5-2010

Investigations of the Dynamical Response in Solids by Time-Dependent Density-Functional Theory

Qinghong Kou
University of Tennessee - Knoxville

To the Graduate Council:

I am submitting herewith a dissertation written by Qinghong Kou entitled "Investigations of the Dynamical Response in Solids by Time-Dependent Density-Functional Theory." I have examined the final electronic copy of this dissertation for form and content and recommend that it be accepted in partial fulfillment of the requirements for the degree of Doctor of Philosophy, with a major in Physics.

Adolfo G. Eguiluz, Major Professor

We have read this dissertation and recommend its acceptance:

Robert Hinde, John J. Quinn, Zhenyu Zhang

Accepted for the Council:
Dixie L. Thompson

Vice Provost and Dean of the Graduate School

(Original signatures are on file with official student records.)

To the Graduate Council:

I am submitting herewith a dissertation written by Qinghong Kou entitled “Investigations of the Dynamical Response in Solids by Time-Dependent Density-Functional Theory”. I have examined the final electronic copy of the dissertation for form and content and recommend that it be accepted in partial fulfillment of the requirements for the degree of Dotor of Philosophy, with a major in physics.

Adolfo G. Eguiluz,
Major Professor

We have read this dissertation
and recommend its acceptance:

Robert Hinde

John J. Quinn

Zhenyu Zhang

Accepted for the Council:

Carolyn R. Hodges
_____
Vice Provost and Dean of the Graduate School

(Original signatures are on file with official student records.)

INVESTIGATIONS OF THE DYNAMICAL RESPONSE IN SOLIDS BY TIME-DEPENDENT DENSITY-FUNCTIONAL THEORY

A Dissertation

Presented for the

Doctor of Philosophy Degree

The University of Tennessee, Knoxville

Qinghong Kou

May 2010

To my kindly son,

To my caring parents

To my beloved boyfriend

To my gentle sister, frank brother-in-law and two lovely nieces

ACKNOWLEDGMENTS

First and foremost, I wish to thank my thesis advisor, Professor Adolfo G. Eguiluz for everything he did for me. I must say I was extremely lucky to have his guidance and support. Without his intuition and physical sense this work could not have been performed. I have learned a lot from him. I wish to thank him again for carefully revising my work.

I want to thank also to Professors John Quinn, Robert Hinde, and Zhenyu Zhang for serving in committee.

The many useful discussions with my colleagues Oscar Restrepo and Claudia Troparevsky are also acknowledged.

I would like to thank to the experimental group form ORNL led by Ben Larsson for the excellent experimental data.

ABSTRACT

The present dissertation studies a joint theoretical-experimental investigation of the dynamical structure factor of wide-gap insulators, using lithium-fluoride as a prototype.

Ground-state (energy bands and electron densities) was calculated using Linear Augmented Plane Wave (LAPW) method and local density approximation (LDA) of density functional theory (DFT). Ab-initio principal is applied to obtain a realistic description of the band structure, which is central to the current research in the condensed matter physics.

Dynamical response function has been evaluated within time-dependent density functional theory (DFT) with an adiabatic approximation (TDLDA), for the exchange-correlation kernel. Our TDLDA spectra contain one adjustable parameter: a "scissors-operator" shift of conduction bands of LDA electronic structure. This parameter is determined in view of the line-shape of the Non-resonant Inelastic X-Ray Scattering (NIXS) cross section for q= 6Å^{-1} along (111) direction. All other spectra are calculated "ab-initio."

The important interplay between band structure and electron dynamics is emphasized within our results. The picture of excitations offers an alternative view to previous investigations involving an approximate solution of the Bethe-Salpeter equation coupled with a more limited range of NIXS data.

TABLE OF CONTENTS

LIST OF TABLES

LIST OF FIGURES

CHAPTER 1

INTRODUCTION

Solid state physics involves application of quantum mechanics (QM) to the electrons in solids. In the first such application, Sommerfeld[1] treated conduction electrons in simple metals as QM particles satisfying the Pauli exclusion principle[2]. Shortly later, Bloch[3] studied the effect of the periodic potential and translational symmetry of crystalline solids on the energy spectra of electrons in solids. The existence of energy bands and band gaps[4] gave insight into why some materials were good conductors, while others were insulators[5]. Band structure calculations[6] were often performed using the knowledge from atomic physics and involved phenomenological parameters, describing the periodic potential that were chosen to give the best fit to observed energy gaps and effective masses. With the improvement in computing capability, researchers were able to attempt first principle calculations without the necessity of introducing adjustable phenomenological parameters. In general, the effective periodic potential contained terms involving the interactions of the electrons with one another through some kind of mean field approximation. For example, the Hartree approximation[7] involves the evaluation of the wavefunctions (WFs) of conduction electrons interacting with other electrons via a self-consistent electron density $\rho\ \vec{r}\ = \sum_i f_0\ E_i\ \left|\Psi_i\ \vec{r}\ \right|^2$, where $\left|\Psi_i\ \vec{r}\ \right|$ is the WF of the ith electron, and $f_0\ E_i$ is the Fermi distribution function. Slater[8] introduced the simple Slater exchange potential (or x-alpha method) by noting that the QM exchange energy was proportional to the cube root of the total density of electrons of the same spin. He accounted for exchange by introducing a potential acting on a electron of spin σ as $V_x\ \vec{r}\ = \alpha\left|\rho_\sigma\ \vec{r}\ \right|^{1/3}$, where $\rho_\sigma\ \vec{r}$ is the density of electrons of spin σ at position $\vec{r}$, and α is a phenomenological constant. Hohenberg demonstrated that the ground-state

energy is uniquely determined by the ground-state density $\rho_\sigma(\vec{r})$ for electrons of each spin σ.

The early Sommerfeld model[1] based on non-interacting electrons was noticed to work better for higher densities. The electron-electron interaction plays an important role in the physically accessible range of densities. However, the main obstacle was to solve the Schrödinger equation for a macroscopic system. It leads to large systems of coupled differential equations making hopeless any attempt to find an exact solution. One of the first attempts to incorporate the electron-electron interaction was provided by Landau[9] theory used for short-range interaction in ^{3}He and applied in condensed matter theory by Silin[10]. It introduces the idea of weakly interacting quasiparticles. Perturbation approaches (e.g Feynmann diagram based method), besides being extremely laborious, are essentially limited by the lack of a small parameter in many cases. Later on, this impeding status was radically changed as Density Functional Theory (DFT) came out in 1964, which led to Walter Kohn winning one half 1998 Nobel Prize in Chemistry.

Hohenberg-Kohn (HK) theorem[11] (DFT) states that there is one to one correspondence between the ground state density $r(\vec{r})$ and the external potential V_{ext}, as well as, a variational principal to search the minimal energy $E[n_0] \leq E[n]$ for the energy functional $E_{V_{ext}}[r]$. Essentially, it allows obtaining the ground-state of a many-electron system by a variation of its density $r(\vec{r})$, a parameter that is far less complicated than the many-electron wave function $\Psi(\vec{r}_1, \vec{r}_2, \ldots, \vec{r}_N)$, where N is the electron number. The theorem could be extended to cover virtual all case of interest (such as, degenerate ground-state systems[12], spin-polarized systems[13], thermal ensembles[14], relativistic systems[15], multicomponent (more than one type of particles) systems[16].

Kohn and Sham[17] turned DFT into a smart way of implementing the HK variational principle in 1965. In the KS scheme, an inhomogeneous many-electron system is treated as a homogeneous many-electron system in the effective potential (mean-field theory). All many-body effects enter one-electron orbital via exchange and correlation potential $V_{xc}(\vec{r})$[18], which can be determined by Quantum Monte-Carlo calculations[19]. Therefore, the density of the interacting system could be powerfully derived from the knowledge of the density for an auxiliary one-particle problem (KS equation). And, the energy functional $E_{xc}[r]$ of the inhomogeneous many-electron system was replaced by its counterpart for a locally-homogeneous electron gas, with the local value of the density, the so-called local density approximation (LDA). LDA turns out to work for many problems where it is not expected to work well[20]. The key point of the victory of the KS scheme is the rigorous introduction of an equivalent orbital picture which is guaranteed to yield the correct density for the correlated system. Furthermore, the KS scheme implemented by the linear augmented planar wave (LAPW) method has achieved the use of the golden dream of the central-field approximation (which goes back all the way to Fermi) in the presence of correlation[21].

Particularly, within the KS scheme, the calculation of electronic structure can be completed through self-consistent cycles by computer. With the significant change in computational environment and infrastructure (CPU speed, memory size, multiple CPU processing and supercomputers), nowadays, the KS DFT is a prevailing method for calculating the ground-state of a many-electron system.

The third generation of DFT is orbital-dependent representations of the exchange-correlation energy functional, the so-called optimized effective potential[22] (OEP). The exchange energy is exactly written in terms of KS orbitals; in addition, the total energy

functional is expressed in terms of the orbitals, which are implicit functionals of the density. A better ground-state can be given according to OEP as long as a researcher has a superior intuition on orbitals. For example, in the second generation of DFT (LDA+U), the total energy functional is hybrid variations of density and orbitals. The parameter "U" of LDA+U in LAPW method is implemented through OEP by the use of the "second-variational" procedure. The initial condition for "U" is an LDA result from the first variation, not physical but closer to the final electronic structure of KS electrons. However, because the macroscopic variable density is replaced by a microscopic variable orbital, and the variational method is critically dependent on the initial condition picked by hand, OEP may lead to a meaningless outcome if the initial WF deviates far from the genuine physical system.

As a counterpart of Hohenberg-Kohn theorem of DFT, the mathematical foundation for the time-dependent (TD) DFT was built up by E. Runge and E. K. U. Gross[23] in 1984. Again, the time-dependent density $r(\vec{r},t)$ of the inhomogeneous many-electron system could be obtained rigorously from a single-particle picture, in terms of the solutions of the time-dependent Kohn-Sham equation, where the time-dependent single-particle potential includes the exchange-correlation (XC) - potential $V_{xc}\left[r(\vec{r},t)\right]$ accounting for the many-body effects. The generalization allows ab-initio calculation of the excited states and thereby makes a whole new arena of phenomena accessible to the first-principle treatment. It works not only for weak probe of molecules[24] and solids[25], but also for matter interacting with the strong laser pulse[26], time-dependent quantum transport[28]. TDDFT is a thriving field, whose impact on the wide area of electron dynamics may eventually rival the enormous influence which ground-state DFT has had on material theory[21]. The above theoretical framework is illustrated in Chapter 2.

DFT is a state of art in which one chooses a realistic path in order to obtain reasonable physical results emerging from the calculations. Particularly, some of the problems which were considered to be rather difficult (for instance, the ferromagnetism of iron) have been easier for DFT experts[29]. It has attained spectacular successes, unthinkable 20 years ago, in describing the electronic structure of the ground state of real solids by applying computational methods which avoid calculations of the many-body wave function. It simplifies enormously the computational work, but also prevents physicists from a deeper understanding of electronic correlations, one of the most fascinating topics of the theory of solids[30].

Models and the many body perturbation theory are other methods of choice for analyzing the properties of the many-electron system. The concept of models can be used everywhere. The goal of the models is to approximate reality and to take into account the most important effects. Strong intuition is needed to set up the model, i.e., to write a physical Hamiltonian $\hat{H}$. Famous models in physics are the Heisenberg model and the Hubbard model. However, without the comparison with measurements, one can never know which nontrivial part of the Hamiltonian $\hat{H}$ is missing. It cannot be used for predicting all properties of different type of the many-body systems. A specific expression of the Hamiltonian is needed for the specific many-particle system. Also, some parameters inside Hamiltonian $\hat{H}$ need to be fitted, which may bring some bias into the calculation. In contrast, DFT is a first-principle method, using "universal" expressions for the Hamiltonian and it can be used to predict properties of realistic systems.

The many body theory can provide physicists with an explicit mathematical form of the genuine many-body interactions in microscopic world, but the infinite perturbative

series forces one to rely on approximations. Many-body perturbation theory (MBPT) reduces the many-particle problem to an effective few-particle problem. All many-body effects are included in an effective interaction kernel. For instance, the solution of the Dyson equation[31], the equation of motion for the one-particle propagator, can provide the single-particle excitation spectrum of the system. The one-particle excitation energies of electronic systems are relevant in photo-electron emission and inverse photo-emission experiments since a single electron is removed or added to the system. The effective interaction kernel[32] includes the electron self energy, which takes into account all exchange and correlation effects on the one-electron level, and which is a non-local and energy-dependent operator. The shielded interaction (or GW) approximation[32,33] is an important approximation for the self-energy operator, where G denotes a single-particle propagator and W stands for the screened interaction, which can be obtained for example using renormalized Hamiltonian approach[28]. Another example is the equation of motion for the two-particle correlation function, the so-called the Bethe-Salpeter equation (BSE), which contains the information of the incident photons creating electron-hole pairs. The two-particle correlation function L is given by the independent propagation L_0 of an electron and the hole, plus a term involving the electron-hole interaction Ξ [34]. MBPT may fail when the external potential is large relative to the unperturbed part of Hamiltonian and cannot be treated as a perturbation.

Correspondingly, electronic excitations in solids can be measured experimentally by inelastic x-ray scattering, electronic energy-loss spectroscopy, and angle-resolved photoemission (the distribution of the electron density of single particle electronic excitations in the reciprocal space), providing valuable information about the intrinsic correlations between electrons in the crystal environment.

Our group has been working on the many-body effects in the correlated systems via electronic excitations of the scattering system for twenty years. First, the dynamical response and the dispersion of the plasmon loss in low atomic number metals, like Al and Na was examined by a generalization of the Dalgarno-Lewis scheme of perturbation theory[35]. Then, the group turns to a realistic treatment of the electronic structure of complex materials. The underlying theoretical framework in our dynamical density-response calculations is TDDFT. The plasmon lifetime in K and its damping mechanism was studied via Padé approximants[36]. The anomalous linewidth dispersion is due to the exchange-correlation effects built into the local spin density approximation (LSDA). Single-particle band structure and dynamical many-body correlations are negligible there. Successively, the group began a theoretical-experimental joint investigation of the dynamical structure factor in 2000. The excitation spectra of correlated electrons in metals (Al, K, and Li) were discussed by a conventional method introducing a numerical broadening factor η[37]. Electron-hole and plasmon excitations in 3d transition metals were reported by ab-initio calculations and inelastic x-ray scattering (IXS) measurements. The evolution of these d states is to move gradually downward crossing the Fermi level as the atomic number increases. It suggests that the optical restricted d-d transition involving d states below and above the Fermi level may happen in transition-metal oxides. This has been observed in TiO_2[38], NiO and CoO[39] by non-resonant IXS at large wavevectors. In addition, the performance of the LSDA+U functional on the ground-state was tested via computations of the electron-hole excitations of NiO compared with NIXS[40] and ellipsometry measurements[41]. Here U describes the on-site Coulomb interaction applying to the non-homogeneous local d shell, a quantity similar to Hubbard model. Furthermore, the complex oxides are extensively explored via charge excitations. One class of oxides ($CaMnO_3$, $LaMnO_3$, CrO_2, etc.) has shown a sharp collective mode.

This feature originates from coherent electron-hole response, mediated by a strong crystal local-field effect (CLFE). It involves two strongly hybridized d and p characters, defined by the bottom edge of the occupied Hubbard band and the empty Hubbard band; whilst, the collective feature of the other class of oxides (NiO and CoO) is inhibited by a third manifold due to O-derived states. Recently, the group has explained a sharp feature in low-energy charge-density excitations of single-crystal MgB_2 displaying a remarkable cosine-like, periodic energy dispersion with momentum transfer $\vec{q}$ along the c* axis, first observed by high resolution NIXS. The physics underlying NIXS data is the strong coupling between the single-particle and collective degrees of freedom, mediated by large CLFE due to charge inhomogeneity normal to the Mg and B layers. As a result, the conventional Landau-damping mechanism does not restrict the collective mode to a small fraction of momentum space. Small-$\vec{q}$ collective channels residing in the single-particle excitation gap of B bonds reappears periodically in higher Brillouin zones[42]. Also, we reveal a collective charge-density excitation at 9eVs induced by CLFE for a large range of momentum transfers in both the hydrated and non-hydrated sodium cobaltates compound for sodium concentrations of $1/3$. The inclusion of water affects the screening at small energies allowing single-particle transitions to be present in the loss spectrum for the small momentum transfers. For the large values of momenta, the loss functions for the hydrated and non-hydrated systems are very similar due to the reduced polarizability of the water molecules. Lately, it was demonstrated that the change in the density response and Wannier functions are caused by metal-to-antiferromagnetic transition in V_2O_3[43]. In the metallic phase, a sharp d-d excitation is observed at $\hbar\omega \sim 2.7\,\mathrm{eV}$ for wave vectors large enough that the sharp plasmonic feature associated with the d-d degrees of freedom is "Landau-damped". Remarkably, the d-d peak also occurs for $\hbar\omega \sim 2.7\,\mathrm{eV}$ in the presence of the insulating gap, a result which is shown to be a signature of a strong d-d

excitonic interaction, absent in the metallic phase. Thus, the strong correlated problem in V_2O_3 has an electron-dynamics counterpart to the opening of the Mott-Hubbard gap, which is a generally trend in similar compounds.

As the LDA/LDA+U is believed to work well in strongly correlated system, in Chapter 3 we try to apply it to one of weakly correlated alkali halides, namely LiF, to investigate the interesting elementary excitations, which provide valuable information about the many-body effects among electrons in the crystal environment. Other goals are to explore the limit of the validity of TDLDA to the extended systems, to check the suitability of computational methods on the ground states and excited states, to understand the difference of the spectra between MBPT and TDDFT, and to expose our views on a decades-long dispute about the nature of excitons (an excited electron is bound to the valence hole it vacated). Moreover, understanding the structure and dynamics of excitons may be helpful to developing technologies for light-emitting diodes[44] or solar energy conversion[45].

With the precious NIXS data available in three principal directions over a wide range of wave vectors, a rigid shift $\Delta = 2.5\text{eV}$ of the TDLDA spectra is determined by using our initial spectrum from the LDA electronic structure referred to the measured dynamical structure factor $S\ \bar{q},\omega$ for a very large wave vector $\bar{q} = 6\dot{\text{A}}^{-1}$ along (111) direction. For this spectrum, the dynamical Coulomb screening effects are gone, the many body effects are not strong and the loss spectrum is basically a replica of the JDOS corresponding to the actual electronic structure of KS electrons. This shift demonstrates that the LDA does not do a good job in wide gap insulators; whilst, the reasonable electronic structure in LiF can be obtained via a scissor shift $\Delta = 2.5\text{eV}$ of conduction bands. All other TDLDA spectra were calculated "ab-initio" and they display a

remarkable semi-quantitative agreement with the NIXS data, along the three high-symmetric directions, from the coherent-response small-*q* regime to the incoherent-response large-*q* regime. This agreement is non-trivial, as the loss line shape changes drastically in both regimes. Furthermore, we do not fix the gap problem in the whole process; however, our calculations excellently agree the NIXS data at the inflexion points for all *q*s.

The important interplay between band structure and electron dynamics is discovered within our technique. The dynamical many-body exchange-correlations in LiF exhibit a rather modest effect since the random phase approximation (RPA) spectra look good under the corrected LDA electronic structure. For the very small wave vector transfer $\vec{q}$ =0.225Å^{-1} // (111), the first two low-energy excitations are dominated by on-site optical allowed transition p→s and p→d respectively, and, the third one is the collective mode characterized by on-site dipole allowed transitions p→d. The excitons in the lowest feature of this wide gap insulator are of Frenkel type where electron and hole reside on the same "extended atom" encompassing different sites, with maxima at $\vec{q}$ =0.75Å^{-1} and 4Å^{-1} in (111). As the wave vector $\vec{q}$ increases, the nature of the spectrum above the gap changes quantitatively, for the evolution of the optical forbidden on-site transition p→p. The competition between the on-site p→p transition and on-site dipole allowed p→d transition lead to CLFE depending strongly in the wave vector $\vec{q}$. The collective mode is damped out at the large wave vector.

In addition, one property related to electronic structure is the dielectric function ε, describing potential reduction in electron systems under external field. We define the "effective" dielectric function $\varepsilon_{eff}\ \vec{q},\omega$ is such that its arithmetic inverse is proportional to the dynamical structure factor. Since the measurable electron-hole spectrum is given as

a direct inverse of $\varepsilon_{eff}\ \vec{q},\omega$, this function allows a certain visualization of some features of the excitation spectrum, such as the distinction between single-particle features and plasmonic features. In other words, $\varepsilon_{eff}\ \vec{q},\omega$ plays the same role for a complex material as the textbook dielectric function plays in case of jellium, so we can use a similar knowledge about dielectric function $\varepsilon\ \vec{q},\omega$ in free electron gas to understand the "effective" dielectric function $\varepsilon_{eff}\ \vec{q},\omega$.

In general, the main goal of this dissertation is to obtain the imaginary part of dynamical response function to connect not only scattering experiments (dynamical structure factor $S\ \vec{q},\omega$) but also optical conductivity experiments, or rather, ellipsometry measurements, which basically measure $\text{Im}\ \vec{q},\omega$ for $\vec{q}\to 0$. New results and insights on the dynamical structure factor are presented for all wave vector transfers $\vec{q}$. The electron-hole interactions (excitonic effects) in LiF are modest. As to the large CLFE for intermediate wave vector $\vec{q}$, dynamical screening is due to highly localized optical forbidden transition.

The dissertation is structured as follows. The next chapter is dedicated to presenting the theoretical framework; the numerical results for LiF together with the comparison with experimental data are presented in Chapter 3 and the conclusions are drawn in the last chapter. Appendixes detailing Dirac equation, LAPW basis functions and their properties and some aspects regarding numerical software are attached at the end of the manuscript.

CHAPTER 2

THEORETICAL PREMISES

2.1 Linear Response Theory

2.1.1 General Consideration

This section is dedicated to the linear response theory and its applications. The derivation provided here follows the explanations of Giuliani and Vignale[31]. There are a lot of problems that require calculating the response of a system to a small time-dependent perturbation. Eventually, its response can be expanded in a power series of the amplitude of perturbation, and the first term to be entirely relevant. Calculation of this response function is what linear response theory does.

As we know, the ground state and the elementary excitations of this system can be described in quantum mechanics. In a very general way, we consider a physical system described by time-independent (many-body) Hamiltonian $\hat{H}_0$. Its eigenvalues and eigenfunctions are E_n and $|\psi_n\rangle$, with occupation probabilities in the equilibrium state f_n. We subject this system to an external perturbation $h\ t$ which is coupled with an observable $\hat{O}$.

The total Hamiltonian is:

$$\hat{H}\ t = \hat{H}_0 + h\ t\ \hat{O} \tag{2.1.1}$$

We suppose that perturbation is turned on at $t = t_0$ and the evolution is adiabatic. The occupation probabilities f_n are constant, not allowing transitions between

orthogonal states. The evolution of the WF, in Schrödinger picture is given by Schrödinger equation:

$$i\hbar\frac{\partial}{\partial t}\left|\psi_n\ \ t\ \right\rangle=\hat{H}\ \ t\ \left|\psi_n\ \ t\ \right\rangle \tag{2.1.2}$$

with the initial condition:

$$\left|\psi_n\ \ t_0\ \right\rangle=\left|\psi_n\right\rangle \tag{2.1.3}$$

Using time-evolution operator U, the WF is:

$$\left|\psi_n\ \ t\ \right\rangle=\hat{U}\ \ t,t_0\ \ \left|\psi_n\right\rangle \tag{2.1.4}$$

The evolution operator can be written as:

$$\hat{U}\ \ t,t_0\ \ =e^{-\frac{i\hat{H}_0\ t-t_0}{\hbar}}\hat{U}_h\ \ t,t_0 \tag{2.1.5}$$

where the part $\hat{U}_h\ \ t,t_0$ due to the external perturbation satisfies the following equation, as a consequence of (2.1.2)

$$i\hbar\frac{\partial}{\partial t}\hat{U}_h\ \ t,t_0\ \ =h\ \ t\ \ \hat{O}\ \ t-t_0\ \ \hat{U}_h\ \ t,t_0 \tag{2.1.6}$$

where the Heisenberg picture version of $\hat{O}$ is

$$\hat{O}\ \ t\ \ =e^{\frac{i\hat{H}_0t}{\hbar}}\hat{O}e^{-\frac{i\hat{H}_0t}{\hbar}}\ . \tag{2.1.7}$$

and the initial condition is $\hat{U}_h\ \ t_0,t_0\ \ =\hat{I}$.

A formal solution of eq. (2.1.6) can be written as:

$$\hat{U}_h\ t,t_0\ = \hat{I} - \frac{i}{\hbar}\int_{t_0}^{t} h\ t'\ \hat{O}\ t'-t_0\ \hat{U}_h\ t',t_0\ dt' \tag{2.1.8}$$

If one is interested only in the first order perturbation expansion [1], the above equation becomes

$$\hat{U}_h^1\ t,t_0\ = \hat{I} - \frac{i}{\hbar}\int_{t_0}^{t} h\ t'\ \hat{O}\ t'-t_0\ dt', \tag{2.1.9}$$

giving a first order expression for the evolution operator as

$$\hat{U}^1\ t,t_0\ = e^{-\frac{i\hat{H}_0\ t-t_0}{\hbar}}\left[\hat{I} - \frac{i}{\hbar}\int_{t_0}^{t} h\ t'\ \hat{O}\ t'-t_0\ dt'\right]. \tag{2.1.10}$$

Any observable $\mathcal{P}$ will have its expectation value at time $t = t_0$

$$\left\langle \hat{\mathcal{P}} \right\rangle_0 = \sum_n f_n \left\langle \psi_n \middle| \hat{\mathcal{P}} \middle| \psi_n \right\rangle, \tag{2.1.11}$$

while after perturbation has been turned on it becomes:

$$\left\langle \hat{\mathcal{P}} \right\rangle_h\ t\ = \sum_n f_n \left\langle \psi_n\ t\ \middle| \hat{\mathcal{P}} \middle| \psi_n\ t\ \right\rangle. \tag{2.1.12}$$

Using eqs. (2.1.4) and (2.1.10) and keeping only the first order in h terms, the above expectation value becomes

$$\begin{aligned}
\left\langle \hat{\mathcal{P}} \right\rangle_h\ t\ &= \sum_n f_n \left\langle \psi_n \middle| \hat{U}^\dagger\ t,t_0\ \hat{\mathcal{P}}\hat{U}\ t,t_0\ \middle| \psi_n \right\rangle \\
&= \sum_n f_n \left\langle \psi_n \middle| \left\{\hat{I} + \frac{i}{\hbar}\int_{t_0}^{t} h\ t'\ \hat{O}\ t'-t_0\ dt'\right\} e^{\frac{i\hat{H}_0\ t-t_0}{\hbar}}\hat{\mathcal{P}}\, e^{-\frac{i\hat{H}_0\ t-t_0}{\hbar}} \right. \\
&\left. \times\left\{\hat{I} - \frac{i}{\hbar}\int_{t_0}^{t} h\ t'\ \hat{O}\ t'-t_0\ dt'\right\} \middle| \psi_n \right\rangle
\end{aligned} \tag{2.1.13}$$

$$\left\langle \hat{P} \right\rangle_h \ t \ = \sum_n f_n \left\langle \psi_n \right| e^{\frac{i\hat{H}_0 \ t-t_0}{\hbar}} \hat{P} e^{-\frac{i\hat{H}_0 \ t-t_0}{\hbar}} \left| \psi_n \right\rangle + \frac{i}{\hbar} \sum_n f_n \left\langle \psi_n \right| \left\{ \int_{t_0}^{t} h \ t' \ \hat{O} \ t'-t_0 \ dt' \right\} \hat{P} \ t \ \left| \psi_n \right\rangle -$$

$$- \frac{i}{\hbar} \sum_n f_n \left\langle \psi_n \right| \hat{P} \ t-t_0 \ \left\{ \int_{t_0}^{t} h \ t' \ \hat{O} \ t'-t_0 \ dt' \right\} \left| \psi_n \right\rangle$$

$$= \left\langle \hat{P} \right\rangle_0 + \frac{i}{\hbar} \sum_n f_n \left\{ \int_{t_0}^{t} h \ t' \ \left\langle \psi_n \right| \ \hat{O} \ t'-t_0 \ \hat{P} \ t-t_0 \ - \hat{P} \ t-t_0 \ \hat{O} \ t'-t_0 \ \left| \psi_n \right\rangle \ dt' \right\}. \tag{2.1.14}$$

Further simplifications can be done using eq. (2.1.7):

$$\left\langle \hat{P} \right\rangle_h \ t \ - \left\langle \hat{P} \right\rangle_0 = \frac{i}{\hbar} \sum_n f_n \left\{ \int_{t_0}^{t} h \ t' \ \left\langle \psi_n \right| \ \hat{O} \ t'-t_0 \ \hat{P} \ t-t_0 \ - \hat{P} \ t-t_0 \ \hat{O} \ t'-t_0 \ \left| \psi_n \right\rangle \ dt' \right\}$$

$$= \frac{i}{\hbar} \sum_n f_n \left\{ \int_{t_0}^{t} h \ t' \ \left\langle \psi_n \right| \left\{ \hat{O} e^{\frac{i\hat{H}_0 \ t'-t}{\hbar}} \hat{P} e^{-\frac{i\hat{H}_0 \ t'-t}{\hbar}} - e^{\frac{i\hat{H}_0 \ t-t'}{\hbar}} \hat{P} e^{-\frac{i\hat{H}_0 \ t'-t}{\hbar}} \hat{O} \right\} \left| \psi_n \right\rangle dt' \right\}$$

$$= - \frac{i}{\hbar} \int_0^{t-t_0} h \ t-t_1 \ \left\langle \left[\hat{P} \ t_1 \ , \hat{O} \right] \right\rangle_0 dt_1 , \tag{2.1.15}$$

where $\left[\ , \ \right]$ stands for commutator, $\left\langle \ldots \right\rangle_0$ denotes the average in thermal equilibrium ensemble, and the transformation of variable $t_1 = t - t'$ has been used.

We define the retarded (causal) linear response function

$$\chi_{\hat{P}\hat{O}} \ t \ = - \frac{i}{\hbar} \theta \ t \ \left\langle \left[\hat{P} \ t \ , \hat{O} \right] \right\rangle_0 \tag{2.1.16}$$

where $\theta \ t_1$ is the Heaviside step function. In this way, we can write the linear response of $\hat{P}$ as

$$\left\langle \hat{P} \right\rangle_1 \ t \ \equiv \left\langle \hat{P} \right\rangle_h \ t \ - \left\langle \hat{P} \right\rangle_0 = \int_0^{t-t_0} \chi_{\hat{P}\hat{O}} \ t_1 \ h \ t-t_1 \ dt_1 , \tag{2.1.17}$$

Now, we can send the time at which the perturbation is turned on to $-\infty$ and rewrite eq. (2.1.17) in the form that is usually used

$$\left\langle \hat{P} \right\rangle_1 \ t \ = \int_0^\infty \chi_{\hat{P}\hat{O}} \ t_1 \ h \ t - t_1 \ dt_1 , \tag{2.1.18}$$

For practical applications we deal with periodic perturbations

$$h \ t \ = h_\omega e^{-i \ \omega + i\eta \ t} + h_\omega^* e^{i \ \omega - i\eta \ t} \tag{2.1.19}$$

The convergence factor $e^{\eta t}$ assures that the perturbation is turned on adiabatically and that at $t = -\infty$, the system is unperturbed. Eventually, $\eta \to 0^+$ limit will be taken in the end. The linear response of eq. (2.1.17) becomes:

$$\begin{aligned} \left\langle \hat{P} \right\rangle_1 \ t \ &= \lim_{\eta \to 0^+} \int_0^\infty \chi_{\hat{P}\hat{O}} \ t_1 \ \left[h_\omega e^{-i \ \omega + i\eta \ \ t - t_1} + h_\omega^* e^{i \ \omega - i\eta \ \ t - t_1} \right] dt_1 \\ &= e^{-i\omega t} h_\omega \lim_{\eta \to 0^+} \int_0^\infty \chi_{\hat{P}\hat{O}} \ t_1 \ e^{i \ \omega + i\eta \ t_1} dt_1 + e^{i\omega t} h_\omega^* \lim_{\eta \to 0^+} \int_0^\infty \chi_{\hat{P}\hat{O}} \ t_1 \ e^{-i \ \omega + i\eta \ t_1} dt_1 \end{aligned} \tag{2.1.20}$$

Understanding that the above integrals represent Fourier components, the expression is written as [31]

$$\left\langle \hat{P} \right\rangle_1 \ \omega \ = h_\omega \chi_{\hat{P}\hat{O}} \ \omega \ , \tag{2.1.21}$$

where, using the definition (2.1.16)

$$\chi_{\hat{P}\hat{O}} \ \omega \ = -\frac{i}{\hbar} \lim_{\eta \to 0^+} \int_0^\infty \left\langle \left[\hat{P} \ t_1 \ , \hat{O} \right] \right\rangle_0 e^{i \ \omega + i\eta \ t_1} dt_1 \ . \tag{2.1.22}$$

A brief look at this expression allows us to represent it like

$$\chi_{\hat{P}\hat{O}}\ \omega = -\frac{i}{\hbar}\lim_{\eta\to 0^+}\sum_n \int_0^\infty f_n \langle\psi_n| e^{\frac{i\hat{H}_0 t_1}{\hbar}} \hat{P} e^{-\frac{i\hat{H}_0 t_1}{\hbar}} \hat{O} - \hat{O} e^{\frac{i\hat{H}_0 t_1}{\hbar}} \hat{P} e^{-\frac{i\hat{H}_0 t_1}{\hbar}} |\psi_n\rangle e^{i\,\omega+i\eta\ t_1} dt_1$$

$$= -\frac{i}{\hbar}\lim_{\eta\to 0^+}\int_0^\infty dt_1 e^{i\,\omega+i\eta\ t_1} f_n \left\{ \langle\psi_n| e^{\frac{i\hat{H}_0 t_1}{\hbar}} \hat{P} \sum_m |\psi_m\rangle\langle\psi_m| e^{-\frac{i\hat{H}_0 t_1}{\hbar}} \hat{O}|\psi_n\rangle \right.$$

$$\left. - \langle\psi_n|\hat{O} e^{\frac{i\hat{H}_0 t_1}{\hbar}} \sum_m |\psi_m\rangle\langle\psi_m| \hat{P} e^{-\frac{i\hat{H}_0 t_1}{\hbar}} |\psi_n\rangle \right\} \qquad .(2.1.23)$$

$$= -\frac{i}{\hbar}\lim_{\eta\to 0^+}\int_0^\infty dt_1 e^{i(\omega+i\eta)t_1} \sum_{nm} f_n \left\{ e^{\frac{i(E_n-E_m)t_1}{\hbar}} \hat{P}_{nm}\hat{O}_{mn} - e^{\frac{i(E_m-E_n)t_1}{\hbar}} \hat{O}_{nm}\hat{P}_{mn} \right\}$$

$$= \frac{1}{\hbar}\lim_{\eta\to 0^+}\left(\sum_{n,m} f_n \frac{\hat{P}_{nm}\hat{O}_{mn}}{\omega-\omega_{mn}+i\eta} - \sum_{n,m} f_m \frac{\hat{O}_{nm}\hat{P}_{mn}}{\omega+\omega_{mn}+i\eta} \right)$$

where $\omega_{mn} = {E_m - E_n}/{\hbar}$. Interchanging m and n in the last sum, the eq. (2.1.23) can be but in much compact form:

$$\chi_{\hat{P}\hat{O}}\ \omega = \frac{1}{\hbar}\lim_{\eta\to 0^+}\sum_{n,m}\frac{f_n - f_m}{\omega-\omega_{mn}+i\eta}\hat{P}_{nm}\hat{O}_{mn}, \qquad (2.1.24)$$

known as Lehman representation[31] which indicates the positions of the poles.

Using the well-known formula:

$$\lim_{\eta\to 0^+}\frac{1}{x+i\eta} = \wp\ x\ - i\pi\delta\ x\ , \qquad (2.1.25)$$

where $\wp\ x$ is the principal value distribution and $\delta\ x$ is the Dirac function, we can separate real and imaginary part in eq. (2.1.24) as

$$\chi_{\hat{P}\hat{O}}\ \omega = \frac{1}{\hbar}\sum_{n,m}\ f_n - f_m\ \hat{P}_{nm}\hat{O}_{mn}\wp\left(\frac{1}{\omega-\omega_{mn}}\right) - \frac{i\pi}{\hbar}\sum_{n,m}\ f_n - f_m\ \hat{P}_{nm}\hat{O}_{mn}\delta\ \omega-\omega_{mn}\ , (2.1.26)$$

Interesting properties of the response functions can be derived starting form the Lehmann representation:

$$\chi_{\hat{P}\hat{O}}\ -\omega\ =\left[\chi_{\hat{P}\hat{O}}\ \ \omega\ \right]^{*}, \tag{2.1.27}$$

Until now, we have used only Hermitian operators, but the theory can be extended to cover all operators, in this case $\chi_{\hat{P}\hat{O}}\ -\omega\ =\left[\chi_{\hat{P}^{\dagger}\hat{O}^{\dagger}}\ \ \omega\ \right]^{*}$. Also interchanging *m* and *n*, at zero frequency we get[31]:

$$\chi_{\hat{P}\hat{O}}\ \ 0\ =\chi_{\hat{O}\hat{P}}\ \ 0\ , \tag{2.1.28}$$

It is important to notice that from eq. (2.1.26), it is immediate that $\chi_{\hat{P}\hat{P}^{\dagger}}\ \ 0$ is real and negative. A close look at the same eq. (2.1.26) reveals another property of response function:

$$\Im m\chi_{\hat{P}\hat{P}}\ \ \omega\ =-\frac{\pi}{\hbar}\left[\sum_{n,m}f_{n}\left|\hat{P}_{nm}\right|^{2}\delta\ \ \omega-\omega_{mn}\ -\sum_{n,m}f_{n}\left|\hat{P}_{nm}\right|^{2}\delta\ \ \omega+\omega_{mn}\ \right], \tag{2.1.29}$$

leading $\Im m\chi_{\hat{P}\hat{P}}\ \ \omega\ >0$ for $\omega<0$ and $\Im m\chi_{\hat{P}\hat{P}}\ \ \omega\ <0$ for $\omega>0$.

We focus now on the physical interpretation of the imaginary part of the response function. Let's consider the Hamiltonian of (2.1.1), where the function $h\ \ t$ is given by (2.1.19). The average power delivered over one period is

$$W=\frac{1}{T}\int_{0}^{T}\frac{\partial}{\partial t}\left\langle\psi_{n}\ \ t\ \left|\hat{H}\ \ t\ \right|\psi_{n}\ \ t\ \right\rangle dt \tag{2.1.30}$$

Using the Schrödinger equation (2.1.2), the above formula transforms (using eq. (2.1.21)) as

$$W = \frac{1}{T}\int_0^T dt\ \left(-i\omega h_\omega e^{-i\omega t} + i\omega h_\omega^* e^{i\omega t}\right)\ \left\langle \hat{O}\right\rangle_1\ t\ = -2\omega\left|h_\omega\right|^2\ \Im m\chi_{\hat{O}\hat{O}}\ \ \omega \qquad (2.1.31)$$

which indicates a energy dissipation for $\omega > 0$ and energy absoption[31] for $\omega > 0$.

The dynamical structure factor[31], characterizing time-dependent fluctuations of $\hat{O}$

$$S_{\hat{O}\hat{O}^\dagger}\ \ \omega\ = \frac{1}{2\pi}\int_{-\infty}^{\infty}\left\langle \hat{O}\ t\ \hat{O}^\dagger\right\rangle_0 e^{i\omega t}dt \qquad (2.1.32)$$

This quantity is actually related to the imaginary part of $\chi_{\hat{O}\hat{O}^\dagger}$

$$\begin{aligned} S_{\hat{O}\hat{O}^\dagger}\ \ \omega\ &= \frac{1}{2\pi}\int_{-\infty}^{\infty}\sum_n f_n \left\langle n\left|e^{\frac{iH_0 t}{\hbar}}\hat{O}e^{-\frac{iH_0 t}{\hbar}}\hat{O}^\dagger\right|n\right\rangle e^{i\omega t}dt \\ &= \frac{1}{2\pi}\int_{-\infty}^{\infty}\sum_{n,m} f_n \left\langle n\left|e^{\frac{iH_0 t}{\hbar}}\hat{O}\right|m\right\rangle\left\langle m\left|e^{-\frac{iH_0 t}{\hbar}}\hat{O}^\dagger\right|n\right\rangle e^{i\omega t}dt \\ &= \frac{1}{2\pi}\int_{-\infty}^{\infty}\sum_{n,m} f_n e^{-i\omega_{mn}t}\left|\hat{O}_{nm}\right|^2 e^{i\omega t}dt = \sum_{n,m} f_n\left|\hat{O}_{nm}\right|^2\delta\ \ \omega-\omega_{mn} \end{aligned} \qquad (2.1.33)$$

If we consider the system at finite temperature T $f_n = e^{-\beta E_n}$, $\beta = \ kT^{\ -1}$,

$$S_{\hat{O}\hat{O}^\dagger}\ \ -\omega\ = e^{-\beta\hbar\omega}S_{\hat{O}^\dagger\hat{O}}\ \ \omega\ . \qquad (2.1.34)$$

Then, eqs. (2.1.33) and (2.1.34) is compared to formula (2.1.26), the fluctuation-dissipation theorem becomes:

$$\Im m\chi_{\hat{O}\hat{O}^\dagger}\ \ \omega\ = -\frac{\pi}{\hbar}\ 1-e^{-\beta\hbar\omega}\ \ S_{\hat{O}\hat{O}^\dagger}\ \ \omega\ . \qquad (2.1.35)$$

We conclude this part by making some comments about analytic properties of response functions and collective modes. We notice form Lehmann representation (2.1.24) that the causal response function is analytic in the complex upper half plane. For finite systems have, the response functions have simple poles, below the real axis. In the thermodynamic limit, the poles are merging producing a branch-cut just infinitesimally

below the real axis[31]. Analytic continuation into the complex lower-half plane may have a pole with finite strength. Such a pole occurring at $\Re e\,\omega + i\Im m\,\omega$, indicates a collective mode with energy $\hbar\Re e\,\omega$ and lifetime $\propto \left|\Im m\,\omega\right|^{-1}$.

2.1.2 Density-density response function of an electron gas in jellium model

The system of interest is a homogeneous non-interacting d-dimensional electron gas. The many-body WFs are Slater determinants of one-particle states. The one-particle states are plane waves $e^{i\vec{k}\cdot\vec{r}}\chi_\sigma$, where χ_σ denotes the spinor. The one particle energy states are $\varepsilon_{\vec{k}\sigma} = \dfrac{\hbar^2 k^2}{2m}$. The calculations are done at 0K.

We evaluate density-density response function using Lehmann representation in eq. (2.1.24). The operators that we use are $\hat{n}_{\vec{q}}$ and $\hat{n}_{-\vec{q}}$. Any eigenstate can be written in second quantization form as

$$\psi_{k_i\sigma_i} = a^\dagger_{k_n\sigma_n} a^\dagger_{k_{n-1}\sigma_{n-1}} \ldots a^\dagger_{k_1\sigma_1} \left|0\right\rangle, \tag{2.1.36}$$

where $a^\dagger_{k_i\sigma_i}$ is electron creation operators and $\left|0\right\rangle$ represents the vacuum state. The electron creation/annihilation operators satisfy the commutation relationships

$$\begin{aligned} a^\dagger_{k_i\sigma_i}, a_{k_j\sigma_j} &= a^\dagger_{k_i\sigma_i} a_{k_j\sigma_j} + a_{k_j\sigma_j} a^\dagger_{k_i\sigma_i} = \delta_{k_i k_j}\delta_{\sigma_i\sigma_j} \\ a_{k_i\sigma_i}, a_{k_j\sigma_j} &= 0 \\ a^\dagger_{k_i\sigma_i}, a^\dagger_{k_j\sigma_j} &= 0 \end{aligned} \quad . \tag{2.1.37}$$

In the initial equilibrium state, the ground sate WF is obtained by occupying all $\vec{k}$ -states with $k \le k_F$. All non-zero contributions to the response function would correspond to transitions between ground state and excited states:

$$\chi_{\hat{n}_{\vec{q}}\hat{n}_{-\vec{q}}}\ \omega\ = \frac{1}{\hbar}\lim_{\eta\to 0^+}\sum_i\left(\frac{1}{\omega-\omega_{i0}+i\eta}\ \hat{n}_{\vec{q}}\ _{0i}\ \hat{n}_{-\vec{q}}\ _{i0}-\frac{1}{\omega-\omega_{0i}+i\eta}\ \hat{n}_{\vec{q}}\ _{i0}\ \hat{n}_{-\vec{q}}\ _{0i}\right), \quad (2.1.38)$$

where 0 stands for ground state and i stand for any excited state. The products of matrix elements involved in this formula are of the following form

$$\frac{1}{L^d}\langle 0|\hat{a}_{\vec{k}'_1\sigma'_1}\ldots\hat{a}_{\vec{k}'_n\sigma'_n}\left(\sum_{\vec{k}\sigma}a^{\dagger}_{\vec{k}+\vec{q}\sigma}a_{\vec{k}\sigma}\right)a^{\dagger}_{\vec{k}_n\sigma_n}\ldots a^{\dagger}_{\vec{k}_1\sigma_1}|0\rangle\langle 0|a_{\vec{k}_1\sigma_1}\ldots a_{\vec{k}_n\sigma_n}\left(\sum_{\vec{k}\sigma}a^{\dagger}_{\vec{k}'\sigma'}a_{\vec{k}'+\vec{q}\sigma'}\right)\hat{a}^{\dagger}_{\vec{k}'_n\sigma'_n}\ldots\hat{a}^{\dagger}_{\vec{k}'_1\sigma'_1}|0\rangle \quad (2.1.39)$$

The terms in (2.1.39) are non-zero only if the bra and ket states differ by one planewave and the respective wavevectors differ by $\vec{q}$. The two sums in eq. (2.1.39) reduce to one. The matrix element appearing first term of eq. (2.1.38) reduced to only $f_{\vec{k}}$ while the second one reduces to $f_{\vec{k}+\vec{q}}$. The energy difference ω_{i0} is the one corresponding to the removal of a particle with $\vec{k}$ and the addition of one with $\vec{k}+\vec{q}$.

The Lindhard response function can be written using one-particle states as [31]:

$$\chi\ q,\omega\ = \lim_{\eta\to 0^+}\frac{1}{L^d}\sum_{\vec{k},\sigma}\frac{f_{\vec{k},\sigma}-f_{\vec{k}+\vec{q},\sigma}}{\hbar\omega+\varepsilon_{\vec{k},\sigma}-\varepsilon_{\vec{k}+\vec{q},\sigma}+i\hbar\eta}, \quad (2.1.40)$$

The summation in (2.1.40) can be transform into integral

$$\chi\ q,\omega\ = 2\int\frac{d^dk}{2\pi\ ^d}\frac{f_{\vec{k}}-f_{\vec{k}+\vec{q}}}{\hbar\omega+\frac{\hbar^2k^2}{2m}-\frac{\hbar^2\ \vec{k}+\vec{q}\ ^2}{2m}+i\hbar\eta}, \quad (2.1.41)$$

Doing simple mathematical steps, the above expression can be written as [1]

$$\chi\ q,\omega\ = \frac{2mk_F^{d-2}\Omega_d}{2\pi\ ^d\hbar^2y}\int_0^1 dx\,x^{d-1}\int\frac{d\Omega_d}{\Omega_d}\frac{1}{w-\frac{y}{2}-x\cos\theta+i\eta}+\ w^+\to w^-\ , \quad (2.1.42)$$

where $w=\frac{m\omega}{\hbar k_F q}$, $x=\frac{k}{k_F}$, $y=\frac{q}{k_F}$ and Ω_d is the solid angle in d dimensions.

The prefactor $\frac{2mk_F^{d-2}\Omega_d}{2\pi^{\ d}\hbar^2}$ is exactly the d dimensional density of states at the Fermi level, which can be expressed as:

$$N_0=\begin{cases}\frac{mk_F}{\pi^2\hbar^2}, & 3D,\\ \frac{m}{\pi\hbar^2}, & 2D,\\ \frac{m}{\pi\hbar^2 k_F}, & 1D.\end{cases} \tag{2.1.43}$$

Using the following notation

$$\psi_d\ z\ =\int_0^1 dx\,x^{d-1}\int\frac{d\Omega_d}{\Omega_d}\frac{1}{z-x\cos\theta}, \tag{2.1.44}$$

which in an antisymmetric function ($\psi_d\ -z\ =-\psi_d\ z\ $),the response function becomes

$$\chi\ q,\omega\ =\frac{N_0}{y}\left[\psi_d\left(w-\frac{y}{2}+i\eta\right)-\psi_d\left(w+\frac{y}{2}+i\eta\right)\right] \tag{2.1.45}$$

The evaluation of $\psi_d\ z\ $ can be done analytically in d =1,2,3,… The integral is evaluated. It is important to remember that the logarithm function has a branch-cut on the negative real axis. The response function is summarized in the following table[31]: Lindhard functions vs. frequency for $q=0.5k_F$ and $q=2.5k_F$ in 1, 2 and 3 dimensions are plotted in Fig. 2.1. In the table we use the notation $\nu_\pm=w\pm\frac{y}{2}$.

Regarding the static limit we can notice, the static response (Lindhard) function exhibits a singular behavior at $q=2k_F$, corresponding to the transitions at the Fermi sea $-k_F\leftrightarrow k_F$. It is important to notice that while the 1D Lindhard function is singular, the

Table 2.1 Real and imaginary part of Lindhard function

	$-\frac{\Re e\chi\ q,\omega}{N_d\ 0}$	$-\frac{\Im m\chi\ q,\omega}{N_d\ 0}$
3D	$\frac{1}{2}-\frac{1-\nu_-}{4y}\ln\left\|\frac{\nu_-+1}{\nu_--1}\right\|+\frac{1-\nu_+}{4y}\ln\left\|\frac{\nu_++1}{\nu_+-1}\right\|$	$\frac{\pi}{4y}\left[\theta\ 1-\nu_-^2\ \ 1-\nu_-^2\ -\theta\ 1-\nu_+^2\ \ 1-\nu_+^2\ \right]$
2D	$1+\frac{1}{y}\Big[\text{sign}\ \nu_-\ \theta\ \nu_-^2-1\ \sqrt{\nu_-^2-1}$ $-\text{sign}\ \nu_+\ \theta\ \nu_+^2-1\ \sqrt{\nu_+^2-1}\Big]$	$\frac{1}{y}\left[\theta\ 1-\nu_-^2\ \sqrt{1-\nu_-^2}-\theta\ 1-\nu_+^2\ \sqrt{1-\nu_+^2}\right]$
1D	$\frac{1}{2y}\ln\left\|\frac{\nu_--1}{\nu_-+1}\right\|-\frac{1}{2y}\ln\left\|\frac{\nu_+-1}{\nu_++1}\right\|$	$\frac{\pi}{2y}\left[\theta\ 1-\nu_-^2\ -\theta\ 1-\nu_+^2\ \right]$

singularity of 2D and 3D responses are only in the derivative. Those singularities are related to Friedel oscillations. The 1D singularity induced so called “Peierls instability”.

The imaginary part is of interest also. According to the above table, it contains the step functions. It is nonzero only in a definite range of frequencies. For 2D and 3D

$$\max\ 0,\omega_-\ q\ \ \le|\omega|\le\omega_+\ q \tag{2.1.46}$$

where

$$\omega_\pm\ q\ =\frac{hq^2}{2m}\pm\frac{hk_F}{m}q\,. \tag{2.1.47}$$

It is nonzero in the area of q,ω plane which describes possible excitations of the electrons from the Fermi sea over the Fermi level, It gives the so called “electron-hole continuum.” The 1D case is determined by the fact the Fermi surface consists in two points $\pm k_F$. Region II from Fig. 2.1 g) is absent.

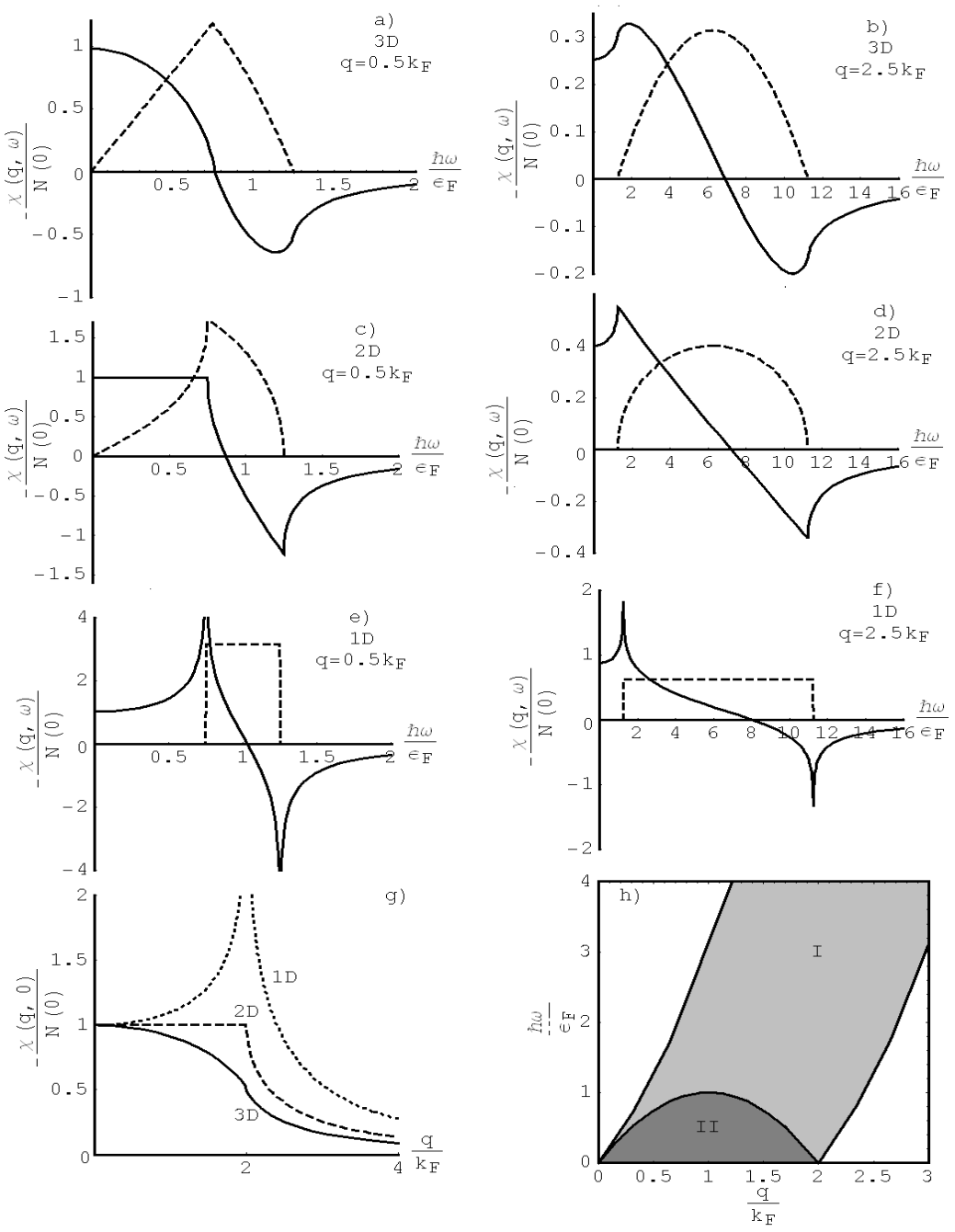

Figure 2.1: Density response function, a)-f) real (solid) and imaginary part (dashed) for 3D, 2D, 1D; g) static response function, electron-hole continuum

We end this section by making some comments about collective modes (plasmons). We try to include electron-electron interaction using Random Phase Approximation (RPA). The density response function is written as [31]

$$\chi_{nn}^{RPA}(q,\omega) = \frac{\chi_0(q,\omega)}{1 - v_q \chi_0(q,\omega)} \tag{2.1.48}$$

When the denominator is zero, the response becomes infinite, signalizing the presence of the collective mode: the plasmons[31]. Expanding the response function in the limit $q \to 0$ and $\frac{\hbar q}{m\omega} \to 0$.

$$\chi_0(q,\omega) \approx \frac{nq^2}{m\omega^2}\left(1 + a_d \frac{q^2 v_F^2}{\omega^2}\right) \tag{2.1.49}$$

with $a_3 = \frac{3}{5}$, $a_2 = \frac{3}{4}$, n being the electron density. Solving the equation

$$1 - v_q \chi_0(q, \Omega_{pl}(q)) = 0 \tag{2.1.50}$$

we obtain the approximate plasmon frequencies

$$\Omega_{pl}(q) \approx \begin{cases} \sqrt{\frac{4\pi n e^2}{m}}\left(1 + \frac{3}{40}\frac{(36\pi)^{\frac{1}{3}} a_B}{n^{\frac{1}{3}}} q^2\right), & 3D, \\ \sqrt{\frac{2\pi n e^2 q}{m}}\left(1 + \frac{3a_B}{8} q\right), & 2D. \end{cases} \tag{2.1.51}$$

The plasmon frequency at zero wavevector is $\sqrt{4\pi n e^2 / m}$ for 3D, while for 2D it is zero at small wavevectors. For large q, the plasma mode enters in the electron-hole continuum becoming Landau damped, decaying in the e-h excitations[31]. The excitation spectrum is presented in Fig 2.2.

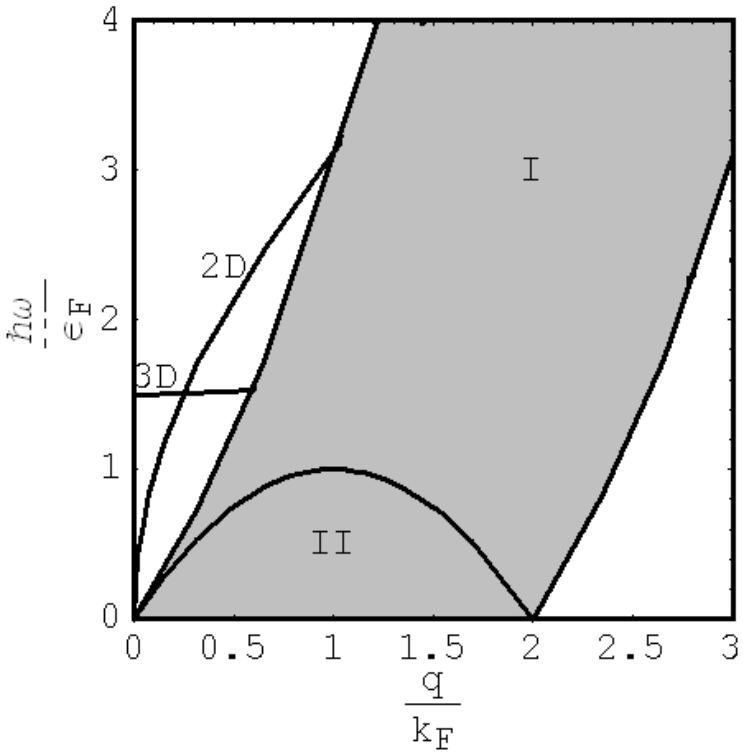

Figure 2.2 Electron-hole continuum and plasmon mode dispersion

2.1.3 Density-density response function of an electron gas in infinite periodic crystals using one-particle picture

The Linhard response function in eq. (2.1.40), which is described in jellium model (electrons move in a uniform positive ion background), dismisses the intrinsic periodicity of crystals, which result in the rather confusing history of various phenomenological "patch ups" of uncontrolled approximations for the many-body problem[37].

A general response of $\langle \hat{P} \rangle$ to $\hat{O}$ for a system described by a one-particle Hamiltonian can be written as a generalization of (2.1.40):

$$\chi_{\hat{n}\hat{n}}\ \ \omega\ = \sum_{\alpha\beta} \frac{f_\alpha - f_\beta}{\hbar\omega + \varepsilon_\alpha - \varepsilon_\beta + i\hbar\eta} \hat{n}_{\alpha\beta}\hat{n}_{\beta\alpha}\,, \tag{2.1.41}$$

where α and β are the one-particle eigenstates. It can also be derived via density-matrix method in single-particle basis.

The eq. (2.1.41) is rewritten in the following form

$$\chi^{\ 0}\ \ \vec{x},\vec{x}'\,|\,\omega\ =\ \sum_{\nu,\nu'} \frac{f_\nu - f_{\nu'}}{E_\nu - E_{\nu'} + \hbar\ \omega + i\eta} \psi_\nu^*\ \vec{x}\ \psi_{\nu'}\ \vec{x}\ \psi_\nu\ \vec{x}'\ \psi_{\nu'}^*\ \vec{x}'\ . \tag{2.1.53}$$

Considering the inherent periodicity, we have

$$\chi^{\ 0}\ \ \vec{x},\vec{x}'\,|\,\omega\ = \chi^{\ 0}\ \ \vec{x}+\vec{R},\vec{x}'+\vec{R}\,|\,\omega \tag{2.1.54}$$

where $\vec{R}$ is a translation vector.

We introduce the Fourier transformation into $\chi^{\ 0}\ \ \vec{x},\vec{x}'\,|\,\omega$,

$$\chi^{\ 0}\ \ \vec{x},\vec{x}'\,|\,\omega\ = \frac{1}{V}\sum_{\vec{q}}\sum_{\vec{q}'} e^{i\vec{q}\cdot\vec{x}} e^{-i\vec{q}'\cdot\vec{x}'} \chi^{\ 0}\ \ \vec{q},\vec{q}'\,|\,\omega\ . \tag{2.1.55}$$

where the wave vectors satisfy Born-Von Karman boundary conditions on a macrocrystal commensurate with the unit cell of the Bravais lattice. Similarly,

$$\chi^{\ 0}\ \ \vec{x}+\vec{R},\vec{x}'+\vec{R}\,|\,\omega\ = \frac{1}{V}\sum_{\vec{q}}\sum_{\vec{q}'} e^{i\vec{q}\cdot\ \vec{x}+\vec{R}}\ e^{-i\vec{q}'\cdot\ \vec{x}'+\vec{R}}\ \chi^{\ 0}\ \ \vec{q},\vec{q}'\,|\,\omega\ . \tag{2.1.56}$$

Comparing with eq. (2.1.55) and (2.1.56) plus the relation in eq. (2.1.54), we get

$$e^{i\,\vec{q}-\vec{q}'\cdot\vec{R}} = 1, \quad \text{namely,}\ \ \vec{q}' = \vec{q} + \vec{G}' \tag{2.1.57}$$

For the computational reason, $\vec{q}$ is rewritten as

$$\vec{q} = \vec{k} + \vec{G} \tag{2.1.58}$$

where, the "reduced" wave vector $\vec{k}$ lies inside the first Brillouin Zone. Inserting eq. (2.1.57) and (2.1.58) into eq. (2.1.55), it becomes

$$\chi^{0}\left(\vec{x},\vec{x}'|\omega\right) = \frac{1}{V}\sum_{\vec{k}}\sum_{\vec{G},\vec{G}'} e^{i\left(\vec{k}+\vec{G}\right)\cdot\vec{x}} e^{-i\left(\vec{k}+\vec{G}'\right)\cdot\vec{x}'} \chi^{0}\left(\vec{k}+\vec{G},\vec{k}+\vec{G}'|\omega\right) .$$

Using the notation

$$\chi^{0}\left(\vec{k}+\vec{G},\vec{k}+\vec{G}'|\omega\right) \equiv \chi^{0}_{\vec{G},\vec{G}'}\left(\vec{k}|\omega\right) ,$$

the above equation becomes

$$\chi^{0}\left(\vec{x},\vec{x}'|\omega\right) = \frac{1}{V}\sum_{\vec{k}}\sum_{\vec{G},\vec{G}'} e^{i\left(\vec{q}+\vec{G}\right)\cdot\vec{x}} e^{-i\left(\vec{q}+\vec{G}'\right)\cdot\vec{x}'} \chi^{0}_{\vec{G},\vec{G}'}\left(\vec{q}|\omega\right) . \tag{2.1.59}$$

Applying the inverse Fourier transformation on eq. (2.1.59), then, we substitute eq. (2.1.53) into it and get density-density response function in the presence of periodic potential

$$\begin{aligned}\chi^{0}_{\vec{G},\vec{G}'}\left(\vec{q}|\omega\right) = & \frac{1}{V}\sum_{\vec{k}}\sum_{n,n'} \frac{f_{\vec{k},n} - f_{\vec{k}+\vec{q},n'}}{E_{\vec{k},n} - E_{\vec{k}+\vec{q},n'} + \hbar\,\omega + i\eta} \\ & \times\left\langle \vec{k},n\left|e^{-i\left(\vec{q}+\vec{G}\right)\cdot\hat{\vec{x}}'}\right|\vec{k}+\vec{q},n'\right\rangle\left\langle \vec{k}+\vec{q},n'\left|e^{i\left(\vec{q}+\vec{G}'\right)\cdot\hat{\vec{x}}}\right|\vec{k},n\right\rangle\end{aligned} \tag{2.1.60}$$

When the KS electronic structure is used in the above equation, it becomes KS response $\chi^{s}_{\vec{G},\vec{G}'}\left(\vec{q}|\omega\right)$. It is discussed in the beginning of section 2.4.

In terms of the expression in eq. (2.1.60), the factors which affect the KS response are the availability of the transition channels, the possibly overlapping WFs of the occupied and empty states, and the selection rules.

2.2 Density Functional Theory

In order to describe the realistic electronic structure in the periodic lattice, we resort to the DFT.

Let us first examine the non-relativistic Hamiltonian in detail:

$$\hat{H} = -\frac{\hbar^2}{2}\sum_i \frac{\tilde{\nabla}^2_{\vec{R}_i}}{M_i} - \frac{\hbar^2}{2}\sum_i \frac{\tilde{\nabla}^2_{\vec{r}_i}}{m_e} + \frac{1}{8\pi\varepsilon_0}\sum_{i'\,j}\frac{e^2}{\left|\vec{r}_i - \vec{r}_j\right|} - \frac{1}{4\pi\varepsilon_0}\sum_{i,j}\frac{e^2 Z_i}{\left|\vec{R}_i - \vec{r}_j\right|} + \frac{1}{8\pi\varepsilon_0}\sum_{i'\,j}\frac{e^2 Z_i Z_j}{\left|\vec{R}_i - \vec{R}_j\right|}, \quad (2.2.1)$$

where, the mass and position of the nucleus are M_i and $\vec{R}_i$ respectively, the mass of the electron at $\vec{r}_i$ is m_e. Then, the Schrödinger equation becomes

$$\hat{H}\Psi\left(\vec{r}_1, z_1, \vec{r}_2, z_2, \ldots, \vec{r}_N, z_N, R_1, R_2, \ldots R_{N_n}\right) = E\Psi\left(\vec{r}_1, z_1, \vec{r}_2, z_2, \ldots, \vec{r}_N, z_N, R_1, R_2, \ldots R_{N_n}\right) \quad (2.2.2)$$

where, $\Psi\left(\vec{r}_1, z_1, \vec{r}_2, z_2, \ldots, \vec{r}_N, z_N, R_1, R_2, \ldots R_{N_n}\right)$ is the many-particle wave function. z_i is the spin coordinate for the i-th electron. Clearly, it is impossible to exactly solve the eq. (2.2.2) regarding the huge number of particles by now.

To approach to an appropriate solution, firstly, the Born-Oppenheimer approximation is made by treating the nuclei as "frozen" at the equilibrium positions. Then, the first term in eq. (2.2.1) disappears; the last term in eq. (2.2.1) reduces to a constant. The Hamiltonian turns into

$$\hat{H} = -\frac{\hbar^2}{2}\sum_i \frac{\tilde{\nabla}^2_{\vec{r}_i}}{m_e} + \frac{1}{8\pi\varepsilon_0}\sum_{i'\,j}\frac{e^2}{\left|\vec{r}_i - \vec{r}_j\right|} - \frac{1}{4\pi\varepsilon_0}\sum_{i,j}\frac{e^2 Z_i}{\left|\vec{R}_{i0} - \vec{r}_j\right|}. \quad (2.2.3)$$

Although the above many-particle Hamiltonian has been simplified, other approximations have to still be used to "solve" the intricate Schrödinger equations. Density functional theory (DFT) is one of the most widely used methods to tackle it and calculate properties of complex electronic systems.

2.2.1 The Hohenberg-Kohn theorem

DFT was formally established in 1964 by Hohenberg and Kohn[11], even though the earliest density functional work was the Thomas-Fermi model[20] done in 1928. For simplicity, DFT is illustrated in the spin non-polarized case first.

In DFT, the Hamiltonian in eq. (2.2.3) is written in three parts

$$\hat{H} = -\frac{\hbar^2}{2}\sum_i \frac{\tilde{\nabla}_{\vec{r}_i}^2}{m_e} + \frac{1}{8\pi\varepsilon_0}\sum_{i'\,j}\frac{e^2}{|\vec{r}_i - \vec{r}_j|} - \frac{1}{4\pi\varepsilon_0}\sum_{i,j}\frac{e^2 Z_i}{|\vec{R}_{i0} - \vec{r}_j|} = \hat{T} + \hat{V}_{ee} + \hat{V}_{ext}. \quad (2.2.4)$$

T is the kinetic energy of the electrons; V_{ee} represents the potential energy due to electron-electron interactions; and V_{ext} denotes for the potential energy in the presence of external potential and the interactions between nuclei and electrons in the material is ascribed to V_{ext}. Other terms might appear due to interaction with other external fields (e.g., incident beam (lights, laser, x-rays, electrons, and neutrons), electrical field, magnetic field, and voltage, etc.). Thus, a many-body system could be viewed as a many-electron system. The wave function $\Psi(\vec{r}_1, z_1, \vec{r}_2, z_2, \ldots, \vec{r}_N, z_N)$ is anti-symmetric to electron permutation.

$$\Psi(\ldots, \vec{r}_i, z_i, \ldots, \vec{r}_j, z_j, \ldots) = -\Psi(\ldots, \vec{r}_j, z_j, \ldots, \vec{r}_i, z_i, \ldots). \quad (2.2.5)$$

The whole theorem is commonly elucidated according to two parts[46]: 1) in the non-degenerate system, there exists a one-to-one mapping between the ground-state

density $r(\vec{r})$ of a many-electron system (atom, molecule, and solid) and the external one-body potential V_{ext}. Therefore, the ground-state mean value of any observable $\hat{O}$ is a unique functional of the ground-state electron density:

$$O[r] = \left\langle \Psi(\vec{r}_1, z_1, \vec{r}_2, z_2, \ldots, \vec{r}_N, z_N) \middle| \hat{O} \middle| \Psi(\vec{r}_1, z_1, \vec{r}_2, z_2, \ldots, \vec{r}_N, z_N) \right\rangle . \qquad (2.2.6)$$

2) As $\hat{O}$ being the Hamiltonian $\hat{H}$, the ground-state total energy functional $E_{V_{ext}}[r]$ has a form of

$$E_{V_{ext}}[r] = \underbrace{T[r] + V_{ee}[r]}_{F_{HK}[r]} + \int d\vec{r}\, r(\vec{r}) n_{ext}(\vec{r}). \qquad (2.2.7)$$

$F_{HK}[r]$ is the Hohenberg-Kohn density functional of an universal many-electron system. The ground-state total energy functional $E_{V_{ext}}[r]$ allows variational access to its minimal value for the ground-state density corresponding to V_{ext}.

In terms of the first theorem, in the non-degenerate system, there exists an invertible relation between the ground-state density $r(\vec{r})$ and the unique external potential V_{ext}. With the knowledge of the ground-state density $r(\vec{r})$, the external potential V_{ext} and the Hamiltonian $\hat{H}$, and hence all the ground-state properties of the system are determined. Reversely, in the non-degenerate system, the external potential V_{ext} which fixes the Hamiltonian $\hat{H}$ gives the unique ground-state density $r(\vec{r})$ of the many-electron system[47] (V-representable). Consequently, the ground-state electron density $r(\vec{r})$ is the basic variable in the many-electron system instead of the many-body wave function Ψ to discover the nature of the atom, molecule and solid.

In the second theorem, the Hohenberg-Kohn density functional $F_{HK}[r]$ is a universal functional of the ground-state density $r(\vec{r})$ for all the many-electron system. It is wholly independent of the system (any number of particles and any external potential).

But, the explicit form of $F_{HK}[r]$ lies in the black- box, the ground-state density has to be obtained via the Rayleigh-Ritz variational principal, where the Euler-Lagrange equation is:

$$\frac{d}{dr(\vec{r})}\left(E_{V_{ext}}[r] - m\left(\int d\vec{r}\, r(\vec{r}) - N\right)\right) = 0 \qquad (2.2.8)$$

2.2.2 The Kohn-Sham equations

A practical procedure to obtain the ground-state density $r(\vec{r})$ is implemented by Kohn and Sham[17] in 1965 based on Hohenberg-Kohn variational principle. The main objective of this formalism is to at most utilize the well-studied homogeneous gas of interacting electrons, which leads to a merit of introducing an auxiliary one-particle problem. The one-particle equation can be solved in the self-consistent process. As a result, all electron (core electrons and valence electrons) and full potential (no shape approximation) ab-initio calculations (only crystal structure and fundamental chemical information is used) within the KS density functional scheme allow complicated and realistic electron structure calculation for all crystalline solids.

Kohn and Sham straighten out the enigmatic universal density functional $F_{HK}[r]$ by proposing that the exact kinetic energy of the interacting electrons is $T[r]$; the kinetic energy of the non-interacting electrons is $T_0[r]$ (assumed that the non-interacting system carries out the same density as the real, interacting one); the difference between them is called the correlation energy V_c:

$$T[r] = T_0[r] + V_c[r]. \qquad (2.2.9)$$

The electron-electron interaction $V_{ee}[r]$ is treated as:

$$V_{ee}[r] = V_{es}[r] + V_x[r] \qquad (2.2.10)$$

$V_{es}[r]$ denotes for the electron-electron electrostatic interaction (or so-called Hartree term). Thus, the Hohenberg-Kohn density functional is rewritten as:

$$F_{HK}[r] = T_0[r] + V_{es}[r] + \underbrace{V_{xc}[r]}_{E_{xc}[r]} + V_{ext}[r]. \tag{2.2.11}$$

$E_{xc}[r]$ stands for the exchange-correlation energy (XC) functional, where the many-body character enters from the electron-electron interaction. The total functional $E_{V_{ext}}[r]$ of the interacting system is formally exact as the following:

$$E_{V_{ext}}[r] = T_0[r] + V_{es}[r] + E_{xc}[r] + V_{ext}[r]. \tag{2.2.12}$$

The unknown energy functional turns out to be $E_{xc}[r]$ (in practice, it needs to be approximately known). Eq. (2.2.12) enlightens us that the full assembly of interacting electrons could be accounted for the non-interacting (independent) electrons moving in an effective potential subject to the Coulomb interaction and the external potential (mean field theory). Accordingly, Kohn and Sham[17] bring in an auxiliary non-interacting one-particle orbital equation, namely, Kohn-Sham Schrödinger-like equation of the ith electron under central-field approximation (for example, only the electron-nuclei interaction is considered here in the V_{ext})

$$\left[-\frac{\hbar^2}{2m_e}\tilde{\nabla}_i^2 + \frac{e^2}{4\pi\varepsilon_0}\int \frac{r(\vec{r}')}{|\vec{r} - \vec{r}'|}d\vec{r}' + u_{xc} - \frac{e^2}{4\pi\varepsilon_0}\sum_j \frac{Z_j}{|\vec{R}_{j0} - \vec{r}|} \right] \psi_i = e_i \psi_i . \tag{2.2.13}$$

u_{xc} is defined as

$$u_{xc} = \frac{d(r(\vec{r})e_{xc})}{dr(\vec{r})}, \tag{2.2.14}$$

where, the universal function e_{xc} is the XC energy density, u_{xc} is the XC potential function at equilibrium state by taking one electron away from the system. The potentials and density are expanded in spherical harmonics (moreover, in lattice harmonics). The eq. (2.2.13) is solved in a self-consistent cycle exactly building upon the invertibility between the unique ground-state density $r(\vec{r})$ and the external potential V_{ext}. The symmetry broken state is initially picked from outside. The convergence criterion is imposed on the ground-state charge density $r(\vec{r})$ of the many-electron system, which is acquired by the single-electron orbital function f_i:

$$r(\vec{r}) = \sum_{i}^{occu.} f_i |f_i(\vec{x})|^2 . \qquad (2.2.15)$$

f_i is the occupation number of the i-th state. The total ground-state energy E of the many-electron system is:

$$E = \sum_i e_i - \underbrace{\frac{1}{2}\int\int \frac{r(\vec{r})r(\vec{r}\,')}{|\vec{r} - \vec{r}\,'|} d\vec{r}d\vec{r}\,'}_{\text{double counting term}} + E_{XC} - \int r(\vec{r})u_{XC}d\vec{r} . \qquad (2.2.16)$$

The KS density functional formalism is generalized in spin-polarized case[13]. The energy functional $E_{V_{ext}}[r^-, r^+]$ of the many-electron system is expressed according to spin densities $r_s(\vec{r})$ (s is the spin index, which denotes for spin-up or spin-down):

$$E_{V_{ext}}[r^-, r^+] = T_0[r^-, r^+] + V_{es}[r^-, r^+] + E_{xc}[r^-, r^+] + V_{ext}[r^-, r^+]. \qquad (2.2.17)$$

After applying the second HK theorem on the above equation and analogue to the case of the non-interacting electron gas moving in the effective potentials, the auxiliary one-particle orbital equation is given pertinent to spin densities $r_s(\vec{r})$ as

$$\left[-\frac{\hbar^2}{2m_e}\nabla_i^2+\frac{e^2}{4\pi\varepsilon_0}\int\frac{\left(r_-(\vec{r}')+r_+(\vec{r}')\right)}{|\vec{r}-\vec{r}'|}d\vec{r}'+u_{xc}^{s}-\frac{e^2}{4\pi\varepsilon_0}\sum_j\frac{Z_j}{|\vec{R}_{j0}-\vec{r}|}\right]f_i^{s}(\vec{r})=e_i f_i^{s}(\vec{r}),$$

(2.2.18)

where, the spin-dependent XC potential function u_{xc}^{s} is

$$u_{xc}^{s}=\frac{d\left(r(\vec{r})e_{xc}\right)}{dr_s(\vec{r})}. \tag{2.2.19}$$

And the ground-state spin density of the many-electron system could be found from spin-dependent single-electron orbital function f_i^{s}:

$$r_s(\vec{r})=\sum_i^{occu.} f_i^{s}\left|f_i^{s}(\vec{x})\right|^2 \text{ and } r(\vec{r})=r_-(\vec{r})+r_+(\vec{r}). \tag{2.2.20}$$

Moreover, the total ground-state energy of the many-electron system is obtained by

$$E=\sum_i e_i-\underbrace{\frac{1}{2}\iint\frac{r(\vec{r})r(\vec{r}')}{|\vec{r}-\vec{r}'|}d\vec{r}d\vec{r}'}_{\text{double counting term}}+E_{XC}-\int r_s(\vec{r})u_{XC}^{s}d\vec{r}, \tag{2.2.21}$$

here, Einstein summation convention is used for the repeated spin index.

It is worthy to note that, such a KS single-electron orbital f_i is not a real electron wave function; and, such KS single-electron energy e_i is not actual electron energy. They only attribute to the description of the many-body ground state. Though, an acceptable agreement with the total energy has been achieved under these solutions, the Kohn-Sham band gap of insulators and semiconductors are roughly 50% smaller than the actual band gap. For example, the LDA gap in LiF is 9eV, while, the actual gap is around 14eV.

2.2.3 The exchange-correlation functional

In the previous section 2.2.2, it has been mentioned that the exact expression of the XC energy functional $E_{XC}[r\text{-},r^{-}]$ is unknown. Thus, several forms of the XC energy functional $E_{XC}[r\text{-},r^{-}]$ have been chosen, such as local spin density approximation[46, 48, 18] (LSDA), generalized gradient approximation[25] (GGA), meta_GGA[26], etc. In all of them, the XC energy functional $E_{XC}[r\text{-},r^{-}]$ could be written as an integral of the energy per electron e_{XC} weighted a probability $r_s(\vec{r})$

$$E_{XC}[r\text{-},r^{-}] = \int d^3r\, r(\vec{r})\, e_{XC}\,. \qquad (2.2.22)$$

The best fit of the energy density function e_{XC} is searched by Perdew[18, 49, 50] via the highly accurate quantum Monte-Carlo simulations[19]. And, LSDA is the simplest one.

LSDA means that in the above integrand of the XC energy functional $E_{XC}[r\text{-},r^{-}]$, the function e_{XC} only explicitly contains the local spin density $r_s(\vec{r})$ or its power terms at the particular position $\vec{r}$, i.e., $e_{XC}(r\text{-}(\vec{r}), r^{-}(\vec{r}))$, without density-gradient $\nabla^n r_s(\vec{r})$ (n=1, 2, 3, ...) correction terms appearing in it.

However, the true XC interaction is non-local; the form of the XC energy functional $E_{XC}[r\text{-},r^{-}]$ should depend on the density not only at the position $\vec{r}$ but also at its neighborhood, which is missing in LSDA. To this extent, LSDA is a rather rude approximation for the XC energy functional $E_{XC}[r\text{-},r^{-}]$. But, it has been demonstrated that LSDA works very well for a large class of properties, even for relatively rapid density variations. How could it happen? To answer this question, the physics of the XC-functional is examined below.

When an actual electron is exposed to "feel" the XC potential, the effective Coulomb potential is written in the following

$$\bar{u}(\vec{r}) = \int d^3r' \frac{1}{4\pi\varepsilon_0} \frac{1}{|\vec{r} - \vec{r}'|} \bar{r}(\vec{r}, \vec{r}'), \tag{2.2.23}$$

where, $\bar{r}(\vec{r}, \vec{r}')$ is the effective density at the position $\vec{r}'$ given by one electron at the position $\vec{r}$. The effective Coulomb energy functional becomes

$$\begin{aligned} E_{Coul}[r] &= E_{es}[r] + E_{xc}[r] = \frac{1}{2} \int d^3r r(\vec{r}) \bar{u}(\vec{r}) \\ &= \frac{1}{2} \int\int d^3r d^3r' r(\vec{r}) \frac{1}{4\pi\varepsilon_0} \frac{1}{|\vec{r} - \vec{r}'|} \bar{r}(\vec{r}, \vec{r}') \end{aligned}. \tag{2.2.24}$$

Then, the XC energy functional $E_{xc}[r]$ could be found

$$E_{xc}[r] = E_{Coul}[r] - E_{es}[r] = \frac{1}{2} \int\int d^3r d^3r' r(\vec{r}) \frac{1}{4\pi\varepsilon_0} \frac{1}{|\vec{r} - \vec{r}'|} \left(\bar{r}(\vec{r}, \vec{r}') - r(\vec{r}') \right) \tag{2.2.25}$$

If the XC-hole density $r_{xc}(\vec{r}, \vec{r}')$ is defined as

$$r_{xc}(\vec{r}, \vec{r}') = \bar{r}(\vec{r}, \vec{r}') - r(\vec{r}'), \tag{2.2.26}$$

the XC energy functional $E_{xc}[r]$ could be rewritten as

$$E_{xc}[r] = \frac{1}{2} \int\int d^3r d^3r' r(\vec{r}) \frac{1}{4\pi\varepsilon_0} \frac{1}{|\vec{r} - \vec{r}'|} r_{xc}(\vec{r}, \vec{r}'). \tag{2.2.27}$$

Compared eq. (2.2.27) with eq. (2.2.24), the XC interaction should be interpreted as the Coulomb interaction between the electron and the XC-hole. The XC-hole density $r_{xc}(\vec{r}, \vec{r}')$, which knows the dynamic correlation, represents a hole where an electron digs about itself because of anti-symmetry (Pauli exclusive principle) and Coulomb correlations.

A practical way to obtain the XC-hole density $r_{xc}(\vec{r},\vec{r}')$ and the XC energy functional $E_{xc}[r]$ is to consider a fictitious system with Hamiltonian

$$\hat{H}(l) = \hat{T} + l\,\hat{H}_{e\text{-}e} + \int V(\vec{r},l)\hat{r}(\vec{r})d\vec{r} \qquad (2.2.28)$$

, where the real parameter l is coupling strength of the electron-electron interaction, which takes values in the range $0 \le l \le 1$. The local potential $V(\vec{r},l)$ is taken in such a way that the expectation value of the density in the ground-state of $H(l)$ has the prescribed value $r(\vec{r})$ independent of l. At l =1, $\hat{H}(1)$ is the true Hamiltonian of electron system with ground-state density $r(\vec{r})$. At l =0, $\hat{H}(0)$ is just the KS Hamiltonian, and $V(\vec{r},0)$ is the KS potential for the system. Making use of this system, the XC energy functional $E_{xc}[r]$ could be derived,

$$E_{xc}[r] = \frac{1}{2}\int_0^1 dl \iint d^3r d^3r' r(\vec{r})r(\vec{r}')\frac{1}{4\pi\varepsilon_0}\frac{1}{|\vec{r}-\vec{r}'|}\left[g_l(\vec{r},\vec{r}')-1\right] \qquad (2.2.29)$$

Comparing eq. (2.2.27) and eq. (2.2.29), the XC-hole density $r_{xc}(\vec{r},\vec{r}')$ could be exactly expressed by the coupling-constant formulae

$$r_{xc}(\vec{r},\vec{r}') = r(\vec{r}')\int_0^1 dl\,\left[g_l(\vec{r},\vec{r}')-1\right] \qquad (2.2.30)$$

where, $g_l(\vec{r},\vec{r}')$ is the pair correlation of inhomogeneous electron liquid system with the density[1] $r(\vec{r})$ and the coupling constant $l\,e^2$. The density $r(\vec{r}')$ is evaluated at l =1.

In LDA, the pair correlation $g_l(\vec{r},\vec{r}')$ becomes $g_l(\vec{r}-\vec{r}')$ for a homogeneous electron liquid of the density $r(\vec{r})$. The XC-hole density $r_{XC}^{LD}(\vec{r},\vec{r}')$ becomes

$$r_{XC}^{LD}(\vec{r},\vec{r}') = r(\vec{r})\int_0^1 dl\,\left[g_l^h(\vec{r}-\vec{r}')-1\right]. \qquad (2.2.31)$$

To compare LDA with the exact form, only exchange effects are considered (which let coupling strength l become trivial) and the multi-pole expansion is further introduced to the LDA XC-hole density $r_{XC}^{LD}(\vec{r},\vec{r}')$,

$$r_{XC}^{LD}(\vec{r},\vec{r}') = (4p)^{-\frac{1}{2}} \sum_{l,m} r_{l,m}^{xc}(\vec{r},u) Y_{l,m}(W), \tag{2.2.32}$$

where, $\vec{u} = \vec{r} - \vec{r}'$ denote for the difference of the two electron positions. If only the monopole (spherical average of the XC-hole) is kept, the XC energy functional $E_{XC}^{LD}[r]$ takes the form of

$$E_{XC}^{LD}[r] = (4p)^{\frac{1}{2}} \int d\vec{r}\, r(\vec{r}) \int_0^{\infty} du\, u r_{00}^{xc}(\vec{x},u). \tag{2.2.33}$$

In addition, the constraint of the charge-conservation sum rule is counted

$$\int d\vec{r}' r_{xc}(\vec{r},\vec{r}') = -1, \tag{2.2.34}$$

which corresponds to the removal of one electron charge. Gunnarsson and Lundqvist[48], whose calculations only include exchange effects, thoroughly explain the origin of the success of the LDA (see Fig. 2.3 and 2.4). Even the line shapes of the exact XC-hole density $r_{xc}(\vec{r},\vec{r}')$ looks dramatically different from that of the LDA XC-hole density $r_{XC}^{LD}(\vec{r},\vec{r}')$ in the Fig. 2.3 (the peak position of the exact XC-hole density $r_{xc}(\vec{r},\vec{r}')$ from eq. (2.2.30) closes to the proton, while peak position of the LDA XC-hole density $r_{XC}^{LD}(\vec{r},\vec{r}')$ from eq. (2.2.32) centered on the electron), the integrand of spherical average of the exchange hole $r_{00}^{xc}(\vec{x},u)$ times u for the XC energy functional $E_{XC}^{LD}[r]$ in eq. (2.2.33) is mostly consistent with the exact result from eq. (2.2.29) in Fig. 2.4. It is remarkable that the simple spherical average LDA XC-hole density $r_{XC}^{LD}(\vec{r},\vec{r}')$ basically describes the XC energy of the many-electron system.

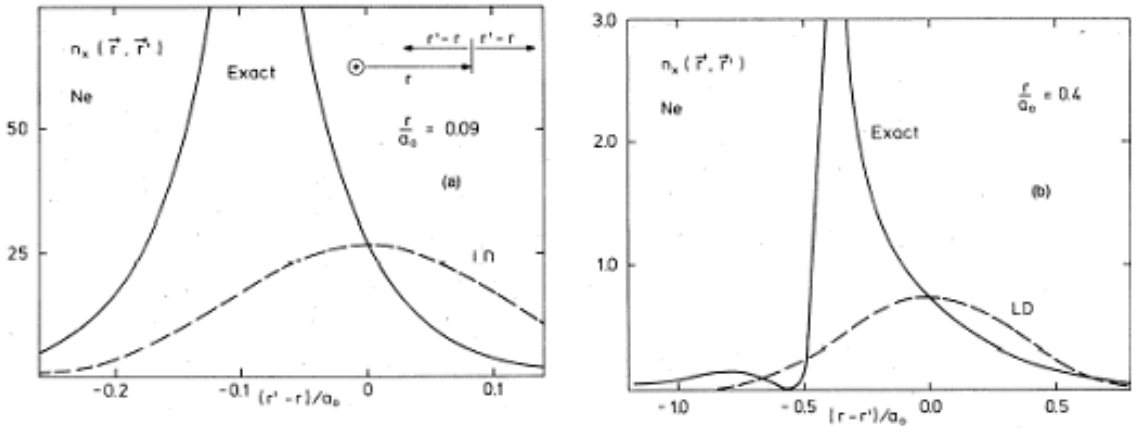

Figure 2.3 Exchange hole $r_x(\vec{r},\vec{r}')$ for a neon atom, where the exact results (continuous line) compare to that of the LDA (dashed line) [13]. The top panel is for r=0.09a_0 and the lower for r=0.4a_0.

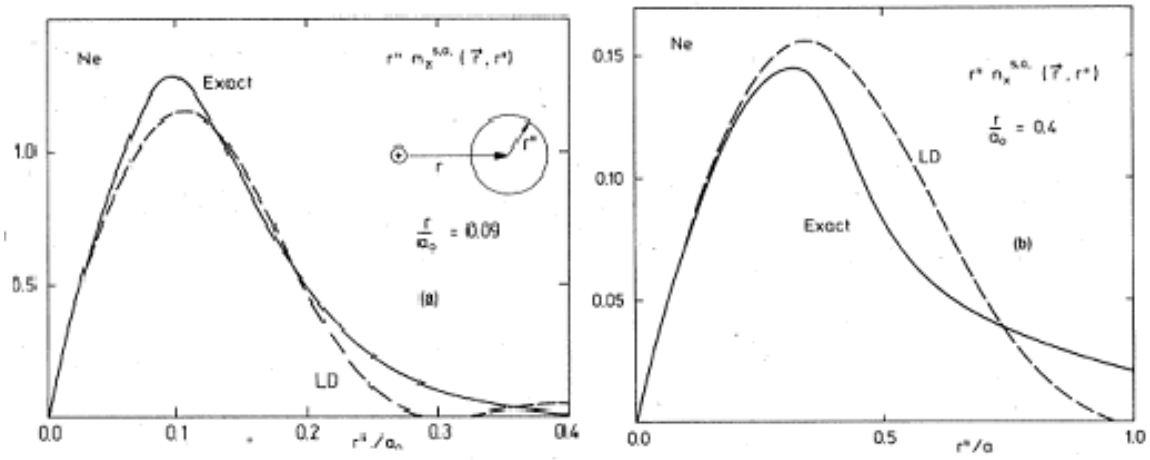

Figure. 2.4 Spherical average of the neon exchange hole times u; the exact results (continuous line) compared with the LDA results (dashed line).

Nevertheless, LSDA has its own shortcoming. It is valid only for slowly varying densities due to missing non-local correction terms in XC energy density function $e_{xc}(r(\vec{r}))$. Errors in exchange energy is typically within 10%; and the smaller correlation being twice large[51]. They cancel partially when sum up together. LSDA also often slightly underestimate equilibrium lattice constant by about 1%, which leads the equilibrium quantities who are sensitive to the lattice constant, say bulk moduli, phonon frequencies, magnetism, and ferroelectricity, to have a few percent errors compared with the measurements[52]. Surface energies are too low[52] either. In addition, LSDA gives ionization energies of atoms, dissociation energies of molecules and cohesive energies errors within 10~20%, while bond lengths agree well with merely error[20] in 2%. Especially, LSDA fails qualitatively on systems where strong localized charges interplay with Coulomb interactions which are key physics in Mott-Hubbard/charge-transfer (anti-ferromagnetic) insulators, like parent compounds of the high-Tc superconductors[29] etc.

The methods going beyond LSDA[46, 48, 18], are GGA[49] and meta-GGA[50], which include low-order density-gradient (like, $\tilde{\nabla}^n r_s(\vec{r})$ (n=1,2)) correction terms in XC energy density function (say, $e_{xc}(r(\vec{r}), \tilde{\nabla} r(\vec{r}))$ or $e_{xc}(r(\vec{r}), \tilde{\nabla} r(\vec{r}), \tilde{\nabla}^2 r(\vec{r}), t)$).

For strong correlated system, a screening parameter "U" which denotes for inhomogeneous "on-site" Coulomb interaction is added on the local orbitals implementing LSDA[54-59].

2.2.4 System with variable particle number, derivative discontinuities and the band gap problem

For realistic applications in condensed matter physics, we must consider systems with very large number of particles $(N >> 1)$. N can be treated as a continuous variable,

tuned by the chemical potential μ. Analogous to the "grand-canonical" ensemble, the operator of interest is[31]:

$$\hat{K} = \hat{H} - m\hat{N} \tag{2.2.35}$$

where $\hat{N}$ is the number of particle operator. As $\left[\hat{K}, \hat{N}\right] = 0$, the eigenstates of K are classified according to the number of particle N. For example, the occupied states and empty states are solutions of the N-electron potential of the KS system, other than the solutions to the (N-1)- and (N+1)-electron potentials. Number of particles N and chemical potential μ are conjugate variables similar to effective single-particle potential $v(\vec{r})$ and density $n_N(\vec{r})$ ($\int n_N(\vec{r})\,d\vec{r} = 1$). However, the actual case is that N is a discrete variable; chemical potential μ is a continuous one. To describe the system with variable particle number, we define the "addition energy" as[31]:

$$m_+(N) = E(N+1) - E(N), \tag{2.2.36}$$

and the "electron affinity (detach an electron from a negative singly-charged system) energy" $A = -m_+(N)$, where $E(N)$ is the energy of the ground-state of $\hat{H}$ (not $\hat{K}$). Likewise, $m_+(N-1)$ is the "first ionization (take an electron from a neutral system) potential I". Throughout the range $m_+(N-1) < \mu < m_+(N)$, the N–electron system will be sustained. The number of particle N does not uniquely determine the chemical potential μ. There is clear discontinuous behavior of dN/dm.

In the one-particle picture, similar to eq. (2.2.7) the total energy can be written like:

$$E_{V-m}[n] = F[n] + \int d\vec{r}\, n(\vec{r})\left[v_{ext}(\vec{r}) - m\right]. \tag{2.2.37}$$

If $F[n]$ were differentiable at all densities and in all "direction" in the space of densities that do not yield integer particle numbers, the stationary condition for energy can be written as:

$$\frac{dF[n]}{dn(\vec{r})} = m - v_{ext}(\vec{r}). \tag{2.2.38}$$

We now try to calculate the discontinuity of the derivative. A fictitious small density fluctuation dn ($\int \delta n \; \vec{r} \; d\vec{r} << 1$) is added (or subtracted) to the density $n_N(\vec{r})$, namely, $n_N^{\pm}(\vec{r}) = n_N(\vec{r}) \pm dn(\vec{r})$. According to the eq. (2.2.38), the derivative discontinuity is[31]

$$\left.\frac{dF[n]}{dn(\vec{r})}\right|_{n_N^+(\vec{r})} - \left.\frac{dF[n]}{dn(\vec{r})}\right|_{n_N^-(\vec{r})} = (m_+(N) - v_{ext}(\vec{r})) - (m_+(N-1) - v_{ext}(\vec{r})) = m_+(N) - m_+(N-1) \equiv E_g \tag{2.2.39}$$

where E_g is the gap in the one-particle excitation spectrum. For example, in the insulating, antiferromagnetic ground-state of parent (undoped) materials, similar reasoning leads to a discontinuity in the kinetic energy functional $E_{g,KS}$

$$\left.\frac{dT_s[n]}{dn(\vec{r})}\right|_{n_N^+(\vec{r})} - \left.\frac{dT_s[n]}{dn(\vec{r})}\right|_{n_N^-(\vec{r})} = E_{g,KS}. \tag{2.2.40}$$

A brief look at equation (2.2.11) convinces us that, the XC functional must present a similar discontinuity

$$V_{xc} = \left.\frac{dE_{xc}[n]}{dn(\vec{r})}\right|_{n_N^+(\vec{r})} - \left.\frac{dE_{xc}[n]}{dn(\vec{r})}\right|_{n_N^-(\vec{r})} = E_g - E_{g,KS}. \tag{2.2.41}$$

As all XC functional expression we use do not have a discontinuity in their derivative, leads to serious underestimation in the gap of solids. Solving the problem for localized *d*- and *f*-electrons embedded into the reservoir of other (delocalized) electrons, a constant *U*-*J*=*I*+*A* is added to the localized levels in the light of

$$2\ d^{n} \rightarrow d^{n+1} + d^{n-1} \tag{2.2.42}$$

where, J represents exchange interaction.

2.3 Time-Dependent Density functional Theory (TDDFT)

With the acceptable solution of the ground state available, the many-body system exposed to a time-dependent external potential was studied. The first efforts for this problem towards KS scheme were taken by Peuckert[60] (1978) and by Zangwill and Soven[61] (1980). A meaningful progress towards a rigorous foundation of TDDFT was made by Deb and Ghosh[62] (1982 and 1983) and by Bartolotti[63] (1981, 1982, 1984 and 1987). Significantly, the exact and general formalism of TDDFT is completed by Runge and Gross[23].

The essentials of Runge and Gross theorem is: 1) in the non-degenerate, interacting, many-electron system evolving in the presence of a time-dependent external potential, there exists a one-to-one correspondence between the time-dependent densities $r(\vec{r},t)$ and the time-dependent external potentials $V(\vec{r},t)$; or, the time-dependent densities $r(\vec{r},t)$ and $r'(\vec{r},t)$ from a same initial state Ψ_0 under the influence of two external potentials $V(\vec{r},t)$ and $V'(\vec{r},t)$ are always different if the potentials differ by more than a purely time-dependent function $V(\vec{r},t) \neq V'(\vec{r},t) + c(t)$. Subsequently, the expectation value of any quantum mechanical operator $\hat{O}(t)$ could be calculated from the knowledge of the time-dependent many-body density as in the following

$$O[r](t) = \left\langle \Psi[r](t) \middle| \hat{O}(t) \middle| \Psi[r](t) \right\rangle, \tag{2.3.1}$$

where, the many-body wave function $\Phi(t)$ is a functional of the time-dependent density

$$\Phi(t) = e^{-i\alpha(t)} \Psi[r](t) \tag{2.3.2}$$

with a pure time-dependent phase $a(t)$ and $\dot{a}(t) = c(t)$. The ambiguity in the phase cancels out in eq. (2.3.1). 2) There exists a stationary point of the quantum mechanical action integral[19] in interacting time-dependent many-electron system

$$A = \int_{t_0}^{t_1} dt \left\langle \Psi[\rho](t) \left| i\frac{\partial}{\partial t} - \hat{H}(t) \right| \Psi[\rho](t) \right\rangle. \quad (2.3.3)$$

At the stationary point, the variational equation is founded

$$\frac{dA[n]}{d\rho(\vec{r},t)} = 0, \quad (2.3.4)$$

where, the functional $A[n]$ can be written as

$$A[n] = \int_{t_0}^{t_1} dt \left\langle \Psi[\rho](t) \left| i\frac{\partial}{\partial t} - \hat{T} - \hat{U} \right| \Psi[\rho](t) \right\rangle - \int_{t_0}^{t_1} dt \int d\vec{r}\, n(\vec{r},t) V(\vec{r},t). \quad (2.3.5)$$

$\hat{T}$ and $\hat{U}$ respectively indicate the kinetic energy and Coulomb interaction in the interacting time-dependent many-electron system.

For the time-dependent density of the interacting system, when V-representability in the corresponding non-interacting system is assumed, a derivative from Runge-Gross theorem could be that a non-interacting system at a given density $\rho(\vec{r},t)$ (the density of non-interacting electrons moving in the effective potential $V_s[\rho](\vec{r},t)$ is identical with the density of Coulomb- interacting ones moving in the external potential $V(\vec{r},t)$) uniquely determines an effective potential $V_s[\rho](\vec{r},t)$; which, in return, ensures a V-representable time-dependent density[64]. By analogy to static KS theory (computationally simple), a fictitious system of non-interacting electrons moving in the effective potential $V_s[\rho](\vec{r},t)$ is defined. The auxiliary time-dependent single-electron (non-interacting) Schrödinger-like orbital equation is

$$i\frac{\partial}{\partial t}\varphi_i(\vec{r},t)=\left(-\frac{\hbar^2\nabla^2}{2m}+u_s[n](\vec{r},t)\right)\varphi_i(\vec{r},t), \tag{2.3.6}$$

with the initial condition

$$\varphi_i(t_0)=\varphi_{i0} \tag{2.3.7}$$

The time-dependent KS potential (or, one-electron effective potential) $u_s[n](\vec{r},t)$ is

$$u_s[n](\vec{r},t)=u(\vec{r},t)+\frac{e^2}{4\pi\varepsilon_0}\int\frac{n(\vec{r}',t)}{|\vec{r}-\vec{r}'|}d\vec{r}'+u_{xc}[n](\vec{r},t), \tag{2.3.8}$$

where, the time-dependent XC potential $u_{xc}[n](\vec{r},t)$ needs to be approximately known. The "adiabatic" local density approximation (ALDA, namely, no time or frequency dependent) is the simplest and possible approximation for $u_{xc}[n](\vec{r},t)$, namely, the ground-state potential of the uniform gas with the instantaneous and local density is used,

$$u_{xc}^{ALDA}[n](\vec{r},t)=\left.\frac{d}{dr}\left(r\varepsilon_{xc}^{\hom}(r)\right)\right|_{r=r(\vec{r},t)}. \tag{2.3.9}$$

$\varepsilon_{xc}^{\hom}(r)$ is the XC energy per electron of static homogenous electron gas. An improved approximation on $u_{xc}[n](\vec{r},t)$ with correct asymptotic $-1/r$ behavior is time-dependent optimized effective potential[65].

The time-dependent density $n(\vec{r},t)$ of the interacting many-electron system is acquired by the non-interacting single-electron orbital function $\varphi_i(\vec{r},t)$:

$$n(\vec{r},t)=\sum_i^{occup} f_i|\varphi_i(\vec{r},t)|^2. \tag{2.3.10}$$

Basically, TDDFT mean field approximation takes into account more correlation effect than DFT mean field approximation, which includes more fluctuations. It has been

used for excited states in the presence of the external perturbation, such as weak probe of molecules and solids, matter interacting with the strong laser pulse, and time-dependent quantum transport.

2.4 Dynamical response within Time-Dependent Density Functional Theory

2.4.1 Response functions and time-dependent mean-field theories in many-body picture

This section is dedicated to a description of linear response in the context of time dependent mean field theories. The difference from the previous sections 2.1.2 is that the exact eigenfunctions of many-body H_0 are not known. The starting point is again the Hamiltonian of eq. (2.1.1). The Hamiltonian will be approximated using mean-field techniques.

$$\hat{H}_0^{MF} = \hat{H}_1 + \hat{V}_0^{MF} \tag{2.4.1}$$

where $\hat{H}_1$ is the non-interacting part and $\hat{V}_0^{MF}$ is one-particle the mean-field potential for the unperturbed system. Hartree-Fock potentials and exchange-correlation potential used in various DFT calculations are examples of mean-field approximated potentials, which is discussed in section 2.2.

Because the mean-field Hamiltonian of (2.4.1) is a one-particle operator, we will use single-particle basis set. According to (2.1.41) a static KS response function would be[31]

$$\chi^{S}_{\hat{P}\hat{O}}\ \omega\ = \sum_{\alpha\beta} \frac{f_\alpha - f_\beta}{\hbar\omega + \varepsilon_\alpha - \varepsilon_\beta + i\hbar\eta} \hat{P}_{\alpha\beta}\hat{O}_{\beta\alpha}\,, \tag{2.4.2}$$

where α and β are the one-particle eigenstates of the Hamiltonian $\hat{H}_0^{MF}$. In the presence of crystal circumstances, the KS response is expressed similar to eq. (2.1.60).

It is worth mentioning that this is not the mean-field response function of the physical system. When a time-dependent external perturbation is applied the mean-field potential becomes time-dependent. The mean-field potential is varies form its ground-state value as the WFs change.

The mean-field potential can be expressed in terms of creation-annihilation operators as

$$\hat{V}^{MF} = \sum_{\alpha\beta} V_{\alpha\beta}^{MF} \hat{a}_\alpha^\dagger \hat{a}_\beta , \tag{2.4.3}$$

where the matrix elements have self-consistent expressions in terms of density matrix $\rho_{\gamma\delta} = \left\langle \hat{a}_\gamma^\dagger \hat{a}_\delta \right\rangle$

$$V_{\alpha\beta}^{MF} = V_{\alpha\beta}^{MF}\left[\rho_{\gamma\delta}\right]. \tag{2.4.4}$$

In the presence of time dependent perturbation, it acquires a small time-dependent component such as

$$\hat{V}^{MF}(t) = \hat{V}_0^{MF} + \hat{V}_1^{MF}(t) , \tag{2.4.5}$$

where the time-dependent component can be written in second quantization form

$$\hat{V}_1^{MF}(t) = \sum_{\alpha\beta} V_{1,\alpha\beta}^{MF}(t)\, \hat{a}_\alpha^\dagger \hat{a}_\beta , \tag{2.4.6}$$

in terms of chain rule, the first order time dependent matrix element being

$$V_{1,\alpha\beta}^{MF}\ t\ =\sum_{\gamma\delta}\left(\frac{\delta V_{\alpha\beta}^{MF}\left[\rho_{\gamma\delta}\right]}{\delta\rho_{\gamma\delta}}\right)_0\rho_{1,\gamma\delta}\ t\ , \tag{2.4.7}$$

with the derivative is calculated of mean-field potential in respect to density matrix evaluate at ground-sate. The density matrix is defined as $\rho_{\gamma\delta}\ t\ =a_\gamma^\dagger a_\delta$. The first order variation of density $\rho_{1,\gamma\delta}\ t$ is calculated self-consistently from an equation similar to (2.1.21)

$$\rho_{1,\gamma\delta}\ \omega\ =\chi_{\rho_{\gamma\delta}\hat{O}}^{MF}h\ \omega\ . \tag{2.4.8}$$

The "fictitious system" locked onto the ground state responds now to two external perturbations $h\ t\ \hat{O}$ and $\sum_{\alpha\beta}V_{1,\alpha\beta}^{MF}\ t\ \rho_{\alpha\beta}$. Using eqs. (2.1.21) and (2.4.8), the response of the observable $\langle\mathcal{P}\rangle_1$ to O can be expressed as

$$\begin{aligned}\langle\mathcal{P}\rangle_1\ \omega\ &=\chi_{\hat{\mathcal{P}}\hat{O}}^{MF}\ \omega\ h\ \omega\ =\chi_{\hat{\mathcal{P}}\hat{O}}^{S}\ \omega\ h\ \omega\ +\sum_{\alpha\beta}\chi_{\hat{\mathcal{P}}\rho_{\alpha\beta}}^{S}\ \omega\ V_{1,\gamma\delta}^{MF}\ \omega\\ &=\chi_{\hat{\mathcal{P}}\hat{O}}^{S}\ \omega\ h\ \omega\ +\sum_{\alpha\beta}\chi_{\hat{\mathcal{P}}\rho_{\alpha\beta}}^{S}\ \omega\ \sum_{\gamma\delta}\left(\frac{\delta V_{\alpha\beta}^{MF}\left[\rho_{\gamma\delta}\right]}{\delta\rho_{\gamma\delta}}\right)_0\rho_{1,\gamma\delta}\ \omega\\ &=\chi_{\hat{\mathcal{P}}\hat{O}}^{S}\ \omega\ h\ \omega\ +\sum_{\alpha\beta\gamma\delta}\chi_{\hat{\mathcal{P}}\rho_{\alpha\beta}}^{S}\ \omega\ \left(\frac{\delta V_{\alpha\beta}^{MF}\left[\rho_{\gamma\delta}\right]}{\delta\rho_{\gamma\delta}}\right)_0\chi_{\rho_{\gamma\delta}\hat{O}}^{MF}h\ \omega\end{aligned} \tag{2.4.9}$$

Choosing $\hat{\mathcal{P}}=\rho_{\alpha\beta}$, this leads to a closed set of equations for the mean-field response function[31]

$$\chi_{\rho_{\alpha\beta}\hat{O}}^{MF}\ \omega\ =\chi_{\rho_{\alpha\beta}\hat{O}}^{S}\ \omega\ +\sum_{\alpha'\beta'\gamma\delta}\chi_{\rho_{\alpha\beta}\rho_{\alpha'\beta'}}^{S}\ \omega\ \left(\frac{\delta V_{\alpha'\beta'}^{MF}\left[\rho_{\gamma\delta}\right]}{\delta\rho_{\gamma\delta}}\right)_0\chi_{\rho_{\gamma\delta}\hat{O}}^{MF} \tag{2.4.10}$$

Defining the interaction kernel as

$$K_{\alpha\beta,\gamma\delta} = \left(\frac{\delta V_{\alpha\beta}^{MF}\left[\rho_{\gamma\delta}\right]}{\delta\rho_{\gamma\delta}} \right)_0 \tag{2.4.11}$$

the eq (2.4.10) can put in closed form

$$\chi_{\rho_{\alpha\beta}\hat{O}}^{MF}\ \omega\ = \chi_{\rho_{\alpha\beta}\hat{O}}^{S}\ \omega\ + \sum_{\alpha'\beta'\gamma\delta} \chi_{\rho_{\alpha\beta}\rho_{\alpha'\beta'}}^{S}\ \omega\ K_{\alpha'\beta',\gamma\delta}\chi_{\rho_{\gamma\delta}\hat{O}}^{MF}\ \omega\ , \tag{2.4.12}$$

respectively in a matrix form

$$\hat{\chi}_{\rho\hat{O}}^{MF}\ \omega\ = \chi_{\rho\hat{O}}^{S}\ \omega\ + \hat{\chi}^{S}\ \omega\ \hat{K}\hat{\chi}_{\rho\hat{O}}^{MF}\ \omega\ , \tag{2.4.13}$$

This allows a formal solution of the mean-field response function[31]

$$\hat{\chi}_{\rho\hat{O}}^{MF}\ \omega\ =\ \hat{I} - \hat{\chi}^{S}\ \omega\ \hat{K}^{\ -1}\ \chi_{\rho\hat{O}}^{f}\ \omega\ , \tag{2.4.14}$$

where

$$\begin{aligned} \hat{\chi}_{\rho\hat{O}\ \ \alpha\beta}^{S}\ \omega\ &\equiv \chi_{\rho_{\alpha\beta}\hat{O}}^{S}\ \omega \\ \hat{\chi}_{\rho\hat{O}\ \ \alpha\beta}^{MF}\ \omega\ &\equiv \chi_{\rho_{\alpha\beta}\hat{O}}^{MF}\ \omega \end{aligned} . \tag{2.4.15}$$

2.4.2 Response function in TDDFT

We consider an electronic system, initially in the ground state, perturbed by a periodic potential $V_1\ \vec{r},t$. As a result, the density will have a time dependent component, and this induces a time-dependence in both Hartree and exchange–correlation potential: These quantities can be written as[31]:

$$
\begin{aligned}
V_1(\vec{r},t) &= V_1(\vec{r},\omega)\, e^{-i\omega t} + V_1^*(\vec{r},\omega)\, e^{i\omega t} \\
n(\vec{r},t) &= n_0(\vec{r}) + n_1(\vec{r},\omega)\, e^{-i\omega t} + n_1^*(\vec{r},\omega)\, e^{i\omega t} \\
V_H(\vec{r},t) &= V_{H,0}(\vec{r}) + V_{H,1}(\vec{r},\omega)\, e^{-i\omega t} + V_{H,1}^*(\vec{r},\omega)\, e^{i\omega t} \\
V_{XC}(\vec{r},t) &= V_{XC,0}(\vec{r}) + V_{XC,1}(\vec{r},\omega)\, e^{-i\omega t} + V_{XC,1}^*(\vec{r},\omega)\, e^{i\omega t}
\end{aligned}
\tag{2.4.16}
$$

The response can be written as a solution of an equation similar to the one in (2.4.12). The interaction potential can be written as[24,31]

$$
V_1[n] = V_{1,H}[n] + V_{1,XC}[n] = \int d^3r' \frac{e^2 n_1(r',\omega)}{|\vec{r}-\vec{r}'|} + \int d^3r' n_1(r',\omega)\, f_{XC}(\vec{r},\vec{r}',\omega) \tag{2.4.17}
$$

The interaction kernel can be expressed

$$
K = \frac{\delta V[n]}{\delta n} = \frac{e^2}{|\vec{r}-\vec{r}'|} + f_{XC}(\vec{r},\vec{r}',\omega) \tag{2.4.18}
$$

The density-response equation is now:

$$
\begin{aligned}
\chi_{nn}^{TD}(r,r',\omega) &= \chi_{nn}^{s}(r,r',\omega) + \\
&+ \int d^3x \int d^3x' \chi_{nn}^{s}(\vec{r},\vec{x},\omega) \left[\frac{e^2}{|\vec{x}-\vec{x}'|} + f_{XC}(\vec{x},\vec{x}',\omega) \right] \chi_{nn}^{TD}(\vec{x}',\vec{r}',\omega)
\end{aligned}
\tag{2.4.19}
$$

similar to mean-field response (2.4.10) (written in $|\vec{r}\rangle$ eigenfunctions).

If using k-space basis set, in a periodic potential, one can write

$$
\chi_{\vec{G},\vec{G}'}^{TD}(\vec{k},\omega) = \chi_{\vec{G},\vec{G}'}^{s}(\vec{k},\omega) + \sum_{\vec{G}_1,\vec{G}_2} \chi_{\vec{G},\vec{G}_1}^{s}(\vec{k},\omega)\, v_{\vec{G}_1}(\vec{k})\, \delta_{\vec{G}_1,\vec{G}_2} + f_{\vec{G}_1,\vec{G}_2}^{XC}(n_0)(k,\omega)\, \chi_{\vec{G}_2,\vec{G}'}^{TD}(k,\omega)
\tag{2.4.20}
$$

2.4.3 Density-density response function and the dielectric constant

For an unperturbed many-electron system, in terms of the "irreducible" polarization (density-response) function $\tilde{\chi}$, we can write the density deviation as

$$n_1(\vec{r},w) = \int d\vec{r}' \chi_{nn}(\vec{r},\vec{r}',w) V_{sc}(\vec{r}',w) \tag{2.4.21}$$

and the screened potential as

$$V_{sc}(\vec{r},w) = V_{ext}(\vec{r},w) + \int d\vec{r}' \frac{e^2}{|\vec{r}-\vec{r}'|} \int d\vec{r}'' \chi_{nn}(\vec{r}',\vec{r}'',w) V_{sc}(\vec{r}'',w). \tag{2.4.22}$$

Immediately, we obtain the exact ("fully dressed") dielectric constant as following

$$\varepsilon(\vec{r},\vec{r}',w) = \delta(\vec{r}-\vec{r}') - \int d\vec{r}'' \frac{e^2}{|\vec{r}-\vec{r}''|} \chi_{nn}(\vec{r}'',\vec{r}',w). \tag{2.4.23}$$

Now, we consider the electron liquid perturbed by an external potential $V_{ext}(\vec{r},t)$. The electrons will move under its influence and the electron density will deviate from its equilibrium value $n_0(\vec{r})$ creating an induced potential $V_1(\vec{r},t)$. A test charge will see the sum of these fields as $V_{sc}(\vec{r},t) = V_{ext}(\vec{r},t) + V_1(\vec{r},t)$ referred usually as screened potential. The induced potential can be written as:

$$\begin{aligned} V_1(\vec{r},t) &= \int d\vec{r}' \frac{e^2 n_1(\vec{r}',t)}{|\vec{r}-\vec{r}'|} = \int_{-\infty}^{\infty} dw e^{iwt} \int d\vec{r}' \frac{e^2 n_1(\vec{r}',w)}{|\vec{r}-\vec{r}'|} \\ &= \frac{e^2}{2\pi} \int_{-\infty}^{\infty} dw e^{-iwt} \int d\vec{r}' \frac{1}{|\vec{r}-\vec{r}'|} \int d\vec{r}'' c_{nn}(\vec{r}',\vec{r}'',w) V_1(\vec{r}'',w) \end{aligned} \tag{2.4.24}$$

where $n_1(\vec{r},t)$ is the change in electron density and $c_{nn}(\vec{r}',\vec{r}'',w)$ is the density-density response function.

The frequency dependent screened potential is given by

$$V_{sc}(\vec{r},w) = V_{ext}(\vec{r},w) + \int d\vec{r}' \frac{e^2}{|\vec{r} - \vec{r}'|} \int d\vec{r}'' c_{nn}(\vec{r}',\vec{r}'',w) V_{ext}(\vec{r}'',w)$$
$$= \int d\vec{r}' V_{ext}(\vec{r}',w) \left[\delta(\vec{r} - \vec{r}') + \int d\vec{r}'' \frac{e^2}{|\vec{r} - \vec{r}''|} c_{nn}(\vec{r}'',\vec{r}',w) \right] \tag{2.4.25}$$

Clearly, the relation of the density-density response function and the dielectric function is[31]

$$\varepsilon^{-1}(\vec{r},\vec{r}',w) = \delta(\vec{r} - \vec{r}') + \int d\vec{r}'' \frac{e^2}{|\vec{r} - \vec{r}''|} c_{nn}(\vec{r}'',\vec{r}',w) \tag{2.4.26}$$

If the "proper" response $\tilde{\chi}$ is replaced by KS response χ^S and the electron liquid experiences a periodic potential, by the use of double Fourier transformation, eq. (2.4.23) and (2.4.26) turns out to be

$$\varepsilon_{\vec{G},\vec{G}'}(\vec{q},w) = \delta_{G,G'} - \sum_{\vec{G}''} v_{\vec{G},\vec{G}''}(\vec{q}) \chi^S_{\vec{G}'',\vec{G}'}(\vec{q},w) \tag{2.4.27}$$

and

$$\left[\varepsilon^{-1}(\vec{q},w)\right]_{\vec{G},\vec{G}'} = \delta_{G,G'} + \sum_{\vec{G}''} v_{\vec{G},\vec{G}''}(\vec{q}) c_{\vec{G}'',\vec{G}'}(\vec{q},w), \tag{2.4.28}$$

where,

$$v_{\vec{G},\vec{G}'}(\vec{q}) = \frac{4\pi e^2}{|\vec{q} + \vec{G}|} \delta_{\vec{G},\vec{G}'}.$$

For the case of homogenous electron liquid, where the response function $c_{nn}(\vec{r},\vec{r}\,',w)$ depends only on the distance $|\vec{r}-\vec{r}\,'|$, a Fourier transformation with respect to $\vec{r}-\vec{r}\,'$ gives

$$V_{sc}(\vec{q},w)=\frac{V_{ext}(\vec{q},w)}{e(\vec{q},w)} \tag{2.4.29}$$

and when using the exact density response

$$e^{-1}(\vec{q},w)=1+v_q c_{nn}(\vec{q},w); \tag{2.4.30}$$

respectively, for the "proper" one,

$$e(\vec{q},w)=1-v_q \chi_{nn}(\vec{q},w). \tag{2.4.31}$$

In RPA, defined by the approximation $\tilde{\chi} \approx \chi^0$ (i.e., the irreducible polarization function is replaced by Lindhard function", or density response for non-interaction electrons moving in an appropriate effective potential), eq. (2.4.31) becomes

$$e(\vec{q},w)=1-v_q c^0(\vec{q},w) \tag{2.4.32}$$

Compared eq. (2.4.28) with eq. (2.4.30), an effective dielectric function is introduced to mimics (formally) the one appropriate for a free-electron gas. It defines the loss function of a complex material as following

$$\frac{1}{e_{eff}(\vec{q},w)}=\left[e^{-1}(\vec{q}-\vec{G}_q,w)\right]_{\vec{G}_q,\vec{G}_q}=e_{\vec{G}_q,\vec{G}_q}(\vec{q}-\vec{G}_q,w)- \sum_{\vec{G},\vec{G}'\neq\vec{G}_q} e_{\vec{G}_q,\vec{G}}(\vec{q}-\vec{G}_q,w)\left(e(\vec{q}-\vec{G}_q,w)\right)^{-1}_{\vec{G},\vec{G}'} e_{\vec{G}',\vec{G}_q}(\vec{q}-\vec{G}_q,w), \tag{2.4.33}$$

where $\vec{G}_{\vec{q}}$ is the reciprocal lattice vector that brings the vector $\vec{q}$ into the Brillouin zone. Substituting eq. (2.4.33) into eq. (2.4.28), we have

$$\mathrm{Im}\frac{-1}{e_{eff}(\vec{q},w)} = -\frac{4pe^2}{\left|\vec{q}+\vec{G}_{\vec{q}}\right|^2}\mathrm{Im}\,c_{\vec{G}_{\vec{q}},\vec{G}_{\vec{q}}}\left(\vec{q}-\vec{G}_{\vec{q}},w\right) = -\frac{4pe^2}{\left|\vec{q}\right|^2}\mathrm{Im}\,c_{\vec{G}_{\vec{q}},\vec{G}_{\vec{q}}}\left(\vec{q}-\vec{G}_{\vec{q}},w\right) \quad (2.4.34)$$

2.5 Dynamical structure factor

The dynamical structure factor $S(q,\omega)$ can be determined experimentally by measuring the double differential cross section $\frac{d^2\sigma}{d\Omega d\omega}$. For a process in which hard X-rays undergo a single scattering event, with transfer of energy $\hbar\omega$ and momentum $\hbar\vec{q}$, it is given by

$$\frac{d^2\sigma}{d\Omega d\omega} = \left(\frac{d\sigma}{d\Omega}\right)_0 S\left(\vec{q},\omega\right) \quad (2.5.1)$$

where $d\sigma/d\Omega\,_0 = r_0^2\left|\vec{e}_i\cdot\vec{e}_f\right|^2\omega_f/\omega_i \approx 10^{-25}\mathrm{cm}^2$ being the Thomson cross section, r_0 is the Bohr radius ($r_0 = e^2/mc^2$) and the remaining variables refer to the polarization vector and frequency of the incident ('i') and scattered ('f') photons[42].

Making use of the fluctuation-dissipation theorem at T=0 (sec. 2.1), the dynamical structure factor $S\left(\vec{q},\omega\right)$ can be expressed as

$$S\left(\vec{q},\omega\right) = -2\hbar V\,\mathrm{Im}\,\chi_{\vec{G},\vec{G}}\left(\vec{q}-\vec{G}\right) . \quad (2.5.2)$$

Because $S\left(\vec{q},\omega\right)$ is an extensive quantity (depend on the amount of material in the system), when the thermodynamic limit is realized for sufficiently large Born-Von-Karman volumes, any residual dependence of $S\left(\vec{q},\omega\right)$ on V is gone. We define a dynamical structure factor $S\left(\vec{q},\omega\right)$ per unit volume as

$$S_V\left(\vec{q},\omega\right) = -2\hbar\,\mathrm{Im}\,\chi_{\vec{G},\vec{G}}\left(\vec{q}-\vec{G},\omega\right) , \quad (2.5.3)$$

thereby defining a scattering cross section per unit volume.

$$\frac{1}{V}\frac{d^2\sigma}{d\Omega d\omega} = \left(\frac{d\sigma}{d\Omega}\right)_0 S\ \vec{q},\omega\ . \qquad (2.5.4)$$

CHAPTER 3

DYNAMICAL RESPONSE STUDIED IN WIDE-GAP INSULATOR

Most ab-intio studies have focused on ground-state properties with the use of DFT. Here, we investigate the suitability of Time-Dependent DFT for the study of the excitations in wide-gap insulator LiF.

The typical alkali halide compound LiF has simple atomic constituents with a NaCl structure. The electronic configuration of the element Li, one ingredient of LiF, is $1s^2 2s^1$ where $2s^1$ is a valence electron; whilst, the electronic configuration of the element F, the other ingredient of LiF, is $1s^2 2s^2 2p^5$ where $2p^5$ are five valence electrons. When the two elements combine into one compound, Li $2s^1$ electron is almost completely transferred to the F $2p^5$ subshell (Fig. 3.1) due to the extremely weak electronegativity of Li and the extremely strong electronegativity of F. After the chemical reaction takes place, they hold together through a large electrostatic force (the binding energy per molecule is around 5eV[66]), thus forming an ionic bonding. The electronic configurations of the Lithium ion (Li^+) and Fluorine ion (F^-) become $1s^2$ and $1s^2 2s^2 2p^6$ respectively. It can be seen in our band character plots (Figure 3.6) and density of state (DOS) plots (Figure 3.7). In reality, the character of the strong ionic-bonding is visualized through LAPW orbital density plots (Fig. 3.2) for the occupied states and empty states near the gap. In contrast to ionic bonding, covalent bonding is characterized by the sharing of electrons between atoms (Fig. 3.3).

When many cations and anions are attracted each other by intermolecular forces, they are arranged in an alternating fashion as demonstrated in the schematic (Fig. 3.4).

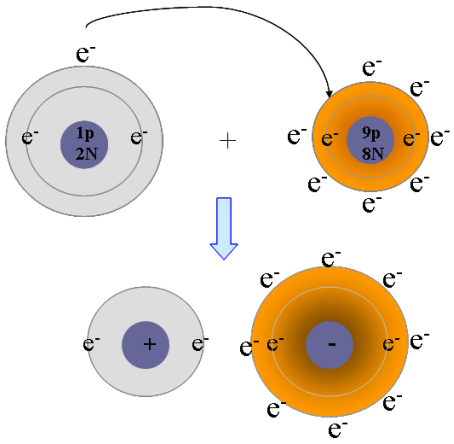

Figure 3.1: During the reaction, lithium on the left loses its one valence electron to fluorine on the right. After the reaction takes place, a positively charged lithium ion (left) and a negatively charged chlorine ion (right) are held together by electrostatic forces, thus forming an ionic bonding.

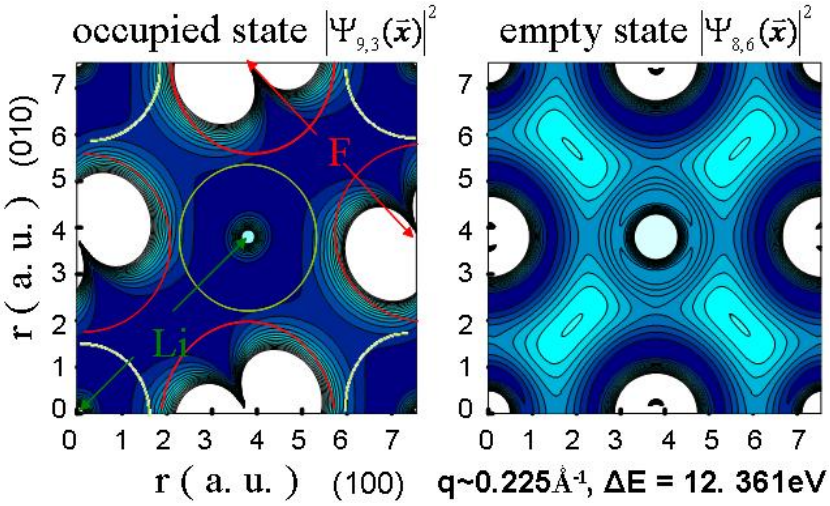

Figure 3.2: Orbital densities for states on both sides of the gap in LiF. White areas represent the highest orbital-density; dark blue areas represent low valences of this; and light cyan areas represent intermediate valences. The occupied state is localized state at the Li site. The empty state is a more delocalized antibonding state. No covelency exists between the Li and F atom.

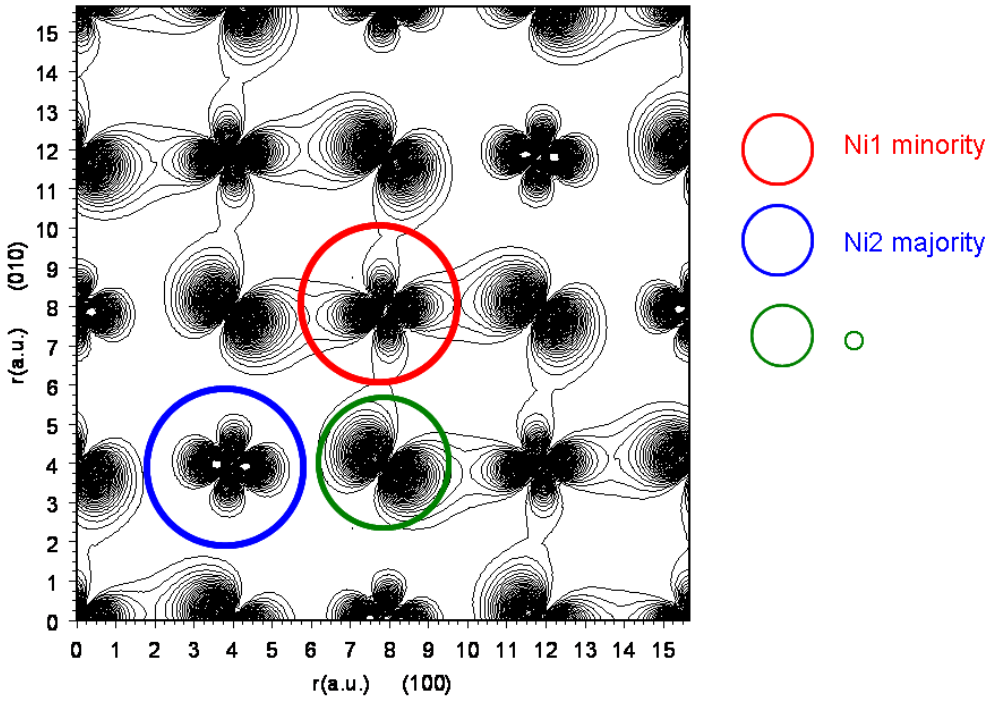

Figure 3.3: Example of covalent bonding between Ni minority and O atom in case of NiO (courtesy of Oscar Restrepo). The figure shows orbital density for Bloch-states near Fermi surface for NiO**.**

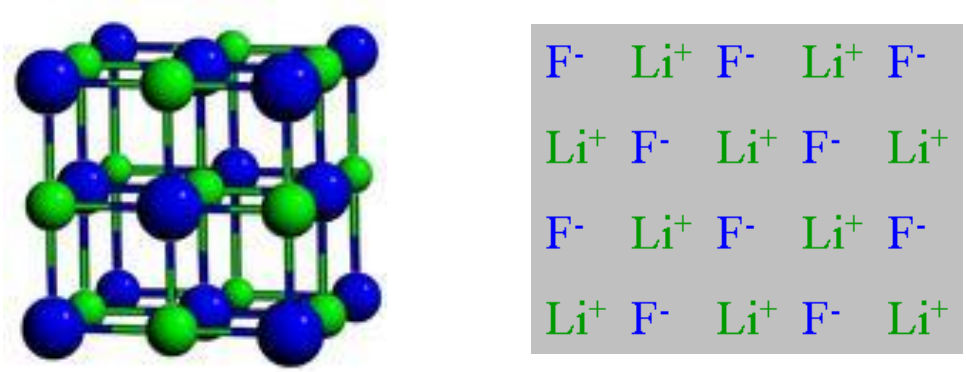

Figure 3.4: The crystal structure of LiF is shown on the left. The blue balls represent Fluorine ions and the smaller balls stand for demonstrate Lithium ions. LiF ionic crystal is schematic on the right.

Such an electronic configuration and crystal structure gives not complicated potential relative to complex oxides[67].

LiF is an F^- centered compound (transitions near gap mostly are from F atom to F atom, similar anions are Cl^- and SO_4^{2-}) exhibiting highly anisotropic physical properties in real space. There remain open questions about the nature of excitons in alkali halides[68], the large gap values, and the discrepancies regarding its fundamental electronic excitations[69].

3.1 Electronic structure

We calculate the electronic structure of the ground-state of LiF from first principles via the LAPW method within DFT. The dimension of the lattice and sampling of the Brillouin Zone (BZ) are 12x12x12 (the so-called k-mesh), with 72 k-points in the irreducible wedge of the BZ. The radius of the atomic-spheres is R^{MT} =1.7a.u and the criterion $R_I^{\min} \cdot G_{\max}$ (see appendix G) to evaluate the accuracy of basis set is set to be 8. The truncated value $\ell_{\max}$ for the spherical harmonics is 10, which is used to expand potential and WF (or charge density) in the KS equation. The energy window separating the core electrons and valence electrons is -6.0Ry, which includes around 300 basis functions; and therefore, the electrons from Li^+ $1s^2$ and from F^- $2s^2 2p^6$ are treated as valence electrons, electrons from F^- $1s^2$ are regarded as core electrons. The upper cut-off energy keeps empty bands up to 5.5Ry above the gap. Between the two energy windows, there are 33 well-converged bands being considered.

The ground-state can be described by band structure and density of states (DOS). Band structure represents the eigenvalues $E_{\vec{k},n}$ vs. the wavevectors $\vec{k}$ along high

symmetry directions for each band *n*. The WF $\psi_{\vec{k},n}$ inside atomic spheres (AS) can be expressed as a sum of angular momentum ℓ and the atomic spheres

$$\psi^{AS}_{\vec{k},n}\ \vec{x}\ = \sum_{I,\ell} \varphi^{I,\ell}_{\vec{k},n}\ \vec{r}\ \Big|_{|\vec{r}|\le R^{I}_{MT}} \tag{3.1.1}$$

and $\varphi^{I,\ell}_{\vec{k},n}$ are ℓ-decomposed amplitudes of the Ith MT sphere. DOS is density of single-particle (e.g., Kohn-Sham-) states given by equation

$$DOS\ \ E\ = 2\sum_{\vec{k}}^{BZ}\sum_{n}\delta\ \ E - E_{\vec{k},n}\ \ , \tag{3.1.2}$$

where, 2 is spin degrees of freedom. It tells the number of modes per unit volume per unit energy at a given energy *E*. Dirac delta function δ in eq. (3.1.2) can be smeared through Gaussian function, namely, $\delta_{\eta}\ \ x\ = \frac{1}{\eta\sqrt{\pi}}\cdot e^{-\frac{x^2}{\eta^2}}$. By recalling the orthonormality of the WF (eq. D.43) and using eq. (3.1.1), the total DOS inside atomic spheres can be further decomposed in terms of angular quantum number ℓ and atomic spheres. They are complementary descriptions to the ground-state within our numerical method.

In reality, the states from core electrons (like $F^- 1s^2$) will not be shown in the band (Fig. 3.5) and DOS plots (Fig. 3.7) for it is less relevant to the present research. On top of Fig. 3.5, the low-lying flat band (the 1st band) around -40eV derives from Li 1s atomic-states; and, the other band involving semi-core states (the 2nd band) around -20eV derives from F 2s atomic-states. At the bottom of Fig. 3.5, the 3rd, 4th and 5th valence bands immediately below Fermi level are composed of occupied states having characters of F 2p atomic-states (Figure 3.6). There are extremely few Li 2s-dominated occupied states because of the strong ionic bonding. The empty states which make up the 6th, 7th, 8th, and 9th conduction bands are sp-, sd-, pd-, or spd-hybridized states around both F and Li atom sites. All of the quantum states can also be understood later through DOS.

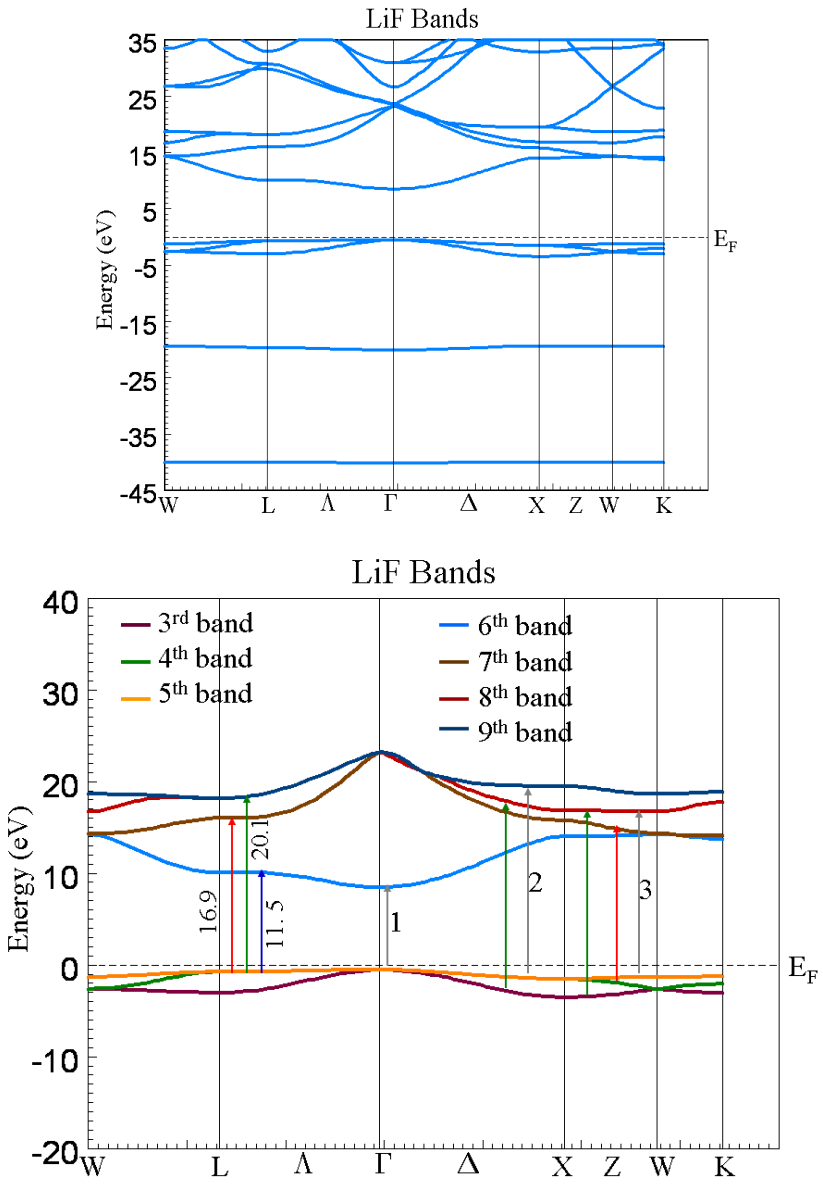

Figure 3.5: The band structure along high-symmetry directions is shown in the energy range from -45ev to 35eV on the top panel; the band from F $1s^2$ core electrons is not included. At the bottom panel, only valence bands and conduction bands near the gap are plotted; one color represents one band. The arrows indicate the flat or parallel parts of the two bands, where the JDOS are relatively high and a large amount of direct transitions may happen subject to the total JDOS, and the selection rules, and the WFs of the occupied and empty states being possibly overlapped.

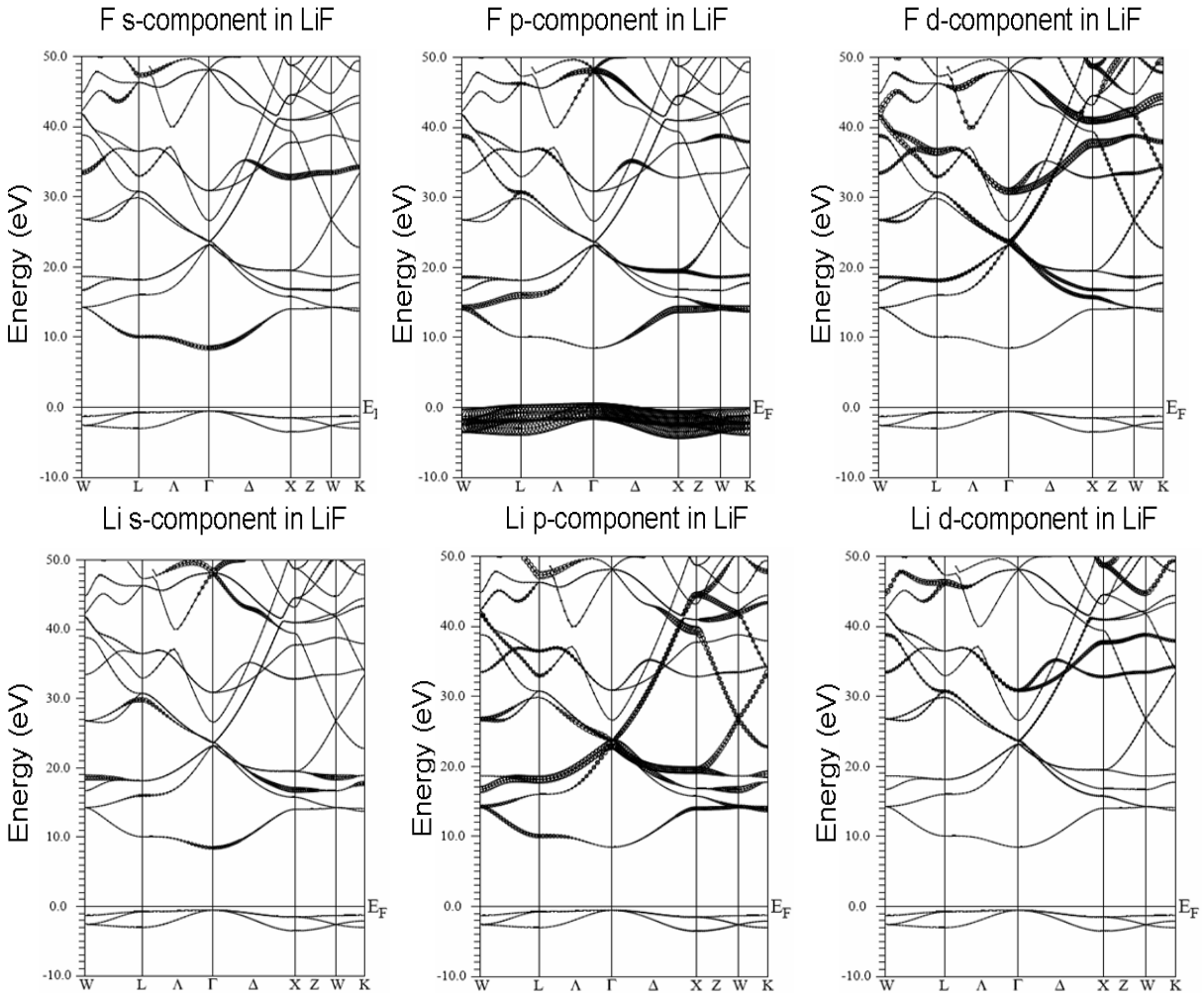

Figure 3.6: Angular momentum character plots. The thickness of the bands accounts for the weight of some ℓ-content of the specific atom of the KS states.

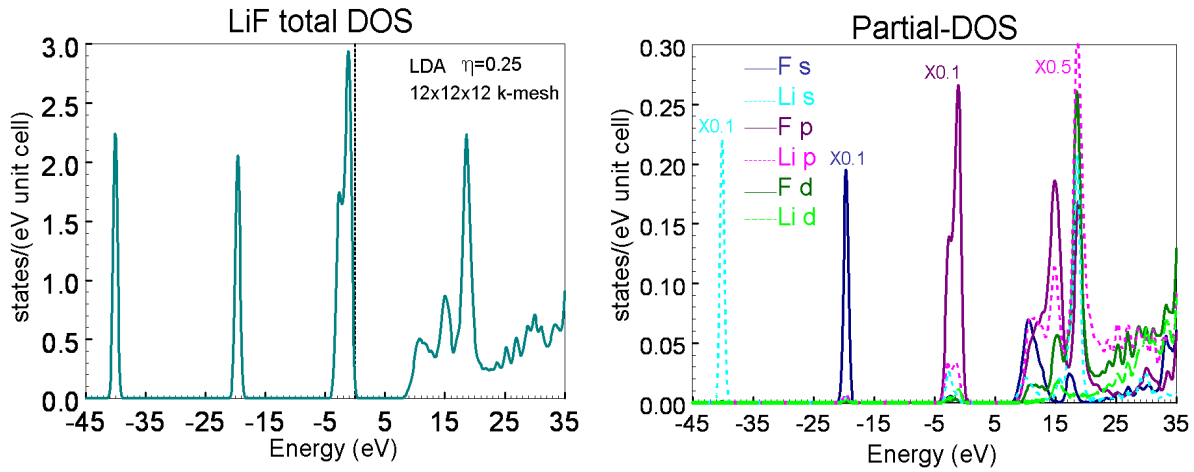

Figure 3.7: LiF total DOS is shown on the left panel. The decomposition of the DOS in angular momentum ℓ and atomic constituents present in the right panel. To present all the peaks in the same scale, we reduce the 4 peaks by times the number nearby.

The available data of DOS are spanned in the same energy range as those of band structure (exclude F^- $1s^2$ core electrons). Clearly, all the occupied states are localized states (Fig. 3.7). The sharp peak around -40eV is composed of Li^+ 1s atomic-like state; the peak around -20eV is made up of F^- 2s atomic-like state; and the peak just below Fermi level is constituted of F^- 2p atomic-like state. Mostly, empty states above Fermi levels are extended. The integral of the DOS between energies E_1 and E_2 for the occupied states is number of electrons in that energy interval. For instance, there are 6 F^- 2p electrons which fall into the energy interval [-5eV, 0],

$$\int_{-5}^{0} dE \cdot DOS\ \ E\ \ \approx 6\,. \tag{3.1.3}$$

A specific way to describe the available channels for the transitions is JDOS, defined as

$$JDOS\ \ \omega, q\ = \sum_{\vec{k}} \sum_{n} \sum_{n'}\ f_{\vec{k},n} - f_{\vec{k}+\vec{q},n'}\ \ \delta\ \ E_{\vec{k},n} - E_{\vec{k}+\vec{q},n'} + \hbar\omega\ , \qquad (3.1.4)$$

where, f is occupation number written as

$$f_{\vec{k},n} = 2 \cdot \frac{1}{e^{E_{\vec{k},n} - E_F \,/\, k_B T} + 1} \qquad (3.1.5)$$

and 2 in eq. (3.1.5) represents spin degeneracy. The Dirac delta function can be expanded by a sequence of Lorentzians, namely, $\delta_\eta\ \ x\ = \frac{1}{\pi} \cdot \frac{\eta}{x^2 + \eta^2}$. Partial-JDOS in atomic spheres can be implemented as same as partial-DOS.

In reality, the total JDOS of LiF and partial-JDOS from F^- anion are shown in Figure 3.8. Partial-JDOS from Li^+ cation is neglected due to very weak charge-transfer effect during excitations; partial-JDOS from interstitial is also neglected because the transitions to interstitial region become appreciable only if the wavevector-transfer q is greater than $4 Å^{-1}$ in our test.

For simplicity, we first discuss qualitatively the excitation channels for small wavevector transfer $q \to 0$ at low energy end from the knowledge of the band structure and DOS. In band structure plot, at the lower panel of Fig. 3.5, the flat or parallel part of the two bands shown by an arrow can be interpreted as a sharp feature in the JDOS for that energy transfer ω. However, the channels at the corresponding frequency may contribute few or zero to real transitions because of not much channels (the 1st light- grey arrow) or the violation of the dipole selection rule (the 2nd light-grey arrow). Similarly, the interpretation of JDOS by DOS is shown in Figure 3.9. This gives us the real transition channels for small q (the left-upper panel of Fig. 3.10). We conclude:

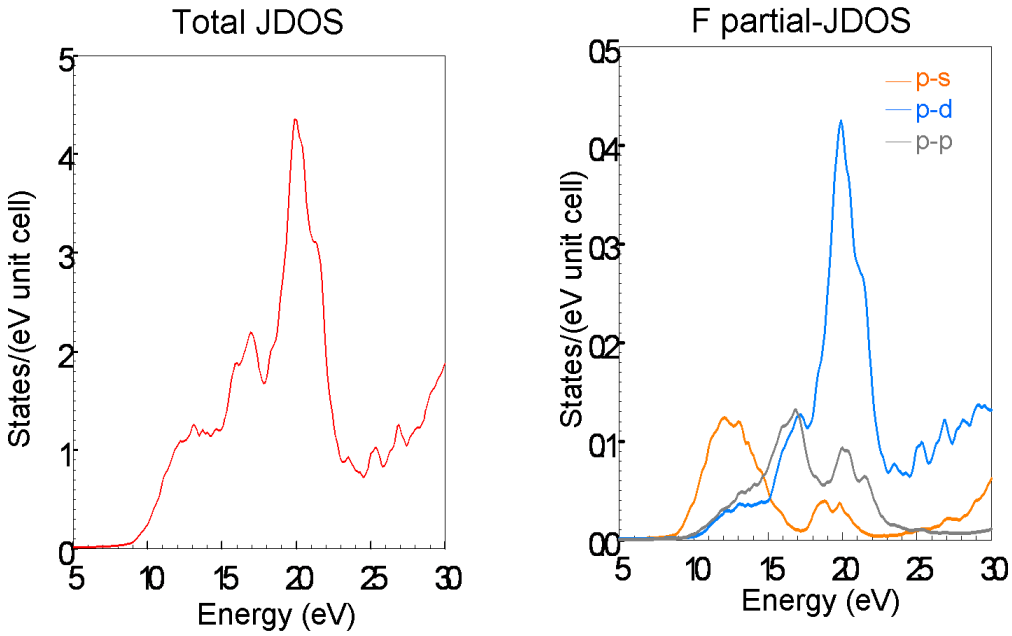

Figure 3.8: The total transition channels of LiF and partial-JDOS from F^- anion.

1. The first feature of real transition channels is from F 2p→ F 3s around 11.5eV.

2. The second feature of real transition channels is from F 2p→ F 3d around 16.9eV.

3. The third feature of real transition channels is from F 2p→ F 3d around 20.1eV.

As *q* increased, the total JDOS of LiF remains nearly unchanged (Fig. 3.10); while, the topology of real transition channels greatly changes (Fig. 3.11). In Fig. 3.11, all real transition channels start at 9eV with an abrupt drop-off around 22eV which gives a collective mode (plasmonic excitations) introduced in sec. 3.3.

It should be noted that the above pedagogical discussion is based on the LDA electronic structure, whose energy gap value is much smaller than the measured optical gap 14.4eV[70]. As mentioned in sec. 2.2, this problem might be involved into that the exchange-correlation potential is discontinuous on adding one particle. In addition, since

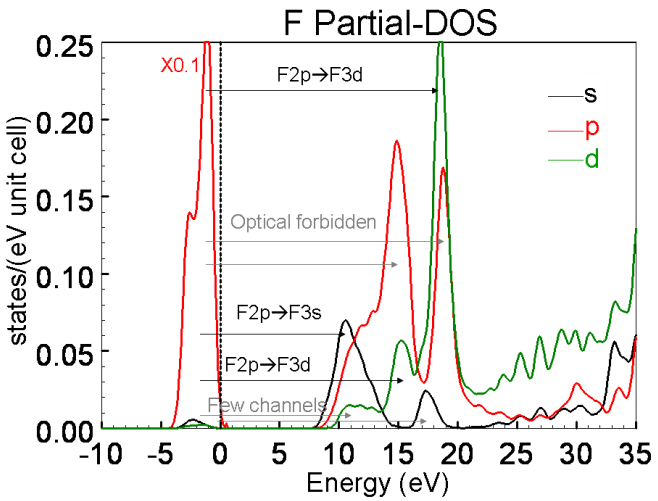

Figure 3.9: Direct transitions are projected in F partial-DOS plot.

very few de-localized electrons embed into an enormous localized electron system and such a rather low density of the conduction electrons leads to little thermal collisions (weak e-e correlations also) in LiF ground-state, the system may be not apt to be treated as a thermal ensemble. Unfortunately, during the determination of Fermi energy E_F, the weight of the states $\left|\vec{k},n\right\rangle$ to generate valence charge density is modified by a Fermi function where the finite temperature formalism[71] is applied in our calculation. Each eigenvalue is temperature broadened using a Fermi function $f_{\vec{k},n} = 2\cdot(1+e^{E_{\vec{k},n}-E_F \,/\, k_B\cdot T})^{-1}$ with a broadening parameter *eval*=0.002*Ry* in replace of k_BT, where 2 takes account into spin degeneracy. The thermal smoothening of the cusp gives a slower rising of the excitation in the JDOS (Fig. 3.11). The LDA part of problem can be solved through the scissor operator presented in the sec. 3.3. For the problem of the onset of JDOS, we should apply zero- temperature formalism to ground-state (namely *eval*=0). Tetrahedron-method may be another feasible option even though convergence is slower than with Gauss- or temperature-smearing. However, the correct electronic structure only translates a constant energy value on the empty bands to enlarge the gap. The physical conclusions made here are still valid for the modified electronic structure.

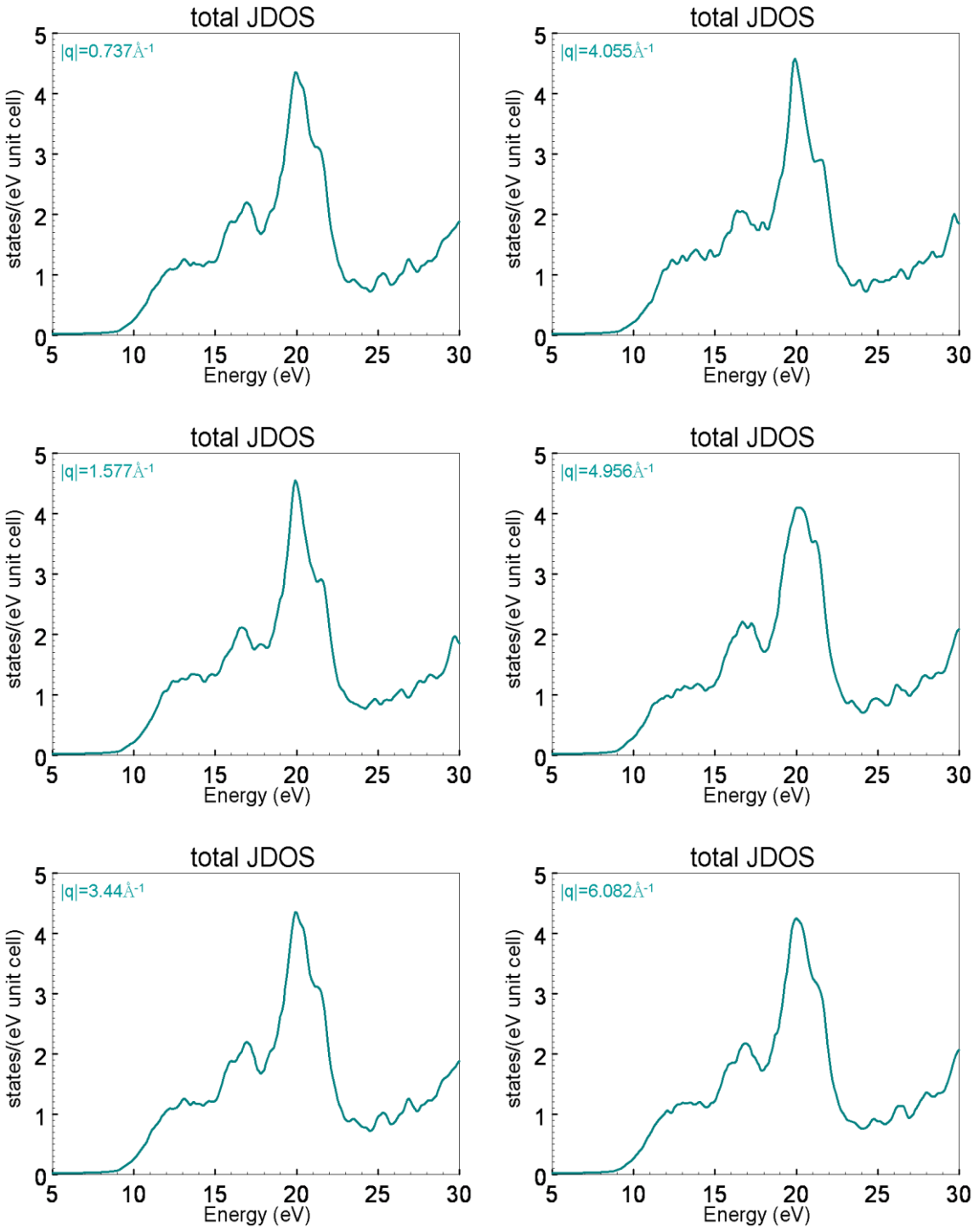

Figure 3.10: The total JDOS over a large range of wavevector transfer *q*s.

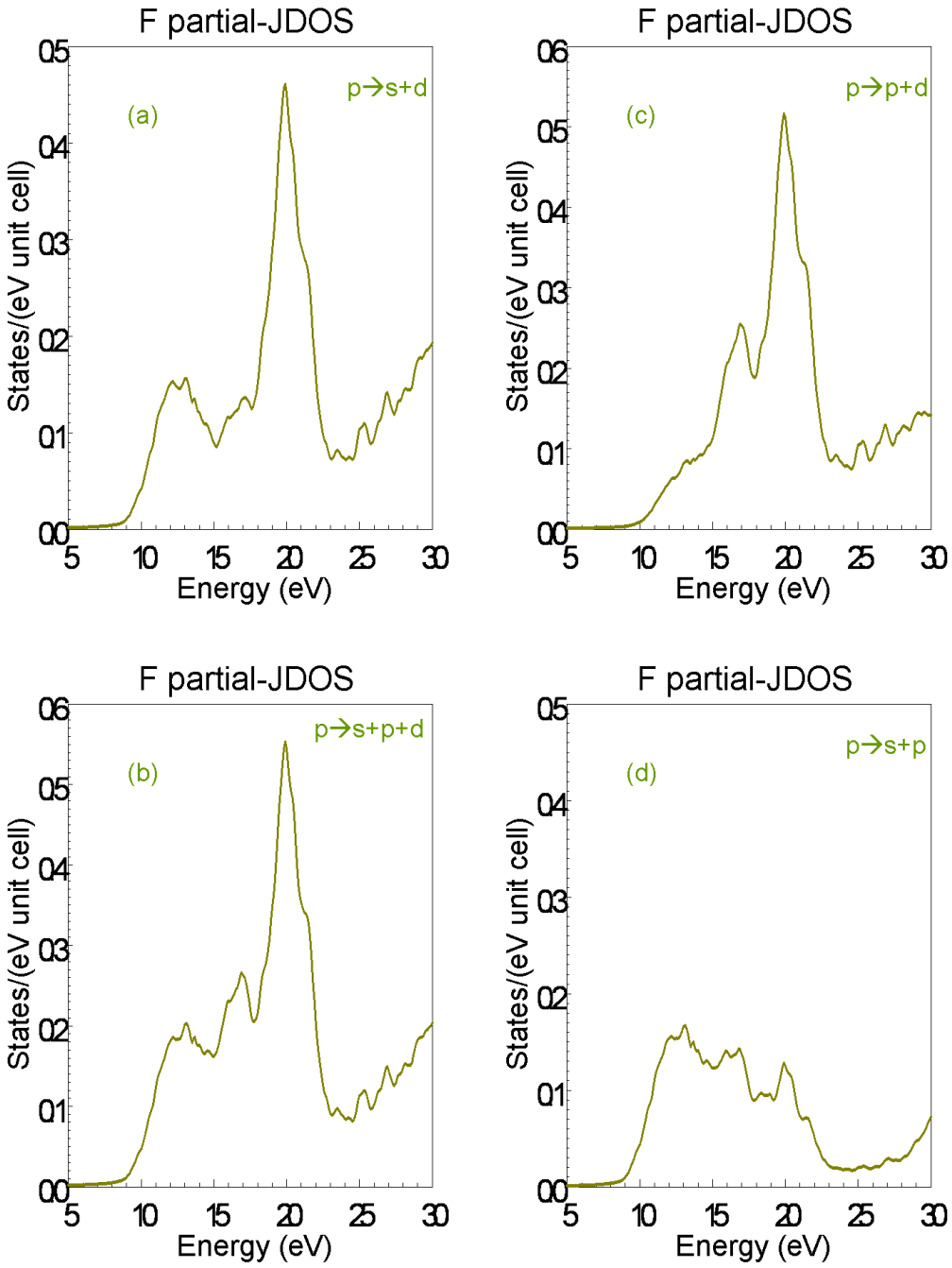

Figure 3.11: The evolution of transition channels for (a) small-, (b) intermediate-, (c) large-, (b) very large- and (d) the largest- *q* regions.

3.2 Experimental data

Non-resonant Inelastic X-ray Scattering (NIXS) experiments measure the double differential cross section and thereby the dynamical structure factor (sec.2.5) of LiF. NIXS, including both energy and directional analysis of scattered photons, comprises a very powerful tool for investigation the electrons in many-particle system by looking at the excitations of this system left behind in the inelastic scattering process[40].

Synchrotron radiation is the light source of NIXS. First-generation synchrotron light sources were basically beamlines built on existing facilities designed for particle physics studies. Second-generation synchrotron light sources were dedicated to the production of synchrotron radiation and employed electron storage ring to harness the synchrotron light. Current (third-generation) synchrotron light sources optimize the intensity of the light by incorporating a long straight sections into the storage ring for insertion devices such as undulator and wiggler magnets. A wiggler has a broader spectrum than an undulator. An undulator creates a narrower and significantly more intense beam of coherent light with selected wavelengths or harmonics which can be tuned by manipulating the magnetic field in the device. Following the two-ring model, it can access to the whole range of x-ray from short-wavelength (high-energy or hard) to vacuum-ultraviolet and long-wavelength (low-energy or soft). Next (fourth-) generation synchrotron light source is the hard x-ray (wavelength less than 1Å) free-electron laser based on a long undulator in a high-energy electron linear accelerator to obtain resonant inelastic X-ray scattering (RIXS) spectroscopy. It would give a peak brightness many orders of magnitude beyond that of the third-generation sources, as well as pulse lengths of 100fs or shorter, and would be more fully coherent. With higher spectral flux of insertion devices in addition to low emittance of the dedicated storage ring, third- and

fourth-generation can bring about the full utilization of all techniques of inelastic scattering[40].The advent of NIXS measurements in this decade is a result of the high intensity of synchrotron sources and the development of high resolution analyzers[72]. One of the astounded findings having been achieved is the d-d dipole forbidden excitations within the gap in NiO and CoO[39]. In fact, it should not have been a surprise in retrospect because it has long been known that quadrupole and higher order multipole scattering is not dipole forbidden. Nevertheless, nobody had thought about measuring for such effects because higher order effects are usually smaller and even the first order effects in NIXS are very low intensity. Furthermore, IXS measurement is still a rather rapidly developing field of measurement with many new things to be discovered.

Earlier measurements by NIXS in LiF were done in [001] direction over small to intermediate wave vector transfers[73]. Also, Larson et al. were interested in LiF as a large band gap insulator for a possible calibration of the quasi-elastic tails similar to CaF_2; and both would be equally good. Thus, Larson et al. restudied LiF and CaF_2 by NIXS using one of the other to be a calibration. The newly NIXS measurements on LiF are discussed below.

The measurements by Larson et al. were performed on the Sector 33 ID XOR-UNI beamline at the Advanced Photon Source at Argonne National Laboratory using 7.59 keV x-rays and a Ge (111) spherical analyzer. Low resolution measurements were made using the high heat-load Si (111) monochromator which has a line width of ~1 eV. Those measurements had approximately 30 times more intensity than high resolution measurement. As a result, the low resolution measurements provide better statistical accuracy and could be performed over a larger range of wave-vector directions and magnitudes, and over greater energy ranges. The non-negligible tails of the quasielastic

peak near $\Delta E = 0$ were removed by scaling quasi-elastic peak measurements on CaF2 to the quasielastic peak heights of measurements on LiF. The measurements of $S(\vec{q},\omega)$ were reduced to absolute units ($eV^{-1}Å^3$) using the first-moment, f-sum rule calibration of the IXS system for Al by μ_{LiF}/μ_{Al}, where μ_{LiF} is the linear absorption coefficient of LiF and μ_{Al} is the linear absorption coefficient for Al[72].

The low resolution measurement data are available over a large range of wave vector transfer in three principal directions [001], [011], and [111]. Below, we choose *q*//[111] to be a representative because all the previous theoretical study are along [001][74]; and the phenomena in [111] are similar to those in [001].

The NIXS data for momentum transfers *q*=0.75 $Å^{-1}$, 1.5 $Å^{-1}$, 3.5 $Å^{-1}$, 4 $Å^{-1}$, 5 $Å^{-1}$, and 6$Å^{-1}$ in [111] are shown in the figure 3.12. The measured gap is around 14.0eV. The swift onset of the spectrum for small and large wavevector transfers $\vec{q}$ shows that conduction electrons in LiF ground-state are scarce because of the big gap. Also, these data are dramatically dependent with momentum transfers. The two extremes (*q*=0.75$Å^{-1}$, and 6$Å^{-1}$) which show the greatly different spectra are compared here. In the region just above the "experimental optical gap[70]" (14.4eV): for small q, there are two sharp features which we are going to explain in terms of dipole allowed excitations; for large q, basically all we have is the onset at the "optical gap," followed by a plateau. In the region about 25 eV**:** for small *q* we have a strong excitation which we are going to explain as a *collective mode* induced by an F 2p→3d feature in the dielectric function; for large *q* that mode is gone. As to *q*'s between both extremes, the spectra show a continuing change between both types of behavior just highlighted. The fact that for large q there are no sharp features will be used below to set the "scissors shift" we will introduce to the LDA band structure (sec. 3.3).

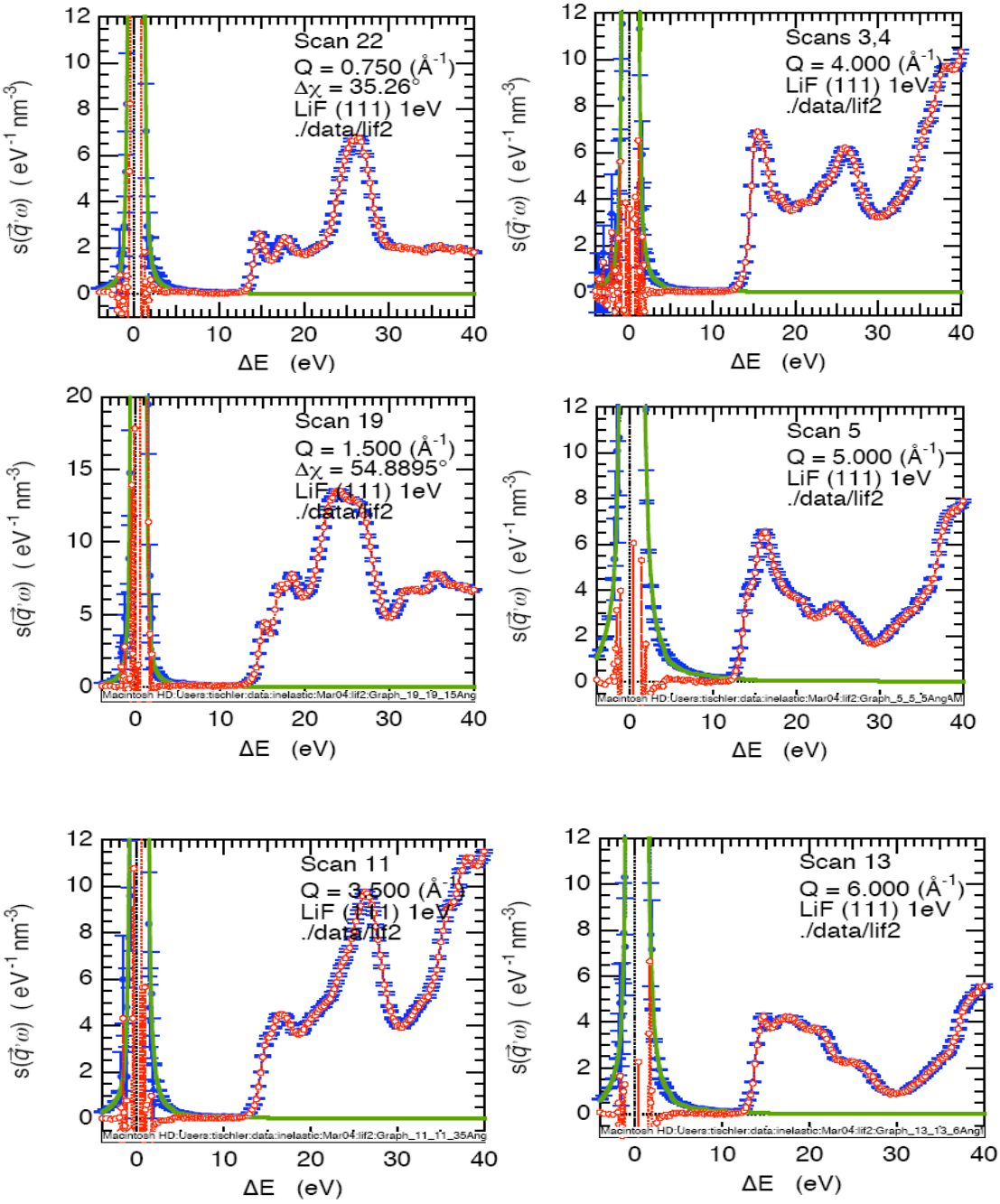

Figure 3.12: The nature of the spectrum above the gap changes qualitatively. The upper left corner corresponds to a relatively small q (IXS does measure for much smaller q's than that one) and bottom right corner corresponds to a large q.

3.3 Theoretical-experimental study of LiF

We perform a realistic description of the charge-density excitations in LiF for a large range of wave vector transfers. We analyze quantum theoretical spectra in the light of the available NIXS data described in the primitive chapter.

3.3.1 The single-particle response for the unperturbed KS system

As discussed in sec. 2.1.3, the KS density-response function is expressed as

$$\chi^{s}_{\vec{G},\vec{G}'}\left(\vec{q}\,|\,\omega\right) = \frac{1}{V}\sum_{\vec{k}}\sum_{n,n'}\left\{\frac{f_{\vec{k},n}-f_{\vec{k}+\vec{q},n'}}{E_{\vec{k},n}-E_{\vec{k}+\vec{q},n'}+\hbar\,\omega+i\eta}\times \left\langle\vec{k},n\middle|e^{-i\,(\vec{q}+\vec{G})\cdot\hat{\vec{x}}'}\middle|\vec{k}+\vec{q},n'\right\rangle\left\langle\vec{k}+\vec{q},n'\middle|e^{i\,(\vec{q}+\vec{G}')\cdot\hat{\vec{x}}}\middle|\vec{k},n\right\rangle\right\}, \tag{3.3.1}$$

where $\eta = 0^{+}$ as is required from Green's function theory, in which (3.3.1) corresponds to a retarded two-particle Green's function and a finite η here allows us to handle the "pole" structure of the "integrand". On the right side of eq. (3.3.1), when $\eta \to 0^{+}$, for the specific frequency ω and momentum transfer *q*, the imaginary part of the fraction term represents the availability of the transition channel; and, the real part of the product of two matrix elements give the probability of the transition. If this product is one, $\mathrm{Im}\,\chi^{s}_{\vec{G},\vec{G}'}\left(\vec{q}\,|\,\omega\right)$ reduces to JDOS for that momentum transfer *q* (see eq. 3.1.4).

In our KS response calculation done by eq.(3.3.1), the truncated value $\ell_{\max}$ for the spherical harmonics is 4, which is used to expand exponential terms and wave-functions. The broadening factor η in the energy-denominator entering the KS response is taken to be 0.2eV and k-mesh is 12x12x12 points. The total 33 bands are included which converged for all relevant energy. Our KS responses are calculated from an optical limit to very large wavevector transfers along [111] direction.

It should be noted that the broadening factor η in eq. (3.3.1) violates conservation laws, such as the equation of continuity (the f-sum rule). However, we have checked that the violation of the f-sum rule incurred by introducing a finite η=0.2 is small (a few percent).

3.3.2 Dynamical response $\chi(q,\omega)$

The dynamical (actual) response discussed in sec. 2.4.2 can be computed by eq. (2.4.20) based on KS response function, random phase approximation (RPA, namely, f_{xc}=0) applied first. The matrix calculation related to the translation reciprocal lattice vector $\vec{G}$ includes crystal local-field effects (CLFEs), which arise when the microscopic electric field varies rapidly over the unit cell. In LiF more $\vec{G}$s are needed to reach an acceptable convergence in the intermediate range of wavevector transfer q as the CLFE is large for that range of qs (Fig. 3.13). We use 65 $\vec{G}$s for all qs in [111] direction to get well-converged dynamical responses.

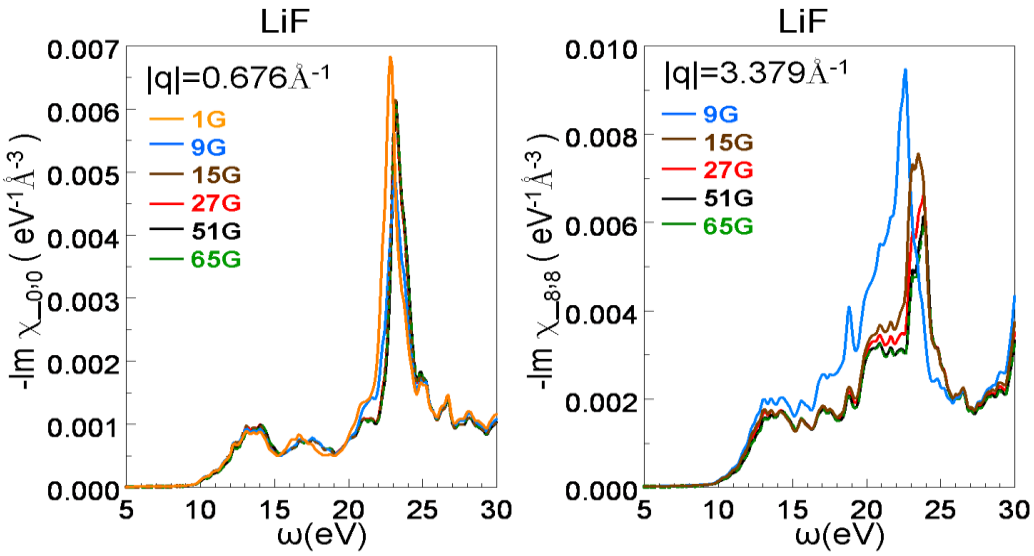

Figure 3.13: For q=0.676Å^{-1}, dynamical response is converged with at least 9 $\vec{G}$ s. For q= 3.379Å^{-1}, dynamical response is reasonably converged with at least 27 $\vec{G}$ s.

3.3.3 The dielectric function, collective mode and dynamical response function

From eq. (2.4.30), for an ideal free electron gas, it is clear that the poles of $1/\varepsilon\ \vec{q},\omega$, or what is equivalent, the relation

$$\varepsilon\ \vec{q},\omega\ = 0 \tag{3.3.2}$$

yields the allowed energy spectrum of the density fluctuations. Eq. (3.3.2) should determine the resonant frequencies associated with the density fluctuations. If $\varepsilon\ \vec{q},\omega\ = 0$, it is possible to have a nonvanishing density fluctuation, and a nonvanishing potential in the electron gas in the absence of a test charge. It also can give the dispersion relation for the existence of polarization waves in the system.

As the effective dielectric function $\varepsilon_{eff}\ \vec{q},\omega$ (eq. 2.4.34) is defined as a comparable quantity of a free-electron gas, it plays the same role for a complex material as the textbook dielectric function $\varepsilon\ \vec{q},\omega$ plays in case of jellium, so we can use a similar knowledge about $\varepsilon\ \vec{q},\omega$ in free-electron gas to understand the "effective" dielectric function $\varepsilon_{eff}\ \vec{q},\omega$. This function allows a certain visualization of the distinction between single-particle features and plasmonic features. In Fig. 3.14, as $\mathrm{Re}\,\varepsilon\ \vec{q},\omega\ =0$ and $\mathrm{Im}\,\varepsilon\ \vec{q},\omega\ \to 0$ around 23eV, we deduce that the 4th feature of dynamical response is a collective mode. This mode start to damp into electron-hole pair after q=1.35Å^{-1} (Fig. 3.15).

When we compare $\varepsilon_{eff}\ \vec{q},\omega$ with the "scalar" (in absence of CLFE) dielectric function (eq. 2.4.27)) $\varepsilon_{\vec{G}_q,\vec{G}_q}\ \vec{q},\omega$ (Fig. 3.15), the structure of $\varepsilon_{eff}\ \vec{q},\omega$ identifies key aspects of the physics of the CLFE. The interplay between rapid frequency variation in

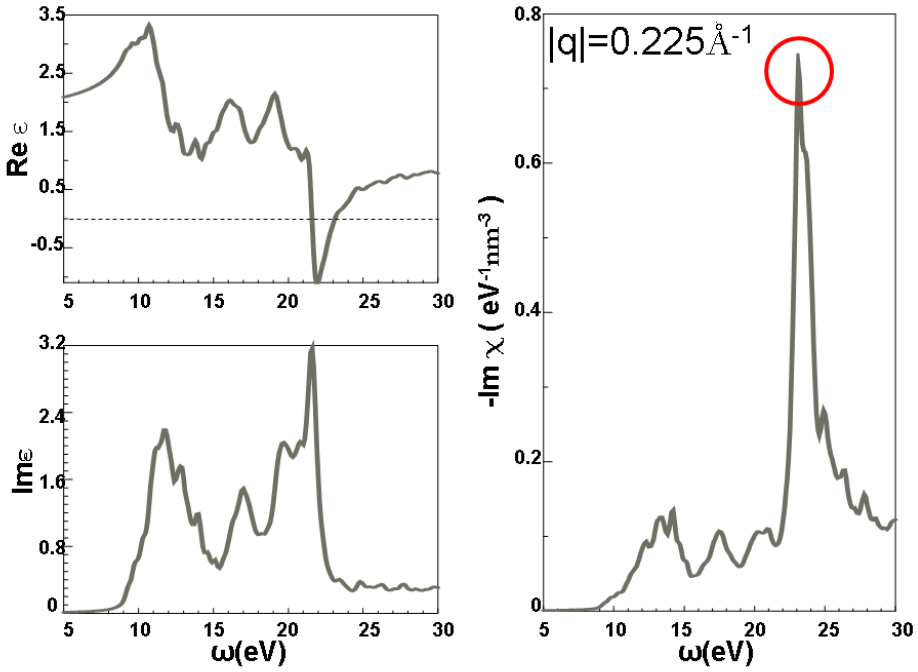

Figure 3.14: The real and imaginary part of $\varepsilon_{eff}\ \bar{q},\omega$ is shown on the left panel. $\mathrm{Re}\,\varepsilon\ \bar{q},\omega$ =0, and $\mathrm{Im}\,\varepsilon\ \bar{q},\omega \rightarrow 0$ around 23eV. On the right panel, the 4th feature of dynamical response done by RPA for the corresponding *q* is a collective mode.

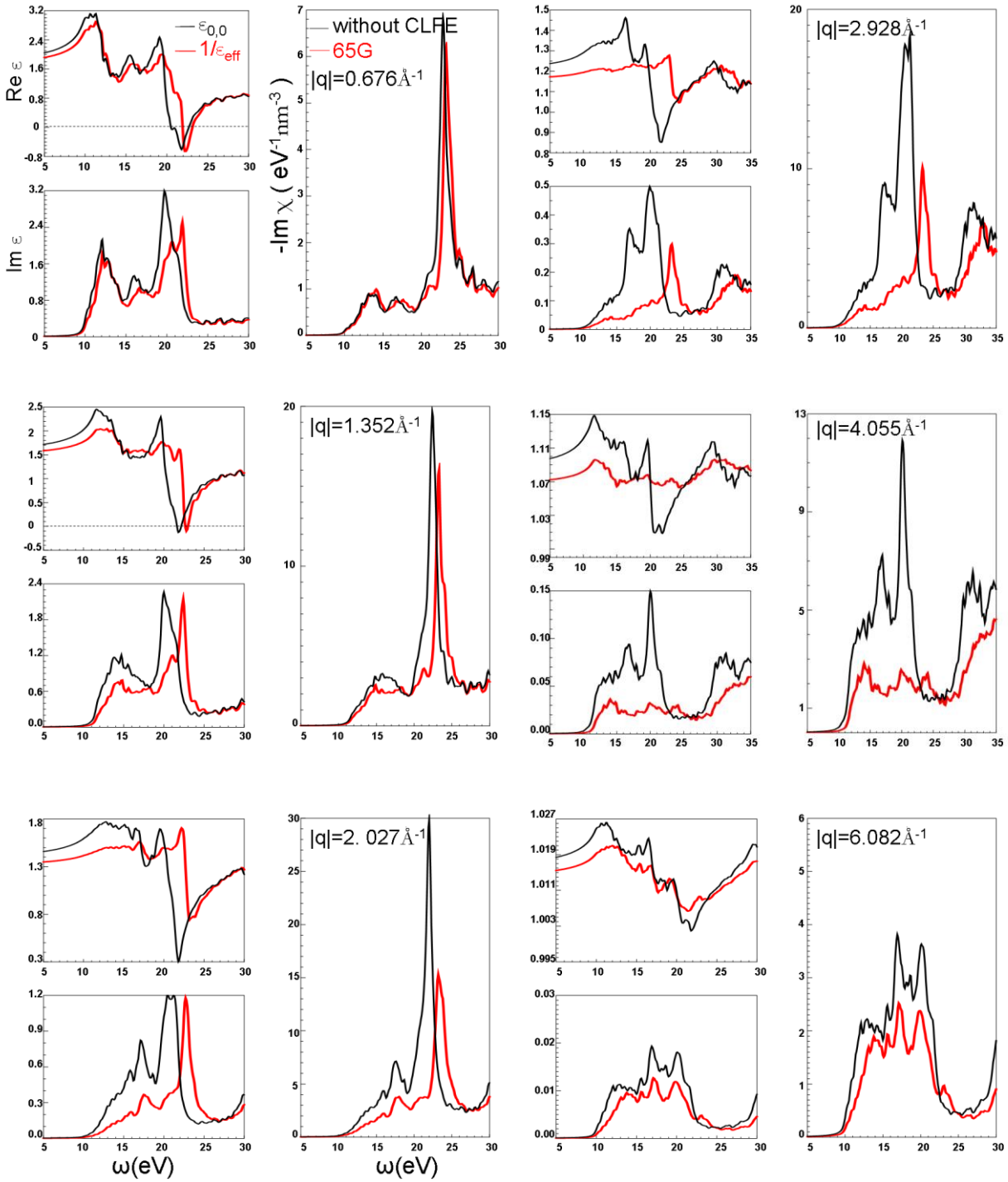

Figure 3.15: The CLFE is displayed through the comparison of $\varepsilon_{eff}\ \ \vec{q},\omega$ with a "scalar" $\varepsilon_{\vec{G}_q,\vec{G}_q}\ \ \vec{q},\omega$ on the left panel. The corresponding dynamical response done by RPA with and without CLFE is shown on the right panel.

$\varepsilon\ \bar{q},\omega$ around "nature" energies for a given material, and its wavevector dependence is displayed. However, it is hard to visualize from the outside the "black-box". From Fig. 3.15, the CLFE is very strong in the intermediate wavevector-transfer range which is between q=2~4Å^{-1}.

3.3.4 Dynamical structure factor $S(q,\omega)$

Through the eq. (2.5.3) and (2.5.4), a joint theoretical-experimental study of the electronic excitations in a scattering system has been done in LiF. The broadening factor η here is chosen to be 0.5eV (Fig. 3.16). It has been found that theoretical spectrums in RPA largely disagree with the measurements for all wavevector transfers (Fig. 3.17). The problem resides in underestimation of the band gap by LDA, where the gap value is 9 eV; while, the optical experimental energy gap is 14.4 eV.

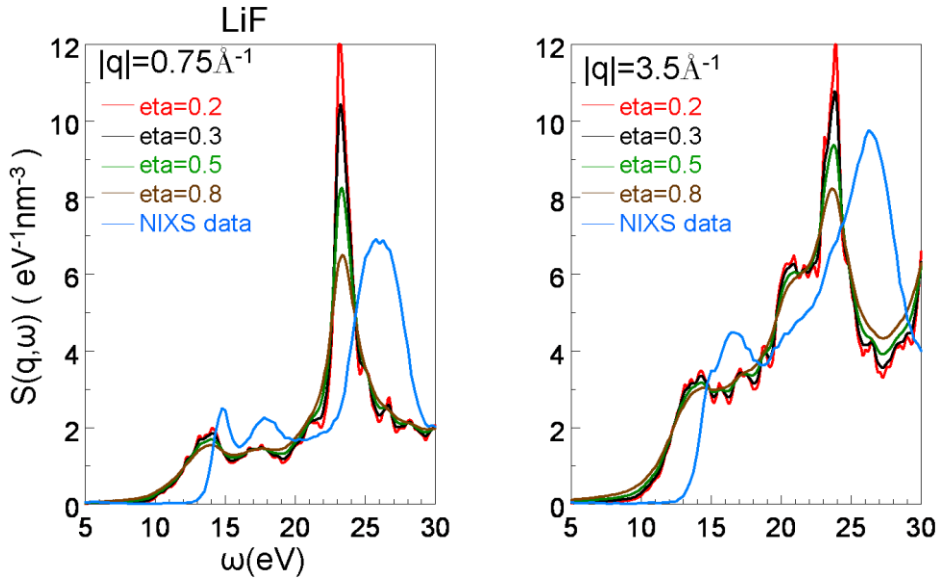

Figure 3.16: The height of the peak around 25eV increases as the broadening parameter η decreases. The comparison of $S(q,\omega)$ with NIXS data is done on a pedagogical-bias and η=0.5 is a compromise choice.

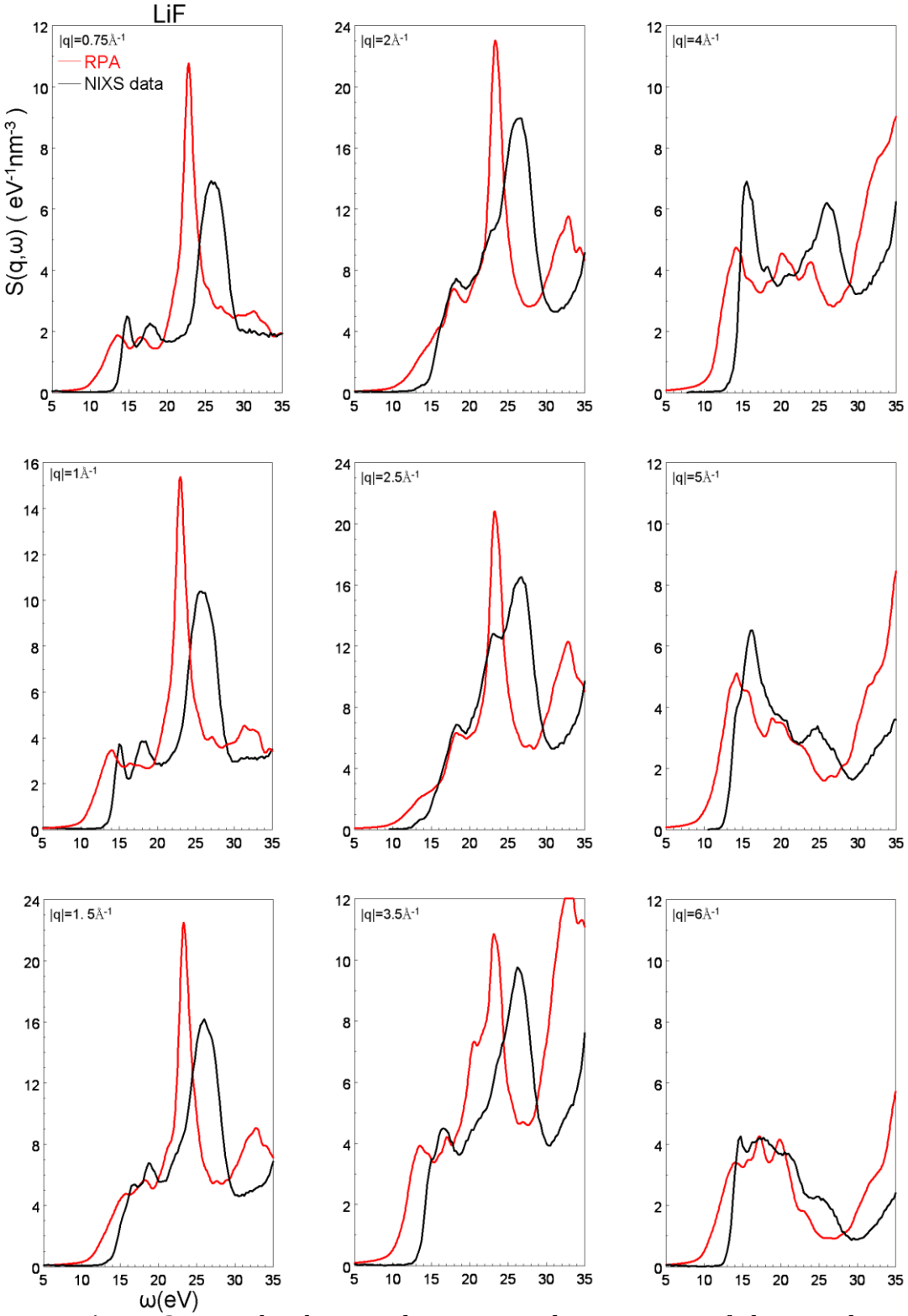

Figure 3.17: The theoretical-experimental comparison of dynamical structure factor for all *q*s in [111] direction. The theoretical spectra are calculated by RPA.

In order to work out the problem, we resort to the dynamical structure factor $S(\vec{q},\omega)$ of the largest wave vector $\vec{q}=6\text{Å}^{-1}$ along (111) direction. For this spectrum, as mentioned in the latter part of chapter 1, all dynamical screening effects (including the CLFE) are basically gone (Fig. 3.15); and the NIXS data (at the right-bottom panel of Fig. 3.12) suggests that there are not strong many-body effects for this *q*. Thus, a shift $\Delta=2.5\text{eV}$ of the TDLDA spectra is determined by using our initial spectrum from the LDA electronic structure referred to NIXS data of the largest wave vector $\vec{q}=6\text{Å}^{-1}$ along [111] direction (Fig. 3.18).

The numerical convergence on ground-state after this shift has been checked by performing calculations with 12x12x12 and 24x24x24 k-meshes without observing appreciable changes in the spectra (Fig. 3.19). Generally, the smallest number of k-points is used for a given level of convergence.

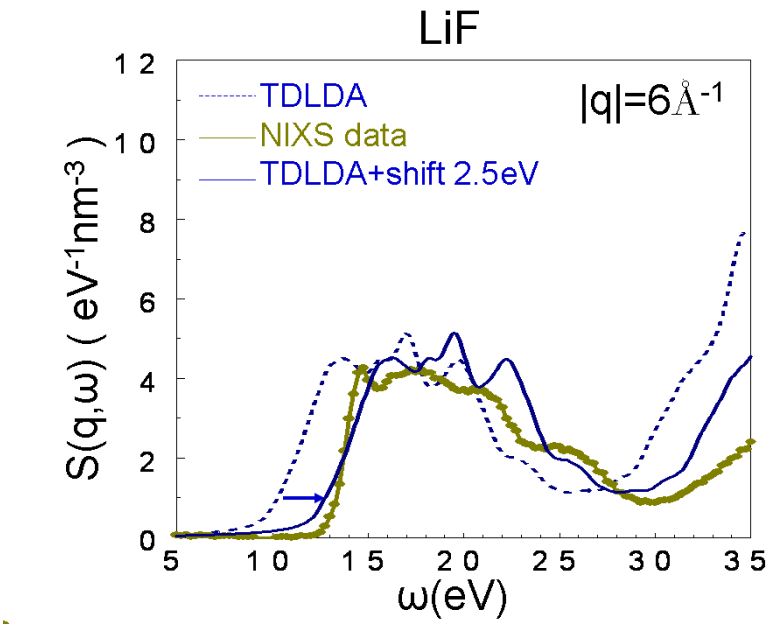

Figure 3.18: Compared with NIXS data, the TDLDA spectrum should be shifted to the high energy end by 2.5eV.

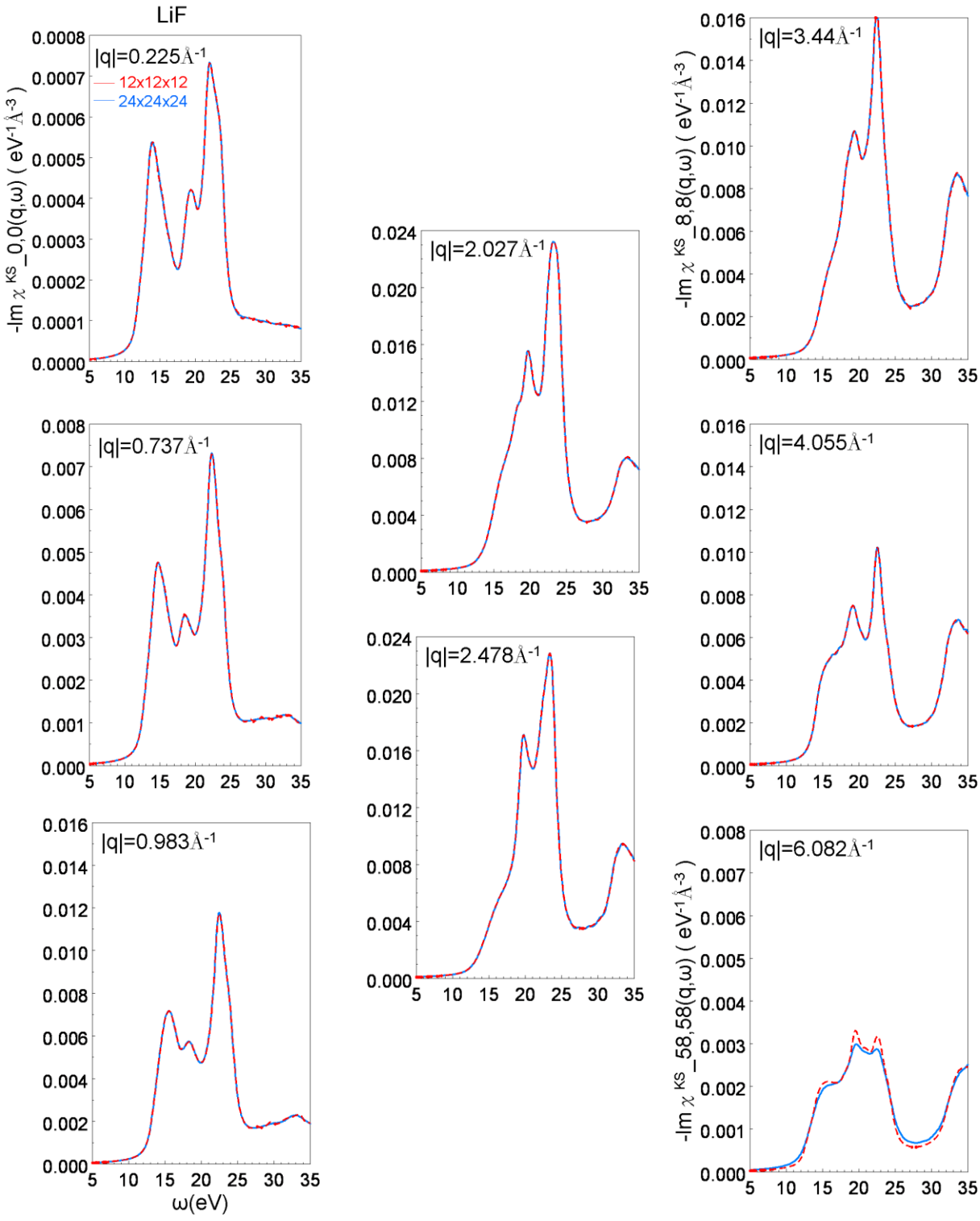

Figure 3.19: The numerical convergence on ground-state after the shift has been checked by 12x12x12 and 24x24x24 k-mesh without appreciable changes in the spectra.

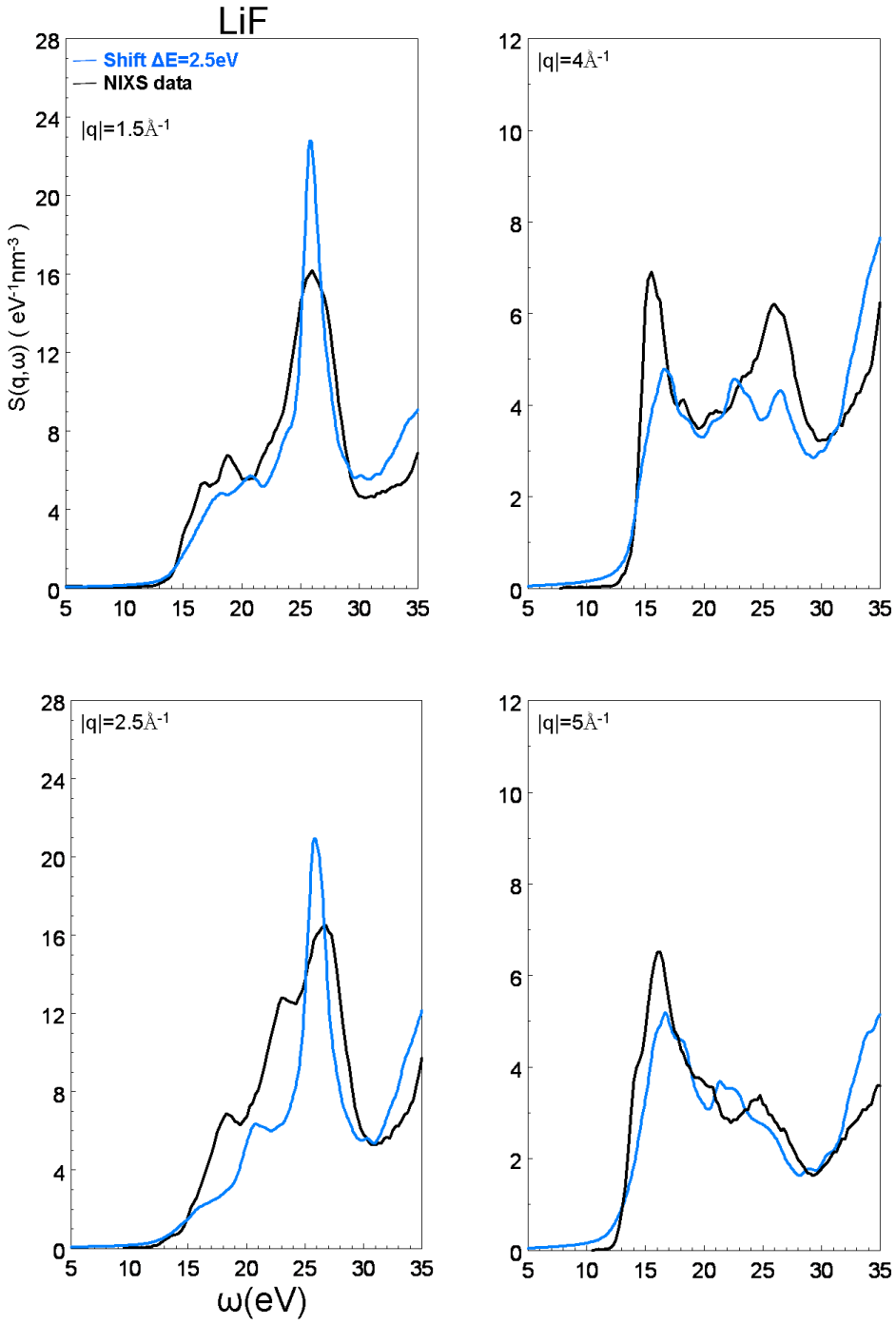

Figure 3.20: The theoretical-experimental comparison of dynamical structure factor for some selective *q*s in [111] direction with the update electronic structure. The theoretical spectra are calculated by RPA.

Then, the dynamical screening effects for all wave vectors, all the way to the optical limit, are treated ab-initio (i.e., without adjusting parameters) (Fig. 3.20, RPA is applied).

Now, we introduce a simplest approximation for many-body kernel f_{xc}, an adiabatic LDA (ALDA),

$$f_{xc}^{ALDA}\left[\rho_0\right]\left(\vec{x},\vec{x}';\omega\right) = \delta\left(\vec{x}-\vec{x}'\right)\frac{d^2}{dn^2}\left(\rho\varepsilon_{xc}^{\hom}\left(\rho\right)\right)\Big|_{\rho=\rho_0\left(\vec{x}\right)} \tag{3.3.3}$$

into eq. (2.4.20). This defines our TDLDA. The spectra (Fig. 3.21) show that the improvement of the calculations is modest. Formally, since the dynamical many-body kernel should be considered in the dynamical many-electron problem even though the exact one is in the black-box, we take TDLDA later on.

So far so good, the huge change in the quantum mechanical response as a function of *q*, leading to major changes in the line shape of the loss function, are ab-initio reproduced very well compared with NIXS data. Especially, even the existence of the large difference 5.4eV between the optical experimental energy gap and LDA band gap, our calculated spectra excellently agree with the gap from NIXS data at the inflexion point, which is around 14eV (Fig. 3.21)! In particular, the microscopic screening by large density fluctuations (CLFE) plays a big role, for an intermediate range of *q*'s (Fig. 3.15). Such effects are not fully guessed at, on the basis of the 6 $Å^{-1}$ spectrum!

The TDLDA spectra without shift are compared with spectra with shift (Fig. 3.22). Changes of line-shapes between them are limited in LiF, which hints that physics does not change due to the shift.

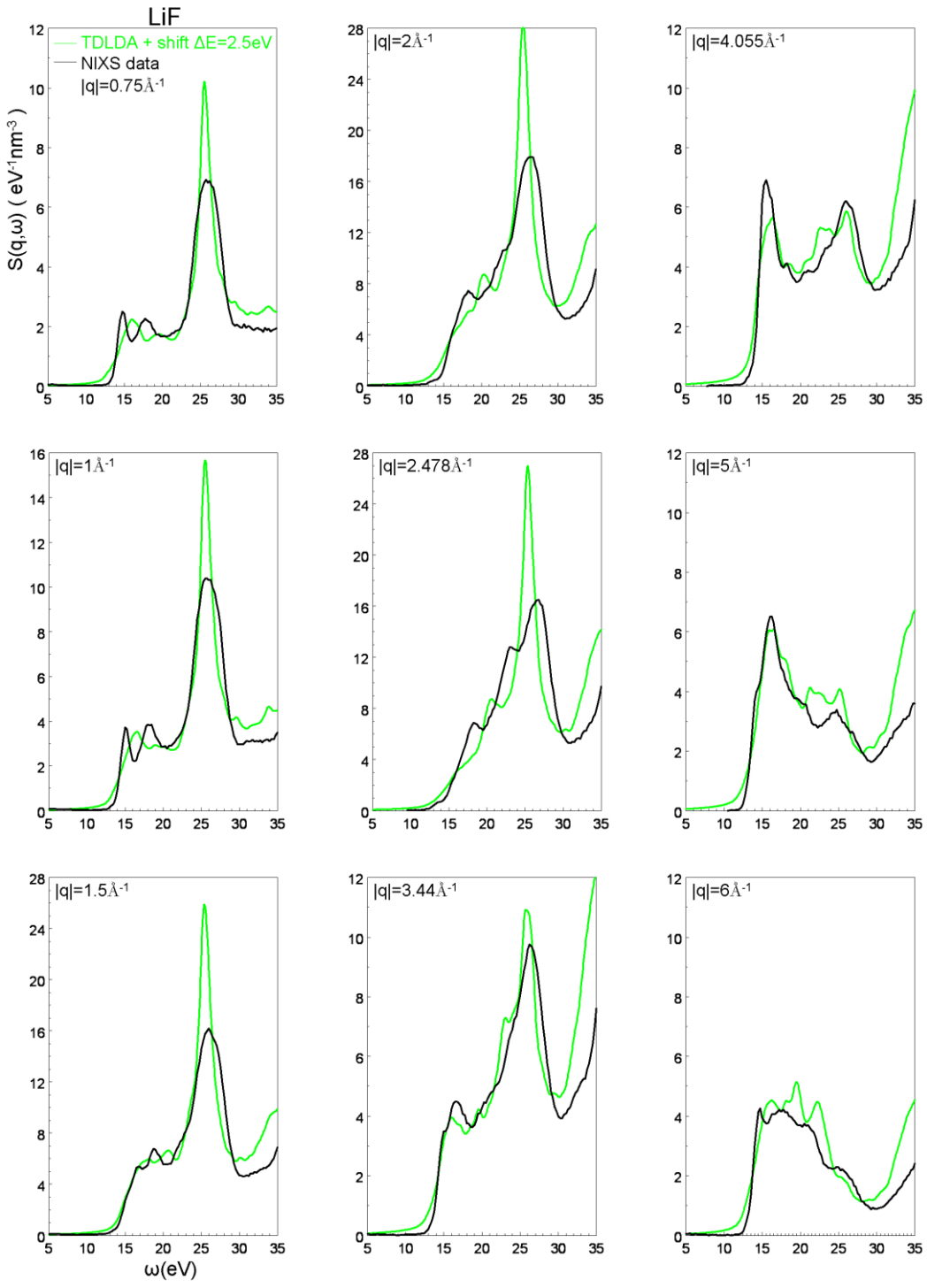

Figure 3.21: The theoretical-experimental comparison of dynamical structure factor for all *q*s in [111] direction. The theoretical spectra are calculated by TDLDA.

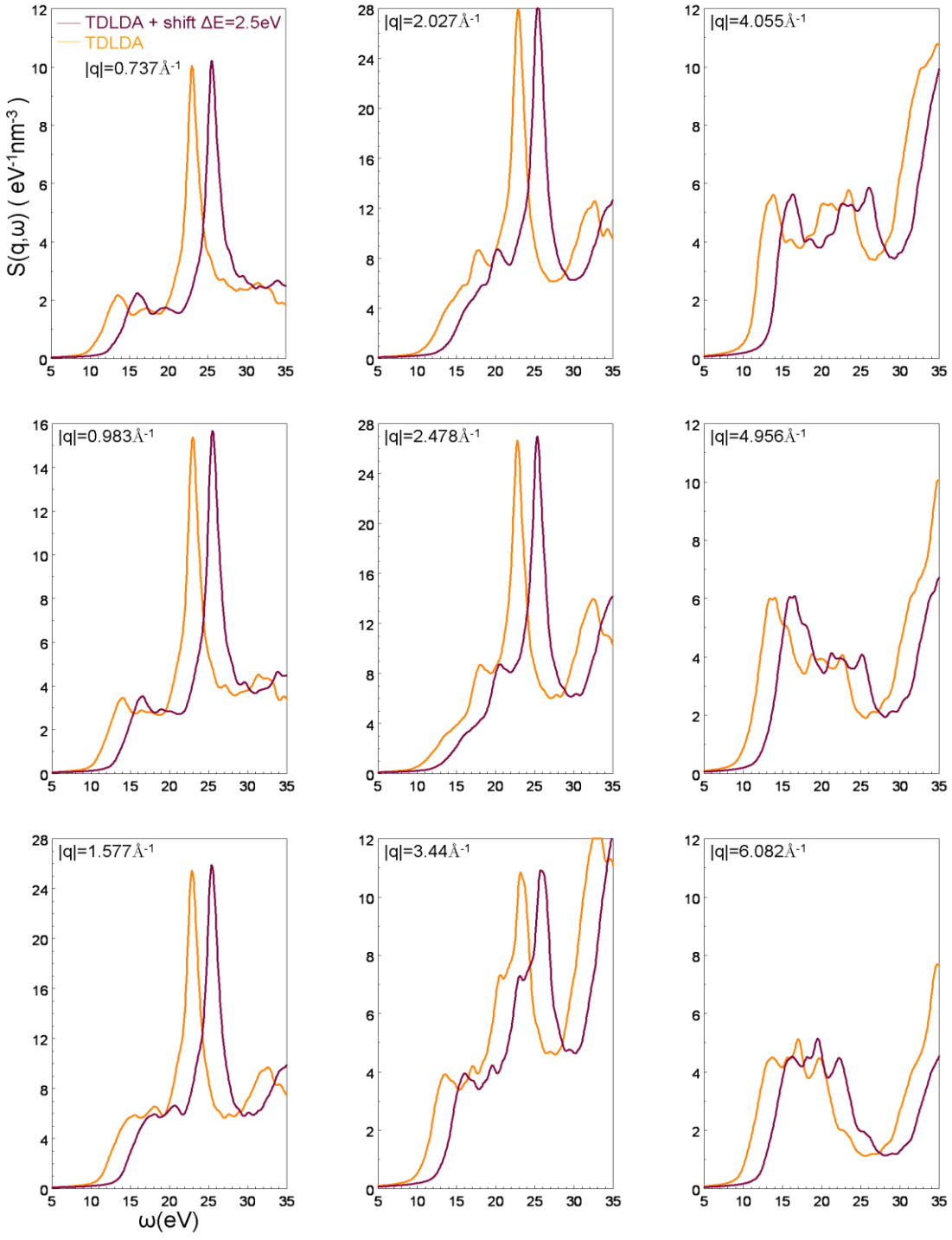

Figure 3.22: The TDLDA spectra with the shift are compared to spectra without shift.

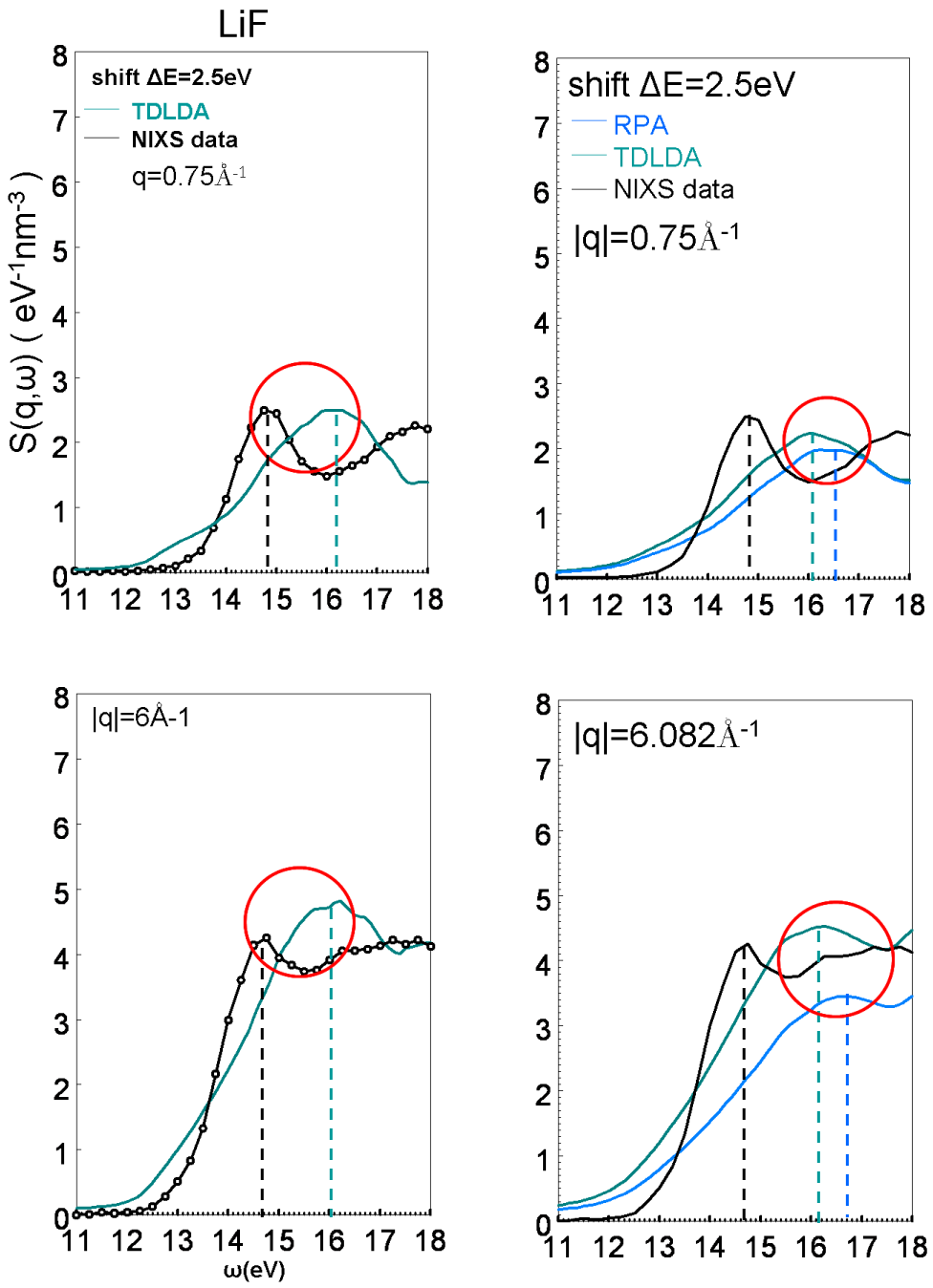

Figure 3.23: On the left panel, the first features are 1.4eV higher than the measurements. On the right panel, fxc only gives 0.5eV shift downward.

But, for the spectrum q=0.75 Å^{-1} and 6Å^{-1}, if we look at the first feature with energy lower than 18eV, they are 1.4eV higher than the measurement (Fig. 3.23). The ALDA kernel f_{XC}^{ALDA} (eq. (3.3.3)) only gives 0.5eV shift downward to the lower energy end which is not enough. To give a big impact on dynamical spectrum for large q, another kernel (the so-called contact model[2]) is introduced here,

$$f_{XC}^{contact}\left(\vec{r},\vec{r}'\right) = -\frac{1}{2}A^{contact}\delta\left(\vec{r}-\vec{r}'\right), \tag{3.3.4}$$

where, A is a constant parameter (expressed in units of $e^2*(a_0)^3$), related to an average value of the expected e-h interaction. It is clear that both ALDA kernel and the contact kernel are local operations. Applying Fourier transformation on eq. (3.3.4), we have

$$f_{XC,contact}^{\vec{G},\vec{G}'}\left(\vec{q}\right) = -\frac{1}{2}A^{contact}\delta_{\vec{G},\vec{G}'}. \tag{3.3.5}$$

We first apply the contact model to the calculation with a 2.5eV shift for the largest q=6Å^{-1} where the dynamical Coulomb screening is weakest among all qs we use (Fig. 3.24). In Fig. 3.24,

1) compared the spectra of A=8.4 with that of A=4.2, the first feature shift to the low energy end about 0.9eV; while the energy difference of the 1st feature between NIXS data and A=4.2 is 1.1eV. There is no change for the 2nd and 3rd feature. But the intensity of the whole spectrum doubly enhanced.

2) the spectrum of A=4.2 is similar to our TDLDA spectrum; and, 4.2 is exactly diagonal value of f_{XC}^{ALDA}, namely, $f_{XC;ALDA}^{\vec{G},\vec{G}}\left(\vec{q}\right) = -A^{contact}$.

3) A=0, the contact model is reduced to the RPA calculation.

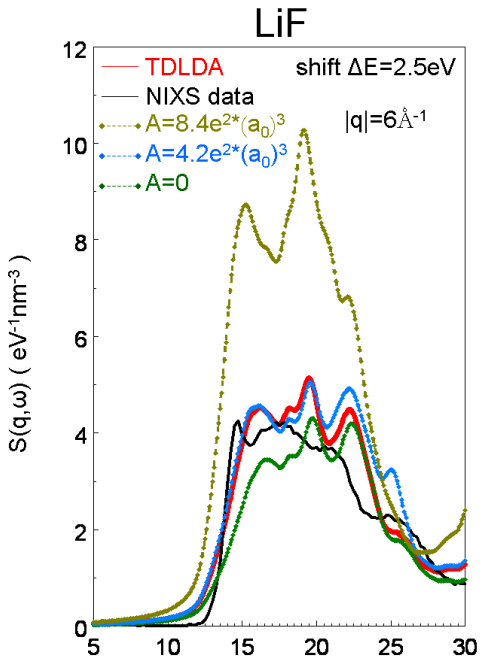

Figure 3.24: The contact model is applied for q=6Å^{-1} with a 2.5eV shift. The spectra roughly keep the same shape but change the intensity.

The contact model looks not totally successful with a shift ΔE=2.5eV. So, we try it on a larger shift ΔE=4.5eV for the same q (Fig. 3.25). However, the result is similar to the discussion above.

For the optical limit, we first introduce a static long-range contribution (LRC) non-local kernel f_{XC}^{static}

$$f_{XC}^{static}\ q\ = -\frac{\alpha^{static}}{q^2}, \tag{3.3.6}$$

where α^{static} is a material-dependent adjustable constant parameter.

We apply the f_{XC}^{static} model to the calculation with a shift 2.5eV for the q=0.75Å^{-1} (Fig 3. 26). We have found:

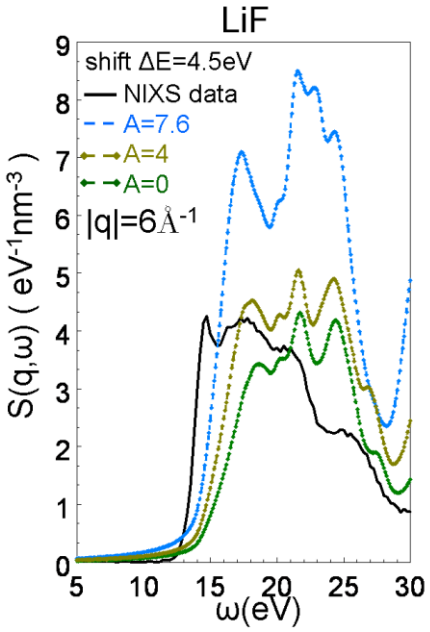

Figure 3.25: The contact model is applied for q=6Å^{-1} with a 4.5eV shift. The spectra still roughly keep the same shape but change the intensity.

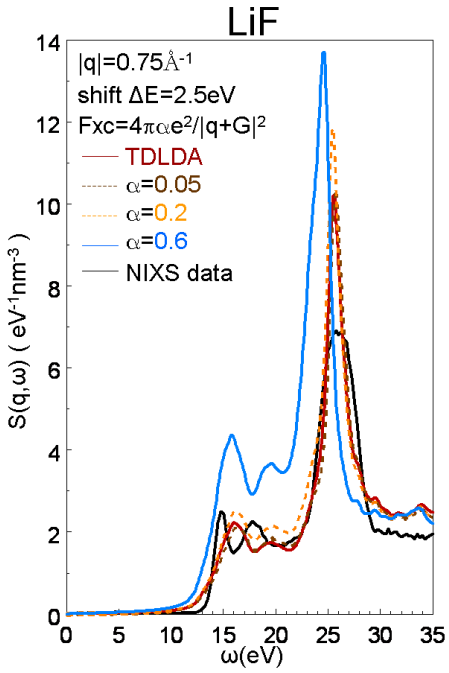

Figure 3.26: The static LRC kernel is applied to the calculation through adjusting parameter α

1) When α=0.05, the spectrum is similar to our TDLDA calculation.

2) When α=0.2, the intensity of spectrum increases without any shifting on the feature positions.

3) When α=0.6, the 1st feature move down by 0.35eV. But, the collective mode move down by 1eV and the intensity of spectrum increases by a large amount,

Clearly, the f_{XC}^{static} model does not help to solve the exciton problem of the 1st feature. Then, we introduce a frequency-dependent LRC kernel

$$f_{XC}^{dyn}\ q\ = -\frac{1}{q^2}\ \alpha + \beta\omega^2\ \ , \tag{3.3.7}$$

where α and β are related to physical quantities, like the dielectric function constant and the plasma frequency.

We apply the f_{XC}^{dyn} model to the calculation for the q=0.225Å^{-1}. When α=1.5 and β=0.0048eV^{-2} is picked, we get similar spectrum as Reining (Fig 3. 27).

Overall, our TDLDA calculations, compared to the new large experimental NIXS data base, suggest that the e-h interaction is modest (Fig. 3.23). The above mentioned energy difference reflects the fact that there is an excitonic binding energy beyond TDLDA, but the height (strength) of the fine structure is comparable with the TDLDA fine structure. We have tried two different type kernels; they do not give us the desired results.

3.3.5 Comparison with previous work

Other authors[73,74,76] have proposed a RPA/GW hybrid method. In order to include

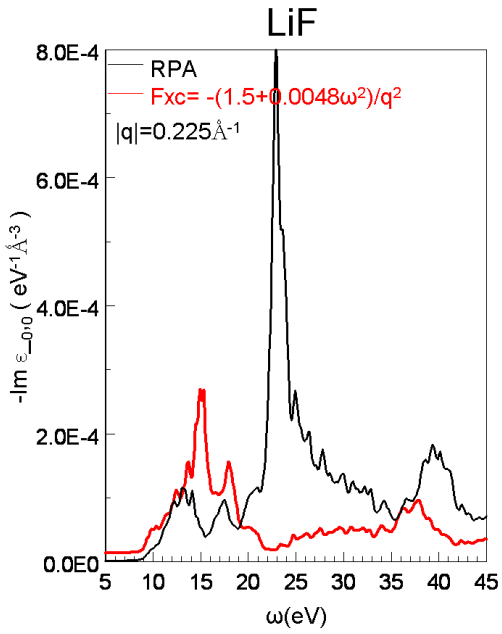

Figure 3.27: The dynamical LRC kernel is applied to the calculation. The spectrum is similar to the Reining's result[76]

excitonic effects in theoretical spectra, they consider the equation of motion for the e–h pair using the two-particle Green's function. It is based on many-body perturbation theory and goes beyond single-particle approximations for the inclusion of excitonic effects.

The x-ray photon with momentum carrying momentum $\vec{q}$ promotes an electron from valence band to conduction band. The excited state WF is obtained by superposing all possible e-h pair WFs $|f\rangle = \sum_{ij,\vec{k}} \psi_{ij}\ \vec{k}\ a^{\dagger}_{i,\vec{k}+\vec{q}} a_{j,\vec{k}} |0\rangle$, where $a^{\dagger}_{i,\vec{k}+\vec{q}}$ creates an electron in the conduction band *i*, and $a_{j,\vec{k}}$ annihilate an electron in the valence band *j*. The e-h pair WF was expanded in terms of LDA single-particle wave functions.

The energy spectrum is obtained by solving the Bethe-Salpeter equation (BSE):

$$\psi_{ij}\left(\vec{k}\right)\left(E_i\left(\vec{k}+\vec{q}\right)-E_j\left(\vec{k}\right)-E\right)=$$
$$-\sum_{i'j'}\int\frac{d\vec{k}'}{2\pi}^3\psi_{i'j'}\left(\vec{k}'\right)\left(2\left\langle i,j;\vec{k}\left|V_{ex}\right|i',j';\vec{k}'\right\rangle-\left\langle i,j;\vec{k}\left|V_{dir}\right|i',j';\vec{k}'\right\rangle\right) \tag{3.3.8}$$

where $E_j\left(\vec{k}\right)$, $E_i\left(\vec{k}+\vec{q}\right)$ are the LDA single-particle energies of valence and conduction electrons, $\left\langle i,j;\vec{k}\left|V_{ex}\right|i',j';\vec{k}'\right\rangle$ and $\left\langle i,j;\vec{k}\left|V_{dir}\right|i',j';\vec{k}'\right\rangle$ represent the exchange screened interaction and direct Coulomb interaction for one e-h pair. The features are shifted by as much as 5eV to higher energies when neglecting direct Coulomb interaction! This method reserves a special role to electron-hole interaction beside the one-body picture.

The inclusion of the e-h interaction drastically alters the spectrum of dynamic structure factor in the case of LiF (Fig. 3.28).

It is noted that the 2nd largest $\vec{q}$ in Fig. 3.29 is similar to our smallest $\vec{q}$. But, we cover a much larger phase space of the excitations (Fig. 3.21). We do overlap with their case q=0.7Å^{-1}, so it is meaningful to compare with them.

Their RPA curves always correspond to a spectrum which is much higher in energy than experiment (e.g., in Soininen and Shirley's calculation, the band gap of the LDA band structure was modified from the LDA value 8.82eV to the GW value of 14.30eV). This is very different from our RPA spectrum, with the "small" value of the shift 2.5eV we use. Then, in their methods, the introduction of the e-h interaction (via Bethe-Salpeter) produces a *large* shift of the spectrum downward (5 eVs). Or in optical limit, via a TDDFT-like method by a long-range contribution model f_{XC}^{LRC}, a sharp feature at the gap develops. The result is that the whole spectrum is controlled by the e-h interaction which in their approaches; and, it may even greatly impact the collective mode in optical limit (Fig. 3.30)!

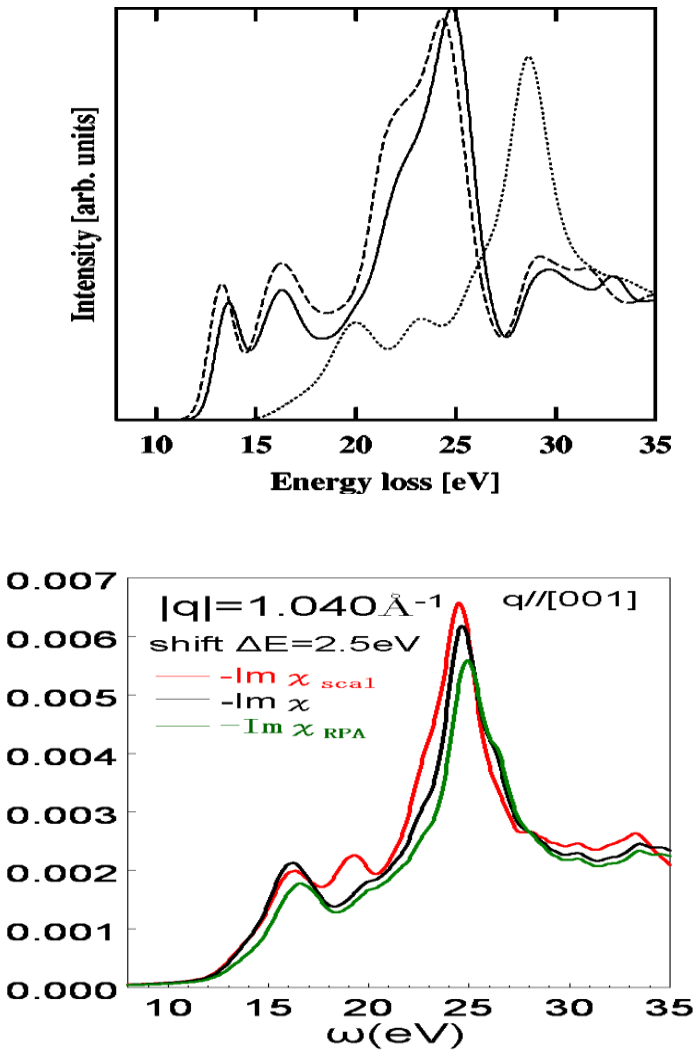

Figure 3.28: On the top panel, it shows theoretical IXS spectrum for LiF for q= 1.12 $Å^{-1}$ // (100) from Soininen-Shirley. The RPA result is given by the dotted line, and the dashed line is the result when CLFE are neglected. The full calculation is given by the solid line. On the bottom panel, the corresponding spectra are calculated by scalar calculation, RPA, and TDDFT respectively.

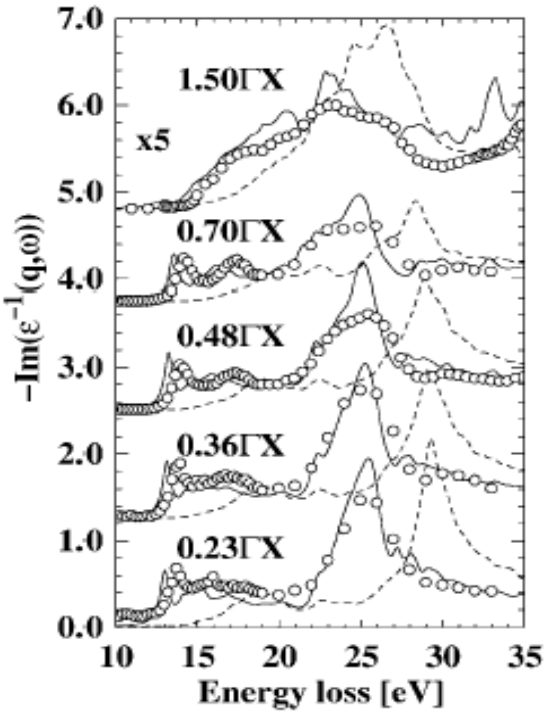

Figure 3.29: The loss spectra of LiF as a function of momentum transfer in the [001] direction calculated by Soininen and Shirley.

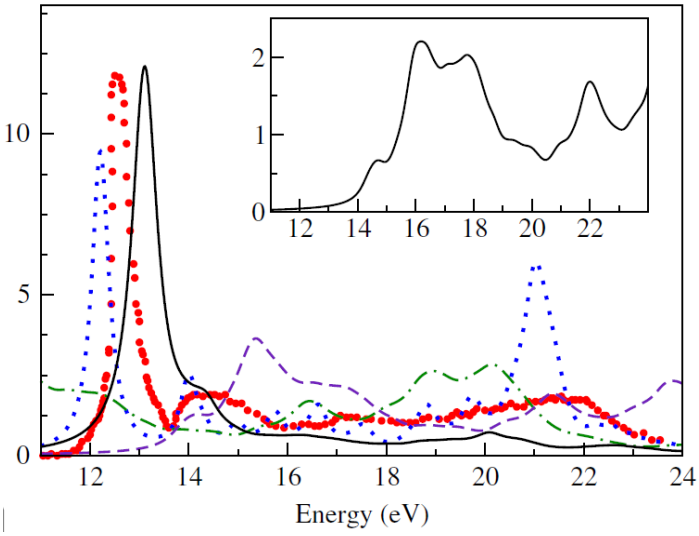

Figure 3.30: Imε of LiF calculated by Reining in optical limit. Dots: optical measurement; dotted curve: BSE; dotted-dashed curve: TDDFT using the f_{XC}^{static}; solid line: TDDFT using the f_{XC}^{dyn}. In the insert: GW-RPA.

Basically, our RPA spectrum is much closer to the NIXS data than those in their work. The inclusion of the "many-body kernel" treated in the ALDA (leading to TDLDA response theory) further improves the agreement with experiment. Our time-dependent density functional theory (TDDFT) calculations offer an alternative picture of the physics of the neutral electron-hole excitations in LiF.

On the discrepancy shifting value, we conduct two types of simply models for the xc kernel on one large and one small q in LiF, to doubly check a combined theoretical method of DFT and MBPT.

The exciton, although appearing at the experimentally predicted value 14eV, suggests that a Frenkel-type exciton is present.

3.3.4 Interplay between electron dynamics and electronic structure

Furthermore, we discuss the relation of the spectrum and the underlying electronic structure. Since dynamical structure factor $S\ \bar{q},\omega$ is proportional to the loss spectrum (Fig. 3.31) and the loss spectrum is mainly a replica of the JDOS (Fig. 3.32), our LDA electronic structure is corrected by a rigid shift all the empty bands upward 2.5eV; whilst, the LDA energy gap is enlarged by 2.5eV, from 9eV to 11.5eV (Fig. 3.33). This rigid shift operator is the so-called "scissor operator". In essence, we use the largest q of NIXS data to check where the "bands should be", for which the LDA does not do a good job, in wide-gap insulators. The update electronic structure is shown by red color (Fig. 3.33). In Fig. 3.32, if JDOS is shifted to the high energy end by 1eV, the 1st feature position in both the update electronic structure and loss spectrum matches well! The e-h combining energy is 1eV in this calculation! At least, the 1st feature of spectra is the exciton!

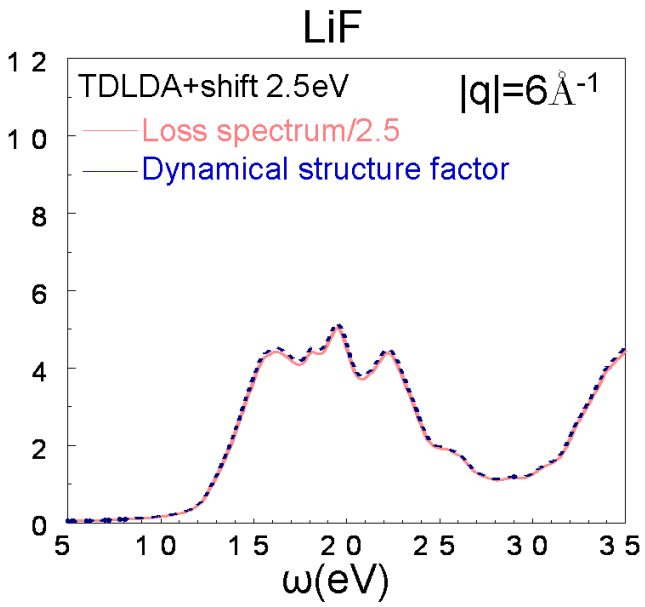

Figure 3.31: Dynamical structure factor is proportional to the loss spectrum. Here, the loss spectrum is reduced by 2.5 than the original data.

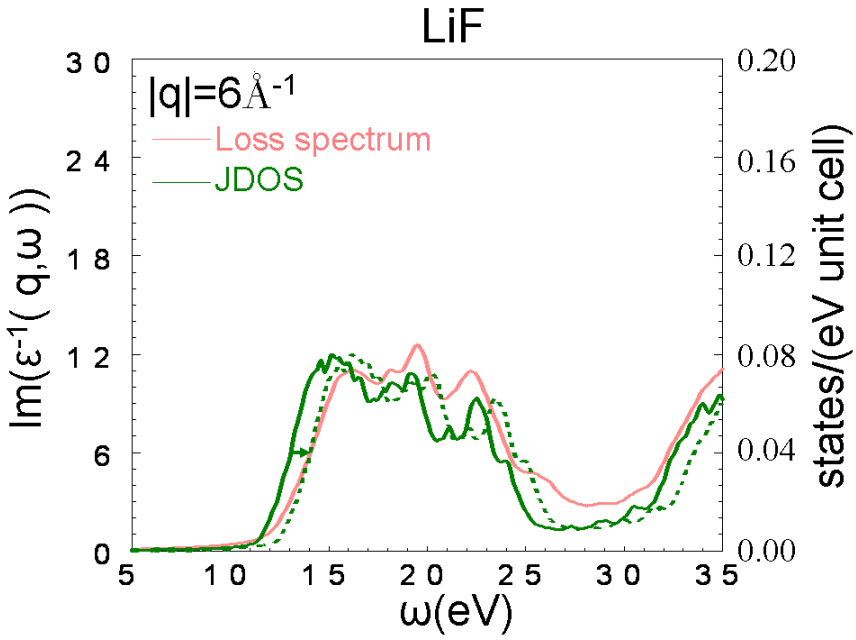

Figure 3.32: The loss spectrum is mainly a replica of the JDOS.

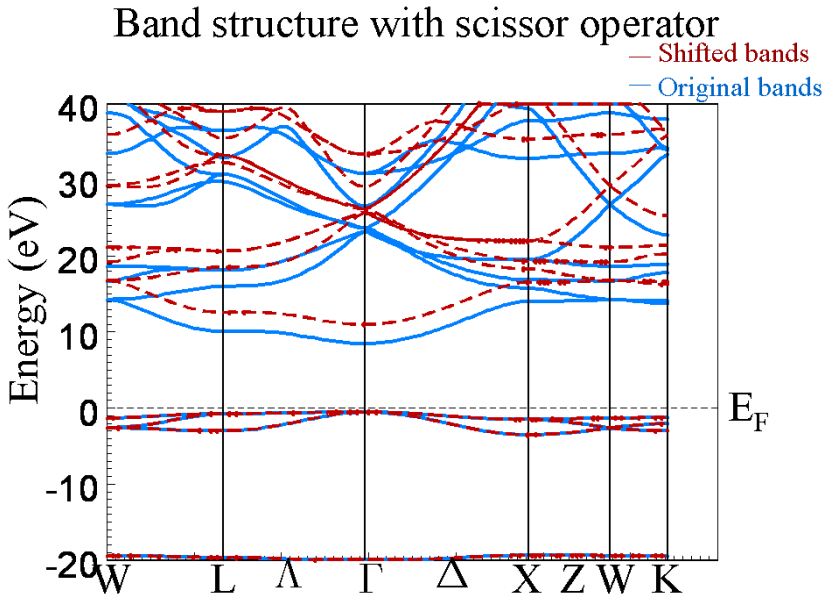

Figure 3.33: The empty bands are lifted by 2.5eV; in addition, LDA energy gap is increased by 2.5eV, from original 9eV to 11.5eV.

At last, we discuss the relation of the collective mode and the underlying electronic structure. The origin of the "wall" in $\varepsilon\ \vec{G}_q,\vec{G}_q;\vec{q},\omega$ (Fig. 3.14) is traced back to JDOS (Fig. 3.11), the energy location (~22eV) of the collective mode is set by the drop-off in the JDOS as we run out of possible p-d channels. This energy scale is cleared visualized in the F^- partial-DOS, associated with the "relative" location of the empty d states and the occupied p states (Fig. 3.9). Although a sharp drop-off in the JDOS is a necessary condition for having a wall in $\varepsilon\ \vec{G}_q,\vec{G}_q;\vec{q},\omega$, it is not a sufficient condition. The strength of the matrix elements (in eq. (3.3.1)) for the imaginary part of KS response function is large, a sharp wall will be presented in $\varepsilon\ \vec{G}_q,\vec{G}_q;\vec{q},\omega$.

LIST OF REFERENCES

LIST OF REFERENCES

Bibliography:

1. A. Sommerfeld, Z. für Physik *Zur Elektronentheorie der Metalle auf Grund der Fermischen Statistik* (*On the Electron Theory Based on the Fermi Statistics*), **47**, 1 and 43 (1927).

2. W. Pauli, Z. für Physik *Über den Zusammenhang des Abschlusses der Elektronengruppen im Atom mit der Komplexstruktur der Spektren* (*On the Connexion Between the Completion of Electron Groups in an Atom with the Complex Structure of Spectra*), **31**, 765 (1925)

3. W. Pauli, Z. für Physik *Über die Quantenmechanik der Elektronen in Kristallgittern* (*About the Quantum Mechanics of the Electrons in Crystal Structures*), **52**, 555 (1928)

4. E. Wigner and F. Seitz, Solid State: Advances in Research and Applications **1**, 97 (1933)

5. A. Wilson, "*The Theory of Electronic Semi-Conductors"* Proc. R. Soc. London A **133**, 458 (1931).

6. C. Kittel, *Introduction to Solid State Physics*, (Wiley; 7th edition, 1995).

7. D. R Hartree,. "*The Wave Mechanics of an Atom with a Non-Coulomb Central Field. Part I-Theory and Methods*" Proceedings of the Cambridge Philosophical Society, **24**, 89-110. (1928) and *The Wave Mechanics of an Atom with a Non-*

Coulomb Central Field. Part II - Some Results and Discussions " Proceedings of the Cambridge Philosophical Society, **46**, 738 (1928).

8. J. C. Slater, *Theory of Complex Spectra*, Phys. Rev. **34**, 1293 (1929).

9. L. D. Landau, *Theory of Fermi-liquids*, Zh. Eksp. Teor. Fiz. **30**, 1058 (1956) [Sov. Phys.- JETP **3**, 920 (1957)], L. D. Landau, *Oscillations in a Fermi-liquid*, Zh. Eksp. Teor. Fiz. **32**, 59 (1956) [Sov. Phys.- JETP **5**, 101 (1957)]

10. V. P. Silin, Zh. Eksp. Teor. Fiz. **33**, 495 (1957), [Sov. Phys.- JETP **6**, 387 (1958)]

11. P. Hohenberg and W. Kohn, *Inhomogeneous Electron Gas*, Phys. Rev. **136**, B864(1964).

12. W. Yang, Y. Zhang, and P. W. Ayers, *Degenerate Ground States and a Fractional Number of Electrons in Density and Reduced Density Matrix Functional Theory*, Phys. Rev. Lett. **84**, 5172 (2000).

13. U. von Barth and J. L. Hedin, *A local exchange-correlation potential for the spin-polarized case:I*, J. Phys. C **5**, 1629(1972); S. H. Vosko, L. Wilk, and M. Nusair, *Accurate spin-dependent electron liquid correlation energies for local spin density calculations: a critical analysis*, Can. J. Phys. **58**, 1200, (1980); W. E. Pickett and J. S. Moodera, *Half Metallic Magnets*, Phys. Today **54**, 39 (2001); H. Eschrig, M. Sargolzaei, K. Koepernik, and M. Richter, *orbital polarization in the Kohn-Sham-Dirac theory*, Europhys. Lett. **72**, 611, (2005); Rudolf Zeller, "*spin polarized DFT calculations and magnetism*", NIC series, Vol. 31, ISBN 3-00-017350-1, pp. 419-455, 2006.

14. N. Marzari, D. Vanderbilt, and M. C. Payne, *Ensemble Density-Functional Theory for ab-intio Molecular Dynamics of Metals and Finite-Temperature Insulators,* Phys. Rev. Lett. **79**, 1337 (1997); M. I. Lubin, O. Heinonen, and M. D. Johnson, *Spin-ensemble density-functional theory for inhomogeneous quantum Hall systems,* Phys. Rev. B **56**, 10373 (1997).

15. E. Engel, S. Keller, A. Facco Bonetti, H. Müller, and R. M. Dreizler, *Local And Non-Local Relativistic Exchange-Correlation Energy Functionals: Comparison To Relativistic Optimized-Potential-Model Results,* Phys. Rev. A **52**, 2750 (1995); E. Engel, S. Keller and R.M. Dreizler, *Generralized Gradient Approximation tor the Rrelativistic Exchange-Only Energy Functional*, Phys. Rev. A **53**, 1367 (1996); E. Engel, S. Keller and R.M. Dreizler, in: "*Electronic Density Functional Theory: Recent Progress and New Directions*", ed. by J.F. Dobson, G. Vignale and M.P. Das (Plenum, New York, 1998); E. Engel, T. Auth, and R. M. Dreizler, *relativistic spin-density-functional theory: Robot solution for single-particle equations for open-subshell atoms*, Phys. Rev. B **64**, 235126 (2001); J. Anton, T. Jacob, B. Fricke, and E. Engel, *Relativistic Density Calculation for Pt2*, Phys. Rev. Lett. **89**, 213001 (2002); J. Anton, B. Fricke, and E. Engel, *Noncollinear and collinear density-functional program for electric and magnetic properties of molecules*, Phys. Rev. A **69**, 012505 (2004); Leonardo Balpassi, Loriano Storchi, Francesco Tarantelli, Antonio Sgamellotti, *Parallelization of a relativistic DFT code*, Future Generations Computer Systems **20**, 739(2004).

16. T. Kreibich, and E. K. U. Gross, *Muticomponent Density-Functional Theory for Electrons and Nuclei*, Phys. Rev. Lett. **86**, 2984 (2001); T. Kreibich, R. Van

Leeuwen and E. K. U. Gross, *Muticomponent Density-Functional Theory*, Springer, Lecture Notes in Physics, 706, 93 (2006).

17. W. Kohn and L. J. Sham, *Self-consistent Equations including Exchange and Correlation Effects*, Phys. Rev. **140**, A1133(1965).

18. J. P. Perdew and Y. Wang, *Accurate and simple analytic representation of the electron-Gas correlation energy*, Phys. Rev. B **45**, 13244(1992).

19. D. M. Ceperly and B. J**.** Alder**,** *Ground State of the Electron Gas by a Stochastic Method*, Phys. Rev. Lett. **45**, 566 (1980).

20. O. Gunnarsson, M. Jonson, and B. I. Lundqvist, *Descriptions Of Exchange And Correlation Effects In A Homogeneous Electron System*, Phys. Rev. B**20**, 3136(1979). R. O. Jones and O. Gunnarsson, *The density functional formalism, its applications and prospects*, Rev. Mod. Phys. **61**, 689(1989).

21. Adolfo G. Eguiluz, Talk on "*Density Functional Theory and its Time-Dependent Extension, in Condensed-Matter Physics*", private communication.

22. S. Pittalis, S. Kurth, N Helbig, and E. K. U. Gross, *Optimized Effective Potential Method in Current-Spin-Density-Functional Theory*, Phys. Rev. A **74**, 062511 (2006); T. Kreibich, S. Kurth, T. Grabo, and E. K. U. Gross, Asymptotic Properties of Optimized Effective Potential, Adv. Quant. Chem. **33**, 31 (1999); M. Petersilka, U. J. Gossmann, and E. K. U. Gross, *Time-Dependent Optimized Effective Potential in the Linear Response Regime*, in "*Electronic Density Functional Theory: Recent Progress and New Direction*", J. F. Dobson, G. Vignale, and M. P. Das, ed(s), (Plenum New York, 1998), P177; T. Grabo, T.

Kreibich, S. Kurth, and E. K. U. Gross, *Orbital Functionals In Density-Functional Theory: The Optimized Effective Potential Method*, in *Strong Correlations in Electronic Structure: Beyond the Local Density Approximation*, edited by v. Anisimov (Gordon and Breach, 1999); T. Grabo, E. K. U. Gross, and M. Lüders, Psi-k Newsletter, 16, 55 (1996).

23. E. Runge and E. K. U. Gross, *Density-Functional Theory for Time-dependent Systems*, Phys. Rev. Lett. **52**, 997(1984).

24. E. K. U. Gross, J. F. Dobson and M. Petersilka, "*Density functional Theory*" edited by R. F. Nalewajski (Springer-Verlag, Berlin, Heidelberg, 1996), Vol. 181, p81; K. Burke and E. K. U. Gross, "*Density Functionals: Theory and Applications*" edited by D. Joubert (Springer, Berlin, 1998), P. 116.

25. Robert van Leeuwen, *Causality and Symmetry in Time-Dependent Density-Functional Theory*, Phys. Rev. Lett. **80**, 1280(1998).

26. T. Kreibich, R. Van Leeuwen and E. K. U. Gross, *Time-Dependent Variational Approach to Molecules in Strong Laser Fields*, Chem. Phys. **304**, 183 (2004); A. Castro, E. Räsänen, A. Rubio and E. K. U. Gross, *Femtosecond laser pulse shaping for enhanced ionization*, Euro. Phys. Lett

27. G. Stefanucci, S. Kurth, E. K. U. Gross, and A. Rubio, *Time dependent transport phenomena, Molecule and nano electronics: analysis, design and simulation*, J. Seminario, ED(s), Elsevier series on Theoretical and Computational Chemistry **17**, 247 (2007); E. Khosravi, S. Kurth, G. Stefanucci and E. K. U. Gross, *The role of bound states in time-dependent quantum transport*, Appl. Phys. A **93**, 355

(2008); G. Stefanucci, S. Kurth, A. Rubio, and E. K. U. Gross, *Time-dependent approach to electron pumping in open quantum systems*, Phys. Rev. B **77**, 075339 (2008); E. Khosravi, G. Stefanucci, S. Kurth and E. K. U. Gross, *Bound States in Ttime-Dependent Quantum Transport: Oscillations and Memory Effects in Current and Density*, Phys. Chem. Chem. Phys. **11**, 4535 (2009); A. Castro and E. K. U. Gross, *Acceleration of optimal quantum control theory algorithms with mixed strategies*, Phys. Rev. E **79**, 056704 (2009).

28. M. S. Hybertsen and S. G. Louie, *Electron correlation in semiconductors and insulators: Band gaps and quasiparticle energies*, Phys. Rev. B **34**, 5390 (1986).

29. P. Fazekas, Lecture Notes on "*Electron Correlation and Magnetism*" (World Scientific, Singapore, 1999)

30. P. Fulde, *Wave-function methods in electronic-structure theory of solids*, Advances in Physics **51**, 909 (2002)

31. Gabriele F. Giuliani and Giovanni Vignale, *Quantum Theory of the Electron Liquid* (Cambridge university press, 2005)

32. J. J. Quinn and R. A. Ferrell "*Electron Self-Energy Approach to Correlation in a Degenerate Electron Gas*", Phys Rev., **112**, 812 (1958)

33. L. Hedin, "*New Method for Calculating the One-Particle Green's Function with Application to the Electron-Gas Problem"* ,Phys. Rev. **139**, A796 (1965).

34. P. Puschnig, dissertation on "*Excitonic Effects in Organic Demi-Conductors, An Ab-initio Study within the LAPW Method*" in 2002; Giovanni Onida, Lucia

Reining, and Angel Rubio, *Electronic excitations: density-functional versus many-body Green's-function approaches*, Rev. Mod. Phys. **74**, 601 (2002).

35. A. A. Quong and Adolfo G. Eguiluz, *First-Principles Evaluation of Dynammical Response and Plasmon Dispersion in Metals*, Phy. Rew. B 70, 3955 (1993).

36. K.-H. Lee and K. J. Chang, *Analytic continuation of the dynamical response function using an N-point padé approximant*, Phys. Rev. B **54**, R8285 (1996).

37. W. Ku and A. G. Eguiluz, *Plasmon Lifetime in K: A Case Study of Correlated Electrons in Solids Amenable to Ab Initio Theory*, Phys. Rev. Lett. **82**, 2350 (1999). A. G. Eguiluz, W. Ku and J. M. Sullivan, "*Dynamical response of correlated electrons in solids probed by inelastic scattering experiments: an ab initio theoretical perspective"*, J. Phys. Chem. Solids **61**, 383 (2000).

38. I. G. Gurtubay, W. Ku, J. M. Pitarke, A. G. Eguiluz, B. C. Larson, J. Tischler, and P. Zschack, *Large crystal local-field effects in the dynamical structure factor of rutile TiO_2*, Phys. Rev. B **70**, 201201(2004); I. G. Gurtubay, J. M. Pitarke, Wei Ku, A. G. Eguiluz, B. C. Larson, J. Tischler, P. Zschack, and K. D. Finkelstein, "*Electron-hole and Plasmon excitations in 3d transition metals: Ab initio calculations and inelastic x-ray scattering measurements"*, Phys. Rev. B **72**, 125117 (2005).

39. B. C. Larson, W. Ku, J. Z. Tischler, C.-C. Lee, O. D. Restrepo, A. G. Eguiluz, P. Zschack, and K. D. Finkelstein, *Nonresonant Inelastic X-Ray Scattering and Energy-Resolved Wannier Function Investigation of d-d Excitations in NiO and CoO*, Phys. Rev. Lett. **99**, 026401(2007).

40. K Hämäläinen and S Manninen, *Resonant And Non-Resonant Inelastic X-Ray Scattering*, J. Phys.: Condens. Matter **13**, 7539 (2001); W. Schülke, *Eelctronic Excitations Investigated By Inelastic X-Ray Scattering Spectroscopy*, J. Phys.: Condens. Matter **13**, 7557 (2001).

41. G. E. Jellison, Jr., and F. A. Modine, "*Two-Modulator Generalized Ellipsometry: Experiment And Calibration"*, Appl. Opt. **36**, 8184 (1997); Two-modulator generalized ellipsometry: theory, Appl. Opt. **36**, 8190 (1997).

42. A. G. Eguiluz, O. D. Restrepo, B. C. Larson, J. Z. Tischler, P. Zschack, and G. E. Jellison, *Electron-hole excitations in NiO: LSDA+U-based calculations vs. inelastic X-ray scattering and ellipsometry measurements*, J. Phys. Chem. Solids **66**, 2281 (2005). Y. Q. Cai, P. C. Chow, O. D. Restrepo, Y. Takano, K. Togano, H. Kito, H. Ishii, C. C. Chen, K. S. Liang, C. T. Chen, S. Tsuda, S. Shin, C. C. Kao, W. Ku, and A. G. Eguiluz, "*Low-Energy Charge-density Excitations in MgB2: Striking Interplay between Single-Particle and Collective Behavior for Large Momenta"*, Phys. Rev. Lett. **97**, 176402 (2006).

43. E. D. Isaacs, P. M. Platzman, M. Metcalf, and J. M. Honig, "*Inelastic X-Ray Scattering Study of the Metal-Antiferromagnetic Insulator Transition in V_2O_3"*, Phy. Rev. Lett. **77**, 1346 (1996); I. V. Solovyev, Z. V. Pchelkina, and V. I. Anisimov, "*Construction of Wannier functions from Localized Atomic Orbitals"*, Phys. Rev. B **75**, 045110 (2007).

44. K. Yang, L. P. Chen, Y. Q. Cai, N. Hiraoka, S. Li, J. F. Zhao, D. W. Shen, H. F. Song, H. Tian, L. H. Bai, Z. H. Chen, Z. G. Shuai, and D. L. Feng, *Inelastic X-*

Ray Scattering Study of Exciton Property in an Organic Molecular Crystal, Phys. Rev. Lett. **98**, 036404 (2007).

45. G. W. Crabtree and N. S Lewis, "*Solar Energy Conversion*", Phys. Today, 60, 31 (2007).

46. S. Cottenier, "*DFT And The Family Of (L)APW-Methods: A Step-By-Step Introduction"*, http://fys.kuleuven.be/iks/nvsf/publications/DFT_and_LAPW.pdf

47. J. T. Chayes, L. Chayes and M. B. Ruskai, "*Density Functional Approach To Quantum Lattice Systems"*, J. Stat. Phys. 38, 497 (1985)

48. O. Gunnarsson, M. Jonson, and B. I. Lundqvist, "*Descriptions of exchange and correlation effects in a homogeneous electron system"*, Phys. Rev. B 20, 3136 (1979).

49. J. P. Perdew, J. A. Chevary, S. H. Vosko, K. A. Jackson, M. R. Pederson, D. J. Singh, and C. Fiolhais, "*Atoms, Molecules, Solids, And Surfaces: Applications Of Generalized Gradient Approximation For Exchange And Correlation"*, Phys. Rev. B **46**, 6671 (1992); Erratum: Phys. Rev. B **48**, 4978 (1993). J. P. Perdew, K. Burke, and M. Ernzerhof, "*Generalized Gradient Approximation Made Simple*," Phys. Rev. Lett. **77**, 3865 (1996).

50. J. Tao, J. P. Perdew, V. N. Staroverov and F. E. Scuseria, "*Climbing the Functional Ladder: Nonemprical Meta-Generalized Gradient Approximation designed for Molecules and Solids"*, Phys. Rev. Lett. **91**, 146401 (2003).

51. J. C. Cuevas, Lecture Note on "*Introduction to Density Functional Theory*", http://www-tfp.physik.uni-karlsruhe.de/~cuevas.

52. Z. Wu and R. E. Cohen, "*More Accurate Generalized Gradient Approximation On Solids"*, Phys. Rev. B **73**, 235116 (2006); L. A. Constantin, J. P. Perdew, and J. Tao, "*Meta-Generalized Gradient Approximation For Exchange-Correlation Hole With An Application To The Jellium Surface Energy"*, Phys. Rev. B **73**, 205104 (2006)

53. A. G. Eguiluz, Lecture Note on "*Density Functional Theory: A Theory of Everything*?" private communication.

54. V. I. Anisimov and O. Gunnarsson, "*Density-Functional Calculation Of Effective Coulomb Interactions In Metals"*, Phys. Rev. B **43**, 7570 (1991).

55. V. I. Anisimov, Jan Zaanen, and O. K. Gunnarsson, "*Band Theory and Mott Insulators: Hubbard U Instead of Stoners I"*, Phys. Rev. B **44**, 943 (1991).

56. V. I. Anisimov, I. V. Solovyev, and M. A. Korotin, "*Density-Functional Theory And Nio Photoemission Spectra"*, Phys. Rev. B **48**, 16929 (1993).

57. A. I. Liechtenstein, V. I. Anisimov, and J. Zaanen, "*Density-Functional Theory And Strong Interactions: Orbital Ordering In Mott Insulators"*, Phys. Rev. B **52**, R5467 (1995).

58. M. T. Czyzyk and G. A. Sawatzky, "*Local-Density Functional And On-Site Correlations: The Electronic Structure Of La2CuO4 And LaCuo3"*, Phys. Rev. B **49**, 14211 (1994).

59. A. B. Shick, A. I. Liechtenstein, W. E. Pickett, "*Implementation Of The LDA+U Method Using The Full-Potential Liearized Augmented Plane-Wave Basis"*, Phys. Rev. B **60**, 10763 (1999).

60. V Peuckert 1978 "*A New Approximation Method For Electron Systems*" J. Phys. C: Solid State Phys. **11** 4945 (1978)

61. A. Zangwill and Paul Soven, "*Density-Functional Approach To Local-Field Effects In Finite Systems: Photoabsorption In The Rare Gases*", Phys Rev A ,**21**, 1561 (1979)

62. Deb B M and Ghosh S K *"Schroedinger Fluid Dynamics Of Many-Electron Systems In A Time-Dependent Density-Functional Framework"* J. Chem. Phys. **77** 342 (1982); Deb B M and Ghosh S K *"New Method For The Direct Calculation Of Electron Density In Many-Electron Systems. I. Application To Closed-Shell Atoms"* Int. J. Quantum Chem. **23** 1 (1983)

63. L. J. Bartolotti, "*Time-Dependent Extension Of The Hohenberg-Kohn-Levy Energy-Density Functional*" ,Phys Rev A ,**24**, 1661 (1981); L. J. Bartolotti, "*Time-Dependent Kohn-Sham Density-Functional Theory*", Phys Rev A, **26**, 2243 (1982); L. J. Bartolotti, ,Phys Rev A, Erratum **27**, 2248 (1983); L. J. Bartolotti, *"Variation-Perturbation Theory Within A Time-Dependent Kohn–Sham Formalism: An Application To The Determination Of Multipole Polarizabilities, Spectral Sums, And Dispersion Coefficients"* J. Chem. Phys. **80**, 5687 (1984) ; L. J. Bartolotti, "*Velocity Form Of The Kohn-Sham Frequency-Dependent Polarizability Equations*", Phys Rev A, **36**, 4492 (1987)

64. R. van Leeuwen, "*Mapping from Densities to Potentials in Time-Dependent Density-Functional*" Theory, Phys. Rev. Lett. **82**, 3863(1999)

65. C. A. Ullrich, U. Gossmann and E. K. U. Gross, "*Time-Dependent Optimized Effective Potential*", Phys. Rev. Lett. **74**, 872(1995)

66. V. I. Anisimov, Jan Zaanen, and O. K. Gunnarsson*, "Band Theory and Mott Insulators: Hubbard U Instead of Stoners I"*, Phys. Rev. **B** 44, 943 (1991)

67. John J. Quinn and Kyung-soo Yi, "Lectures on Solid State Physics", P85, Springer, 1st edition, 2009.

68. A. W. Overhauser, *Multiplet Structure of Excitons in Ionic Crystals*, Phys. Rev. **101**, 1702 (1956).

69. J. R. Fields, P. C. Gibbons and S. E. Schnatterly, *Electronic Excitations in LiF*, Phys. Rev. Lett. **21**, 430 (1977).

70. D. M. Roessler and W. C. Walker, *Optical Constants of Magnesuum Oxide and Lithium Fluoride in the Far Ultraviolet*, J. Opt. Soc. Am. **57**, 835 (1967).

71. Neil W. Ashcroft and N. David Mermin, Solid State Physics, Thomsom Learning Inc., 1st edition, 1976.

72. J. Z. Tischler, B. C. Larson, P. Zschack, A. Fleszar and A. G. Eguiluz, *Interplay between inelastic X-ray scattering and ab initio density-response calculations: Insight into the electronic correlations in aluminum*, Phys. Stau. Sol. 237, 280 (2003)

73. W. A. Caliebe, J. A. Soininen, Eric L. Shirley, C. –C. Kao, and K. Hämäläinen, *Dynamical Structure Factor of Diamond and LiF Measured Using Inelastic X-Ray Scattering*, Phys. Rev. Lett. 84, 3907 (2000). L. X. Benedict and E. L.

Shirley, *Ab initio calculation of $\varepsilon_2(\omega)$ including the electron-hole interaction: Application to GaN and CaF_2*, Phys. Rev. B **59**, 5441 (1999); J. A. Soininen and E. L. Shirley, *Effects of electron-hole interaction on the dynamical structure factor: Application to nonresonant inelastic x-ray scattering*, Phys. Rev. B, 61, 16423 (2000).

74. M. Rohlfing, and S. G. Louie, *Electron-hole in semiconductors and insulators*, Phys. Rev. Lett. **81**, 2312 (1998), M. Rohlfing, and S. G. Louie, *Electron-hole excitations from first principles*, Phys Rev B, **62**, 4927 (2000).

75. D. Pines, "*Elementary excitations in solids"* (W. A. Benjamine, Inc.), 1963.

76. S. Botti, A. Schindlmayr, R. Del Sole and L. Reining, *Time-dependent density-functional theory for extended systems*, Rep. Prog. Phys. 70, 357 (2007), S. Botti, A. Fourreau, F. Nguyen, Y-O Renault, F. Sottile and L. Reining, *Energy dependence of exchange-correlation kernel of time-dependent density functional theory: A simple model for solids*

77. J. J. Sakurai, "*Advanced Quantum Mechanics*" (Addison Wesley. 1967).

78. D. J. Singh, "*Planewaves, Pseudopotentials and The LAPW Method*" (Kluwer Academic Publishers, 1994). P. Blaha, K. Schwarz, G. K. H. Madsen, D. Kvasnicka and J. Luitz, "WIEN2k, "*An Augmented Plane Wave + Local Orbitals Program for Calculating Crystal Properties*" (Karlheinz Schwarz, Techn. Universität Wien, Austria), 2001. ISBN 3-9501031-1-2.

79. P. Blaha, K. Schwarz, et al., "*WIEN2k - Usersguide*", http://www.wien2k.at/reg_user/textbooks/

80. D. Singh, "*Simultaneous Solution Of Diagonalization And Self-Consistency Problems For Transition-Metal Systems*", Phys. Rev. **B** 40, 5428 (1989). D. Singh, "*Ground-state Properties of Lanthanum*: *Treatment Of Extended-Core States"*, Phys. Rev. B **43**, 6388 (1991).

81. J. P. Perdew, K. Burke, and M. Ernzerhof, "*Generalized Gradient Approximation Made Simple"*, Phys. Rev. Lett. **77**, 3865 (1996)..

82. J. P. Perdew, S. Kurth, A. Zupan, P. Blaha, "*Accurate Density Functional With Correct Formal Properties: A Step Beyond The Generalized Gradient Approximation"*, Phys. Rev. Lett. **82**, 2544 (1999); *Erratum:*, Phys. Rev. Lett. **82**, 5179 (1999).

83. J. P. Perdew, A. Ruzsinszky, G. Csonka, O. A. Vydrov, G. E. Scuseria, L. A. Constantin, X. Zhou, and K. Burke, "*Restoring The Density-Gradient Expansion For Exchange In Solids And Surfaces"*, Phys. Rev. Lett. **100**, 136406 (2008); Erratum: "*Restoring the Density-Gradient Expansion for Exchange in solids and Surfaces"*, Phys. Rev. Lett. **102**, 039902 (2009). A. E. Mattsson, R. Armiento, and T. R. Mattsson, Comment on "*Restoring the Density-Gradient Expansion for Exchange in Solids and Surfaces*", Phys. Rev. Lett. **101**, 239701 (2008). John P. Perdew et al., Reply:, Phys. Rev. Lett. **101**, 239702 (2008).

84. J. Stoer, R. Bulirsch, "*Intoduction to numerical Analysis"*, Springer-Verlag, New York, 1993).

85. D. Singh, H. Krakauer, and C. S. Wang, "*Accelerating The Convergence Of Self-Consistent Linearized Augmented-Plane-Wave Calculations"*, Phys. Rev. **B** 34, 8391 (1986)

86. John David Jackson, "Classical Electrodynamics" (John Wiley and Sons Inc., 3rd Edition, 1999), p471

87. D. D. Koeling and G. O. Arbman, "*Use Of Energy Derivative Of The Radial Solution In An Augmented Plane Wave Method: Application To Copper"*, J. Phys. F: Met. Phys., **5**, 2041 (1975); D. D. Koeling and B. N. Harmon, "*A Technique For Relativistic Spin-Polarized Calculations"*, J. Phys. C: Solid State Phys., **10**, 3107 (1977); D. D. Koeling, Technical Notes "*Linearized Form Of The APW Method*", J. Phys. Chem. Solids, **33**, 1335 (1972).

88. M. E. Rose, "*Elementary Theory of Angular Momentum*" (Dover Publications, INC. New York, 1995)

89. .B. Kohler, S. Wilke, M. Scheffler, R. Kouba, C. Ambrosch-Draxl, "*Force Calculation And Atomic Structure Optimization For The Full-Potential Linearized Augmented Plane-Wave Code WIEN"*, Computer Physics Communications, **94**, 31 (1996).

90. C. Ambrosch-Draxl and J. O. Sofo, "*Linear Optical Properties Of Solids Within The Full-Potential Linearized Augmented Planewave Metho"d*, Computer Physics Communications, **175**, 1 (2006).

91. P. E. Blöchl, O. Jepsen, and O. K. Anderson, "*Improved Tetrahedron Method For Brillioun Zone Integrations"*, Phys. Rev. B **43**, 6388 (1991); A. H. Macdonald, S.

H. Vosko, and P. T. Coleridge, *Extensions Of The Tetrahedron Method For Evaluation Spectral Properties Of Solids*, J. Phys. C: Solid State Phys., **12**, 2991(1979).

APPENDICES

APPENDIX A

DIRAC EQUATION

Dirac equation is the relativistic generalization of Schrödinger equation, describing a spin-$\frac{1}{2}$. In the presence of an electromagnetic field and an external potential is written as[77]

$$i\hbar\frac{\partial\psi}{\partial t} = H\psi = \left[c\vec{\alpha}\cdot\left(\vec{p} - \frac{e\vec{A}}{c}\right) + \beta mc^2 + V\right]\psi \tag{A.1}$$

where c is the speed of light, $\vec{p} = -i\hbar\vec{\nabla}$, and the 4×4 matrices are written in terms of Pauli matrices

$$\alpha_i = \begin{pmatrix} 0 & \sigma_i \\ \sigma_i & 0 \end{pmatrix} \quad \beta = \begin{pmatrix} 1 & 0 \\ 0 & -1 \end{pmatrix} \tag{A.2}$$

with

$$\sigma_1 = \begin{pmatrix} 0 & 1 \\ 1 & 0 \end{pmatrix} \quad \sigma_2 = \begin{pmatrix} 0 & -i \\ i & 0 \end{pmatrix} \quad \sigma_3 = \begin{pmatrix} 1 & 0 \\ 0 & -1 \end{pmatrix} \tag{A.3}$$

The eigensystem problem in the presence of an spherical potential V written as

$$\left(-i\hbar c\vec{\alpha}\cdot\vec{\nabla} + \beta mc^2 + V(r)\right)\psi(\vec{r}) = E\psi(\vec{r}) \tag{A.4}$$

In this case, the Hamiltonian commute with J^2, J_z, and $K = \beta\vec{\Sigma}\cdot\vec{J} - \hbar\beta/2$, where $\vec{J} = \vec{L} + \hbar\vec{\Sigma}/2$, $\Sigma_i = \begin{pmatrix} \sigma_i & 0 \\ 0 & \sigma_i \end{pmatrix}$ and $\vec{L} = \vec{r}\times\vec{p}$ is the angular momentum. The proof that these commutators are zero can be easily done using $[x_i, p_j] = i\hbar\delta_{ij}$, $[\beta, \alpha_i] = -2\alpha_i$ and Pauli matrix property $[\sigma_i, \sigma_j] = 2ie_{ijk}\sigma_k$ with e_{ijk} being the Levi-Civita tensor. The wavefunctions will be indexed by j, m, and κ $\psi_{n\kappa jm}$ with

$J^2 y_{nkjm} = j(j+1)\hbar^2 y_{nkjm}$, $J_z y_{nkjm} = m y_{nkjm}$, $K y_{nkjm} = k\hbar y_{nkjm}$ One can notice that $K^2 = \hat{J}^2 + 1/4$, which leads to $k = \pm\left(j + 1/2\right)$. It is clear that the Hamiltonian does not commute individually with angular momentum and spin operators, and only the total angular momentum is a good quantum number. Adding the angular and spin momentum $j = l \pm 1/2$. By noticing that $\vec{S}\cdot\vec{J} = \vec{J}^2 - \vec{L}^2 - 3\hbar^2/4$ and introducing it into the definition of $\hat{K}$, it is clear that $k > 0$ corresponds $j = l + 1/2$, $(k = l + 1)$ and $k > 0$ corresponds to $j = l - 1/2$, $(k = -l)$

With the these facts in mind, we can write the general solution of eq. (A.4) as

$$y_{nkjm} = \begin{pmatrix} f_{nkj}(r)\, j_{kjm} \\ i g_{nkj}(r) \dfrac{\vec{S}\cdot\vec{r}}{r} j_{kjm} \end{pmatrix} \tag{A.5}$$

where

$$j_{kjm} = \begin{cases} \sqrt{\dfrac{j+m-1}{2j}}\, Y^{m-\frac{1}{2}}_{j-\frac{1}{2}} \begin{pmatrix} 1 \\ 0 \end{pmatrix} + \sqrt{\dfrac{j-m-1}{2j}}\, Y^{m+\frac{1}{2}}_{j-\frac{1}{2}} \begin{pmatrix} 0 \\ 1 \end{pmatrix}, & k > 0 \\ \sqrt{\dfrac{j-m-1}{2j}}\, Y^{m-\frac{1}{2}}_{j+\frac{1}{2}} \begin{pmatrix} 1 \\ 0 \end{pmatrix} - \sqrt{\dfrac{j+m+1}{2j}}\, Y^{m+\frac{1}{2}}_{j+\frac{1}{2}} \begin{pmatrix} 0 \\ 1 \end{pmatrix}, & k < 0 \end{cases} \tag{A.6}$$

The radial functions satisfy the following equations:

$$\begin{aligned} &-\frac{\hbar^2}{2M}\frac{1}{r^2}\frac{d}{dr}\left(r^2 \frac{df_{nkj}}{dr}\right) + \left[V + \frac{\hbar^2}{2M}\frac{l(l+1)}{r^2}\right] f_{nkj} - \frac{\hbar^2}{4M^2c^2}\frac{dV}{dr}\frac{df_{nkj}}{dr} - \\ &-\frac{\hbar^2}{4M^2c^2}\frac{dV}{dr}\frac{1-k}{r} f_{nkj} = e\, f_{nkj} \end{aligned} \tag{A.7}$$

and

$$\frac{dg_{nkj}}{dr} + \frac{1+k}{r} g_{nkj} = \frac{1}{\hbar c}(V - e) f_{nkj} \tag{A.8}$$

where $e = E - mc^2$ and $M = m + \left(E - mc^2 - V(r)\right)/2c^2$.

In eq. (A.7), we need notice that the first two terms are similar to the non-relativistic Schrödinger equation, the relativistic effects being included only in the mass *M*.. Kinetic energy, potential, and centrifugal term are all present. The last two terms are clearly relativistic corrections $\left(\mu\ 1/\left(Mc^2\right)\right)$. They are Darwin term and spin-orbit coupling term. If one considered spin-orbit term as small, the eq. (A.7) and (A.8) depend only on *n* and l. They are solved using the same techniques as the non-relativistic counterparts. Spin-orbit can later be added perturbatively using the Hamiltonian:

$$H_{SO} = \frac{\hbar^2}{4M^2c^2}\frac{1}{r}\frac{dV}{dr}\vec{L}\times\vec{s} \tag{A.9}$$

APPENDIX B

LAPW METHOD

The linearized augmented plane wave (LAPW) method is one of choices to solve the KS equations. It is used to calculate the density-functional-based electronic structure and total energy calculation. Modern implementations allow the use of a number of approximations to exchange and correlation (LDA, GGA, and LDA+U, among others) and make no approximations to the shape of the crystal potential in order to obtain a physically reasonable result via all-electron ab initio electronic-structure calculation. In practice, core and valence electrons are treated separately[†]. All (chemical) kinds of atoms are treated on the same footing[†]. Like most modern electronic-structure methods, the LAPW method is a variational expansion approach which solves the equations of DFT by approximating KS wave function as a finite linear combination of basis functions.

The basis set used for expanding the eigenstates of the solid state Hamiltonian is required to be unbiased (it should not, in a hidden way, force the solution into a built-in direction) and efficient (the total number of basis functions included in it should be as low as possible).

The LAPW basis is constructed to be reasonably accurate and efficient for the solution of KS problem. The solutions are rapidly varying and atomic-like (like isolated-atom solutions) near the atoms but more smoothly varying and not atomic-like

[†] A relativistic treatment for core electrons is required. In a new development (super-LAPW), for example, core electrons could be regarded as valence electrons with arbitrary number of local orbitals allowed.

[†] the same R^{MT}, $R_I^{\min} \cdot G_{\max}$, $\ell_{\max}$ and energy window

throughout the rest of the unit cell. The primitive unit cell is partitioned into two regions: non-overlapping atom-centered spheres (so-called muffin tin (MT) spheres) and the remaining interstitial (figure B.1), like in APW. The I[th] atomic sphere is presented in the primitive unit cell. $\vec{x}$ is the position vector starting from the origin of the primitive unit cell, $\vec{X}_I$ indicates the position of the I[th] sphere with respect to the same origin, and the $\vec{r}$ vector is referred to a local coordinate that originates at the center of each sphere. The relation among $\vec{x}$, $\vec{X}_I$, and $\vec{r}$ is $\vec{x} = \vec{X}_I + \vec{r}$.. The LAPW basis functions are then constructed by connecting plane waves (sinusoidal functions) in the interstitial region to linear combinations of atomic-like functions in the spheres. The atomic-like nature of the LAPW basis in the vicinity of the atoms leads to an efficient representation, whilst the plane wave nature in the interstitial region allows highly accurate solutions for any atomic arrangement: close-packed or open, high-symmetry or low, surfaces or bulk[78].

However, instead in the APW method the radial function is constructed only at the unknown eigenvalue E_l^I (the single-particle orbital energy) and lacks variational freedom to allow WF changing as the band energy deviates from this reference. It will take more time to repeat the same procedure solving the secular equation to reach density and energy tolerance. In the LAPW method the energy dependent radial part $u_l^I(r, \varepsilon_{\vec{k}}^n)$ of the basis function for the valence states (which leak out of the MT sphere) is linearized by a Taylor expansion at the energy $E_{1,l}^I$ (near the center of the l- valence-band). The radial part can be written as

$$u_l^I(r, \varepsilon_{\vec{k}}^n) = u_l^I(r, E_{1,l}^I) + (E_{1,l}^I - \varepsilon_{\vec{k}}^n) \underbrace{\left.\frac{\partial u_l^I(r,E)}{\partial E}\right|_{E=E_{1,l}^I}}_{\dot{u}_l^I(r, E_{1,l}^I)} + O(E_{1,l}^I - \varepsilon_{\vec{k}}^n)^2 , \qquad \text{(B.1)}$$

where $\varepsilon_{\vec{k}}^{n}$ is the eigenenergy of the n^{th} band for the given $\vec{k}$ wave vector, $\dot{u}_l^I(r,\varepsilon_{\vec{k}}^{n})$ is the energy derivative of $u_l^I(r,\varepsilon_{\vec{k}}^{n})$. This approximation is justified if one finds the eigenvalue

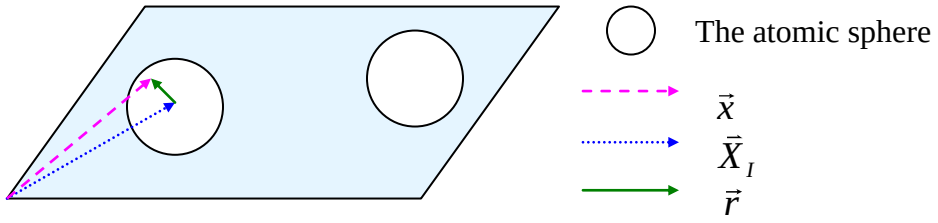

Figure B.1: The Ith atomic sphere in the primitive unit cell.

not far from $E_{1,l}^I$. Using plane wavefunctions in the interstitial region and spherical harmonics for the MT sphere, the basis ϕ function can be written as follows:

$$\phi^{I,\vec{k}+\vec{G}}(\vec{x}) = \begin{cases} \dfrac{1}{\sqrt{N\Omega_0}} e^{i(\vec{k}+\vec{G})\cdot\vec{x}} & \vec{x} \in \text{Interstitial} \\ \sum_{\ell,m} Y_\ell^m(\hat{r})\ \ A_{\ell,m}^{I,\vec{k}+\vec{G}} u_\ell^I(r,E_{1,\ell}^I) + B_{\ell,m}^{I,\vec{k}+\vec{G}} \dot{u}_\ell^I(r,E_{1,\ell}^I) & \vec{r} \in \text{I-Sphere} \end{cases}, \qquad \text{(B.2)}$$

where Ω_0 denotes for the volume of the unit cell, the Y_l^m means spherical harmonics, $\hat{r}$ represents the directional angle of $\vec{r}$ in spherical coordinates. The coefficients A and B are determined using the continuity of the function ϕ and its slope on the MT sphere surface.

The basis set can be slightly modified to account for the effect of low-lying valence states (so called semi-core states). They lie far from the linearization energy $E_{1,l}^I$ and are not entirely confined to the core. Considering such a state with a principal quantum number one less than the corresponding valence state but with the same angular momentum quantum number ℓ is done by adding another single radial function $u_l^I(r,E_{2,l}^I)$ to the basis function, which describes the much more free-atom-like behavior

of the semi-core state (a sharp peak in DOS at energy $E_{2,l}^{I}$). A new type of basis function (so called "local orbital") is introduced as

$$\phi_{\ell,m}^{I,LO}(\vec{x}) = \begin{cases} 0 & \vec{x} \in \text{Interstitial} \\ Y_l^m(\hat{r})\ \ A_{l,m}^{I,LO} u_l^I(r, E_{1,l}^I) + B_{l,m}^{I,LO} \dot{u}_l^I(r, E_{1,l}^I) + C_{l,m}^{I,LO} u_l^I(r, E_{2,l}^I) & \vec{r} \in \text{I-Sphere} \end{cases}. \quad \text{(B.3)}$$

A and B and C are determined again from the continuity of the function, its slope and normalization condition at boundary between MT sphere and interstitial region. An example is provided by 3p-state that appears in the calculations regarding nickel atom.

Thus, all eigenenergies can be obtained with a single diagonalization. The calculation of the radial functions $u_l^I(r, E_{1,l}^I)$ and its corresponding energy derivative $\dot{u}_l^I(r, E_{1,l}^I)$ is introduced in appendix D.

Since the non-interacting single-electron moves in the periodic lattice in the micro-model, the wave function can be viewed as linearized by a set of $\vec{G}$ vectors:

$$\Psi_{\vec{k},n}^{I}\ \ \vec{x}\ \ = \sum C_n\ \ \vec{k} + \vec{G}\ \ \phi^{LAPW}(\vec{x}) \qquad \text{(B.4)}$$

where $\phi^{LAPW}(\vec{x})$ stands for any of the expressions (B.2) and (B.3), and the summation is done over all available quantum numbers and reciprocal space wavevectors. Details are provided in Appendix D.1 (see eq. (D.3)).

To limit the set of the plane waves, all $\vec{G}$ vectors are chosen within the region $G \le G_{\max}$, which corresponds to a sphere with radius $G_{\max}$ centered at the origin of reciprocal lattice. The maximum of the wave vector $\vec{G}$ can be determined from the lower cut-off energy E_{cut}. In LiF, if $E_{cut} = -6Ry = 3E_h$, the corresponding $G_{\max}$ is equal to $\sqrt{2E} \approx 2.45\ a.u.^{-1}$ in C.G.S. units. The volume of this $G_{\max}$ sphere $4\pi G_{\max}^3/3$ is 61.6a.u.$^{-3}$, the volume of the first BZ $(2\pi/a)^3/2$ is 0.283a.u.$^{-3}$ (fcc

lattice constant is 7.6 a.u.). Because the 1st BZ only contains $1\vec{G}$ (the summation of two wave vectors inside 1st BZ always confine in the 1st BZ), the number of plane waves needed is at least 218. In fact, there are around 300 plane waves in use to give an accurate enough calculation[46].

The accuracy of the LAPW basis set is judged by the product $R^{\min} \cdot G_{\max}$, where $R^{\min}$ stands for the smallest muffin tin radius among all (chemical) kinds of atoms. Because the smallest muffin tin radius $R^{\min}$ is increased, the steep behavior of the wave function in the remaining interstitial region is decreased and fewer plane waves will be needed to describe the smoother parts of the wave function in that region. Thus, the criterion becomes that the product $R^{\min} \cdot G_{\max}$ should be kept the same in order to give the same accuracy. Reducing $G_{\max}$ means reducing the size of the matrices, and a larger $R^{\min}$ can significantly lower the computation time. Nevertheless, $R^{\min}$ cannot be too large, since the spherical harmonics are not appropriate to describe the wave function far away from the nuclei.

In practice, the infinite terms in eq. (2.5.2) have to be truncated at some value $\ell_{\max}$. For a given $\ell_{\max}$, $Y_m^{\ell_{\max}}(\theta,\phi)$ can have at most $2\ell_{\max}$ nodes along a great circle (i.e. $\theta = 0 \to 2\pi$ for any fixed ϕ) of the *I*–sphere. There are $2\ell_{\max} / 2\pi R_I = \ell_{\max} / \pi R_I$ nodes per unit length. The plane wave with the shortest period $2\pi / G_{\max}$ has $2 / 2\pi / G_{\max} = G_{\max} / \pi$ nodes per unit length. If the number of nodes per unit length of a plane wave matches the number of nodes per unit length of $\ell_{\max}$, this yields the condition $R_I G_{\max} = \ell_{\max}$ which can be used to determine a good $\ell_{\max}$. LAPW calculations are generally well converged for $R_I G_{\max}$ in the range 7.5~9, this results in $\ell_{\max} \approx 8$. However, a finite value for $\ell_{\max}$ means that the matching at the sphere boundaries will not be exact for each LAPW basis[79].

One aspect worth mentioning is that the exchange-correlation potential functional used by WIEN2k to solve the Kohn-Sham equations is of the form of the local spin density approximation (LSDA)[80]. More modern expressions that consider density-gradient terms (e.g. generalized gradient approximation – GGA) are also used[49,81-83]. The other aspect, as I mentioned in section 2.2.3, is that LSDA postulates that the exchange-correlation energy due to a particular density could be found by dividing the material into infinitesimally small volumes (*r*-grid) with a constant density. Each such volume contributes to the total exchange correlation energy by an amount equal to the exchange correlation energy of an identical volume filled with a homogeneous electron gas, which has the same overall density as the original material has in this volume. It is expected to perform well for systems with a slowly varying density. While, GGA goes beyond LSDA, it makes the exchange-correlation contribution of every infinitesimal volume not only dependent on the local density in that volume, but also on the density in the neighboring volumes, which leads to the gradient of the density played a role[46].

Next, the KS equation for each k-point in the irreducible zone (IZ) will be solved in a self-consistent way. Given an input charge density ρ_{in} (the initial electron density is calculated by considering that all electrons belong to atoms, ignoring the crystal structure); the corresponding spherical symmetric potential can be worked out. The obtained secular equation size is quite big. The Hilbert space can be reduced by applying symmetry operations on WF to decrease basis set. The secular equation can be solved using various numerical techniques[84] (i.e., Cholesky decomposition, or LU decomposition, or Lanczos). In this way the Kohn-Sham wave functions are obtained. This yields an output density ρ_{out}, which in general differs from the input ρ_{in}. Then, an input for the next iteration ρ_{in}' is constructed by using the input ρ_{in} and output ρ_{out}

densities from the recent iterations by Broyden's second method[85]. The advantage of this numerical method over Newton's method is because the Jacobian matrix is not needed. The whole procedure is repeated and the final solution to the wave functions is found out when input charge density to the self-consistent loop yields an output equal to it within a specified tolerance.

At last, the physical quantities can be obtained by this ground-state, for example, DOS, which is defined as:

$$DOS\ \ E\ \ = \sum_{\nu} \delta\ \ E_{\nu} - E\ \ = 2 \sum_{\vec{k},j} \delta\ \ E_{\vec{k},j} - E \tag{B.5}$$

where, the factor of 2 takes account of the spin degeneracy.

The core electrons were treated as in free atoms (neglecting electron-electron interactions from other atoms), but subject to the potential due to the valence electrons.

APPENDIX C

SECULAR EQUATION AND OVERLAP MATRIX

Finding energies and electron densities requires solving the eigenproblem posed by eq. (2.2.18). The wavefunction can be written in terms of LAPW basis set given by eqs., (B.2) and (B.3). The secular equation that must be solved involves the Hamiltonian matrix with the elements:

$$H_{GG\phi}\left(\vec{k}\right)= \left\langle f^{I,\vec{k}+\vec{G}} \middle| H \middle| f^{I,\vec{k}+\vec{G}\phi} \right\rangle . \tag{C.1}$$

As the basis wavefunctions are not necessary orthogonal, there is an overlap matrix *S* also

$$S_{GG\phi}\left(\vec{k}\right)= \left\langle f^{\vec{k}+\vec{G}} \middle| f^{\vec{k}+\vec{G}\phi} \right\rangle . \tag{C.2}$$

The integrals in scalar products are done over the whole crystal volume containing both interstitial part and MT spheres. The MT sphere contributions can also be divided into spherical ($l = 0$ part of the potential and the kinetic energy) and non-spherical ($l \neq 0$) potential terms. The above matrix elements become

$$H_{\vec{G},\vec{G}\phi}\left(\vec{k}\right)= \int_{\text{interstitial}} d^3\vec{r}\, e^{-i\left(\vec{k}+\vec{G}\right)\vec{r}} \left[T + V_{PW}\right] e^{i\left(\vec{k}+\vec{G}\phi\right)\vec{r}} + \sum_I \left[H^I_{\vec{G},\vec{G}\phi}\left(\vec{k}\right) + V^{I,NS}_{\vec{G},\vec{G}\phi}\left(\vec{k}\right) \right]. \tag{C.3}$$

As the basis wavefunctions are not necessary orthogonal, there is an overlap matrix *S* also

$$S_{\vec{G},\vec{G}\phi}\left(\vec{k}\right)= \frac{1}{\Omega} \int_{\text{interstitial}} d^3\vec{r}\, e^{i\left(\vec{G}\phi - \vec{G}\right)\vec{r}} + \sum_I S^I_{\vec{G},\vec{G}\phi}\left(\vec{k}\right). \tag{C.4}$$

where *T* stands for kinetic energy operator, *NS* stands for the non-spherical contributions and *I* indexes the MT spheres.

We need to estimate integrals over the interstitial region. Using Fourier series expansion, we can write

$$\frac{1}{\Omega}\int_{\text{interstitial}} d^3\vec{r}\, f(\vec{r}) = \frac{1}{\Omega}\sum_{\vec{G}} f_{\vec{G}} \int_{\text{interstitial}} d^3\vec{r} e^{-i\vec{G}\cdot\vec{r}} = \frac{1}{\Omega}\sum_{\vec{G}} f_{\vec{G}} \left[\int_{\text{unit cell}} - \sum_I \int_{I^{th}\text{ sphere}}\right] e^{-i\vec{G}\cdot\vec{r}} d^3\vec{r}$$

$$= \sum_{\vec{G}} f_{\vec{G}}\delta(\vec{G}) - \sum_{I,\vec{G}} \frac{e^{-i\vec{G}\cdot\vec{R}_I} f_{\vec{G}}}{\Omega}\int_{I^{th}} d^3\vec{r} e^{-i\vec{G}\cdot(\vec{r}-\vec{R}_I)} = \sum_{\vec{G}} f_{\vec{G}}\left[\delta(\vec{G}) - \sum_I \frac{e^{-i\vec{G}\cdot\vec{R}_I}}{\Omega}\int_{I^{th}} d^3\vec{r}' e^{-i\vec{G}\cdot\vec{r}'}\right]$$

$$= \sum_{\vec{G}} f_{\vec{G}}\left[\delta(\vec{G}) - \sum_I \frac{4\pi e^{-i\vec{G}\cdot\vec{R}_I}}{\Omega G}\int_{I^{th}} r'\sin(Gr')dr'\right] = \sum_{\vec{G}} f_{\vec{G}}\left[\delta(\vec{G}) - \sum_I \frac{4\pi R_I^2 e^{-i\vec{G}\cdot\vec{R}_I} j_1(GR_I)}{\Omega G}\right]$$

. (C.5)

where j_1 is the spherical Bessel function of the first order and δ is the Kronecker symbol. If we use the notation $\Omega(\vec{G}) \equiv d_{\vec{G},0} - \sum_I \frac{4\pi R_I^2 e^{-i\vec{G}\cdot\vec{R}_I} j_1(GR_I)}{\Omega G}$, the interstitial matrix elements are found to be

$$\int_{\text{inter}} d\vec{r} e^{-i(\vec{k}+\vec{G})\cdot\vec{r}} [T + V_{PW}] e^{i(\vec{k}+\vec{G}')\cdot\vec{r}} = \sum_{\vec{G}''} V_{PW}(\vec{G}'')\Omega(\vec{G}-\vec{G}'-\vec{G}'') + \frac{\hbar^2(\vec{k}+\vec{G}')^2}{2m}\Omega(\vec{G}-\vec{G}') \tag{C.6}$$

and

$$\frac{1}{\Omega}\int_{\text{interstitial}} d^3\vec{r} e^{i(\vec{G}'-\vec{G})\cdot\vec{r}} = \Omega(\vec{G}-\vec{G}'). \tag{C.7}$$

The spherical terms are easily evaluated by using the definitions of the basis functions (B.2) and the orthonormality of the spherical functions. The relevant matrix elements are:

$$H^{I}_{G,G'}(\vec{k}) = \sum_{lm} \left[\left(A^{I,\vec{k}+\vec{G}}_{l,m}\right)^{*} A^{I,\vec{k}+\vec{G}'}_{l,m} + \left(B^{I,\vec{k}+\vec{G}}_{l,m}\right)^{*} B^{I,\vec{k}+\vec{G}'}_{l,m} \right] E^{I}_{l} + \frac{1}{2} \left[\left(A^{I,\vec{k}+\vec{G}}_{l,m}\right)^{*} B^{I,\vec{k}+\vec{G}'}_{l,m} + \left(A^{I,\vec{k}+\vec{G}}_{l,m}\right)^{*} B^{I,\vec{k}+\vec{G}'}_{l,m} \right] \tag{C.8}$$

and

$$S^{I}_{G,G'}(\vec{k}) = \sum_{lm} \left[\left(A^{I,\vec{k}+\vec{G}}_{l,m}\right)^{*} A^{I,\vec{k}+\vec{G}'}_{l,m} + \left(B^{I,\vec{k}+\vec{G}}_{l,m}\right)^{*} B^{I,\vec{k}+\vec{G}'}_{l,m} \right]. \tag{C.9}$$

The calculation of non-spherical elements is more complicated using integrals of the type $\int_{0}^{R_I} r^2 f_\ell^I\ r, E_\ell^I\ g_\ell^I\ r, E_\ell^I\ V\ r\ dr$, where f and g are functions of the set u and $\dot{u}$.

APPENDIX D

ORTHONOMALITY OF THE WAVE FUNCTION $\Psi_{\vec{k},n}(\vec{x})$ IN THE LAPW BASIS FOR THE VALENCE STATE

D.1 The wave function $\Psi^{I}_{\vec{k},n}\ \vec{x}$ in the LAPW basis for the valence state

In absence of external magnetic field, spin-orbital coupling and spin polarization, for a given wave vector $\vec{k}$ and band index n, the electron wavefunction in the interstitial region for the valence state is expressed as:

$$\Psi_{\vec{k},n}(\vec{x}) = \sum_{\vec{G}} \left\langle \vec{x} \middle| \vec{k}+\vec{G} \right\rangle \left\langle \vec{k}+\vec{G} \middle| \Psi \right\rangle = \frac{1}{\sqrt{N\Omega_0}} \sum_{\vec{G}} C_n\ \vec{k}+\vec{G}\ e^{i\,\vec{k}+\vec{G}\cdot\vec{x}} \qquad \text{(D.1)}$$

where N is the total number of the primitive unit cells in the macrocrystal and Ω_0 is the primitive unit cell volume.

For MT sphere region, we can write a similar expansion, considering both LAPW extended and local orbitals. The local orbitals are restricted to the particular atom and ℓ for which they are relevant. For a given wave vector $\vec{k}$ and band index n, the electron wavefunction in the crystal in the I$^{\text{th}}$ atomic sphere for the valence state is expressed as:

$$\Psi^{I}_{\vec{k},n}\ \vec{x}\ = \sum_{\vec{G}} C_n\ \vec{k}+\vec{G}\ \phi^{I,\vec{k}+\vec{G}}(\vec{x}) + \sum_{\{\vec{H}^{I}_{\ell LO}\}} C^{LO}_n\ \vec{k}+\vec{H}^{I}_{\ell LO}\ \sum_m \phi^{I,LO}_{\ell,m}(\vec{x})\delta_{\ell,\ell^{LO}} \quad \text{(D.2)}$$

where $\{H^{I}_{\ell lo}\}$is a subgroup of reciprocal vectors $\{\vec{G}\}$ related to the I$^{\text{th}}$ atomic sphere. They are determined by the value ℓ of the local orbital. The number of $H^{I}_{\ell lo}$ vectors for a specific ℓ^{lo} is given by $2\ell^{lo}+1\ N$, where N is the total number of the same kind atoms in the crystallographically nonequivalent atom basis of the primitive unit cell.

Details about these vectors are provided in Appendix D. Functions $\phi^{I,\vec{k}+\vec{G}}(\vec{x})$ and $\phi_{\ell,m}^{I,LO}(\vec{x})$ are the LAPW+LO basis set defined in Appendix B (Eqs. (B.2)-(B.3)).

It is important to remember that the functions in the interstitial region and those in the MT spheres and their derivatives are continuous. In order to impose these conditions, we use the spherical wave expansion of the plane wave[86]:

$$\frac{1}{\sqrt{N\Omega_0}}e^{i\ \vec{k}+\vec{G}\ \cdot\vec{x}} = \frac{1}{\sqrt{N\Omega_0}}e^{i\cdot\ \vec{r}+\vec{X}_I} = \frac{4\pi}{\sqrt{N\Omega_0}}e^{i\ \vec{k}+\vec{G}\ \cdot\vec{X}_I}\sum_{\ell,m} i^{\ell}\ j_{\ell}\ \left|\vec{k}+\vec{G}\right| r\ \ Y_{\ell m}^{*}\ \ \Omega_{\vec{k}+\vec{G}}\ \ Y_{\ell m}\ \ \Omega_{\vec{r}} \quad \text{(D.3)}$$

The equations used to determine *A* and *B* from Eq. (B.2) are now:

$$\begin{aligned}
&\frac{4\pi}{\sqrt{N\Omega_0}}e^{i\ \vec{k}+\vec{G}\ \cdot\vec{X}_I} i^{\ell}\ j_{\ell}\ \left|\vec{k}+\vec{G}\right| R_{MT}^{I}\ \ Y_{\ell m}^{*}\ \ \Omega_{\vec{k}+\vec{G}} = A_{\ell,m}^{I,\vec{k}+\vec{G}} u_{\ell}^{I}\ \ R_{MT}^{I}, E_{1,\ell}^{I} + B_{\ell,m}^{I,\vec{k}+\vec{G}} \dot{u}_{\ell}^{I}\ \ R_{MT}^{I}, E_{1,\ell}^{I} \\
&\frac{4\pi}{\sqrt{N\Omega_0}}e^{i\ \vec{k}+\vec{G}\ \cdot\vec{X}_I} i^{\ell}\ j_{\ell}'\ \left|\vec{k}+\vec{G}\right| R_{MT}^{I}\ \ Y_{\ell m}^{*}\ \ \Omega_{\vec{k}+\vec{G}} = A_{\ell,m}^{I,\vec{k}+\vec{G}} u_{\ell}'^{I}\ \ R_{MT}^{I}, E_{1,\ell}^{I} + B_{\ell,m}^{I,\vec{k}+\vec{G}} \dot{u}_{\ell}'^{I}\ \ R_{MT}^{I}, E_{1,\ell}^{I}
\end{aligned} \quad \text{(D.4)}$$

where the derivatives are taken in respect to *r*. Similar equations can be derived for the local orbitals of eq. (B.3). j_ℓ is the ℓ^{th} order spherical Bessel function, $Y_{\ell m}$ are the spherical harmonics.

A redefinition of coefficients seems natural:

$$\begin{aligned}
&\frac{4\pi\ \ R_{MT}^{I}}{\sqrt{N\Omega_0}}^{2} e^{i\ \vec{k}+\vec{G}\ \cdot\vec{X}_I} i^{\ell} Y_{\ell m}^{*}\ \ \Omega_{\vec{k}+\vec{G}}\ \ a_{0,\ell,m}^{I,\vec{k}+\vec{G}} = A_{\ell,m}^{I,\vec{k}+\vec{G}} \\
&\frac{4\pi\ \ R_{MT}^{I}}{\sqrt{N\Omega_0}}^{2} e^{i\ \vec{k}+\vec{G}\ \cdot\vec{X}_I} i^{\ell} Y_{\ell m}^{*}\ \ \Omega_{\vec{k}+\vec{G}}\ \ a_{1,\ell,m}^{I,\vec{k}+\vec{G}} = B_{\ell,m}^{I,\vec{k}+\vec{G}}
\end{aligned} \quad \text{(D.5)}$$

where, R_{MT}^{I} is the muffin tin radius of the I$^{\text{th}}$ atom.

A similar redefinition occurs for the coefficients of LO orbitals:

$$\frac{4\pi\ R_{MT}^{I}}{\sqrt{N\Omega_0}}^{2} e^{i\ \vec{k}+\vec{G}\ \cdot\vec{X}_I} i^{\ell} Y_{\ell m}^{*}\ \ \Omega_{\vec{k}+\vec{H}}\ \ a_{0,\ell,m}^{I,\vec{k}+\vec{H},LO} = A_{\ell,m}^{I,LO}$$

$$\frac{4\pi\ R_{MT}^{I}}{\sqrt{N\Omega_0}}^{2} e^{i\ \vec{k}+\vec{G}\ \cdot\vec{X}_I} i^{\ell} Y_{\ell m}^{*}\ \ \Omega_{\vec{k}+\vec{H}}\ \ a_{1,\ell,m}^{I,\vec{k}+\vec{H},LO} = B_{\ell,m}^{I,LO} \qquad \text{(D.6)}$$

$$\frac{4\pi\ R_{MT}^{I}}{\sqrt{N\Omega_0}}^{2} e^{i\ \vec{k}+\vec{G}\ \cdot\vec{X}_I} i^{\ell} Y_{\ell m}^{*}\ \ \Omega_{\vec{k}+\vec{H}}\ \ a_{2,\ell,m}^{I,\vec{k}+\vec{H},LO} = C_{\ell,m}^{I,LO}$$

Due to symmetry the dependence on *m* of the coefficients will be dropped, and using the newly defined $a_{\ell,0}^{I,\vec{k},\vec{G}}, a_{\ell,1}^{I,\vec{k},\vec{G}}, a_{\ell,0}^{I,lo}, a_{\ell,1}^{I,lo}, a_{\ell,2}^{I,lo}$ we can write a more detailed expression of the wavefunction inside MT spheres:

$$\Psi_{\vec{k},n}^{I}\ \ \vec{x}\ = \frac{4\pi\ R_{MT}^{I}}{\sqrt{N\Omega_0}}^{2} \sum_{l}\sum_{m} i^{\ell} Y_{\ell,m}(\Omega_{\vec{r}}) \Bigg\{ \sum_{\vec{G}} \Big[C_n\ \ \vec{k}+\vec{G}\ \ Y_{\ell,m}^{*}\ \ \Omega_{\vec{k}+\vec{G}}\ \ e^{i\ \vec{k}+\vec{G}\ \cdot\vec{X}_I}$$

$$a_{\ell,0}^{I,\vec{k},\vec{G}} u_{\ell}^{I}\ \ r, E_{1,l}^{I}\ + a_{\ell,1}^{I,\vec{k},\vec{G}} \dot{u}_{\ell}^{I}\ \ r, E_{1,l}^{I}\ \ \Big] + \sum_{\{\vec{H}_{\ell lo}^{I}\}} \Big[C_n^{lo}\ \ \vec{k}+\vec{H}_{\ell lo}^{I}\ \ Y_{\ell,m}^{*}\Big(\Omega_{\vec{k}+\vec{H}_{\ell lo}^{I}}\Big)\delta_{\ell lo,\ell} \qquad \text{(D.7)}$$

$$\cdot e^{i\left(\vec{k}+\vec{H}_{\ell lo}^{I}\right)\cdot\vec{X}_I} \left(a_{\ell,0}^{I,lo} u_{\ell}^{I}\left(r, E_{1,l}^{I}\right) + a_{\ell,1}^{I,lo} \dot{u}_{\ell}^{I}\left(r, E_{1,l}^{I}\right) + a_{\ell,2}^{I,lo} u_{\ell}^{I,lo}\left(r, E_{2,l}^{I}\right) \right) \Big] \Bigg\}$$

In all LAPW calculations $u_{\ell}^{I}(r, E_{1,l}^{I})$ is the solution to the radial Schrödinger-like equation with the spherically averaged crystal potential at the linearization energy $E_{1,l}^{I}$, $\dot{u}_{\ell}^{I}(r, E_{1,l}^{I})$ its energy derivative, and $u_{\ell}^{I,lo}(r, E_{2,l}^{I})$ corresponds to the local orbital contribution at the linearization energy $E_{2,l}^{I}$.

The function $u_{\mathrm{l}}^{I}(r, E_{1,l}^{I})$ is the solutions of the equation[87]

$$\left(h_{\mathrm{l}}^{I} - e\right) u_{\mathrm{l}}^{I}\left(r, E_{1,l}^{I}\right) = 0\,, \qquad \text{(D.8)}$$

with

$$h_l^I = -\frac{1}{r}\frac{d^2}{dr^2}r + \frac{l(l+1)}{r^2} + u^I(r). \tag{D.9}$$

The normalization condition can be added to the radial solutions inside I-sphere as

$$\int_0^{R_{MT}} r^2 \left(u_l^I\left(r, E_{1,l}^I\right)\right)^2 dr = 1. \tag{D.10}$$

The radial functions $u_l^I(r, E_{1,l}^I)$ are determined by eq. (D.8), (D.9), (D.10) and orthogonal condition.

We differentiate the eq. (D.8) in respect to energy, the energy derivative $\dot{u}_l\left(r, E_{1,l}^I\right)$ will be obtained by

$$\left(h_l^I - e\right)\dot{u}_l\left(r, E_{1,l}^I\right) = u_l^I\left(r, E_{1,l}^I\right) \tag{D.11}$$

This is an inhomogeneous equation with the free term being $u_l^I(r, E_{1,l}^I)$, a solution of the homogeneous eq. (D.8). By differentiating the normalization condition eq. (D.10) with respect to energy E, we know immediately that $\dot{u}_l\left(r, E_{1,l}^I\right)$ and $u_l^I(r, E_{1,l}^I)$ are orthogonal

$$\int_0^{R_{MT}} r^2 \dot{u}_l\left(r, E_{1,l}^I\right) u_l^I\left(r, E_{1,l}^I\right) dr = 0. \tag{D.12}$$

Considering the expectation value of h_l^I between $u_l^I(r, E_{1,l}^I)$ and $u_l^I(r, E_{1,l}^I + d)$, using

$$\left(\left(h_l^I\right)_{ij}\right)^+ = \left(h_l^I\right)_{ij}, \tag{D.13}$$

and the Taylor expansion at some energy $E_{1,l}^I$ of $u_l^I(r, E_{1,l}^I + d)$

$$u_l^I(r, E_{1,l}^I + \delta) = u_l^I(r, E_{1,l}^I) + \delta \cdot \dot{u}_l^I(r, E_{1,l}^I) + \cdots, \tag{D.14}$$

the standard integration by parts gives the condition

$$R^2\left[u_l^I(R)\right]\dot{u}_l^I(R) - u_l^I(R)\left[\dot{u}_l^I(R)\right] = 1 \qquad \text{(D.15)}$$

Combining eq. (D.9), (D.11), (D.12) and (D.15), the energy derivative $\dot{u}_l^I\left(r, E_{1,l}^I\right)$ can be obtained. Eq. (D.14) is founded up to a normalization constant which can be determined easily:

$$N_\ell \equiv \int_0^R r^2 \cdot \dot{u}_\ell^I\ \left(r, E_{1,l}^I\right) \cdot \dot{u}_\ell^I\ \left(r, E_{1,l}^I\right)\ d\vec{r} \qquad \text{(D.16)}$$

In the course of getting radial functions $u_l^I(r, E_{1,l}^I)$, we need to know that the radial functions $u_l^I(r, E_{1,l}^I)$ themselves may not correspond to something physical, but, it does not harm since they are only part of a basis function, not the searched eigenfunction itself. And because they are close to how the actual eigenfunction will look like in that region of the crystal, they will do their job as basis function very efficiently.

If relativistic effects are considered, the radial functions are found as solutions of Dirac equation like:

$$\begin{aligned}
u_\ell^I(r, E_{1,l}^I) &= \frac{1}{r}\begin{pmatrix} P_\ell^I(r, E_{1,l}^I) \\ i\alpha Q_\ell^I(r, E_{1,l}^I)(-\vec{\sigma}\cdot\hat{r}) \end{pmatrix} \\
\dot{u}_\ell^I(r, E_{1,l}^I) &= \frac{1}{r}\begin{pmatrix} \dot{P}_\ell^I(r, E_{1,l}^I) \\ i\alpha \dot{Q}_\ell^I(r, E_{1,l}^I)(-\vec{\sigma}\cdot\hat{r}) \end{pmatrix} \\
u_\ell^{I,lo}(r, E_{2,l}^I) &= \frac{1}{r}\begin{pmatrix} P_\ell^{I,lo}(r, E_{2,l}^I) \\ i\alpha Q_\ell^{I,lo}(r, E_{2,l}^I)(-\vec{\sigma}\cdot\hat{r}) \end{pmatrix}
\end{aligned} \qquad \text{(D.17)}$$

$P_\ell^I(r, E)$ is major component of the radial solution, $Q_\ell^I(r, E)$ is the minor component , α : Fine structure constant, $\vec{\sigma}$: Pauli matrix vector.

Note that in WIEN2k, electron spins are taken to be either spin-up or spin-down,

$$\chi_s = |+\rangle = \begin{pmatrix} 1 \\ 0 \end{pmatrix} \equiv \chi_+ \text{ or } \chi_s = |-\rangle = \begin{pmatrix} 0 \\ 1 \end{pmatrix} \equiv \chi_- . \tag{D.18}$$

In the spin-polarized system, atoms with spin-up (majority spin) and spin-down (minority spin) electron are considered as two different kinds of atoms. The ground-state files consist of two sets: one is for the spin-up case; the other is for the spin-down case. The wave functions use the expression similar to eq. (D.7), but a spin index s is added to the summation, C and a coefficients, and the radial function u and its energy derivative $\dot{u}$.

A general expression of spinor χ_s is

$$\chi_s = \begin{pmatrix} \langle + | \alpha \rangle \\ \langle - | \alpha \rangle \end{pmatrix} \equiv \begin{pmatrix} c_+ \\ c_- \end{pmatrix} = c_+ \chi_+ + c_- \chi_- \tag{D.19}$$

where, $|\alpha\rangle$ is an arbitrary state ket, $|\alpha\rangle = |+\rangle\langle + | \alpha\rangle + |-\rangle\langle - | \alpha\rangle$. It has appeared in the package exciting, an add-on to WIEN2k code. Spin-orbit interactions can be also considered. The code uses a second variational step and regards the scalar-relativistic eigenfunctions as basis.

D.2 The orthonormality of the Bloch state wave functions in macro crystal

Considering an ideal fictitious perfect macrocrystal, the complete set of Bloch statekets is $|\vec{k}, n\rangle$, where the wave vector $\vec{k}$ is within the 1st Brillouin Zone, $\vec{k} = \sum_{i=1}^{3} m_i b_i / N_i$ ($0 \le m_i \le N_i - 1$ integer), n is band index.

The orthonormality condition of the Bloch states can be written as

$$\langle \vec{k}, n | \vec{k}', n' \rangle = \delta_{\vec{k},\vec{k}'} \delta_{n,n'} \tag{D.20}$$

where $\langle \vec{k}, n | \vec{k}', n' \rangle$ is an inner product between the Bloch state bra $\langle \vec{k}, n |$ and the Bloch state ket $| \vec{k}', n' \rangle$.

The band index n appears in the left side of the eq. (D.20) because for a given $\vec{k}$ there are many solutions to the Schrödinger equation, they are indexed by n. These Bloch states $| \vec{k}, n \rangle$ are orthogonal for a given wave vector $\vec{k}$ as proved in the following.

Setting the Hamiltonian operator of the macrocrystal is $\hat{H}_{KS}$, the eigenvalues are $E_{\vec{k},n}$ with the eigenstates $| \vec{k}, n \rangle$, we have

$$\hat{H}_{ks} | \vec{k}, n \rangle = E_{\vec{k},n} | \vec{k}, n \rangle, \text{ and } \hat{H}_{ks} | \vec{k}, n' \rangle = E_{\vec{k},n'} | \vec{k}, n' \rangle$$

for each state respectively. Thus, the Hamiltonian matrix element becomes

$$\langle \vec{k}, n | \hat{H}_{KS} | \vec{k}, n' \rangle = E_{\vec{k},n} \langle \vec{k}, n | \vec{k}, n' \rangle = E_{\vec{k},n'} \langle \vec{k}, n | \vec{k}, n' \rangle$$

The above equation can be rewritten as the following

$$E_{\vec{k},n} - E_{\vec{k},n'} \langle \vec{k}, n | \vec{k}, n' \rangle = 0 \qquad \text{(D.21)}$$

If the states are non-degenerate, there exists $E_{\vec{k},n} \neq E_{\vec{k},n'}$. Then $\langle \vec{k}, n | \vec{k}, n' \rangle = 0$, which means the two arbitrary states are orthogonal for a given vector $\vec{k}$. So, generally, all the non-degenerate wave functions are orthogonal with each other. By setting the self-integral of the Bloch state wave function equal to one, we get orthonormal wave function.

If there are number of *p* Bloch states are such that energy eigenvalues are degenerate, they form a subspace group p in the Hilbert space, in which $E_{\vec{k},n} = E_{\vec{k},n'}$. We can apply a procedure, like Graham Schmidt, on these eigenstates and obtain

orthonormal wave functions and we get all orthonormal Bloch state wave functions with a given $\vec{k}$.

The wave vector of an electron appears in the left side of the eq. (D.20), because the inner product of two Bloch states with the same band index n is non-zero only when $\vec{k}-\vec{k}'$ = 0. It is zero when $\vec{k}-\vec{k}' \neq 0$. For this stationary quantum mechanics system, the proof is as the following.

Inserting the closure relation, and setting the volume of a macrocrystal is Ω ,

$$\left\langle \vec{k},n\middle|\vec{k}',n'\right\rangle = \int_{\Omega} d^3x \left\langle \vec{k},n\middle|\vec{x}\right\rangle \left\langle \vec{x}\middle|\vec{k}',n'\right\rangle = \int_{\Omega} d^3x \Psi^*_{\vec{k},n}(\vec{x})\Psi_{\vec{k}',n'}(\vec{x}) \qquad \text{(D.22)}$$

Because of the periodic lattice, we can cover the total integral area through moving the first primitive unit cell Ω_0 from its origin by a lattice vector $\vec{R}$. The integral becomes

$$\left\langle \vec{k},n\middle|\vec{k}',n'\right\rangle = \sum_{\vec{R}} \int_{\Omega_0} d^3x \Psi^*_{\vec{k},n}(\vec{x}+\vec{R})\Psi_{\vec{k}',n'}(\vec{x}+\vec{R}) \qquad \text{(D.23)}$$

Using Bloch's theorem, $\Psi_{\vec{k}',n'}(\vec{x}+\vec{R}) = e^{i\vec{k}'\cdot\vec{R}}\Psi_{\vec{k}',n'}(\vec{x})$, $\Psi^*_{\vec{k},n}(\vec{x}+\vec{R}) = e^{-i\vec{k}\cdot\vec{R}}\Psi^*_{\vec{k},n}(\vec{x})$, the equation becomes

$$\left\langle \vec{k},n\middle|\vec{k}',n'\right\rangle = \sum_{\vec{R}} \int_{\Omega_0} d^3x e^{-i\vec{k}\cdot\vec{R}}\Psi^*_{\vec{k},n}(\vec{x})e^{i\vec{k}'\cdot\vec{R}}\Psi_{\vec{k}',n'}(\vec{x}) = \sum_{\vec{R}} e^{i(\vec{k}'-\vec{k})\cdot\vec{R}} \int_{\Omega_0} d^3x \Psi^*_{\vec{k},n}(\vec{x})\Psi_{\vec{k}',n'}(\vec{x}) \text{ .(D.24)}$$

We rewrite eq. (D.24) as below

$$\left\langle \vec{k},n\middle|\vec{k}',n'\right\rangle = \frac{(1-e^{i(\vec{k}'-\vec{k})\cdot N_1\vec{a}_1})(1-e^{i(\vec{k}'-\vec{k})\cdot N_2\vec{a}_2})(1-e^{i(\vec{k}'-\vec{k})\cdot N_3\vec{a}_3})}{(1-e^{i(\vec{k}'-\vec{k})\cdot\vec{a}_1})(1-e^{i(\vec{k}'-\vec{k})\cdot\vec{a}_2})(1-e^{i(\vec{k}'-\vec{k})\cdot\vec{a}_3})} \int_{\Omega_0} d^3x \Psi^*_{\vec{k},n}(\vec{x})\Psi_{\vec{k}',n'}(\vec{x}) \text{ .} \qquad \text{(D.25)}$$

where N_1, N_2, N_3 is the number of the primitive unit cell respectively along X, Y, Z axis in the macrocrystal.

Note that in the above equation $e^{i(\vec{k}'-\vec{k})\cdot N_i\vec{a}_i}=1$, because

$$(\vec{k}'-\vec{k})\cdot N_1\vec{a}_1=\sum_{i=1}^{3}(\frac{m_i'}{N_i}b_i-\frac{m_i}{N_i}b_i)N_1\vec{a}_1=\sum_{i=1}^{3}(m_i'-m_i)\cdot\frac{N_1}{N_i}2\pi\cdot\delta_{i1}=2\pi(m_1'-m_1)$$

$$(\vec{k}'-\vec{k})\cdot N_2\vec{a}_2=\sum_{i=1}^{3}(\frac{m_i'}{N_i}b_i-\frac{m_i}{N_i}b_i)N_2\vec{a}_2=\sum_{i=1}^{3}(m_i'-m_i)\cdot\frac{N_2}{N_i}2\pi\cdot\delta_{i2}=2\pi(m_2'-m_2)$$

$$(\vec{k}'-\vec{k})\cdot N_3\vec{a}_3=\sum_{i=1}^{3}(\frac{m_i'}{N_i}b_i-\frac{m_i}{N_i}b_i)N_3\vec{a}_3=\sum_{i=1}^{3}(m_i'-m_i)\cdot\frac{N_3}{N_i}2\pi\cdot\delta_{i3}=2\pi(m_3'-m_3)$$

where m_i' and m_i are integers ($0\le m_i, m_i'\le N_i-1$ integer).

If $\vec{k}'-\vec{k}\neq\vec{G}$, the denominators are different from zero, and the scalar product becomes zero. If $\vec{k}'-\vec{k}=\vec{G}$, the L'Höpital's rule applied to the factor in front of the integral in the right side of eq. (D.25) makes the inner product $\langle\vec{k},n|\vec{k}',n'\rangle$:

$$\langle\vec{k},n|\vec{k}',n'\rangle=N_1N_2N_3\delta_{\vec{k}-\vec{k}',\vec{G}}\int_{\Omega_0}d^3x\Psi^*_{\vec{k},n}(\vec{x})\Psi_{\vec{k}',n'}(\vec{x})=N\delta_{\vec{k}-\vec{k}',\vec{G}}\int_{\Omega_0}d^3x\Psi^*_{\vec{k},n}(\vec{x})\Psi_{\vec{k}',n'}(\vec{x})$$

where $N=N_1N_2N_3$ is the total number of the primitive unit cell in the macrocrystal.

By setting $\vec{G}=0$, we restrict $\vec{k}-\vec{k}'$ in the first Brillouin Zone without missing any physical information, because for a given n, the eigenstates and eigenvalues are periodic functions of $\vec{G}$ in the reciprocal lattice:

$$\begin{aligned}\Psi_{n,\vec{k}'+\vec{G}}(\vec{x})&=\Psi_{n,\vec{k}}(\vec{x}),\\ \varepsilon_{n,\vec{k}'+\vec{G}}&=\varepsilon_{n,\vec{k}}.\end{aligned}\qquad\text{(D.26)}$$

From eq. (D.24) to eq. (D.26), it tells us that

$$\sum_{\vec{R}}e^{i(\vec{k}'-\vec{k})\cdot\vec{R}}=N\delta_{\vec{k}-\vec{k}',\vec{G}}=N\delta_{\vec{k},\vec{k}'}\qquad\text{(D.27)}$$

The inner product $\left\langle \vec{k},n\middle|\vec{k}',n'\right\rangle$ is rewritten as the following

$$\left\langle \vec{k},n\middle|\vec{k}',n'\right\rangle = N\delta_{\vec{k},\vec{k}'}\int\limits_{\Omega_0} d^3x\Psi^*_{\vec{k},n}(\vec{x})\Psi_{\vec{k}',n'}(\vec{x}) = \begin{cases} N\int\limits_{\Omega_0} d^3x\Psi^*_{\vec{k},n}(\vec{x})\Psi_{\vec{k},n'}(\vec{x}) & if\ \vec{k}=\vec{k}', \\ 0 & if\ \vec{k}\neq\vec{k}'. \end{cases} \quad \text{(D.28)}$$

Thus, it is true that the Bloch state wave functions in the stationary quantum mechanical system satisfy eq. (D.20).

$$\left\langle \vec{k},n\middle|\vec{k}',n'\right\rangle = N\delta_{\vec{k},\vec{k}'}\int\limits_{\Omega_0} d^3x\Psi^*_{\vec{k},n}(\vec{x})\Psi_{\vec{k}',n'}(\vec{x}) = \delta_{\vec{k},\vec{k}'}\int\limits_{\Omega} d^3x\Psi^*_{\vec{k},n}(\vec{x})\Psi_{\vec{k}',n'}(\vec{x}) = \delta_{\vec{k},\vec{k}'}\delta_{n,n'}$$

D.3 The inner product of wave functions for a valence state in the LAPW basis

D.3.1 Contribution from the interstitials

For a given $\vec{k}$ and n, the state wavefunction in the interstitial regions is presented in eq. (D.1), its norm can be evaluated as:

$$\begin{aligned} \left\langle \Psi_{\vec{k},n}\middle|\Psi_{\vec{k}',n'}\right\rangle_{\text{interstitials}} &= N\delta_{\vec{k},\vec{k}'}\int\limits_{\text{interstitial}} d^3x\Psi^*_{\vec{k},n}\ \vec{x}\ \Psi_{\vec{k}',n'}\ \vec{x} \\ &= \delta_{\vec{k},\vec{k}'}\frac{1}{\Omega_0}\sum_{\vec{G}\ ,\ \vec{G}'} C^*_n\ \vec{k}+\vec{G}\ C_{n'}\ \vec{k}'+\vec{G}'\int\limits_{\text{interstitial}} d^3x e^{-i\ \vec{k}+\vec{G}\ \cdot\vec{x}} e^{i\ \vec{k}'+\vec{G}'\ \cdot\vec{x}}, \quad \text{(D.29)} \\ &= \delta_{\vec{k},\vec{k}'}\frac{1}{\Omega_0}\sum_{\{\vec{G},\vec{G}'\}} C^*_n\ \vec{k}+\vec{G}\ C_{n'}\ \vec{k}'+\vec{G}'\int\limits_{\text{interstitial}} d^3x e^{-i\ \vec{k}+\vec{G}-\vec{k}'-\vec{G}'\ \cdot\vec{x}} \end{aligned}$$

where the volume of the integral on the right side of the eq. (D.29) is an interstitial volume of a primitive unit cell. In order to evaluate the integral above, we evaluate it over the whole primitive unit cell and subtract its value at the MT spheres

$$\int_{\text{interstitial}} d^3x e^{-i\,\vec{k}+\vec{G}-\vec{k}'-\vec{G}'\cdot\vec{x}} = \int_{\text{all space}} d^3x e^{-i\,\vec{k}+\vec{G}-\vec{k}'-\vec{G}'\cdot\vec{x}} - \int_{\text{all MT's}} d^3x e^{-i\,\vec{k}+\vec{G}-\vec{k}'-\vec{G}'\cdot\vec{x}}$$

$$= \Omega_0 \delta_{\vec{k}+\vec{G},\vec{k}'+\vec{G}'} - \sum_I \int_{\substack{\text{sphere centered} \\ \text{at the I}^{\text{th}}\text{ atom}}} d^3x e^{-i\,\vec{k}+\vec{G}-\vec{k}'-\vec{G}'\cdot\vec{x}} \qquad \text{(D.30)}$$

We substitute $\vec{x} = \vec{X}_I + \vec{r}$ and use the spherical wave expansions of a vector plane wave as in eq. (C.3) into the second term on right side of the eq. (C.30). It becomes

$$\int_{\substack{\text{sphere centered} \\ \text{at the I}^{\text{th}}\text{ atom}}} d^3x e^{-i\,\vec{k}+\vec{G}-\vec{k}'-\vec{G}'\cdot\vec{x}} = e^{-i\,\vec{k}+\vec{G}-\vec{k}'-\vec{G}'\cdot\vec{x}_I}$$

$$\cdot\left[4\pi \sum_{l=0}^{\infty} (-i)^l \sum_m Y_{lm}(\Omega_{\vec{k}+\vec{G}-\vec{k}'-\vec{G}'}) \int_0^{R_{MT}} dr r^2 j_l \left|\vec{k}+\vec{G}-\vec{k}'-\vec{G}'\right| r \int d\Omega_r Y_{lm}^* \;\Omega_r \right] \qquad \text{(D.31)}$$

Using the orthonormality of the spherical harmonics:

$$\int_0^{2\pi} d\phi \int_{-1}^{1} d\,\cos\theta\; Y_{l,m}^*(\Omega_{\vec{r}}) Y_{l',m'}(\Omega_{\vec{r}}) = \delta_{l,l'}\delta_{m,m'},$$

and $Y_{00} = \sqrt{\frac{1}{4\pi}}$, we have

$$\int d\Omega_r Y_{lm}^* \;\Omega_r \;=\; 4\pi^{\;1/2} \int d\Omega_r Y_{00} \;\Omega_r \; Y_{lm}^* \;\Omega_r \;=\; 4\pi^{\;1/2} \delta_{l,0}\delta_{m,0} \qquad \text{(D.32)}$$

Introducing the result from eq. (D.32) into eq. (D.31), gives

$$\int_{\substack{\text{sphere centered} \\ \text{at the I}^{\text{th}}\text{ atom}}} d^3x e^{-i\,\vec{k}+\vec{G}-\vec{k}'-\vec{G}'\cdot\vec{x}} = e^{-i\,\vec{k}+\vec{G}-\vec{k}'-\vec{G}'\cdot\vec{x}_I} \left[4\pi \int_0^{R_{MT}} dr r^2 j_0 \left|\vec{k}+\vec{G}-\vec{k}'-\vec{G}'\right| r \right] \qquad \text{(D.33)}$$

Substituting eq. (D.33) and eq. (D.30) into eq. (D.29), gives

$$\left\langle \Psi_{\vec{k},n} \middle| \Psi_{\vec{k}',n'} \right\rangle_{\text{interstitials}} = \delta_{\vec{k},\vec{k}'} \left\{ \sum_{\vec{G}} C_n^* \ \vec{k}+\vec{G} \ C_{n'} \ \vec{k}+\vec{G} \ - \frac{4\pi}{\Omega_0} \sum_I e^{-i \ \vec{k}+\vec{G}-\vec{k}'-\vec{G}' \cdot \vec{x}_I} \right.$$

$$\left. \cdot \left[\sum_{\vec{G}\ ,\ \vec{G}'} C_n^* \ \vec{k}+\vec{G} \ C_{n'} \ \vec{k}'+\vec{G}' \int_0^{R_{MT}} drr^2 j_0 \ \left| \vec{k}+\vec{G}-\vec{k}'-\vec{G}' \right| r \ \right] \right\} \tag{D.34}$$

We evaluate the integral of the Spherical Bessel function on the right side of eq. (D.34) below. Setting

$$\int_0^{R_{MT}} drr^2 j_0 \ \left| \vec{k}+\vec{G}-\vec{k}'-\vec{G}' \right| r \ \equiv \int_0^{R_{MT}} drr^2 j_0 \ Kr \ ,$$

where we define $K = \left| \vec{k}+\vec{G}-\vec{k}'-\vec{G}' \right|$.

For K=0, we have

$$\int_0^{R_{MT}} drr^2 j_0 \ Kr \ = \frac{R_{MT}^3}{3}. \tag{D.35}$$

For $K \neq 0$,

$$\int_0^{R_{MT}} drr^2 j_0 \ Kr \ = \int_0^{R_{MT}} drr^2 \frac{\sin \ Kr}{Kr}.$$

Setting $r' = Kr$, we have

$$\int_0^{R_{MT}} drr^2 j_0 \ Kr \ = \frac{1}{(K)^3} \int_0^{K \cdot R_{MT}} dr'r' \sin \ r' \ = \frac{1}{(K)^3} \int_0^{K \cdot R_{MT}} -r' \ d\cos r' \ .$$

Applying standard integration by parts on above equation, yields

$$\int_0^{R_{MT}} dr r^2 j_0\ \ Kr\ \ = \frac{1}{(K)^3}\left\{ -Kr\cos(Kr)\Big|_0^{R_{MT}} + \int_0^{K\cdot R_{MT}} dr' \cos\ \ r' \right\}$$
$$= -\frac{R_{MT}}{(K)^2}\cos(KR_{MT}) + \frac{1}{(K)^3}\sin(Kr)\Big|_0^{R_{MT}} = -\frac{R_{MT}}{(K)^2}\cos(KR_{MT}) + \frac{1}{(K)^3}\sin(KR_{MT}) \quad \text{.(D.36)}$$

Making use of eqs. (D.35) and (D.36) in eq. (D.34) gives:

$$\left\langle \Psi_{\vec{k},n} \middle| \Psi_{\vec{k}',n'} \right\rangle_{\text{interstitials}} = \delta_{\vec{k},\vec{k}'} \sum_{\vec{G}\ ,\ \vec{G}'} C_n^*\ \ \vec{k}+\vec{G}\ \ C_{n'}\ \ \vec{k}'+\vec{G}' \left\{ \delta_{\vec{k}+\vec{G},\vec{k}'+\vec{G}'} \left[1 - \frac{4\pi}{\Omega_0} \sum_I \frac{R_{MT}^I\ \ ^3}{3} \right] \right.$$

$$\left. + \frac{4\pi}{\Omega_0}(\delta_{\vec{k}+\vec{G},\vec{k}'+\vec{G}'} - 1) \sum_I e^{-i\ \vec{k}+\vec{G}-\vec{k}'-\vec{G}'\ \cdot\vec{x}_I} \left[-\frac{R_{MT}^I}{(K)^2}\cos(KR_{MT}^I) + \frac{1}{(K)^3}\sin(KR_{MT}^I) \right] \right\} \quad \text{(D.37)}$$

where $K = \left|\vec{k}+\vec{G}-\vec{k}'-\vec{G}'\right|$.

D.3.2 Contribution from the atomic spheres:

For a given $\vec{k}$ and n, the norm of the wavefunction presented in eq. (D.7) is expressed as:

$$\left\langle \Psi_{\vec{k},n} \middle| \Psi_{\vec{k}',n'} \right\rangle_{\text{atomic spheres}} = N \sum_I \int_{\substack{\text{sphere centered} \\ \text{at the I}^{\text{th}}\ \text{atom}}} d^3\vec{r}\, \Psi_{\vec{k},n}^{*I}\ \ \vec{r}\ \ \Psi_{\vec{k}',n'}^{I}\ \ \vec{r}$$

$$= \frac{16\pi^2}{\Omega_0} \sum_I\ \ R_{MT}^I\ \ ^4 \int_{\substack{\text{sphere centered} \\ \text{at the I}^{\text{th}}\ \text{atom}}} d^3\vec{r} \times \sum_{lm}\sum_{l'm'} Y_{lm}^*(\Omega_{\vec{r}})Y_{l'm'}(\Omega_{\vec{r}})$$

$$\left\{ \sum_{\mu,\mu'} A_{\ell,m,\mu}^{*I,\vec{k},n} A_{\ell',m',\mu'}^{I,\vec{k}',n'} u_{\ell,\mu}^{*I}\ \ r\ \ u_{\ell',\mu'}^{I}\ \ r \sum_{\mu,\gamma'} A_{\ell,m,\mu}^{*I,\vec{k},n} B_{\ell',m',\gamma'}^{I,\vec{k}',n'} u_{\ell,\mu}^{*I}\ \ r\ \ u_{\ell,\gamma'}^{I}\ \ r \right. \quad \text{(D.38)}$$

$$\left. + \sum_{\gamma,\mu'} B_{\ell,m,\gamma}^{*I,\vec{k},\vec{H},n} A_{\ell',m',\mu'}^{I,k',\vec{G}',n'} u_{l,\gamma}^{*I}\ \ r\ \ u_{l',\mu'}^{I}\ \ r \sum_{\gamma,\gamma'} B_{l,m,\gamma}^{*I,\vec{k},n} B_{l',m',\gamma'}^{I,\vec{k}',n'} u_{l,\gamma}^{*I}\ \ r\ \ u_{l',\gamma'}^{I}\ \ r \right\}$$

where the summation is over all the atoms in the primitive unit cell, the indexes $\mu = 0,1$ and $\gamma = 0,1,2$ refer to:

$$\begin{aligned} u^I_{l,0}\ r &= u^I_l\ r \\ u^I_{l,1}\ r &= \dot{u}^I_l\ r \\ u^I_{l,2}\ r &= u^{I,lo}_l\ r \end{aligned} \quad . \tag{D.39}$$

We will evaluate it for the most general (relativistic case) using the radial functions provided by Eq. (D.17).

The following relationships involving Pauli matrices are useful. The matrices are:

$$\sigma_x = \begin{pmatrix} 0 & 1 \\ 1 & 0 \end{pmatrix}, \quad \sigma_y = \begin{pmatrix} 0 & -i \\ i & 0 \end{pmatrix}, \quad \sigma_z = \begin{pmatrix} 1 & 0 \\ 0 & -1 \end{pmatrix}.$$

and they obey the following commutation and anti-commutation relations

$$\sigma_i, \sigma_j = 2\delta_{i,j}, \quad \left[\sigma_i, \sigma_j\right] = 2i\varepsilon_{ijk}\sigma_k$$

where, ε_{ijk} is Levi-Civita symbol,

We have,

$$\vec{\sigma}\cdot\hat{r}^{\ \dagger}\ \vec{\sigma}\cdot\hat{r} = (\hat{x}\sigma_x^\dagger + \hat{y}\sigma_y^\dagger + \hat{z}\sigma_z^\dagger)\cdot(\hat{x}\sigma_x + \hat{y}\sigma_y + \hat{z}\sigma_z)^2 = \hat{\mathrm{I}}$$

and

$$\begin{aligned} \vec{\sigma}\cdot\vec{\mathrm{A}}\quad \vec{\sigma}\cdot\vec{\mathrm{B}} &= \sigma_i \mathrm{A}_i \sigma_j \mathrm{B}_j = \sigma_i \mathrm{A}_i \sigma_i \mathrm{B}_i + i\varepsilon_{ijk}\sigma_k \mathrm{A}_i \mathrm{B}_j \\ &= \vec{\mathrm{A}}\cdot\vec{\mathrm{B}} + i\vec{\sigma}\cdot(\mathrm{A}\times\mathrm{B}) \end{aligned} \quad .$$

Immediate consequence are $\vec{\sigma}\cdot\hat{r}\quad\vec{\sigma}\cdot\hat{r} = \mathrm{I}.$ and $\vec{\sigma}\cdot\hat{r}^{\ \dagger}\ \vec{\sigma}\cdot\hat{r} = \mathrm{I}$

Thus,

$$u^{*I}_{l,\mu}\ \ r\ \ u^{I}_{l',\mu'}\ \ r\ \ = \frac{1}{r^2}\ \ P^{*I}_{l,\mu}(r)P^{I}_{l',\mu'}(r) + \alpha^2 Q^{*I}_{l,\mu}(r)Q^{I}_{l',\mu'}(r)\ \ \vec{\sigma}\cdot\hat{r}\ \ ^{\dagger}\ \ \vec{\sigma}\cdot\hat{r}$$

$$= \frac{1}{r^2}\ \ P^{*I}_{l,\mu}(r)P^{I}_{l',\mu'}(r) + \alpha^2 Q^{*I}_{l,\mu}(r)Q^{I}_{l',\mu'}(r)$$

For the same reason,

$$u^{*I}_{l,\mu}\ \ r\ \ u^{I}_{l',\gamma'}\ \ r\ \ = \frac{1}{r^2}\ \ P^{*I}_{l,\mu}(r)P^{I}_{l',\gamma'}(r) + \alpha^2 Q^{*I}_{l,\mu}(r)Q^{I}_{l',\gamma'}(r)$$

$$u^{*I}_{l,\gamma}\ \ r\ \ u^{I}_{l',\mu'}\ \ r\ \ = \frac{1}{r^2}\ \ P^{*I}_{l,\gamma}(r)P^{I}_{l',\mu'}(r) + \alpha^2 Q^{*I}_{l,\gamma}(r)Q^{I}_{l',\mu'}(r)$$

$$u^{*I}_{l,\gamma}\ \ r\ \ u^{I}_{l',\gamma'}\ \ r\ \ = \frac{1}{r^2}\ \ P^{*I}_{l,\gamma}(r)P^{I}_{l',\gamma'}(r) + \alpha^2 Q^{*I}_{l,\gamma}(r)Q^{I}_{l',\gamma'}(r)$$

Using again the orthonormality of the spherical harmonics, we obtain

$$\left\langle \Psi_{\vec{k},n} \middle| \Psi_{\vec{k}',n'} \right\rangle_{\text{atomic spheres}} = N\delta_{\vec{k},\vec{k}'} \sum_{I} \int_{\substack{\text{sphere centered} \\ \text{at the I}^{\text{th}}\text{ atom}}} d^3\vec{r}\,\Psi^{*I}_{\vec{k},n}\ \ \vec{r}\ \ \Psi^{I}_{\vec{k}',n'}\ \ \vec{r}$$

$$= \delta_{\vec{k},\vec{k}'} \frac{16\pi^2}{\Omega_0} \sum_{I}\ \ R^{I}_{MT}\ \ ^4 \times \sum_{l,m} \left\{ \sum_{\mu,\mu'} A^{*I,\vec{k},n}_{l,m,\mu} A^{I,\vec{k}',n'}_{l,m,\mu'} U^{I}_{l,\mu,\mu'} \right. \tag{D.40}$$

$$\left. + \sum_{\mu,\gamma'} A^{*I,\vec{k},n}_{l,m,\mu} B^{I,\vec{k}',n'}_{l,m,\gamma'} U^{I}_{l,\mu,\gamma'} + \sum_{\gamma,\mu'} B^{*I,\vec{k},n}_{l,m,\gamma} A^{I,\vec{k}',n'}_{l,m,\mu'} U^{I}_{l,\gamma,\mu'}\ \ + \sum_{\gamma,\gamma'} B^{*I,\vec{k},n}_{l,m,\gamma} B^{I,\vec{k}',n'}_{l,m,\gamma'} U^{I}_{l,\gamma,\gamma'} \right\}$$

where we define:

$$
\begin{aligned}
U^I_{l,\mu,\mu'} &= \int_0^{R_{MT}} dr \;\; P^{*I}_{l,\mu}(r)P^I_{l,\mu'}(r) + \alpha^2 Q^{*I}_{l,\mu}(r)Q^I_{l,\mu'}(r) \\
U^I_{l,\mu,\gamma'} &= \int_0^{R_{MT}} dr \;\; P^{*I}_{l,\mu}(r)P^I_{l,\gamma'}(r) + \alpha^2 Q^{*I}_{l,\mu}(r)Q^I_{l,\gamma'}(r) \\
U^I_{l,\gamma,\mu'} &= \int_0^{R_{MT}} dr \;\; P^{*I}_{l,\gamma}(r)P^I_{l,\mu'}(r) + \alpha^2 Q^{*I}_{l,\gamma}(r)Q^I_{l,\mu'}(r) \\
U^I_{l,\gamma,\gamma'} &= \int_0^{R_{MT}} dr \;\; P^{*I}_{l,\gamma}(r)P^I_{l,\gamma'}(r) + \alpha^2 Q^{*I}_{l,\gamma}(r)Q^I_{l,\gamma'}(r)
\end{aligned}
\tag{D.41}
$$

Also, according to eq. (D.10), (D.12) and (D.16), we have

$$
\begin{aligned}
&U^I_{\ell,s,0,0} = 1 && U^I_{\ell,s,1,1} = N_\ell \\
&U^I_{\ell,s,0,1} = U^I_{\ell,s,1,0} = 0 && U^I_{\ell,s,0,2} = U^I_{\ell,s,2,0} \\
&U^I_{\ell,s,1,2} = U^I_{\ell,s,2,1} && U^I_{\ell,s,2,2} = 1
\end{aligned}
\tag{D.42}
$$

The whole WF norm can be calculated as the sum of the results in eq. (D.37) and (D.40)

$$
\left\langle \Psi_{\vec{k},n} \middle| \Psi_{\vec{k}',n'} \right\rangle = \left\langle \Psi_{\vec{k},n} \middle| \Psi_{\vec{k}',n'} \right\rangle_{\text{atomic spheres}} + \left\langle \Psi_{\vec{k},n} \middle| \Psi_{\vec{k}',n'} \right\rangle_{\text{interstitial}} \tag{D.43}
$$

Eq. (D.43) is required to satisfy eq. (D.20), namely, $\left\langle \vec{k},n \middle| \vec{k}',n' \right\rangle = \delta_{\vec{k},\vec{k}'}\delta_{n,n'}$.

The Bloch state wavefunction of the I$^{\text{th}}$ atomic sphere is abbreviated as

$$
\Psi^I_{\tilde{\vec{k}},n}\;\; \vec{x} \;\; = \frac{4\pi \;\; R^I_{MT}}{\sqrt{N}\sqrt{\Omega_0}}^2 \sum_l \sum_m \sum_\beta Y^*_{lm}(\Omega_{\vec{r}}) A^{I,\tilde{\vec{k}},n}_{l,m,\beta} u^I_{l,\beta} \;\; r \tag{D.44}
$$

where

$$
A^{I,\tilde{\vec{k}},n}_{l,m,\beta} = \begin{cases} A^{I,\tilde{\vec{k}},n}_{l,m,\mu} & \mu = 0,1 \\ B^{I,\tilde{\vec{k}},n}_{l,m,\gamma} & \gamma = 0,1,2 \text{ for local orbital} \end{cases} . \tag{D.45}
$$

APPENDIX E

KOHN-SHAM RESPONSE FUNCTION IN LAPW BASIS

E.1 Rotational properties of Bravais lattice and the crystal system

Considering a symmetry operator $\hat{S}$ acting on a position eigenket $|\vec{x}\rangle$ of a crystal system, we have

$$\hat{S}|\vec{x}\rangle = |\mathcal{R}\,\vec{x} + \vec{\tau}_{\ \mathcal{R}}\rangle \tag{E.1}$$

where $\mathcal{R}$ is a orthogonal rotation operation of the point group of the crystal system and $\vec{\tau}_{\ R}$ is a partial lattice constant translation related to $\mathcal{R}$. Then, applying the operatorial identity $\hat{S}^{-1}\cdot\hat{S} = \hat{\mathrm{I}}$ to the position eigenket $\vec{x}$ we get:

$$\hat{S}^{-1}\hat{S}|\vec{x}\rangle = \hat{S}^{-1}|\mathcal{R}\,\vec{x} + \vec{\tau}_{\ \mathcal{R}}\rangle = |\vec{x}\rangle.$$

Defining $\vec{y} \equiv \mathcal{R}\,\vec{x} + \vec{\tau}_{\ \mathcal{R}}$, we have $\vec{x} \equiv \mathcal{R}^{-1}_{\ \ \vec{y} - \vec{\tau}_{\ \mathcal{R}}}$. The above equation becomes

$$\hat{S}^{-1}|\vec{y}\rangle = |\mathcal{R}^{-1}_{\ \ \vec{y} - \vec{\tau}_{\ \mathcal{R}}}\rangle = |\mathcal{R}^{-1}\vec{y} - \mathcal{R}^{-1}\vec{\tau}_{\ \mathcal{R}}\rangle, \tag{E.2}$$

describing the action of the inverse operation $\hat{S}^{-1}$.

A direct consequence of eqs. (E.2) and (E.1) is that:

$$\hat{S}^{\dagger}\hat{\vec{x}}\hat{S}|\vec{x}\rangle = \hat{S}^{-1}\hat{\vec{x}}|\mathcal{R}\,\vec{x} + \vec{\tau}_{\ \mathcal{R}}\rangle = \hat{S}^{-1}\left[\hat{\vec{x}}|\mathcal{R}\,\vec{x} + \vec{\tau}_{\ \mathcal{R}}\rangle\right] = \hat{S}^{-1}\left[\vec{x}|\mathcal{R}\,\vec{x} + \vec{\tau}_{\ \mathcal{R}}\rangle\right].$$

When the action of $\hat{S}^{-1}$ on the whole function (of x) $\vec{x}|\mathcal{R}\,\vec{x} + \vec{\tau}_{\ \mathcal{R}}\rangle$ is same as on the eigenvalue $\vec{x}$ and eigenfunction $|\mathcal{R}\,\vec{x} + \vec{\tau}_{\ \mathcal{R}}\rangle$ separately,

$$\begin{aligned}\hat{S}^{-1}\left[\vec{x}|\mathcal{R}\,\vec{x} + \vec{\tau}_{\ \mathcal{R}}\rangle\right] &= \left[\mathcal{R}^{-1}\vec{x} - \mathcal{R}^{-1}\vec{\tau}_{\ \mathcal{R}}\right]|\mathcal{R}^{-1}\left[\mathcal{R}\,\vec{x} + \vec{\tau}_{\ \mathcal{R}}\right] - \mathcal{R}^{-1}\vec{\tau}_{\ \mathcal{R}}\rangle \\ &= \left[\mathcal{R}^{-1}\vec{x} - \mathcal{R}^{-1}\vec{\tau}_{\ \mathcal{R}}\right]|\,\vec{x}\rangle = \left[\mathcal{R}^{-1}\hat{\vec{x}} - \mathcal{R}^{-1}\vec{\tau}_{\ \mathcal{R}}\right]|\,\vec{x}\rangle\end{aligned} \tag{E.3}$$

Let us consider a rotation operation $\mathcal{R}$ acting on a scalar product $\vec{k}\cdot\vec{x}$. As roational orthogonal operations conserve the scalar product, we can write

$$\begin{aligned}\mathcal{R}\vec{k}\cdot\mathcal{R}\vec{x}=\vec{k}\cdot\vec{x}=\mathcal{R}^{-1}\vec{k}\cdot\mathcal{R}^{-1}\vec{x}\\ \vec{k}\cdot\mathcal{R}\vec{x}=\mathcal{R}^{-1}\vec{k}\cdot\vec{x}\\ \vec{k}\cdot\mathcal{R}^{-1}\vec{x}=\mathcal{R}\vec{k}\cdot\vec{x}\end{aligned} \qquad \text{(E.4)}$$

The result of the operator $\hat{S}$ acting on a crystal wavefunction $\left|\vec{\underset{\sim}{k}},n\right\rangle$ can be evaluated as follows. First, we use the completeness relation $\int d^3x\left|\vec{x}\right\rangle\left\langle\vec{x}\right|=\hat{\mathrm{I}}$ and the orthogonality of $\hat{S}\quad\hat{S}^{\dagger}=\hat{S}^{-1}$ and we obtain:

$$\hat{S}\left|\vec{\underset{\sim}{k}},n\right\rangle=\int d^3x\left|\vec{x}\right\rangle\left\langle\vec{x}\right|\hat{S}\left|\vec{\underset{\sim}{k}},n\right\rangle=\int d^3x\left|\vec{x}\right\rangle\left\langle\mathcal{R}^{-1}\vec{x}-\mathcal{R}^{-1}\vec{\tau}\ \ \mathcal{R}\ \ \right|\vec{\underset{\sim}{k}},n\Big\rangle.$$

It is obvious that the periodic part $w_{\vec{\underset{\sim}{k}},n}$ of the Bloch wavefunction $\left|\vec{\underset{\sim}{k}},n\right\rangle$ does not change under symmetry operation. Using eq. (E.4), we can write the following relation:

$$\begin{aligned}\left\langle\mathcal{R}^{-1}\vec{x}-\mathcal{R}^{-1}\vec{\tau}\ \ \mathcal{R}\ \ \right|\vec{\underset{\sim}{k}},n\Big\rangle&=e^{i\vec{k}\cdot\mathcal{R}^{-1}\left[\vec{x}-\vec{\tau}\ \mathcal{R}\ \right]}w_{\vec{\underset{\sim}{k}},n}\ \ \mathcal{R}^{-1}\vec{x}-\mathcal{R}^{-1}\vec{\tau}\ \ \mathcal{R}\\ &=e^{i\mathcal{R}\vec{k}\cdot\left[\vec{x}-\vec{\tau}\ \mathcal{R}\ \right]}w_{\mathcal{R}\vec{\underset{\sim}{k}},n}\ \ \vec{x}\ \ =e^{-i\left(\mathcal{R}\vec{k}\right)\cdot\vec{\tau}\ \mathcal{R}\ s}\left\langle\vec{x}\right|\mathcal{R}\vec{\underset{\sim}{k}},n\Big\rangle\end{aligned}$$

This allows us to put $\hat{S}\left|\vec{\underset{\sim}{k}},n\right\rangle$ in a much simpler form:

$$\hat{S}\left|\vec{\underset{\sim}{k}},n\right\rangle=\int d^3xe^{-i\mathcal{R}\vec{k}\cdot\vec{\tau}\ \mathcal{R}}\ \left|\vec{x}\right\rangle\left\langle\vec{x}\right|\mathcal{R}\vec{\underset{\sim}{k}},n\Big\rangle=e^{-i\mathcal{R}\vec{k}\cdot\vec{\tau}\ \mathcal{R}}\ \left|\mathcal{R}\vec{\underset{\sim}{k}},n\right\rangle.$$

Namely, the relation between the wavefunctions $\left|R\vec{\underset{\sim}{k}},n\right\rangle$ and $\left|\vec{\underset{\sim}{k}},n\right\rangle$ is

$$\left|\mathcal{R}\vec{\underset{\sim}{k}},n\right\rangle=e^{i\mathcal{R}\vec{\underset{\sim}{k}}\cdot\vec{\tau}\ \mathcal{R}}\ \hat{S}\left|\vec{\underset{\sim}{k}},n\right\rangle. \qquad \text{(E.5)}$$

These symmetry properties will be used to derive KS response below.

E.2 Kohn-Sham response function in LAPW basis

The Kohn-Sham response function of a macrocrystal is written as

$$\chi_{\vec{G}\vec{G}'}\left(\vec{q},\omega\right) = \frac{1}{N\Omega_0}\sum_{\vec{k}}^{BZ}\sum_{n,n'}\frac{f_{\vec{k},n} - f_{\vec{k}+\vec{q},n'}}{E_{\vec{k},n} - E_{\vec{k}+\vec{q},n'} + \hbar\,\omega + i\eta} \times\left\langle \vec{k},n\left| e^{-i\left(\vec{q}+\vec{G}\right)\cdot\vec{x}}\right|\vec{k}+\vec{q},n'\right\rangle\left\langle \vec{k}+\vec{q},n'\left| e^{i\left(\vec{q}+\vec{G}'\right)\cdot\vec{x}}\right|\vec{k},n\right\rangle \tag{E.6}$$

where *BZ* stands for the Brillouin zone. The sum over wave vectors $\vec{k}$ in eq. (E.6) can be rewritten as a sum over special *k*-points $\underset{\sim}{\vec{k}}$ in the irreducible Brillouin zone (*BIZ*) and over the star of each $\underset{\sim}{\vec{k}}$ (all points obtained by applying symmetry operations on $\underset{\sim}{\vec{k}}$). As each point of the star is obtained by applying a unique symmetry operation to $\underset{\sim}{\vec{k}}$, the sum over points of the star is replaced by summing over all symmetry operations.

Any vector $\vec{k}$ from the Brillouin zone can be expressed as

$$\vec{k} = \mathcal{R}\,\underset{\sim}{\vec{k}} \tag{E.7}$$

where $\mathcal{R}$ is the unique operation that brings $\vec{k}$ in the *BIZ* vector $\underset{\sim}{\vec{k}}$. The vector $\vec{k}+\vec{q}$ does not necessary lie into *BZ*, but the translation with the reciprocal lattice vector $\vec{G}_{\vec{q}}\ \vec{k}$ will bring it into the *BZ*. A symmetry operation $\mathcal{R}_1$ will bring it into *IBZ* as

$$\underset{\sim}{\vec{k}}' = \mathcal{R}_1^{-1}\left[\mathcal{R}\,\underset{\sim}{\vec{k}} + \vec{q} - \vec{G}_{\vec{q}}\ \vec{k}\ \right]. \tag{E.8}$$

For every $\vec{k}$ there are unique $\mathcal{R}, \mathcal{R}_1$ and $\vec{G}_{\vec{q}}\ \vec{k}$ which brings the aforementioned vectors to the *IBZ*.

Introducing expression (E.7) and (E.8) into eq. (E.6), we have:

$$\chi_{\vec{G}\vec{G}'}\left(\vec{q},\omega\right)=\frac{1}{N\Omega_0}\sum_{\underset{\sim}{\vec{k}}}^{BIZ}\sum_{\mathcal{R}}\sum_{n,n'}\frac{f_{\mathcal{R}\underset{\sim}{\vec{k}},n}-f_{\mathcal{R}'\underset{\sim}{\vec{k}}'+\vec{G}_{\vec{q}},n'}}{E_{\mathcal{R}\underset{\sim}{\vec{k}},n}-E_{\mathcal{R}'\underset{\sim}{\vec{k}}'+\vec{G}_{\vec{q}},n'}+\hbar\left(\omega+i\eta\right)}$$
$$\times\left\langle\mathcal{R}\underset{\sim}{\vec{k}},n\left|e^{-i\left(\vec{q}+\vec{G}\right)\cdot\hat{\vec{x}}}\right|\mathcal{R}_1\underset{\sim}{\vec{k}}'+\vec{G}_{\vec{q}},n'\right\rangle\left\langle\mathcal{R}_1\underset{\sim}{\vec{k}}'+\vec{G}_{\vec{q}},n'\left|e^{i\left(\vec{q}+\vec{G}'\right)\cdot\hat{\vec{x}}}\right|\mathcal{R}\underset{\sim}{\vec{k}},n\right\rangle \quad ,(E.9)$$

where $\underset{\sim}{\vec{k}}'$, $\vec{G}_{\vec{q}}$ and $\mathcal{R}_1$ are uniquely determined by $\underset{\sim}{\vec{k}}$, $\vec{q}$ and $\mathcal{R}$.

Owing to the symmetry properties, the eigenvalues and the occupation numbers respectively satisfy the following relations:

$$\begin{aligned}f_{\mathcal{R}\underset{\sim}{\vec{k}},n}&=f_{\underset{\sim}{\vec{k}},n}\\ f_{\mathcal{R}'\underset{\sim}{\vec{k}}'+G_{\vec{q}},n'}&=f_{\underset{\sim}{\vec{k}}',n'}\\ E_{\mathcal{R}\underset{\sim}{\vec{k}},n}&=E_{\underset{\sim}{\vec{k}},n}\\ E_{\mathcal{R}'\underset{\sim}{\vec{k}}'+G_{\vec{q}},n'}&=E_{\underset{\sim}{\vec{k}}',n'}\end{aligned}\quad . \qquad (E.10)$$

The following identity

$$\left|\mathcal{R}_1\underset{\sim}{\vec{k}}'+\vec{G}_{\vec{q}}\ \ \vec{k}\ \ ,n'\right\rangle=e^{i\vec{G}_{\vec{q}}\ \vec{k}\cdot\vec{x}}\left|\mathcal{R}_1\underset{\sim}{\vec{k}}',n'\right\rangle, \qquad (E.11)$$

can further simplify the calculations. Introducing expressions (E.10) and (E.11) into eq. (E.9), we get

$$\chi_{\vec{G}\vec{G}'}\left(\vec{q},\omega\right)=\frac{1}{N\Omega_0}\sum_{\underset{\sim}{\vec{k}}}^{BIZ}\sum_{\mathcal{R}}\sum_{n,n'}\frac{f_{\underset{\sim}{\vec{k}},n}-f_{\underset{\sim}{\vec{k}}',n'}}{E_{\underset{\sim}{\vec{k}},n}-E_{\underset{\sim}{\vec{k}}',n'}+\hbar\left(\omega+i\eta\right)}$$
$$\times\left\langle\mathcal{R}\underset{\sim}{\vec{k}},n\left|e^{-i\ \vec{q}+\vec{G}\cdot\hat{\vec{x}}}\right|\mathcal{R}_1\underset{\sim}{\vec{k}}',n'\right\rangle\left\langle\mathcal{R}_1\underset{\sim}{\vec{k}}',n'\left|e^{i\ \vec{q}+\vec{G}'\cdot\hat{\vec{x}}}\right|\mathcal{R}\underset{\sim}{\vec{k}},n\right\rangle \quad .(E.12)$$

Now, it's time to remember the result of symmetry operations acting on wavefunctions of eq. (E.5) and the matrix element that appears in equation (E.12) transforms as

$$\begin{aligned}\left\langle \mathcal{R}\vec{\underset{\sim}{k}},n\left|e^{-i\ \vec{q}+\vec{G}\ \cdot\hat{\vec{x}}}\right|\mathcal{R}_1\vec{\underset{\sim}{k}}',n'\right\rangle &= \left\langle \mathcal{R}\vec{\underset{\sim}{k}},n\left|e^{-i\ \vec{q}+\vec{G}\ \cdot\hat{\vec{x}}}\right|\mathcal{R}\ \ \mathcal{R}^{-1}\mathcal{R}_1\vec{\underset{\sim}{k}}'\ \ ,n'\right\rangle \\ &= \int d^3x e^{i\left[\left(\mathcal{R}_1\vec{\underset{\sim}{k}}'\right)-\left(\mathcal{R}\vec{\underset{\sim}{k}}\right)\right]\cdot\vec{\tau}\ \mathcal{R}}\left\langle\vec{\underset{\sim}{k}},n\left|S^{\dagger}e^{-i\ \vec{q}+\vec{G}\ \cdot\hat{\vec{x}}}S\right|x\right\rangle\left\langle x\right|\ \mathcal{R}^{-1}\mathcal{R}_1\ \ \vec{\underset{\sim}{k}}',n'\right\rangle\end{aligned} \tag{E.13}$$

Using the relation in eq. (E.3) the whole operator term becomes

$$\begin{aligned}\hat{S}^{\dagger}e^{-i\ \vec{q}+\vec{G}\ \cdot\hat{\vec{x}}}\hat{S}\left|\vec{x}\right\rangle &= e^{-i\ \vec{q}+\vec{G}\ \cdot\left(\hat{S}^{\dagger}\hat{\vec{x}}\hat{S}\right)}\left|\vec{x}\right\rangle \\ &= e^{-i\ \vec{q}+\vec{G}\ \cdot\left(\mathcal{R}^{-1}\ \hat{\vec{x}}-\vec{\tau}\ \mathcal{R}\ \right)}\left|\vec{x}\right\rangle = e^{-i\left[\mathcal{R}\ \vec{q}+\vec{G}\ \right]\cdot\hat{\vec{x}}}\ e^{i\left[\mathcal{R}\ \vec{q}+\vec{G}\ \right]\cdot\vec{\tau}\ \mathcal{R}}\ \left|\vec{x}\right\rangle\end{aligned}$$

The first matrix element of eq. (E.12) can finally be written as

$$\begin{aligned}&\left\langle \mathcal{R}\vec{\underset{\sim}{k}},n\left|e^{-i\ \vec{q}+\vec{G}\ \cdot\hat{\vec{x}}}\right|\mathcal{R}_1\vec{\underset{\sim}{k}}',n'\right\rangle \\ &= e^{i\left[\left(\mathcal{R}_1\vec{\underset{\sim}{k}}'\right)-\left(\mathcal{R}\vec{\underset{\sim}{k}}\right)\right]\cdot\vec{\tau}\ \mathcal{R}}\ e^{i\left[\mathcal{R}\left(\vec{q}+\vec{G}\right)\right]\cdot\vec{\tau}\left(\mathcal{R}\right)}\left\langle\vec{\underset{\sim}{k}},n\left|e^{-i\left[\mathcal{R}\ \vec{q}+\vec{G}\ \right]\cdot\hat{\vec{x}}}\right|\mathcal{R}'\vec{\underset{\sim}{k}}',n'\right\rangle\end{aligned} \tag{E.14}$$

where $\mathcal{R}'=\mathcal{R}^{-1}\mathcal{R}_1$.

In a similar manner, one can write the second matrix element of eq. (E.12) as:

$$\begin{aligned}&\left\langle \mathcal{R}_1\vec{\underset{\sim}{k}}',n'\left|e^{-i\ \vec{q}+\vec{G}'\ \cdot\hat{\vec{x}}}\right|\mathcal{R}\vec{\underset{\sim}{k}},n\right\rangle \\ &= e^{-i\left[\left(\mathcal{R}_1\vec{\underset{\sim}{k}}'\right)-\left(\mathcal{R}\vec{\underset{\sim}{k}}\right)\right]\cdot\vec{\tau}\ \mathcal{R}}\ e^{-i\left[\mathcal{R}\ \vec{q}+\vec{G}'\ \right]\cdot\vec{\tau}\ \mathcal{R}}\left\langle\mathcal{R}'\vec{\underset{\sim}{k}}',n'\left|e^{-i\left[\mathcal{R}\ \vec{q}+\vec{G}\ \right]\cdot\hat{\vec{x}}}\right|\vec{\underset{\sim}{k}},n\right\rangle^{*}\end{aligned}. \tag{E.15}$$

Putting eq. (E.14), (E.15) and (E.16) into eq. (E.12), we have an expression for the Kohn-Sham response function:

$$\chi_{\vec{G}\vec{G}'}\left(\vec{q},\omega\right) = \frac{1}{N\Omega_0}\sum_{\underset{\sim}{\vec{k}}}^{BIZ}\sum_{\mathcal{R}}\sum_{n,n'}\frac{f_{\underset{\sim}{\vec{k}},n} - f_{\underset{\sim}{\vec{k}}',n'}}{E_{\underset{\sim}{\vec{k}},n} - E_{\underset{\sim}{\vec{k}}',n'} + \hbar\,\omega + i\eta}\, e^{i\left[\mathcal{R}\,\vec{G}-\vec{G}'\right]\cdot\vec{\tau}\,\mathcal{R}} \times$$
$$\times\left\langle \underset{\sim}{\vec{k}},n\left| e^{-i\left[\mathcal{R}\,\vec{q}+\vec{G}\right]\cdot\hat{\vec{x}}}\right| R'\underset{\sim}{\vec{k}}',n'\right\rangle\left\langle \underset{\sim}{\vec{k}},n\left| e^{-i\left[\mathcal{R}\,\vec{q}+\vec{G}'\right]\cdot\hat{\vec{x}}}\right| R'\underset{\sim}{\vec{k}}',n'\right\rangle^{*} \quad \text{.(E.16)}$$

The first matrix element can be further written as below via the completeness relation and eq. (E.5)

$$\left\langle \underset{\sim}{\vec{k}},n\left| e^{-i\left[\mathcal{R}\left(\vec{q}+\vec{G}\right)\right]\cdot\hat{\vec{x}}}\right| R'\underset{\sim}{\vec{k}}',n'\right\rangle = \int d^3x\left\langle \underset{\sim}{\vec{k}},n\middle|\vec{x}\right\rangle e^{-i\left[\mathcal{R}\,\vec{q}+\vec{G}\right]\cdot\vec{x}}\left\langle \vec{x}\middle|\mathcal{R}'\underset{\sim}{\vec{k}}',n'\right\rangle$$
$$= e^{i\left[\mathcal{R}'\underset{\sim}{\vec{k}}'\right]\cdot\vec{\tau}\,\mathcal{R}'}\int d^3x\Psi_{\underset{\sim}{\vec{k}},n}\left(\vec{x}\right) e^{-i\mathcal{R}\left(\vec{q}+\vec{G}\right)\cdot\vec{x}}\left\langle \vec{x}\middle|\hat{S}'\middle|\underset{\sim}{\vec{k}}',n'\right\rangle \quad \text{.(E.17)}$$
$$= e^{i\left(\mathcal{R}'\underset{\sim}{\vec{k}}'\right)\cdot\vec{\tau}\left(\mathcal{R}'\right)}\int d^3x\Psi_{\underset{\sim}{\vec{k}},n}\left(\vec{x}\right) e^{-i\left[\mathcal{R}\left(\vec{q}+\vec{G}\right)\right]\cdot\vec{x}}\Psi_{\underset{\sim}{\vec{k}}',n'}\left(\mathcal{R}'^{-1}\left(\vec{x}-\vec{\tau}\left(\mathcal{R}'\right)\right)\right)$$

E.2.1 Evaluation of the density matrix element in the atomic spheres

From eq. (E.17), the contribution from the atomic spheres (or Muffin Tins) to this matrix element is given by:

$$\left\langle \underset{\sim}{\vec{k}},n\left| e^{-i\left[\mathcal{R}\left(\vec{q}+\vec{G}\right)\right]\cdot\hat{\vec{x}}}\right| \mathcal{R}'\underset{\sim}{\vec{k}}',n'\right\rangle_{MT} = e^{i\left(\mathcal{R}'\underset{\sim}{\vec{k}}'\right)\cdot\vec{\tau}\,\mathcal{R}'}\, ME\_MT_{n,n'}\left(\mathcal{R},\underset{\sim}{\vec{k}},\vec{q}+\vec{G}\right) \quad \text{(E.18)}$$

where

$$ME\_MT_{n,n'}\ \mathcal{R},\vec{\underset{\sim}{k}},\vec{q}+\vec{G}$$

$$= N\sum_{I}\int_{Sphere} d^3x\Psi^{I}_{\vec{\underset{\sim}{k}},n}\ \vec{x}\ e^{-i\left[\mathcal{R}\ \vec{q}+\vec{G}\right]\cdot\vec{x}}\Psi^{I}_{\vec{\underset{\sim}{k}}',n'}\ \mathcal{R}'^{-1}\ \vec{x}-\vec{\tau}\ \mathcal{R}' \tag{E.19}$$

As we mentioned in Appendix B, $\vec{x}=\vec{x}_I+\vec{r}$, where $\vec{x}_I$ is the position of the I[th] atom in the primitive unit cell and $\vec{r}$ is the distance measured from the center of that atom. When a symmetry operation is applied on the I^{th} atom, it turns into its equivalent atom in the global system

$$\mathcal{R}'^{-1}\ \vec{x}_I-\vec{\tau}\ \mathcal{R}'\ =\vec{x}_I+\vec{R}_I\,,$$

where $\vec{R}_I$ is the primitive lattice vector that brings the new atom position inside the primitive unit cell. Therefore,

$$\Psi^{I}_{\vec{\underset{\sim}{k}}',n'}\ \mathcal{R}'^{-1}\ \vec{x}-\vec{\tau}\ \mathcal{R}'\ =e^{i\vec{\underset{\sim}{k}}'\cdot\vec{R}_I}\left\langle\vec{x}_I+\mathcal{R}'^{-1}\vec{r}\,\middle|\,\vec{\underset{\sim}{k}}',n'\right\rangle=e^{i\vec{\underset{\sim}{k}}'\cdot\vec{R}_I}\Psi^{I}_{\vec{\underset{\sim}{k}}',n'}\ \vec{x}_I+\mathcal{R}'^{-1}\vec{r} \tag{E.20}$$

According to the wave function of the I^{th} atomic sphere written in eq. (E.44):

$$\Psi^{*I}_{\vec{\underset{\sim}{k}},n}\ \vec{x}\ =\Psi^{*I}_{\vec{\underset{\sim}{k}},n}\ \vec{x}_I+\vec{r}\ =\frac{4\pi\ R^{I}_{MT}{}^{2}}{\sqrt{N}\sqrt{\Omega_0}}\sum_{l}\sum_{m}\sum_{\beta}Y^{*}_{lm}\ \Omega_{\vec{r}}\quad A^{I,n,\vec{\underset{\sim}{k}}}_{l,m,\beta}{}^{*}\ u^{*I}_{l,\beta}\ r \tag{E.21}$$

$$\Psi^{I}_{\vec{\underset{\sim}{k}}',n'}\ \vec{x}_I+\mathcal{R}'^{-1}\vec{r}\ =\frac{4\pi\ R^{I}_{MT}{}^{2}}{\sqrt{N}\sqrt{\Omega_0}}\sum_{l'}\sum_{m'}\sum_{\beta'}Y_{l'm'}\ \Omega_{\mathcal{R}'^{-1}\vec{r}}\ A^{I,n',\vec{\underset{\sim}{k}}'}_{l',m',\beta'}u^{I}_{l',\beta'}\ r \tag{E.22}$$

Using the spherical wave expansion on the exponential term below, we have

$$e^{-i\left[\mathcal{R}(\vec{q}+\vec{G})\right]\cdot\vec{x}} = e^{-i\left[\mathcal{R}(\vec{q}+\vec{G})\right]\cdot\vec{x}_I+\vec{r}}$$

$$= e^{-i\left[\mathcal{R}(\vec{q}+\vec{G})\right]\cdot\vec{x}_I}\left[4\pi\sum_{l''=0}^{\infty}(i)^{l''}\, j_{l''}\left|\mathcal{R}\,\vec{q}+\vec{G}\right|r\sum_{m''=-l''}^{l''}Y^{*}_{l''m''}\left(\Omega_{\mathcal{R}\,-\vec{q}-\vec{G}}\right)Y_{l''m''}\,\Omega_{\vec{r}}\right] \quad \text{(E.23)}$$

Substituting eqs. (E.20) - (E.23) into eq.(E.19) the contribution to the first matrix element from the atomic spheres is given by

$$ME\_MT_{n,n'}\;\;\mathcal{R},\vec{k},\vec{q}+\vec{G}$$

$$= N\sum_{I}\int_{Sphere} d^3x\Psi^{I}_{\vec{k},n}\;\;\vec{x}\;\;e^{-i\mathcal{R}\left(\vec{q}+\vec{G}\right)\cdot\vec{x}}\Psi^{I}_{\vec{k}',n'}\;\;\mathcal{R}'^{-1}\;\;\vec{x}-\vec{\tau}\;\;\mathcal{R}'$$

$$= N\sum_{I=1}^{Na}\frac{4\pi^{\;3}\;R_{MT}^{I\;4}}{N\Omega_0}e^{-i\mathcal{R}(\vec{q}+\vec{G})\cdot\vec{x}_I}e^{i\vec{k}'\cdot\vec{R}_I}\times\sum_{l''=0}^{\infty}(i)^{l''}\sum_{m''=-l''}^{l''}Y^{*}_{l''m''}\left(\Omega_{\mathcal{R}\,-\vec{q}-\vec{G}}\right)$$

$$\times\sum_{l}\sum_{m}\sum_{l'}\sum_{m'}\int d\Omega_{\vec{r}}Y^{*}_{lm}\;\;\Omega_{\vec{r}}\;\;Y_{l''m''}\left(\Omega_{\vec{r}}\right)Y_{l'm'}\left(\Omega_{\mathcal{R}'^{-1}\vec{r}}\right)\sum_{\beta}\sum_{\beta'}\int_{0}^{R_{MT}^{I}}dr$$

$$\left\{P^{*I}_{l,\beta}(r)P^{I}_{l',\beta'}(r)+\alpha^2Q^{*I}_{l,\beta}(r)Q^{I}_{l',\beta'}(r)\right\}j_{l''}\left(\left|\mathcal{R}\left(\vec{q}+\vec{G}\right)\right|r\right)\times\left(A^{I,\vec{k},n}_{l,m,\beta}\right)^{*}A^{I,\vec{k}',n'}_{l',m',\beta'}$$

where functions *P* and *Q* are defined in eq. (E.44).

Applying the rotational properties of the spherical harmonics[77]

$$Y_{l'm'}\,\Omega_{\mathcal{R}'^{-1}\vec{r}}\;=\mathcal{R}'Y_{l'm'}\,\Omega_{\vec{r}}\;=\sum_{m'''=-l'}^{l'}D^{l'}_{m'''m'}\;\mathcal{R}'\,Y_{l'm'''}\,\Omega_{\vec{r}}$$

into the above equation, we get

$$ME\_MT_{n,n'}\ \mathcal{R},\vec{\underset{\sim}{k}},\vec{q}+\vec{G}$$

$$= N\sum_{I}\int_{Sphere} d^3x\Psi^{I}_{\vec{\underset{\sim}{k}},n}\ \vec{x}\ e^{-i\left[\mathcal{R}\left(\vec{q}+\vec{G}\right)\right]\cdot\vec{x}}\Psi^{I}_{\vec{\underset{\sim}{k}}',n'}\ \mathcal{R}'^{-1}\ \vec{x}-\vec{\tau}\ \mathcal{R}'$$

$$= N\sum_{I=1}^{Na}\frac{4\pi^{\ 3}\ R_{MT}^{I\ \ 4}}{N\Omega_0}e^{-i\left[\mathcal{R}(\vec{q}+\vec{G})\right]\cdot\vec{x}_I}e^{i\vec{\underset{\sim}{k}}'\cdot\vec{R}_I}\times\sum_{l''=0}^{\infty}(i)^{l''}\sum_{m''=-l''}^{l''}Y^{*}_{l''m''}\left(\Omega_{\mathcal{R}\ -\vec{q}-\vec{G}}\right)$$

$$\times\sum_{l}\sum_{m}\sum_{l'}\sum_{m'}\sum_{m'''=-l'}^{l'}\int d\Omega_{\vec{r}}Y^{*}_{lm}\left(\Omega_{\vec{r}}\right)Y_{l''m''}\left(\Omega_{\vec{r}}\right)Y_{l'm'''}\left(\Omega_{\vec{r}}\right)D^{l'}_{m'm'''}\left(\mathcal{R}'\right)\sum_{\beta}\sum_{\beta'}\int_{0}^{R_{MT}^{I}}dr$$

$$\left\{P^{*I}_{l,\beta}(r)P^{I}_{l',\beta'}(r)+\alpha^2Q^{*I}_{l,\beta}(r)Q^{I}_{l',\beta'}(r)\right\}j_{l''}\left(\left|\mathcal{R}\left(\vec{q}+\vec{G}\right)\right|r\right)\times\left(A^{I,\vec{\underset{\sim}{k}},n}_{l,m,\beta}\right)^{*}A^{I,\vec{\underset{\sim}{k}}',n'}_{l',m',\beta'}$$

, (E.24)

where, the Gaunt coefficients (the product of three spherical harmonics) are determined through Wigner 3*j* symbols.

E.2.2 Evaluation of the density matrix element in the interstitial space

From eq. (C.18), the contribution from the interstitial to the first matrix element is given by

$$\left\langle\vec{\underset{\sim}{k}},n\left|e^{-i\mathcal{R}\ \vec{q}+\vec{G}\ \cdot\hat{\vec{x}}}\right|\mathcal{R}'\vec{\underset{\sim}{k}}',n'\right\rangle_{INT}=e^{i\left(\mathcal{R}'\vec{\underset{\sim}{k}}'\right)\cdot\vec{\tau}\left(R'\right)}ME\_INT_{n,n'}\ \mathcal{R},\vec{\underset{\sim}{k}},\vec{q}+\vec{G}\qquad(E.25)$$

where

$$ME\_INT_{n,n'}\ \mathcal{R},\vec{\underset{\sim}{k}},\vec{q}+\vec{G}$$

$$=N\int_{\substack{\text{Interstitial}\\ \text{in unit cell}}}d^3x\ \Psi^{*,I}_{\vec{\underset{\sim}{k}},n}\ \vec{x}\ \ e^{-i\left[\mathcal{R}\ \vec{q}+\vec{G}\ \right]\cdot\vec{x}}\Psi^{I}_{\vec{\underset{\sim}{k}}',n'}\ \mathcal{R}'^{-1}\ \vec{x}-\vec{\tau}\ \mathcal{R}'\qquad.(E.26)$$

According to the wave function of the I^{th} atomic sphere written in eq. (C.1):

$$\Psi^{*}_{\vec{\underset{\sim}{k}},n}\ \ \vec{x}\ = \frac{1}{\sqrt{N\Omega_0}}\sum_{\vec{G}''} C^{*}_{n}\ \ \vec{\underset{\sim}{k}}+\vec{G}''\ \ e^{-i\left(\vec{\underset{\sim}{k}}+\vec{G}''\right)\cdot\vec{x}} \tag{E.27}$$

$$\begin{aligned}\Psi_{\vec{\underset{\sim}{k}}',n'}\ \ \mathcal{R}'^{-1}\ \ \vec{x}-\vec{\tau}\ \ \mathcal{R}'\ \ &= \frac{1}{\sqrt{N\Omega_0}}\sum_{\vec{G}'''} C_{n'}\ \ \vec{\underset{\sim}{k}}'+\vec{G}'''\ \ e^{i\left(\vec{\underset{\sim}{k}}'+\vec{G}'''\right)\cdot\left(\mathcal{R}'^{-1}\left(\vec{x}-\vec{\tau}\ \mathcal{R}'\ \right)\right)} \\ &= \frac{1}{\sqrt{N\Omega_0}}\sum_{\vec{G}'''} e^{-i\left[\mathcal{R}'\left(\vec{\underset{\sim}{k}}'+\vec{G}'''\right)\right]\cdot\vec{\tau}\left(\mathcal{R}'\right)} C_{n'}\ \ \vec{\underset{\sim}{k}}'+\vec{G}'''\ \ e^{i\left[\mathcal{R}'\left(\vec{\underset{\sim}{k}}'+\vec{G}'''\right)\right]\cdot\vec{x}}\end{aligned} \tag{E.28}$$

Substituting eqs.(E.27) and (E.28) into eq.(E.26), the contribution to the matrix element from the interstitial region is written as

$$\begin{aligned}ME\_INT_{n,n'}\ \ \mathcal{R},\vec{\underset{\sim}{k}},\vec{q}+\vec{G}\ \ &= \frac{N}{N\Omega_0}\sum_{\vec{G}''}\sum_{\vec{G}'''} C^{*}_{n}\ \ \vec{\underset{\sim}{k}}+\vec{G}''\ \ C_{n'}\ \ \vec{\underset{\sim}{k}}'+\vec{G}''' \\ & e^{-i\left[\mathcal{R}'\left(\vec{\underset{\sim}{k}}'+\vec{G}'''\right)\right]\cdot\vec{\tau}\left(\mathcal{R}'\right)} \times \int_{\substack{\text{Interstitial}\\ \text{in unit cell}}} d^3x\ \ e^{-i\left[\vec{\underset{\sim}{k}}+\vec{G}''+\mathcal{R}\left(\vec{q}+\vec{G}\right)-R'\left(\vec{\underset{\sim}{k}}'+\vec{G}'''\right)\right]\cdot\vec{x}}\ \cdot\end{aligned}$$

The integral of the plane wave in the above equation is evaluated as same as that in eq. (C.30), the first matrix element in the interstitial region becomes

$$ME\_INT_{n,n'}\ \mathcal{R},\underset{\sim}{\vec{k}},\vec{q}+\vec{G}\ =\sum_{\vec{G}''}\sum_{\vec{G}'''}C_n^*\ \underset{\sim}{\vec{k}}+\vec{G}''\ C_{n'}\ \underset{\sim}{\vec{k}}'+\vec{G}'''\ e^{-i\left[\mathcal{R}'\left(\underset{\sim}{\vec{k}}'+\vec{G}'''\right)\right]\cdot\vec{\tau}\ \mathcal{R}'}$$

$$\times\begin{cases}1-\dfrac{4\pi}{\Omega_0}\displaystyle\sum_I\dfrac{R_{MT}^{I\ 3}}{3} & \text{if } |\vec{K}|=0\\ -\dfrac{4\pi}{\Omega_0}\displaystyle\sum_I e^{-i\vec{K}\cdot\vec{x}_I}\left[-\dfrac{R_{MT}^I}{|\vec{K}|^2}\cos|\vec{K}|R_{MT}^I+\dfrac{1}{|\vec{K}|^3}\sin|\vec{K}|R_{MT}^I\right] & \text{if } |\vec{K}|\neq 0\end{cases} \tag{E.29}$$

where $\vec{K}=\underset{\sim}{\vec{k}}+\vec{G}''+\mathcal{R}\left(\vec{q}+\vec{G}\right)-\mathcal{R}'\left(\underset{\sim}{\vec{k}}'+\vec{G}'''\right)$.

Eq. (E.16) for the Kohn-Sham response function has an ultimate version presented below

$$\chi_{\vec{G},\vec{G}'}\ \vec{q},\omega\ =\frac{1}{N\Omega_0}\sum_{\underset{\sim}{\vec{k}}}^{BIZ}\sum_{\mathcal{R}}\sum_{n,n'}\frac{f_{\underset{\sim}{\vec{k}},n}-f_{\underset{\sim}{\vec{k}}',n'}}{E_{\underset{\sim}{\vec{k}},n}-E_{\underset{\sim}{\vec{k}}',n'}+\hbar\ \omega+i\eta}e^{i\left[\mathcal{R}\ \vec{G}-\vec{G}'\right]\cdot\vec{\tau}\left(\mathcal{R}\right)}$$

$$\times\left[ME\_MT_{n,n'}\ \mathcal{R},\underset{\sim}{\vec{k}},\vec{q}+\vec{G}\ +ME\_INT_{n,n'}\ \mathcal{R},\underset{\sim}{\vec{k}},\vec{q}+\vec{G}\ \right] \tag{E.30}$$

$$\times\left[ME\_MT_{n,n'}\ \mathcal{R},\underset{\sim}{\vec{k}},\vec{q}+\vec{G}'\ +ME\_INT_{n,n'}\ \mathcal{R},\underset{\sim}{\vec{k}},\vec{q}+\vec{G}'\ \right]^*$$

with the matrix element expression in eqs. (E.24) and (E.29).

Note that in eq. (E.24) if the rotation matrix $\mathcal{R}_{LOC}$ that transforms the general coordinate system $\vec{r}$ into the local system $\vec{r}'=\mathcal{R}_{LOC}\cdot\vec{r}$ is not an identity matrix,

$$Y_{lm}\ \Omega_{\vec{r}}\ =Y_{lm}\ \Omega_{\mathcal{R}_{LOC}^{-1}\vec{r}'}\ =\mathcal{R}_{LOC}Y_{lm}\ \Omega_{\vec{r}'}\ =\sum_{m'=-l}^{l}D_{m'm}^{l'}\ \mathcal{R}_{LOC}\ Y_{lm'}\ \Omega_{\vec{r}'}\ .$$

Meanwhile, local rotation matrices $\mathcal{R}_I$ change the atom position $\boldsymbol{X}_I$ in the global coordinate system to a position in a local coordinate system $\boldsymbol{X}_I'$ for each atomic site in this way:

$$X_I' = \mathcal{R}_I X_I .$$

The matrix element expression in eq. (E.24) for each atom could use wavefunction got in the local system because the local rotation matrix $\mathcal{R}_{LOC}$ is unit matrix (plane waves are naturally in the local system), and rotation matrices $\mathcal{R}_I$ for each kind of atom are the same. The only difference in the local reference frame is that nonequivalent atom of the same kind become equivalent (having the same site symmetry). Thus, the position variable of a wavefunction in eq. (E.20) becomes

$$R'^{-1}\ \vec{x}_I - \vec{\tau}\ R' = \vec{x}_{IR} + \vec{R}_{IR}$$

where, $\vec{x}_{IR}$ is one of the positions of this kind of atom in the local system and $\vec{R}_{IR}$ is a primitive lattice vector. The eq. (E.24) turns into

$$ME\_MT_{n,n'}\ \mathcal{R}, \vec{\tilde{k}}, \vec{q}+\vec{G}$$

$$= N \sum_I \int_{Sphere} d^3x \Psi^I_{\vec{\tilde{k}},n}\ \vec{x}\ e^{-i\left[\mathcal{R}\left(\vec{q}+\vec{G}\right)\right]\cdot\vec{x}} \Psi^I_{\vec{\tilde{k}}',n'}\ \mathcal{R}'^{-1}\ \vec{x}-\vec{\tau}\ \mathcal{R}'$$

$$= N \sum_{I=1}^{Na} \frac{4\pi^{\ 3}\ R_{MT}^{I\ \ 4}}{N\Omega_0} e^{-i\left[\mathcal{R}(\vec{q}+\vec{G})\right]\cdot\vec{x}_I} e^{i\vec{\tilde{k}}'\cdot\vec{R}_{IR}} \times \sum_{l''=0}^{\infty} (i)^{l''} \sum_{m''=-l''}^{l''} Y^*_{l''m''}\left(\Omega_{\mathcal{R}\ -\vec{q}-\vec{G}}\right)$$

$$\times \sum_l \sum_m \sum_{l'} \sum_{m'} \sum_{m'''=-l'}^{l'} \int d\Omega_{\vec{r}} Y^*_{lm}\left(\Omega_{\vec{r}}\right) Y_{l''m''}\left(\Omega_{\vec{r}}\right) Y_{l'm'''}\left(\Omega_{\vec{r}}\right) D^{l'}_{m'm'''}\left(\mathcal{R}'\right) \sum_\beta \sum_{\beta'} \int_0^{R^I_{MT}} dr$$

$$\left\{P^{*I}_{l,\beta}(r) P^I_{l',\beta'}(r) + \alpha^2 Q^{*I}_{l,\beta}(r) Q^I_{l',\beta'}(r)\right\} j_{l''}\left(\left|\mathcal{R}\left(\vec{q}+\vec{G}\right)\right| r\right) \times \left(A^{I,\vec{\tilde{k}},n}_{l,m,\beta}\right)^* A^{I,\vec{\tilde{k}}',n'}_{l',m',\beta'}$$

. (E.31)

In fact, we use eq. (E.31), (E.29) and (E.30) to calculate KS response in the local system.

APPENDIX F
THE GROUND-STATE DATA FILE IN THE ABSENCE OF EXTERNAL MAGNETIC FIELD AND SPIN-ORBIT COUPLING

These files are obtained from WIEN2k, a commercial code which solves KS equations by using LAPW method. Orthogonality of the KS orbitals is used as a validation criterion for the data in the files. Afterwards, these data are used to calculate the dynamical charge response. Below, we provide a description of files given by WIEN2k:

case.struc

An example of the structure file is given for silicon in the following:

```
-------------------------------------------top of file-------------------------------------------line#

T F                                                                                                1
10.26121700000000       10.26121700000000       10.26121700000000                                  2
1.570796326794897       1.570796326794897       1.570796326794897                                  3
270.1074883993305       1                                                                          4
        2                                                                                          5

0.6123235974036595          0.0000000000000000E+000  0.0000000000000000E+000                   6
0.0000000000000000E+000  0.6123235974036595          0.0000000000000000E+000                   7
0.0000000000000000E+000  0.0000000000000000E+000  0.6123235974036595                            8

-0.6123235974036595      0.6123235974036595      0.6123235974036595                             9
0.6123235974036595      -0.6123235974036595      0.6123235974036595                             10
0.6123235974036595       0.6123235974036595     -0.6123235974036595                             11
```

0.1250000000000000 0.1250000000000000 0.1250000000000000 12

0.8750000000000000 0.8750000000000000 0.8750000000000000 13

0.0000000000000000E+000 0.0000000000000000E+000 1.000000000000000 14

0.0000000000000000E+000 1.000000000000000 0.0000000000000000E+000 15

1.000000000000000 0.0000000000000000E+000 0.0000000000000000E+000 16

0.0000000000000000E+000 0.0000000000000000E+000 0.0000000000000000E+000 17

-1.000000000000000 0.0000000000000000E+000 0.0000000000000000E+000 18

0.0000000000000000E+000 -1.000000000000000 0.0000000000000000E+000 19

0.0000000000000000E+000 0.0000000000000000E+000 -1.000000000000000 20

0.0000000000000000E+000 0.0000000000000000E+000 0.0000000000000000E+000 21

1.000000000000000 0.0000000000000000E+000 0.0000000000000000E+000 22

0.0000000000000000E+000 1.000000000000000 0.0000000000000000E+000 23

0.0000000000000000E+000 0.0000000000000000E+000 1.000000000000000 24

0.4073582315219531 25

29 26

8 8 8 27

----------bottom of file----------

line 1: format (L2,x,A4)

a,b

a T/F relativistic (non-relativistic) calculations

b F(cc) lattice type

line 2: format (3G25.16)

Bravais lattice constants in a.u (1 a.u.=0.529177 Å).

line 3: format (3G25.16)

Angles between the three primitive vectors of Bravais lattice

line 4: format (G25.16,I5)

unitvolume, nat

univolume Primitive unit cell volume in a.u.^{3}

nat Total number of different kinds of atoms in the primitive unit cell (a unique atomic basis set), which are (chemically) different even in the local systems.

line 5: format (*)

Total number of (crystallographically) nonequivalent atoms for each kind of atoms in the primitive unit cell.

In our case, there are only two nonequivalent atoms of the same kind per unit cell.

line 6-8:format (*)

Transformation matrix from the Bravais reciprocal lattice (β') to the Cartesian coordinate system (k) $k \leftarrow \beta'$.

line 9-11:format (*)

Transformation matrix from the primitive reciprocal lattice (β) system to the Cartesian system (k) $k \leftarrow \beta$.

line 12:format (*)

Position of the 1st nonequivalent atom in primitive lattice system α

line 13:format (*)

Position of the 2nd nonequivalent atom in primitive lattice system α

This procedure (line 12 and 13) is repeated for all atoms in the nonequivalent atom basis set.

The descriptions from Line 1 to 13 are within the general coordination-system.

line 14-16:format (*)

ROTIJ Rotation matrix of the position of the 1st nonequivalent atom.

line 17:format (*)

TAUIJ Non-primitive translation of the 1st nonequivalent atom after rotation.

In our case, this local rotation matrix changes the 1st atom in itself.

This procedure (line 14-17) is repeated for all atoms in the nonequivalent atom basis set.

line 18-20:format (*)

ROTIJ Rotation matrix of the position of the 2nd nonequivalent atom.

line 21:format (*)

TAUIJ Non-primitive translation of the 2nd nonequivalent atom after rotation.

In our case, this local rotation matrix changes the 2nd atom into the 1st one.

Local rotation matrices change the global coordinate system to a local coordinate system for each atom. Atoms of the same kind become same[68].

line 22-24:format (*)

ROTLOC Rotation matrix $\mathcal{R}_{LOC}$ that transforms the general coordinate system $\vec{r}$ into the local system $\vec{r}' = \mathcal{R}_{LOC}\vec{r}$.

Lines 22-24 are repeated for each kind of atoms.

Especially, in the local system, the density and potential are expanded by a symmetrized spherical harmonics (lattice harmonics) to minimize the number of LM combinations. And the interpretation of the partial charges requires a proper orientation of the coordinate system.

line 25:format (*)

EFERMI Fermi Energy in Rydbergs (the zero corresponds to the average potential in the interstitial region).

line 26:format (*)

num_kpoint Number of special wave vector $\vec{k}$ in the wedge (irreducible zone of BZ or PZ)

line 27:format (*) A mesh of k-points in BZ or PZ is called k-mesh

case.radwf

This is the radial part of the KS wave function of different kind of atoms for si:

----------top of file ----------line #

1 781 0.1000000000000000E-03 0.1269677891350786E-01 2.000000000000000 1

0.1000000000000000E-03 0.1012777725233957E-03 0.1025718720730069E-03 0.1038825072710885E-03 2

0.1052098894056130E-03 0.1065542324643330E-03 0.1079157531692775E-03 0.1092946710116900E-03 3

0.1106912082874132E-03 0.1121055901327245E-03 0.1135380445606311E-03 0.1149888024976277E-03 4

……..……

……

0.1806828230483254E+01 0.1829915385157326E+01 0.1853297541150258E+01 0.1876978467907845E+01 195

0.1900961983040826E+01 0.1925251952940320E+01 0.1949852293401132E+01 0.1974766970253013E+01 196

0.2000000000000000E+01 197

0 0 198

0.1206693719154186E-02 -0.8469012334153209E-02 0.1739369261122543E-03 -0.1220752167038603E-02 199

0.1222031333256928E-02 -0.8576657249305038E-02 0.1761477418383877E-03 -0.1236268470269575E-02 200

0.1237563895259563E-02 -0.8685670379226295E-02 0.1783866580161249E-03 -0.1251981992618618E-02 201

……..……

……

0.9644760316379138 -0.4792678811228312 -0.2695014889483754 -0.3609135830838770 977

0.9525676814531685 -0.4870904114716960 -0.2911270824362163 -0.3641712171838272 978

0.9398130209594196 -0.4944112673013740 -0.3134194456704765 -0.3671387608257123 979

1 1 980

0.6218224000938161E-06 0.6080735414772907E-03 0.7183809816910824E-07 0.7024971561025428E-04

0.1445048727685413E-05 0.1413097851280930E-02 981

0.6356243214545141E-06 0.6215702942474135E-03 0.7343261097772329E-07 0.7180897280382157E-04

0.1477122916230055E-05 0.1444462860671727E-02 982

……..……

……

2.499063066653207 5.610682790172643 -0.9584766858701888E-02 -0.1404237130911250 8015

2.828609456991570 6.271132923997019 -0.1759362253787647E-01 -0.1752950448359072 8016

3.201652005852213 7.009405482276383 -0.2774398002511145E-01 -0.2169576247373168 8017

10 0 8018

0.6348338890816690E-46 0.8119499500491326E-42 0.5178103130007400E-47 0.6622772744284051E-43 8019

0.7256921940834644E-46 0.9281573508772036E-42 0.5919200417988130E-47 0.7570633147307683E-43 8020

0.8295542654716781E-46 0.1060996515776939E-41 0.6766364575721910E-47 0.8654152643328452E-43 8021

……..……

……

2.553575669162728 6.403702807490168 -0.7219328935980500E-02 -0.1285767030036476 8797

2.928140333737076 7.251027260265472 -0.1462615165169869E-01 -0.1645022040036292 8798

3.357684452093923 8.210550990854122 -0.2423743949158455E-01 -0.2082347055616752 8799

----------bottom of file ----------

line 1: format (2i4,3G25.16)

number,max_r_mesh, R0,dx,Rmt

number The 1st kind of atoms

max_r_mesh Maximum number of radial mesh points

R0 Initial length in the logarithmic mesh

dx Step to construct the logarithmic mesh

Rmt Radius of the muffin tin atomic sphere

line 2-197: format (4E24.16)

rmesh r points are constructed according to the equation $r_n = R_0 e^{n \cdot dx}$ in the logarithmic mesh, where n = 0,1,2,…., (max_r_mesh-1)

line 198: format (*)

numl, isloc

numl =0 Number of ℓ (angular momentum) component ($0 \le$ numl ≤ 10).

isloc =0 No local orbitals.

line 199-979: format (4G25.16)

$P_\ell, Q_\ell, \dot{P}_\ell, \dot{Q}_\ell$ Used to construct the Dirac radial functions $u_\ell^I(r)$ and $\dot{u}_\ell^I(r)$.

They are ordered in the same way as r-mesh.

$$u_\ell^I(r) = \frac{1}{r}\begin{pmatrix} P_\ell^I(r) \\ i\alpha Q_\ell^I(r)(-\vec{\sigma}\cdot\hat{r}) \end{pmatrix}$$

$$\dot{u}_\ell^I(r) = \frac{1}{r}\begin{pmatrix} \dot{P}_\ell^I(r) \\ i\alpha \dot{Q}_\ell^I(r)(-\vec{\sigma}\cdot\hat{r}) \end{pmatrix}$$

P_ℓ Major component

Q_ℓ Minor component (relativistic)

$\dot{P}_\ell$ Energy derivative of the major component

$\dot{Q}_\ell$ Energy derivative of the minor component

line 980: format (11X, I2, 10X, I2)

numl, isloc

numl=1 ℓ component

isloc =1 Has local orbitals.

line 981-1761: format (6G25.16)

$P_\ell, Q_\ell, \dot{P}_\ell, \dot{Q}_\ell, P_\ell^{local}, Q_\ell^{local}$ Used to construct the radial functions $u_{\ell,m,s}^I(r)$, $\dot{u}_{\ell,m,s}^I(r)$ and $u_{\ell,m,s}^{I,local}(r)$.

$$u_\ell^{I,lo}(r) = \frac{1}{r}\begin{pmatrix} P_\ell^{I,lo}(r) \\ i\alpha Q_\ell^{I,lo}(r)(-\vec{\sigma}\cdot\hat{r}) \end{pmatrix}$$

P_ℓ^{local} Major component for the local orbitals

Q_ℓ^{local} Minor component for the local orbitals

The same format is used for all ℓ components as it can be seen from line 8018, where the data are for ℓ =10 with no local orbital contribution (isloc=0).

The entire format is repeated for each kind of atoms.

In absence of external magnetic field, spin-orbit coupling and spin polarization, the only quantum number needed is ℓ.

case.kg2

For a given wave vector $\vec{k}$ in the wedge (irreducible zone of BZ or PZ) and a band index *n*, coefficients $C_n\ \vec{k}+\vec{G}$ are those defined in Eq. (D.9):

----------top of file ----------line #

0.0000000000000000E+00 0.0000000000000000E+00 0.0000000000000000E+00 1 289 67 1 67 1

0 0 0 -1 -1 -1 1 -1 -1 -1 1 -1 -1 -1 1 1 1 -1 1 -1 1 -1 1 1 1 1 1 1 0 0 -2

0 -2 0 -2 0 0 2 0 0 0 2 0 0 0 2 0 -2 -2 -2 0 -2 -2 -2 0 2 0 -2 2 -2 0

0 2 -2 0 -2 2 -2 2 0 -2 0 2 2 2 0 2 0 2 0 2 2 -1 -1 -3 -1 -3 -1 1 -1 -3

……..……

……

4 -2 4 -4 4 2 -4 2 4 0 6 0 0 0 6 4 4 2 4 2 4 -2 4 4 2 4 4 0 -2 -6

0 -6 -2 -2 0 -6 2 0 -6 -2 -6 0 2 -6 0 0 2 -6 0 -6 2 -6 0 -2 -6 -2 0 6 0 -2

6 -2 0 -6 2 0 -6 0 2 6 2 0 6 0 2 0 6 -2 0 -2 6 -2 6 0 2 6 0 -2 0 6

2 0 6 0 6 2 0 2 6 2

-1 -1 -1 1 -1 -1 -1 1 -1 -1 -1 1 1 1 -1 1 -1 1 3

1 -6.203512927989510 3.9062500000000639E-003 4

0.3740374925775061E-15 -0.8395204094233819E-02 0.7686056914887067E-02

0.1844298950106750E-01 -0.3452425051045617E-01 -0.3452425051027610E-01

0.1844298950112365E-01 0.7686056914918202E-02 -0.8395204094503173E-02

……..……

……

-0.1339245276284827E-05 -0.8024665559394769E-06 -0.8024665571432173E-06 5

-0.5054299033951716E-02 -0.5054299036069679E-02 0.7161350077237138E-01

-0.3058994864175180 -0.3008451873803917 0.7666779980861987E-01 6

2 -6.203512927989504 3.9062500000000639E-003 7

0.1117323476067929E-14 0.1971085424616810E-01 -0.1771619677045144E-01

0.3009001839228489E-01 0.7337032624606389E-02 0.7337032624468631E-02

0.3009001839255692E-01 -0.1771619677085551E-01 0.1971085424643695E-01

……..……

……

0.7285330822991943E-02 203

0.5392611589050057E-17 -0.2073807122691731E-16 -0.3427507956411751E-16

-0.3429717570000177E-16 -0.5688770619415353E-17 0.2934130472511674E-17 204

0.1250000000000000E+00 0.1250000000000000E+00 -0.1250000000000000E+00 2 307 68 1 68 205

0 0 0 -1 -1 1 -1 -1 -1 1 -1 1 -1 1 1 1 -1 -1 -1 1 -1 1 1 1 0 -2 0 -2 0 0

0 0 2 1 1 -1 0 0 -2 2 0 0 0 2 0 -2 -2 0 0 -2 2 -2 0 2 0 -2 -2 -2

……..……

……

0 6 -2 2 6 0 -2 -6 -2 -6 -2 -2 2 -6 2 -6 2 2 2 -2 6 -2 2 6 0 0 0 -1 -1 1 206

-1 -1 -1 1 -1 1 1 -1 -1 -1 1 -1 207

1 -6.203550813341432 3.1250000000000511E-002 208

-0.1296615706515974E-11 0.3699287606971739E-10 0.2744077414692920E-01

0.3754367791326569E-01 -0.1010290378376723E-01 -0.7302369285534880E-02

0.2713653478907228E-01

……..……

……

-0.1802871161265438E-03 209

0.6093503007041291E-01 0.2426683479956198 0.1142345429576091

0.3139304522207872 0.9614041916769867E-01 0.3603460130642538 210

2 -6.203550813341426 3.1250000000000511E-002 211

-0.1382555736104320E-12 0.3704988977510143E-11 0.2750876676926200E-01

-0.1001002412198162E-01 0.3751879088953358E-01 0.2711854648068082E-01

-0.7235235945340163E-02 0.1988331053953430E-01

……..……

……

-0.2913684626296956E-02 -0.2623701359144162E-02 0.4102101626576705E-02

0.1396643966884592E-03

0.4179292507232789E-05 -0.5674576001750915E-05 -0.1220435484959635E-04

-0.1158498814665050E-04 0.5809206525591932E-16 -0.5146165396592846E-16

74 5.430141734215908 0.0000000000000000E+000

0.2599408096627260 0.2467489052777631 0.8901483668179954E-01

-0.1208629131615090 0.1042614459570057 0.2128560116550380

0.7678795380508640E-01 -0.2242359047101155 -0.6285035029954454E-01

0.8501809224802944E-01 0.1724190153722392 0.6128817582687615E-01

……..……

……

0.5059266473170637E-02 -0.6511828380540403E-02 6410

0.1220435484965858E-04 0.1158498814657759E-04 0.4179292507249952E-05

-0.5674576001742430E-05 0.6018251450364120E-16 0.1504394159370309E-17 6411

----------bottom of file ----------

line 1: format (3E24.16,A11,4I4)

a,b,c, name_spkp, num_basis, num_eigenvalue, nband_min, nband_max

a,b,c Coordinates of the 1st $\vec{k}$ -point in the wedge in conventional reciprocal lattice system

name_spkp Ordinal number of the given $\vec{k}$ -point in the wedge

num_basis Maximum number of basis vectors $\vec{G}$ for this $\vec{k}$ -point

num_eigenvalue Maximum number of eigenvalues $E_{\vec{k},n}$ for this $\vec{k}$ -point

nband_min Ordinal number of the first band for this $\vec{k}$ -point

nband_max Ordinal number of the last band for this $\vec{k}$ -point

line 2: format (2200(3I4,x))

a,b,c $\vec{G}$ vectors in conventional reciprocal lattice system is utilized to construct the LAPW basis.

line 3: format (2200(3I4,x))

$\vec{H}^I_{\ell^{lo}}$ vectors (Eq. C.6) corresponding to the local orbitals (subgroup of $\vec{G}$ vectors) of the I^{th} atomic sphere. The total number of vectors $\vec{H}^I_{\ell^{lo}}$ is $2\ell^{lo}+1\,N$ for every ℓ^{lo}, where N is the total number of the nonequivalent atoms of the same kind. In

this case, $N = 2$ and only $\ell^{lo} = 1$ is consdiered, so the total number of $\vec{H}^{I}_{\ell^{lo}}$ vectors is six:

-1 -1 -1 1 -1 -1 -1 1 -1 -1 -1 1 1 1 -1 1 -1 1

If we have more than one ℓ^{lo} component for the local orbitals, the vectors $\vec{H}^{I}_{\ell^{lo}}$ will be listed as an ascending order of ℓ^{lo}.

When there is more than one kind of atoms, the vectors $\vec{G}$ and the coefficients $C_n\ \vec{k}+\vec{G}$ used to construct the wave functions for the interstitials and the atomic sphere are the same, except for the contribution of the local orbitals, where the vectors $\vec{H}^{I}_{\ell^{lo}}$ are listed according to the corresponding atom.

line 4: format (*)

bandindex, eigenvalue, weight

bandindex	Band index n
eigenvalue	Eigenvalue $E_{\vec{k},n}$ (in Ry) for k vector and band index n
	The zero energy is chosen as the average potential in the interstitial region.
weight =	$f_{\vec{k},n} \times$ (number of points in the star of k)/(number of reciprocal primitive unit cells or size of k-mesh).

line 5: format (2200(G25.16))

eigenvector	For a given special wave vector $\vec{k}$ in the wedge and the band index n , eigenvector is given in terms of reciprocal lattice vectors $\vec{G}$.

line 6: format (2200(G25.16))

These six eigenvectors are used to construct the local orbitals and are denoted as $C_n^{local}\ \vec{k}+\vec{H}^I_{\ell^{lo}}$.

line 7-204:

The format of lines 4 to 6 is repeated for all the bands (n from 2 to 67)

line 205-6411:

The format of lines1-204 is repeated for the entire special wave vectors $\vec{k}$ in the wedge

case.abclo

This file presents coefficients of the radial part of the local orbitals for silicon:

----------top of file ----------line #

7.9595649267803781E-002 0.1746947408861206 0.9973312931702077 1

----------bottom of file ----------

line 1: format (*)

a,b,c	coefficients necessary to construct the local orbitals. They are written for each kind of atoms in the ascending order of ℓ^{lo}. For Si, there are two nonequivalent atoms of the same kind and the only contribution to the local orbitals which comes from $\ell^{lo}=1$.
A	$a^{I,local}_{\ell,0}$
B	$a^{I,local}_{\ell,1}$
C	$a^{I,local}_{\ell,2}$

The entire format is repeated for each kind of atoms in local system.

case.ab

Coefficients of the radial part of the non-local wave functions are given below for silicon:

----------top of file ----------line #

128		1
0.3671508107800111	-0.4944186307593381	2
0.2199956637885180	0.1861754913917260E-01	3
0.2199956637885180	0.1861754913917260E-01	4
0.2199956637885180	0.1861754913917260E-01	5
0.2199956637885180	0.1861754913917260E-01	6
0.2199956637885180	0.1861754913917260E-01	7
0.2199956637885180	0.1861754913917260E-01	8
0.2199956637885180	0.1861754913917260E-01	9
0.2199956637885180	0.1861754913917260E-01	10
0.1764188505661603	0.1132435655331141	11
0.1764188505661603	0.1132435655331141	12
.....		
.....		
0.2621655790213903E-02	0.3759233847986692E-01	93120
0.2621655790213903E-02	0.3759233847986692E-01	93121
0.2621655790213903E-02	0.3759233847986692E-01	93122
0.2621655790213903E-02	0.3759233847986692E-01	93123
0.2621655790213903E-02	0.3759233847986692E-01	93124
0.2621655790213903E-02	0.3759233847986692E-01	93125

0.2621655790213903E-02 0.3759233847986692E-01 93126

0.2621655790213903E-02 0.3759233847986692E-01 93127

----------bottom of file ----------

line 1: format (*)

iblock	Total number of the basis vectors $\vec{G}$ which are used for calculating coefficients $a_{\ell,0}^{I,\vec{k},\vec{G}}$ and $a_{\ell,1}^{I,\vec{k},\vec{G}}$.

line 2-93127: format (2G25.16)

a,b	Coefficients used to construct the non local orbital part of the wave functions in the atomic sphere region in local system.
A	$a_{\ell,0}^{I,\vec{k},\vec{G}}$
B	$a_{\ell,1}^{I,\vec{k},\vec{G}}$

The process is repeated for every basis vectors $\vec{G}$, every angular momentum ℓ, every special $\vec{k}$ in the wedge, and each kind of atoms.

APPENDIX G

TEST IMPORTANT PARAMETERS IN WIEN2K

WIEN2k is a program mostly focused on LAPW method (partly on APW). It comprises the atomic forces[89] and the linear optical properties[90] based on the electronic structure which it creates.

The motivation of this test is to check the convergence of the most important parameters in WIEN2k with LAPW method and see how to solve the KS problem accurately and efficiently. The calculation material is chosen to be nickel owing to its significant magnetism and rich band characters (local orbital vs. delocalized orbital), but not too complicated electronic structure, compared with simple metal Al.

The calculated density of states (DOS) and band structure for the valence state of Ni in LAPW are shown below. From the sharp peak in DOS (Figure G.1), the flat band in band structure (Figure G.2), and band character plot (Figure G.3) in electrons with minority- spin, it can be seen that the largest contribution to the DOS near the Fermi level is provided by the d-component. From the wave functions dominated by s, p, d component at the Γ point (Figure G.4), it is also known that s-controlled Bloch state is quite delocalized. It has finite amplitude at neighboring sites. In energy space, this nature translates into a broad band (about 8eV). Compared with s-controlled state, d-governed state is pretty localized in the vicinity of the atom where it originates. The amplitude at the position of the nearest neighbor is so small that tunneling or hopping is not efficient.

Therefore, the possibility of the large DOS in d-governed band in its electronic

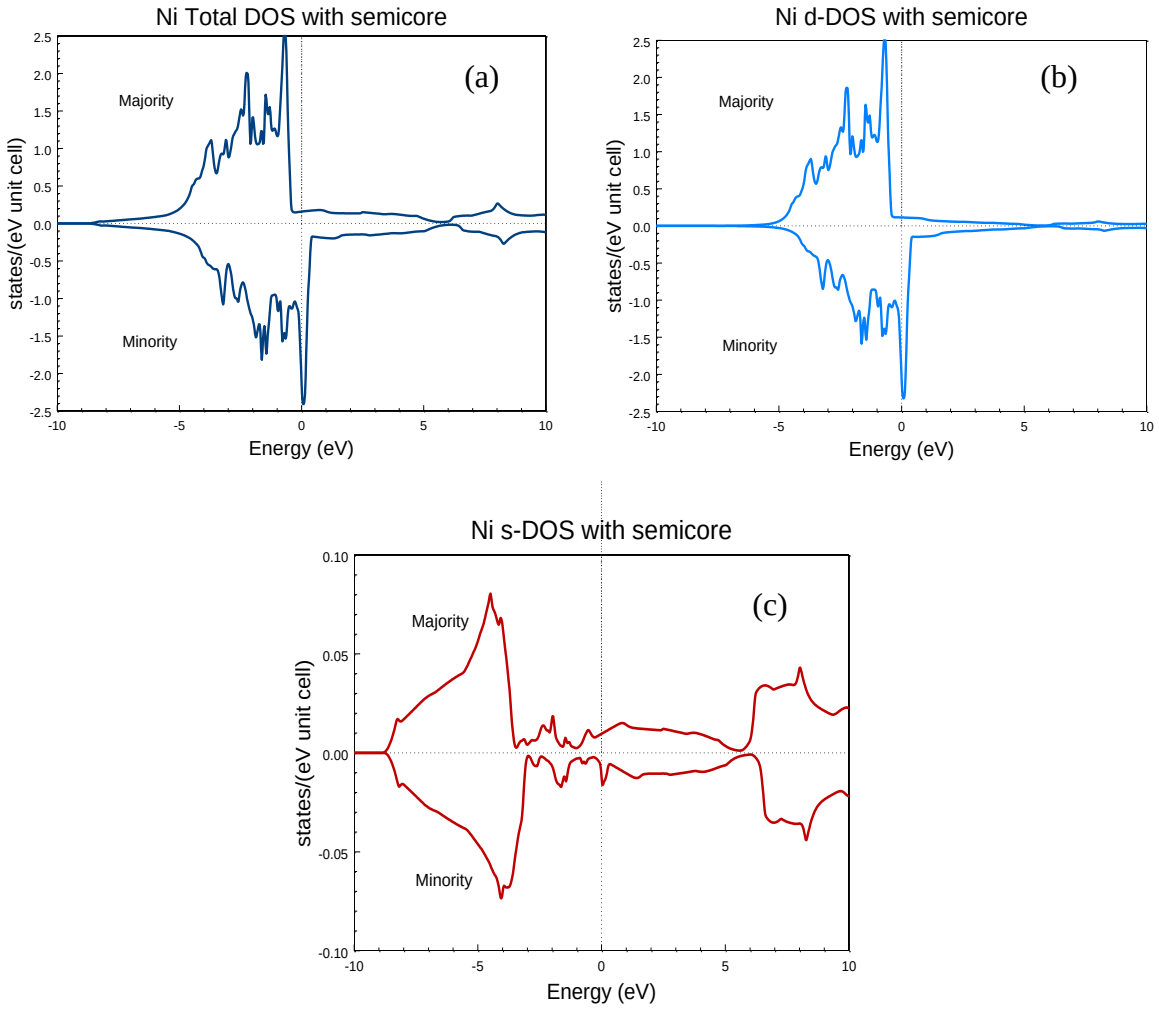

Figure G.1 (a) Calculated DOS (0~2.5states/eV*unit cell) of nickel with LAPW. The exchange splitting is about 0.8eV (the number obtained by finding the difference between the upper edge of the total DOS of majority and minority spin electron). (b) The d-DOS (0~2.5states/eV*unit cell) of majority and minority spin electron in nickel. (c) The s-DOS (0~0.1states/eV*unit cell) of majority and minority spin electron in nickel.

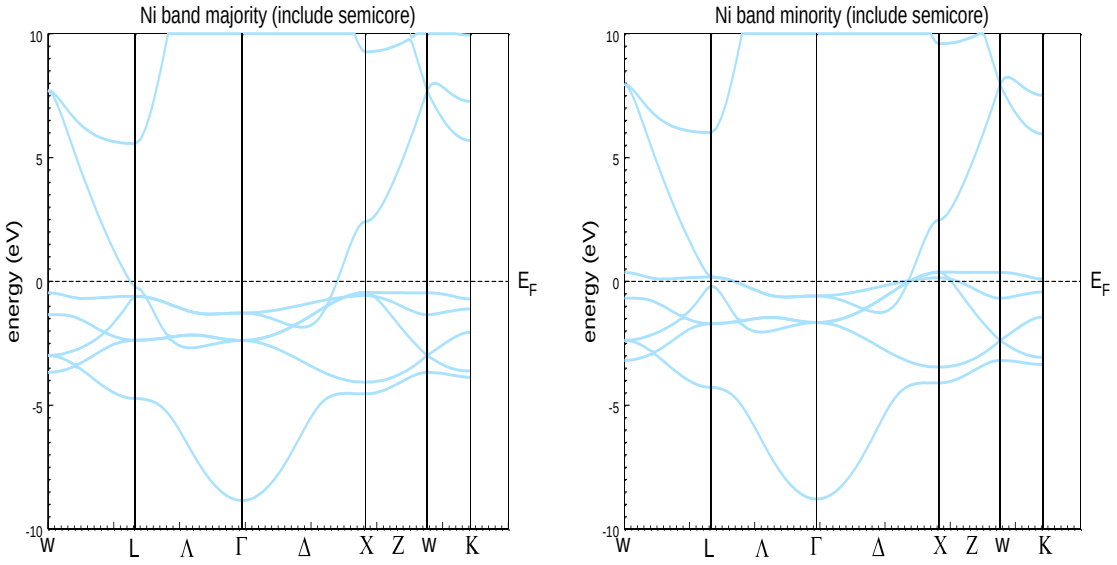

Figure G.2 The band structure of the majority and minority spin electron for nickel.

structure results because nickel has a large number (8 compared with the maximum number of 10) of d electrons in one atom and relatively narrow d-bandwidth (about 3eV) in DOS/bands (Figure G.2/Figure G.4) near or at the Fermi level. Furthermore, due to small s-content in partial DOS, the exchange splitting in s-component is small. It is clearly that the differing occupation of the d bands for majority and minority spins at the Fermi level leads to the magnetization (Figure G.1). The Stoner gap (defined as the distance between the upper edge of the d-band of majority spin electron and the Fermi energy) is 0.4eV.[†]

[†] In figure G. 4, three nodes can be recognized in the s-controlled Bloch state, two nodes in the p-dominated state, and no nodes in the d-governed state. The rule for the number of the nodes of the wave function is that they are $(n-l-1)$, where n is the principal quantum number, l is the azimuthal (orbital angular momentum) quantum number. Also, it can be found that there is finite amplitude at the site of the atom for the s-controlled state, zero amplitude at the same site for the p-

Based on the interpretation in section 2.4., it can be learned that there exists a number of parameters inside WIEN2k. Also it can be noted that the summation of the k points in DOS is over the first Brillouin zone by the tetrahedron method[80]. The direct consequence is that the size of the k-mesh will affect the DOS a little when the Fermi-Dirac distribution function is not constant just below or above the Fermi level. It happens because in WIEN2k the Fermi-Dirac distribution function is applied to specify the occupied states for constructing the charge density[†] and it is modified by the thermal broadening factor ($k_B \cdot T$, where k_B is Boltzman constant). Thus, changing the parameter will vary the result of the calculated physical quantities. This poses the issue of what is the impact on the density-functional-based electronic structure and total energy calculation when the parameter is changed in WIEN2k, or, if the calculations are convergent or not with the adjustable parameters. If they were not convergent, it would be a disaster because it is hard to decide which calculation is better. In principle, the calculations should be convergent with the adjustable parameters. The electronic structure and total

---

dominated state and d-governed state. The behavior is produced by the centrifugal potential term $\frac{l(l+1)\hbar^2}{2mr^2}$ in Kohn-sham equation.

[†] Expressed as $n\ \vec{x}\ = \sum_{\vec{k},j} f_{\vec{k},j} \left|\Psi_{\vec{k},j}(\vec{x})\right|^2$, where f is the Ferimi-Dirac distribution function.

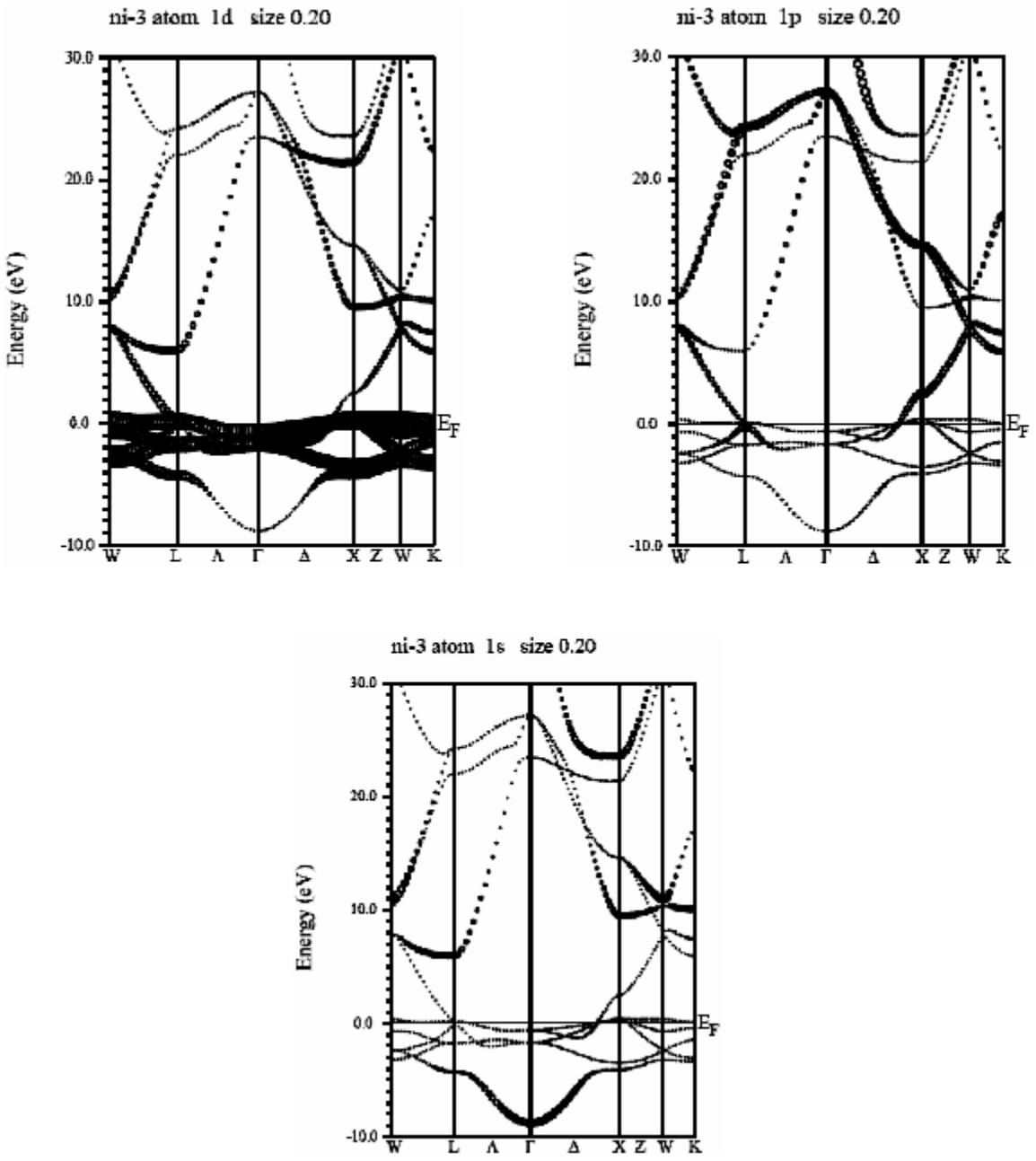

Figure G.3 Band character plots of the minority spin electron. From left to right and top to bottom, are d, p, s components respectively.

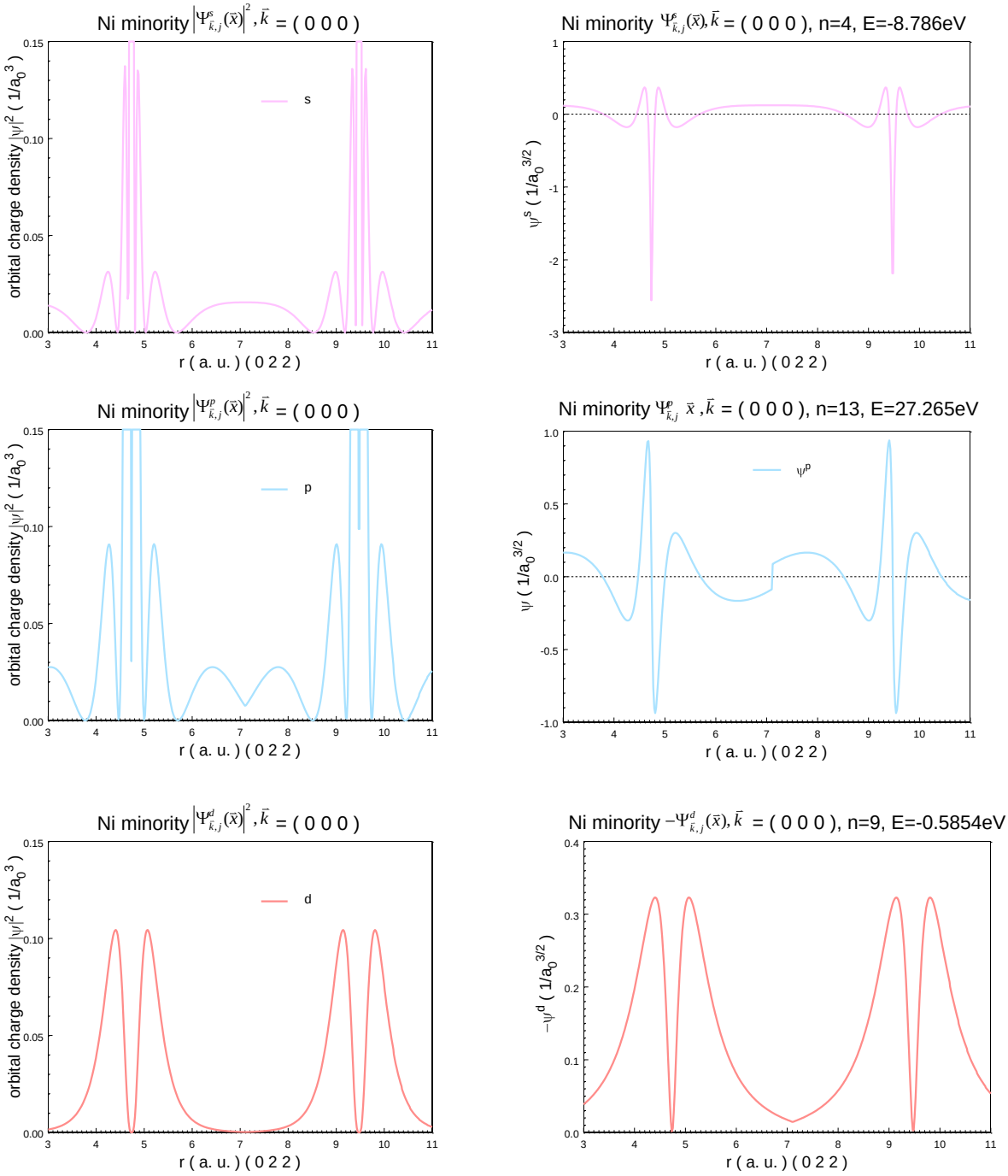

Figure G.4 Plots of |ψ|2 (left side) and |ψ| (right side) Pink color presents s-domianted orbital, blue color presents p-dominated orbital, red color presents d-dominated orbital.

energy determine the nature of the calculating material. Several tests are applied below to answer the question.

The first test is to study the effect of the choice of the atomic sphere radius R_{MT}. Firstly, the bands are compared in different radius ($R_{MT}=2.1a_0$ and $R_{MT}=2.3a_0$, where a_0 is the Bohr radius[†]) with different basis-set cutoff ($R_I^{\min} \cdot G_{\max} = 7, 8, 9 \text{ and } 10$), but the same linearization energies and local orbital, and the same k-mesh (Figure G.5).[†]

Apparently the convergence of the calculation with different $R_I^{\min} \cdot G_{\max}$ in $R_{MT}=2.1a_0$ is better than in $R_{MT}=2.3a_0$. It confirms that:

1. The smaller R_{MT} will make the calculations more expensive because more plane waves are needed, but a little bit more accurate because the plane waves are better basis functions to reduce the linearization error.

2. The R_{MT} cannot be too large because the spherical harmonics is not appropriate to describe the wave function far away from the nuclei.

3. The R_{MT} should be chosen as large as possible, but not too large, to achieve a promise of the accuracy and efficiency!

[†] $1\, a_0 = 0.529\ \mathring{\text{A}}$

[†] The energy which separates the core and the valence state is -6.0Ry. k-mesh is equal to 512. It is the same in the whole document except specified.

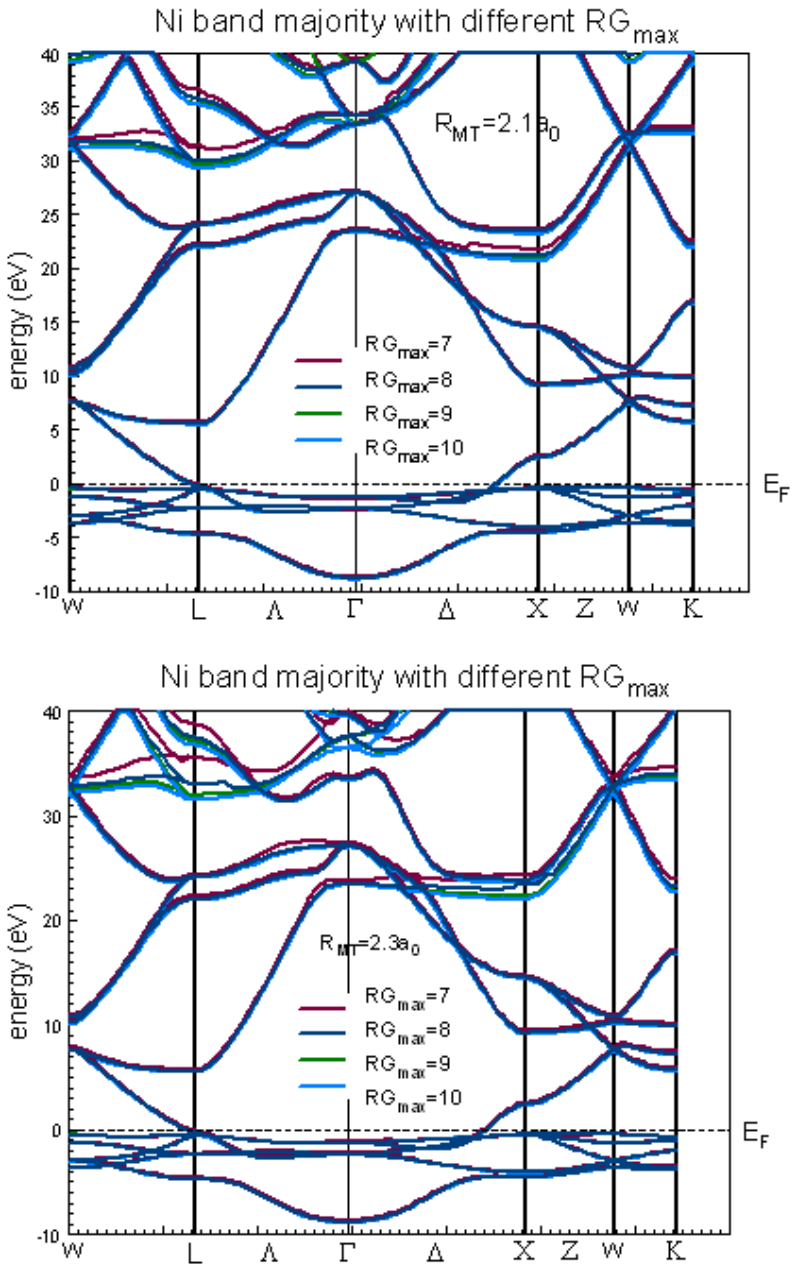

Figure G.5. The band structure for $R_{MT}=2.1a_0$ and $R_{MT}=2.3a_0$ with different basis-set cutoff, but the same linearization energies and local orbital, and the same *k*-mesh. The convergence of the calculation in $R_{MT}=2.1a_0$ is better than in $R_{MT}=2.3a_0$.

Secondly, the bands and DOS with R_{MT}=2.1a_0 and R_{MT}=2.3a_0 are evaluated in the same basis-set cutoff $R_I^{\min} \cdot G_{\max} = 8$, the same linearization energies and local orbital, and the same k-mesh (Figure G.6), which gives the same accuracy of the computation. It is obviously that the two curves in each plot merge well below 20eV and start to split above 20eV, which means the calculations do not converge well at high energy.[†] It will be seen to be improved by adding local orbital above the Fermi level in the next test.

The second test is to stabilize the bands above 20eV with different R_{MT} by adding local orbitals with energy in the region well above the Fermi level. This not only increases the basis set but provides the flexibility of the basis set in that energy region. The ground state is calculated in the two sphere radii 2.3a_0 and 2.1a_0 with local orbital ℓ=0, 1, 2, and 3. The total DOS are compared in the same content with local orbital and without local orbital at R_{MT}=2.3a_0 and 2.1a_0 (Figure G.7)

.It is clear that:

1. The curves go on different paths above 20eV without local orbital, like the curve with R_{MT}=2.1a_0 and the curve with R_{MT}=2.3a_0.

2. For ℓ=0, 1, and 3, what is common in the plots is that there is no appreciable difference in total DOS with and without local orbital in the same radius. For example, the curve with R_{MT}=2.3 a_0 +local orbitals meets the curve with R_{MT}=2.3a_0 well.

[†] It may be because: 1) the more accurate computation is needed by adjusting parameters, 2) the linearized method is not a precise technique, 3) the formula for exchange correlation functional is not exact for the high energy states, 4) the density functional theory (DFT) model is not suited to describe the unoccupied states and only more evolved methods , like GW approximation or time dependent-DFT, may help, etc.

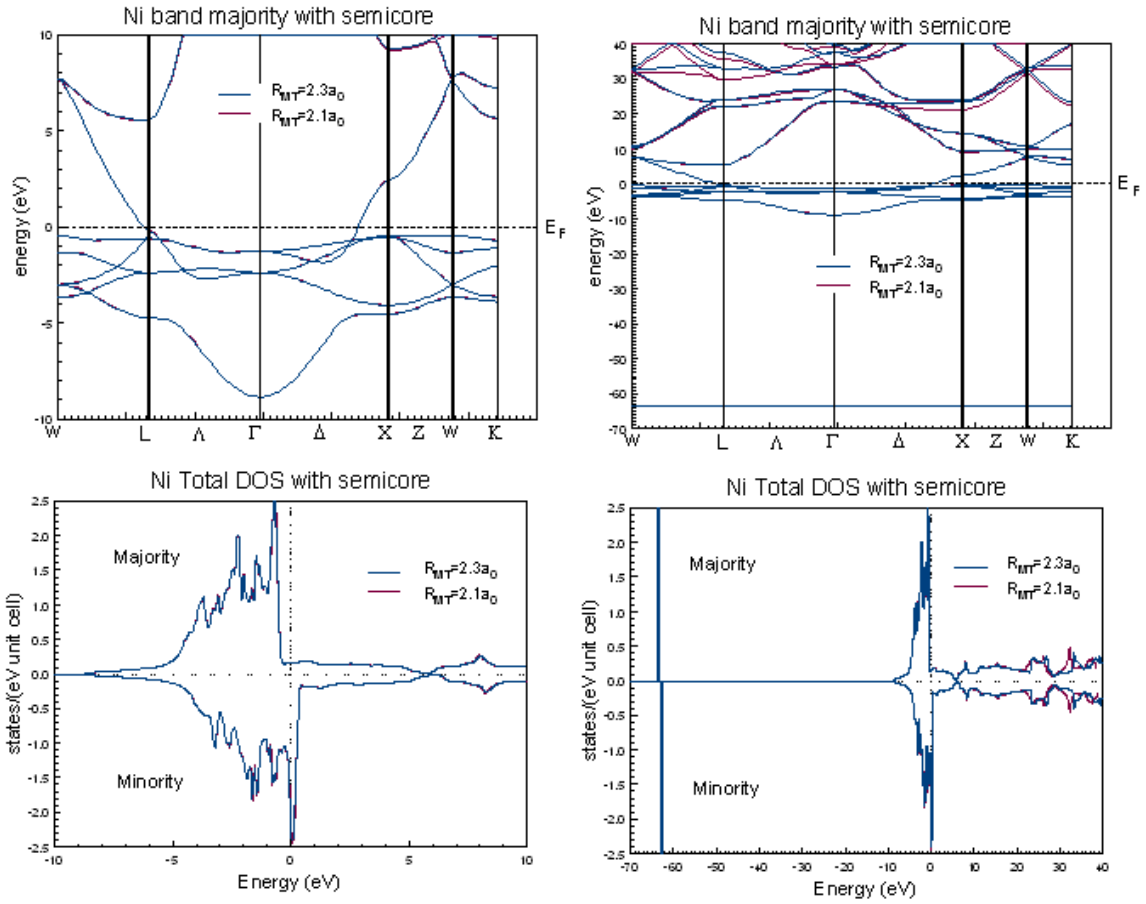

Figure G.6. The bands and DOS with $R_{MT}=2.1a_0$ and $R_{MT}=2.3a_0$ are plotted in the same basis-set cutoff $R_I^{\min} \cdot G_{\max} = 8$, the same linearization energies and local orbital, and the same k-mesh. The curves come together below 20eV, and split above 20eV.

3. The magnificent thing comes out that for $\ell = 2$ component the curves in R_{MT}=2.3 a_0 and 2.1 a_0 meet well with local orbital and they do not merge the curve without local orbital at high energy above 20eV. For instance, the curve with RMT=2.3 a_0 +lo meets the curve with R_{MT}=2.1 a_0 +local orbital well, and the curve with R_{MT}=2.3 a_0 +lo does not meet the curve with R_{MT}=2.3 a_0.† Thus, the calculations above 20eV are improved with different Rmt only by adding local orbital $\ell = 2$.

The third test is to estimate the consequence of the variety of the temperature broadening factors.† Firstly, the DOS is examined in the same temperature broadening factor with different *k*-mesh (*k*=216, 512, 4096) (Figure G.8). It is found that the sampling of the *k* points does affect the computation of the DOS due to the summation of the k points in the first Brillouin zone, the calculated d-DOS arrives a good precision since k=512 and the total DOS only has little disagreement in the range of 5eV to 10eV and above 23eV.† The total energy and the magnetic moment appear having an erratic behavior towards the exact value because the number of k points is not a variational parameter (Figure G.9). Secondly, the DOS is plotted in the *k*-mesh (*k*=512) with different temperature broadening factors ($E_{val} = k_B \cdot T = 0.002Ry$ and $0.006Ry$) (Figure 10) by tetra method. curves agree well, which expresses that the DOS is not sensitive to this change of the temperature broadening factor in nickel when k-mesh gives sufficient accuracy.

† Does it mean that d-content prevails over other contents in that energy region?

† In this test, $R_I^{\min} \cdot G_{\max} = 8$ and Rmt=2.3a0.

† No band shift is observed.

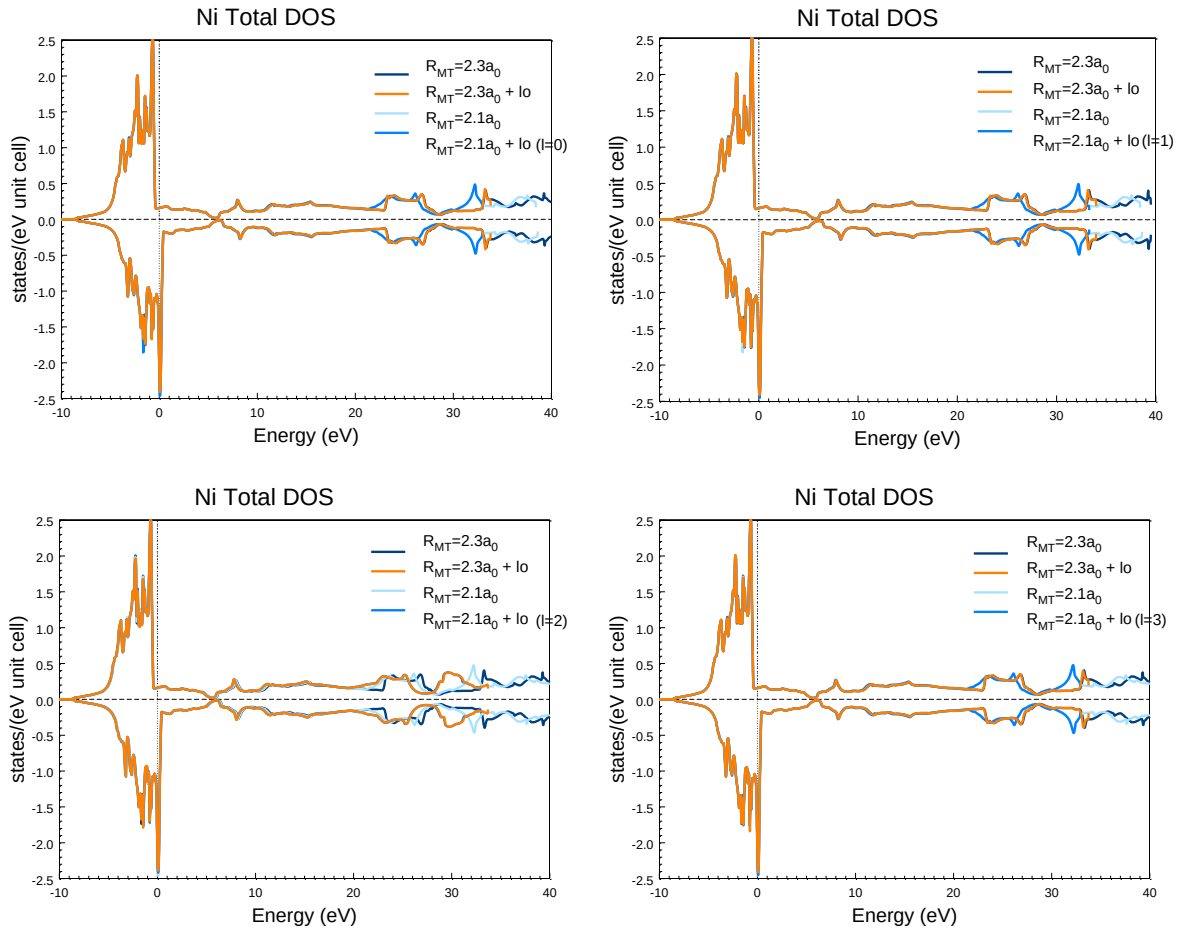

Figure G.7. The total DOS are compared in the same content local orbital and no local orbital with Rmt=2.3*a*0 and 2.1*a*0. The curves diverge above 20eV without local orbital. For ℓ =0, 1, and 3, there is no appreciable difference in total DOS with and without local orbital in the same radius. For $\ell = 2$ component the curves in Rmt=2.3*a*0 and 2.1*a*0 meet well with local orbital and they do not join the curve without local orbital at high energy above 20eV.

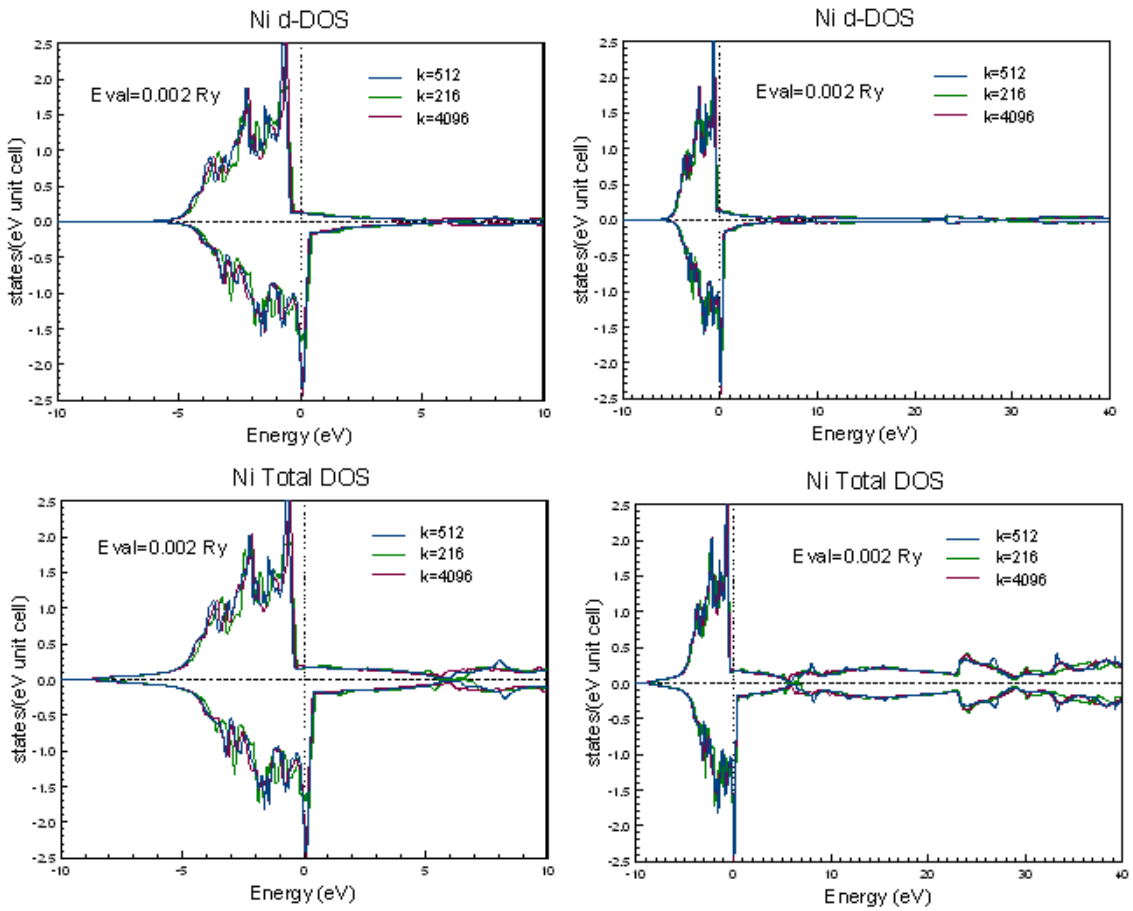

Figure G.8. The DOS is examined for the same temperature broadening factor with different k-mesh (k=216, 512, 4096). It is found that the sampling of the k points do affect the computation of the DOS. The figures in the left panels are details of those in the corresponding right panels.

The fourth test is to search for the change of the bands/DOS with and without putting the semicore states in the core state. The bands/DOS is drawn with Ecore< 4.5Ry and 6.0Ry respectively (Figure G.11).[†] It can be seen that up to 40eV there is no appreciable difference between the case in which semicore states are considered and treated like valence states and the case in which they are not considered.

The fifth test is to check the result of adjusting the charge convergence (cc) parameter in the self consistent cycle. The bands is schemed with cc=0.001, 0.0001 and 0.00001 correspondingly (Figure G.12). In the plots, the three curves become one and the computations reach enough accuracy after 0.001. The total energy remains the same as cc becomes smaller (Figure G.13).

The sixth test is to inspect the effect of the choice of the $\vec{G}$ basis vector sets with the definite muffin tin radius, namely the different basis-set cutoff $R_I^{\min} \cdot G_{\max}$ will be used with the same $R_I^{\min}$. Because the product $R_I^{\min} \cdot G_{\max}$ judges the accuracy of the computation and $R_I^{\min}$ is unchanged, in this test the accuracy of the computation becomes determined by $\vec{G}_{\max}$ if the same k-mesh, the same linearization energie,s and the same local orbital are applied; and the more $\vec{G}$ vectors are used, the more accurate the computation would be. After the adequate level of accuracy is reached, the further improvement will become not apparently as the $\vec{G}$ vector set is increased. With this in mind, the band structure is plotted in different scale (–10eV to 10eV and -10eV to 40eV) with R_{MT}=2.1 a_0 (Figure G.14). It can be found that the curves well match in the range of

[†] $R_I^{\min} \cdot G_{\max} = 8$ and Rmt=2.3a0.

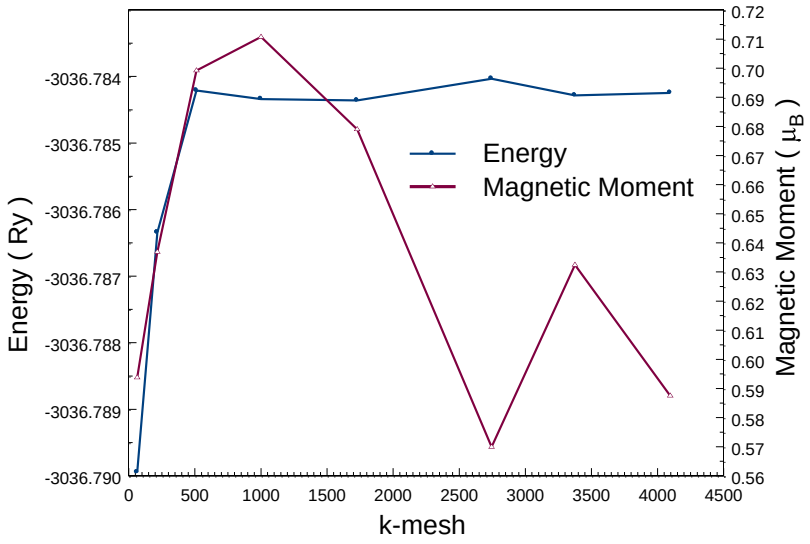

Figure G.9. The total energy and the magnetic moment appears an erratic behavior towards the exact value because the number of k points is not a variational parameter.

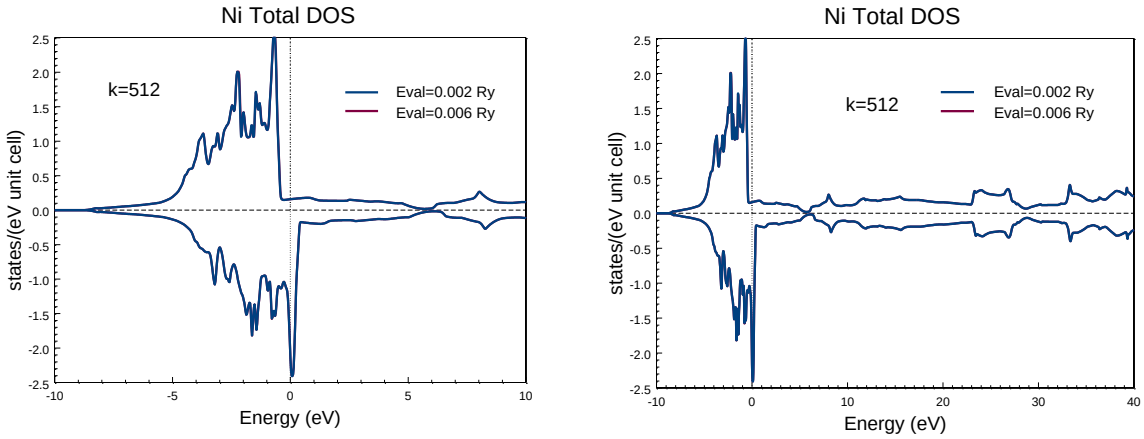

Figure G.10. The DOS agree well in the k-mesh (k=512) with temperature broadening factors (E_{val}=0.002Ry and 0.006Ry) The left panel is a detail of the right one.

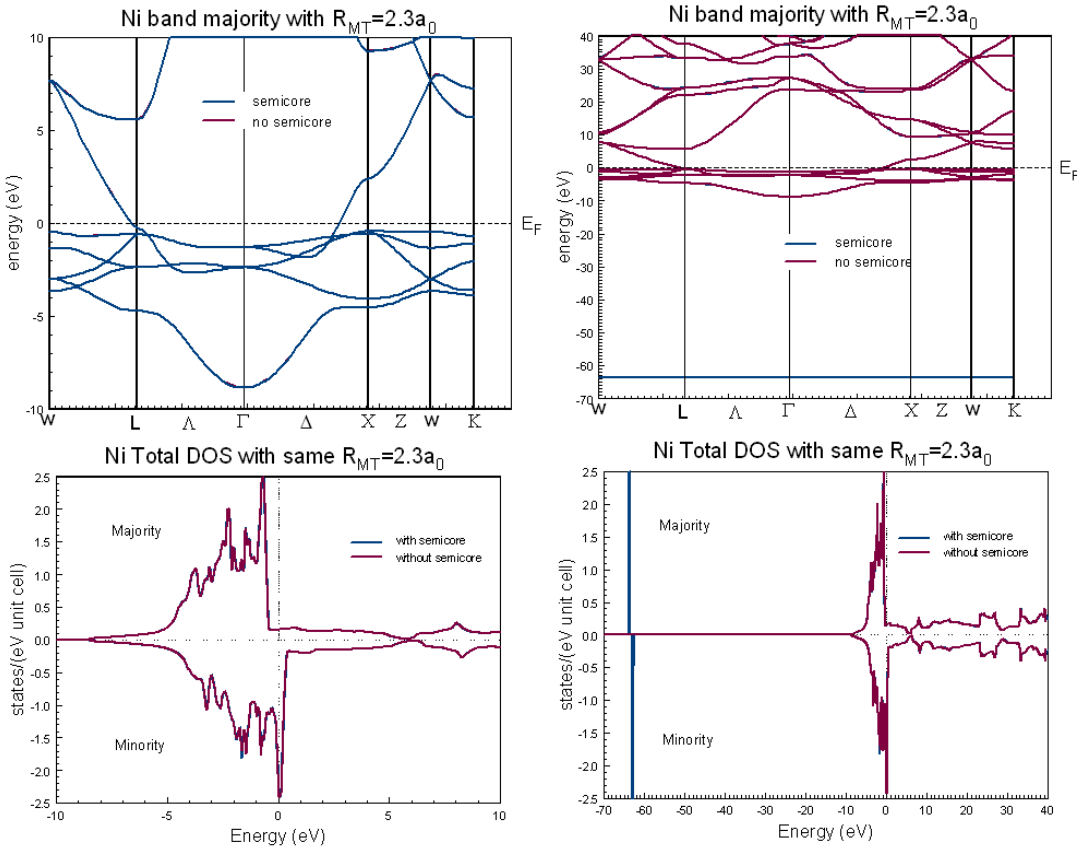

Figure G.11. The bands/DOS match perfectly with Ecore< 4.5Ry and 6.0Ry respectively.

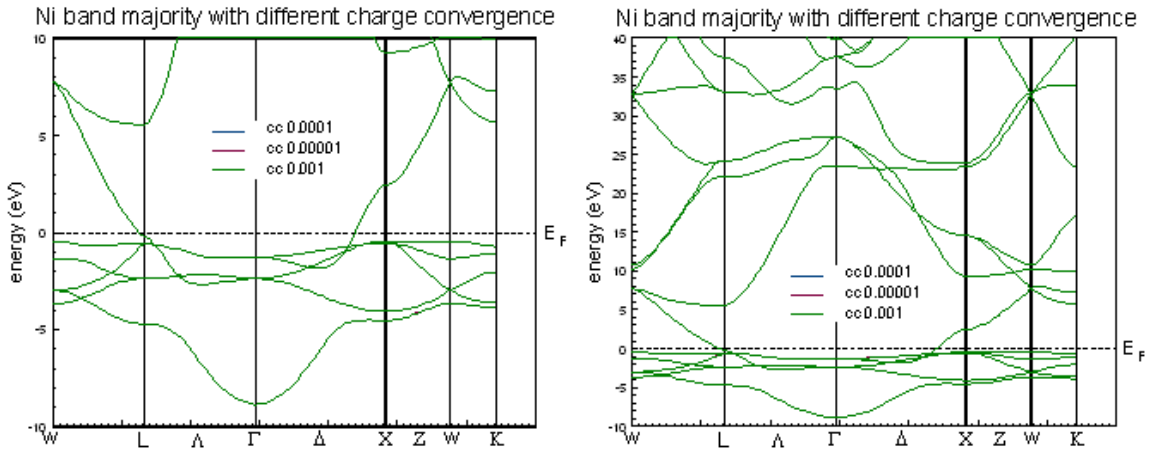

Figure G.12. The bands is drawn with the criteria of the charge convergence 0.001, 0.0001 and 0.00001 correspondingly. Due to excellent convergence, the curves seem to overlap

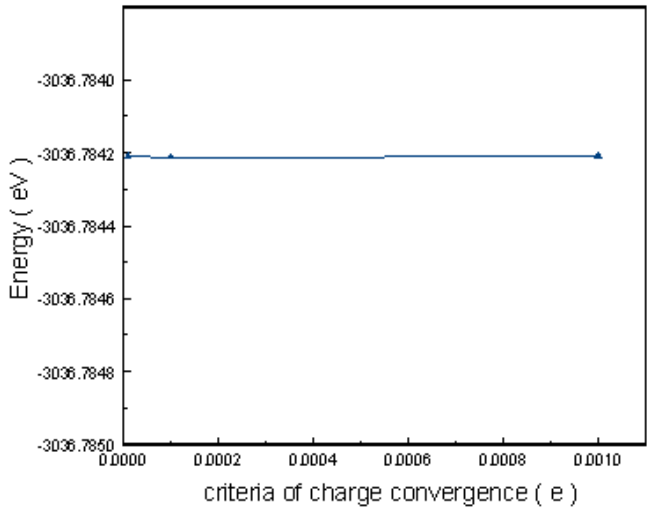

Figure G.13. Energy plotted as function of charge convergence criteria

-10eV to 10eV. It demonstrates that in this range the calculations are convergence with all the selected the $\vec{G}$ vector sets and the calculation have arrived at reasonable accuracy from $R_I^{\min} \cdot G_{\max} = 8$. Above 20eV the bands in $R_I^{\min} \cdot G_{\max} = 7$ stay away from the corresponding ones in larger basis-set cutoffs ($R_I^{\min} \cdot G_{\max} = 8, 9 \text{ and } 10$) and the states with larger basis-set cutoffs begin to split above 30eV. It tells that the LAPW basis set is only good in a limited energy region. In fact, a basis set is chosen to be large enough to be accurate, but only just large enough in order not to waste computer time. Moreover, the calculated total energy and magnetic moment are shown below (Figure G.15). They change monotonically because the number of the plane waves is a variational quantity. The convergence of the total energy is acceptable for $R_I^{\min} \cdot G_{\max} \geq 8$, while the convergence of the magnetic moment become acceptable for $R_I^{\min} \cdot G_{\max} \geq 7$.

The seventh test is to observe the outcome of the alteration of the formula used for the exchange-correlation functional $V_{xc}(n)$ in LDA/LSDA. The plots are made with three forms of functional (Figure G.16). The agreement of the calculated bands is excellent in nickel.

The eighth test is to draw the total energy vs. the lattice constant in the neighborhood of the minimum energy by least square method (Figure G.17). The lattice constant for the minimum energy predicted by the fitting curve is a=6.4905a_0, the experimental value at T=0K is 6.5 a_0.

In summary, the better electronic-structure and total energy calculation in WIEN can be made by a proper choice of the basis-set cutoff $R_I^{\min} \cdot G_{\max}$, k-mesh, a temperature broadening factor, lattice constant, exchange correlation potential, convergence parameter, and linearization energy and local orbitals.

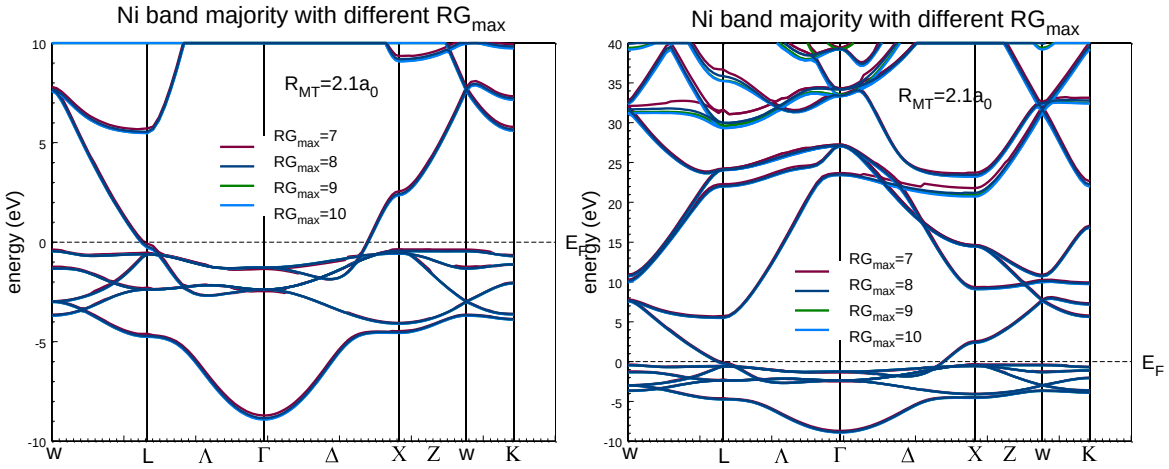

Figure G.14. The band structure with different $R_I^{\min} \cdot G_{\max}$ in different energy scale.

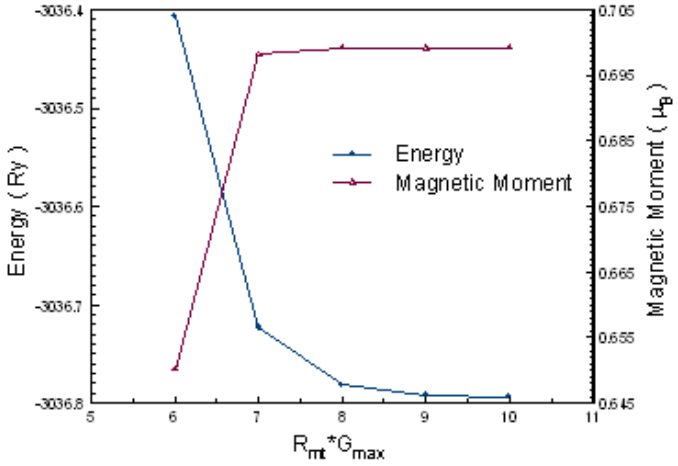

Figure G.15. The total energy and magnetic moment vs. $R_I^{\min} \cdot G_{\max}$. Their variation is monotonically .

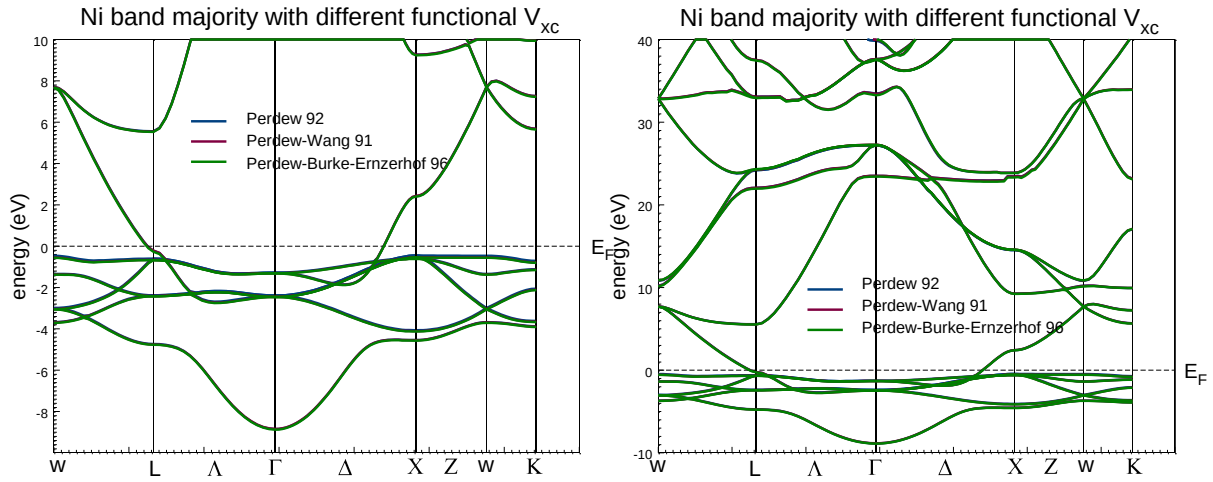

Figure G.16. The bands are plotted with three forms of the exchange-correlation functional $V_{xc}(n)$ in LDA/LSDA.

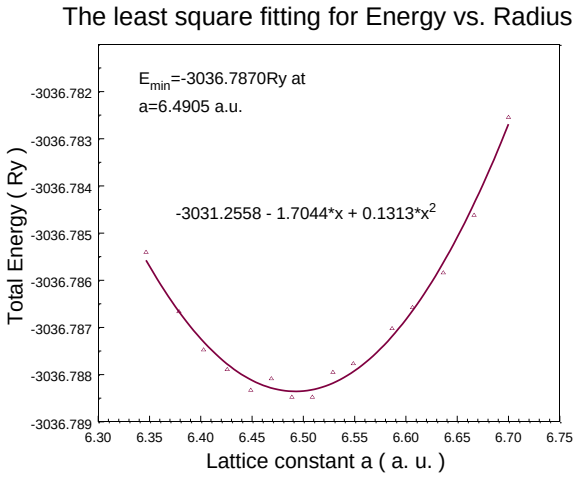

Figure G.17. The total energy vs. the lattice constant in the neighborhood of the minimum energy

VITA

Qinghong Kou was born on April 21, 1969 in Wuhan, P. R. of China. She graduated from University of Hubei with a Bachelor of Science degree in July 1989 and from Wuhan University with a Master of Science in 2001. She entered University of Tennesee as a graduate student during the Fall of 2001 and will graduate in 2009.